TRICUSPID VALVE MECHANICS: UNDERSTANDING THE EFFECT OF ANNULAR DILATATION AND PAPILLARY MUSCLE DISPLACEMENT

A Thesis
Presented to
The Academic Faculty

by

Erin M. Spinner

In Partial Fulfillment
of the Requirements for the Degree
Doctor of Philosophy in the
School of Biomedical Engineering

Georgia Institute of Technology & Emory University
December 2011

TRICUSPID VALVE MECHANICS: UNDERSTANDING THE EFFECT OF ANNULAR DILATATION AND PAPILLARY MUSCLE DISPLACEMENT

Approved by:

Dr. Ajit P. Yoganathan PhD, Advisor
Department of Biomedical Engineering
Emory University/Georgia Institute of Technology

Dr. Stamatios Lerakis MD
Division of Cardiology
Emory University

Dr. David H. Adams MD
Department of Cardiothoracic Surgery
The Mount Sinai Medical Center

Dr. John N. Oshinski PhD
Deparment of Radiology & Biomedical Engineering
Emory University/Georgia Institute of Technology

Dr. Rudolph Gleason PhD
Department of Mechanical Engineering
Georgia Institute of Technology

Dr. W. Robert Taylor MD, PhD
Division of Cardiology & Biomedical Engineering
Emory University/Georgia Institute of Technology

Date Approved: July 25, 2011

In memory of my loving father.

ACKNOWLEDGEMENTS

This has been an amazing journey, one of which I couldn't have done without the help of so many.

Thank you to Dr. Y for taking a chance on me and never giving up. I hope I have helped to show him that the tricuspid valve truly is important to study. I also want to thank him for contributing to my success: introducing me to so many amazing people and allowing me to present my research at conferences all around the world. The CFM lab has been an experience I will take with me always and never forget. I want to thank the members of my committee. Dr. Adams, your insight and experience was priceless. It was a pleasure working with you on the Circulation paper, and your suggestions helped to strengthen my research. I appreciate you taking time to assist me. Dr. Lerakis, thank you for giving us the opportunity to branch out to *in vivo* work. It was truly a pleasure working with you and your team at Emory. You were always available for me and made me smile. Dr. Taylor, I appreciate your insight and spirit. It was always a pleasure talking with you. You were there to support me throughout my entire journey in graduate school and for that I am forever grateful. Dr. Oshinski, I thank you for your imaging expertise and playing an instrumental role in helping me to get my

first paper published. Dr. Gleason, for keeping me in touch with my roots in mechanical engineering and strengthening my investigation of the mechanics. You are an inspiration in keeping balance and making sure to make time for the things that you care about. To all my committee members, I thank you for your positive attitude. I am truly blessed to have the pleasure of working with such amazing clinicians and scientists, a dream come true.

Thank you to the members of the CFM lab, both past and present. To Kartik B. and Kartik S. for always supporting me and helping me through the tough times. Not sure I could have stuck in there without your encouragement. To Murali and Jorge, for setting such high standards and always keeping me in check and pushing me to work even harder than I thought possible. Diane and Maria for being there to talk with. Maria, it has been a pleasure, you are a great person and great friend. JP, for making me laugh and being such a hard worker. Chirs and Yap for keeping me company at conferences and always being up for a good time. The new post docs, Neela, Shiva, Lucia, Reza and Arvind, for taking over the administrative tasks and giving me time to work on my thesis. Swetha, Min, Bradon, Lauren, Elaine and Andrew, best of luck with your future in the CFM lab. I especially have to thank my amazing undergraduate Lauren whom I am forever grateful for and so proud. She always made me smile and made my

life so much easier. Lauren, I know you are destined for great things. Dana and Patrick, whom were also instrumental in the success of my thesis. Dr. Thourani, for allowing me to observe my first open heart surgery and your constant enthusiasm, you always made me excited about science.

Thank you to my friends whom helped me to maintain balance and always have fun. Ashley, so many memories and many more to come. You were always there for me whenever I needed you. Jeremy, thanks for being up for anything and being such a great person. So many others: Gina, Casey, Randy, Fernie, Chris, Julia, Laura, Carolyn, Alyssa, Nnenna, Rachel, Jay, Ken, Barbara. Ginny, Lisa, Anna and Joseph, I will never forget you all and am so thankful for your kindness.

Thank you to those closest to me. Andrés, I love you, and couldn't imagine making it through this journey without you. Your dedication to your work and science was inspirational. You were always there to make me laugh and smile, even if I tried so hard to resist. I can't wait for our future together. Gina, my sister, for paving the way for me and always being so supportive and proud of me, I love you. Mom, for being such a strong women and teaching me so much, I love you. You are an inspiration to me, and I hope that I can be to my kids what you have been for me. Dad, whom I miss so much, for giving me direction. I love you and thank you.

TABLE OF CONTENTS

LIST OF TABLES

LIST OF FIGURES

LIST OF SYMBOLS AND ABBREVIATIONS

TV	Tricuspid Valve
MV	Mitral Valve
TR	Tricuspid Regurgitation
RV	Right Ventricle
LV	Left Ventricle
RVEDA	Right Ventricular End Diastolic Area
LVEDA	Left Ventricular End Diastolic Area
PM	Papillary Muscle
APM	Anterior Papillary Muscle
SPM	Septal Papillary Muscle
PPM	Posterior Papillary Muscle
RLL	Residual Leaflet Length
PA	Pulmonary Artery
SA	Septal/Anterior
PS	Posterior/Septal
AP	Anterior/Posterior

SUMMARY

Tricuspid regurgitation (TR), back flow of blood from the right ventricle to the right atrium, has been reported in approximately 85% of the population, with 16% having mild or severe TR. Patients with untreated moderate to severe TR are likely to experience decreased exercise capacity and have increased morbidity and mortality, thus affecting the patient's quality of life. Current methods of repair offer limited rates of success, and many patients require further operations to correct returning levels of TR. Incomplete repair may be due to incomplete understanding of the functional anatomy and mechanics of the TV and the underlying causes of TR.

It was hypothesized that **alterations in the geometry of tricuspid valve annular and subvalvular apparatus induced by ventricular dilatation determine the severity of TR**. *In vivo* measurements of papillary muscle (PM) position in patients with single or biventricular dilatation revealed PM displacement away from the center of the annulus as compared to control patients. Additionally, pulmonary arterial pressure, annulus area, ventricular size and apical displacement of the anterior PM were highly correlated with the severity of TR. An *in vitro* right-heart simulator was developed to investigate isolated mechanics of TR. Through these *in vitro* studies it was demonstrated that the tricuspid valve begins to leak at only 40% dilation, much lower than the mitral valve. Additionally, it was shown that isolated PM displacement resulted in significant TR. The highest levels of TR were achieved with a combination of annular dilatation and PM displacement. Alterations in leaflet coaptation, as quantified by measuring the amount of leaflet available for coaptation and leaflet mobility were observed with annular dilatation and

PM displacement, both isolated and combined. The changes in leaflet coaptation resulted in redistribution of the forces on the chords originating from the anterior PM and inserting into the anterior and posterior leaflets.

The findings herein provide the clinical and scientific community with a mechanistic understanding of the tricuspid valve to further improve intervention and repair of TV disease.

CHAPTER 1

INTRODUCTION

Tricuspid regurgitation (TR), back flow of blood from the right ventricle to the right atrium through the tricuspid valve (TV), a once ignored disease, has been rapidly gaining interest of clinicians in the cardiovascular field[1, 2]. If left untreated, TR can worsen over time and have detrimental effects on morbidity and mortality[1, 3]. As with any new treatment, the specific surgical repair techniques and replacement valve design specifications for TR therapies remains controversial and is often only done in conjunction with other valve repairs[3, 4 2].

Functional tricuspid valve regurgitation (TR) is increasingly recognized as a source of morbidity in patients with severe left sided valvular heart disease, particularly those with chronic mitral valve regurgitation[5, 6]. Early investigators believed functional TR would resolve after surgical correction of left sided valve disease[7] and did not advocate concomitant tricuspid surgery. As it was recognized that severe TR often persisted despite corrective, left-sided valve surgery[8], and that reoperation for severe functional TR was perilous, interest grew in simultaneously repair of the tricuspid valve along with the mitral valve. Tricuspid valve dilatation was soon thereafter recognized as the primary mechanism of functional TR and remodeling annuloplasty with a prosthetic ring, became the treatment of choice for most surgeons[9-11]. More recent studies have further clarified the role of annular dilatation centered around the right ventricular free wall portion of the tricuspid annulus as the primary lesion [12, 13] and thus target of remodeling strategies, and American and European Guidelines recommend concomitant

annular remodeling for severe annular dilatation or for moderated to severe TR in patients undergoing left-sided valve surgery [14, 15].

Currently, treatment options are limited for correction of TR. Past research has focused primarily on the mitral and aortic valves, and as a result, the mechanisms which are responsible for TR have yet to be elucidated and remain understudied. Though TV repairs have been attempted, 30% of current repairs fail, requiring patients to return to the operating room[16]. This recurrent TR is likely due to an incomplete understanding of the tricuspid valve apparatus and alterations associated with different diseases. While it is widely accepted that annular dilatation[9, 17] and pulmonary hypertension[18, 19] contribute to TR, it is uncertain as to which other factors which may be involved and the relative contribution of these factors to disease progression. Previous studies have identified changes in ventricular geometry as well as papillary muscle (PM) displacement as contributing factors to TR. As a result of PM displacement, the valve leaflets may become tethered, thus restricting the motion and preventing proper coaptation. Leaflet tethering itself may be used as a predictor of TR[20-22]. Additionally, changes in the ventricle geometry may directly affect the PMs as they are directly connected to the ventricular wall. It is believed that RV dilatation may result in displacement of the anterior PM (APM)[23, 24], while another study reported displacement of the septal PM (SPM) towards the center of the RV with LV dilatation [25]. However, these prior studies were unable to directly correlate these finding to the magnitude of TR.

Though numerous studies have been conducted to understand the normal and disease mitral valve (MV), studies on the mechanics of the TV are lacking. Perhaps an oversimplification of the relationship between the valves is responsible for the direct use

of MV repair techniques to TV disease. While various aspects of the two valves are certain to overlap, the difference in valve structure warrants studies specifically investigating the TV. Efforts to provide a better understanding of the valve have been ongoing [12, 17, 21, 23, 26], but have mostly been conducted *in vivo*, which often restrict the ability to complete a detailed mechanistic investigation of the valve under both normal and disease conditions.

Interestingly functional mitral regurgitation has been much more carefully studied on the lab bench and by imaging techniques and is recognized to involve primarily posterior papillary muscle displacement, leading to leaflet tethering and a compromised zone of leaflet coaptation [27]. It is generally accepted that with annular dilatation, TR will occur [21, 22, 28] but the mechanism by which this occurs has yet to be demonstrated. As in functional mitral regurgitation, another possible mechanism for TR is papillary muscle (PM) displacement, which may result from right ventricular dilatation. The role of PM displacement is much less well defined in functional TR, and this may have important clinical implications. It is possible one of the mechanisms of recurrent TR after tricuspid valve repair with an annuloplasty ring, which occurs in up to 30 percent of patients[16], is failure to address the leaflet tethering, due to PM displacement. Understanding the mechanisms of TR will lead to improved diagnosis and treatment.

With displacement of the PMs the chords become tethered and the leaflets lose the ability to move freely and properly coapt. While leaflet tethering has been observed clinically it is not clear as to what actually causes the tethering whether it is due to annular dilatation or PM displacement or a combination of the two. Along with leaflet

mobility, chordal forces may also be affected by these disease conditions, as they are an integral part of the system. If a chord's force is significantly increased it may become elongated or in extreme cases rupture, both of which would be detrimental to proper valve function. By investigating chordal forces we can begin to identify which chords may be responsible for certain types of tethering. We believe that disease conditions may lead to restricted leaflet mobility thereby altering the chordal forces. It is important to understand these interactions to provide surgeons with sufficient information to make appropriate repairs, which aim to restore the valve to its normal state. Through this study we intend to provide a more complete picture of how disease alters TV annular and sub valvular geometry, thus affecting leaflet mobility and changing the force distribution on the tendinous chords.

In general the extreme lack of data and general understanding of the tricuspid valve warrants a thorough investigation. While clinical data has been analyzed they are often retrospective in nature. Carefully designed studies which aim to understand certain aspects of TV disease are therefore necessary. These sentiments have been shared both in literature and again and again at clinical conferences. The clinicians are inquiring for data to assist in their understanding and to aid in their development of tricuspid valve specific treatments.

The overall goal of this thesis was to understand the mechanisms which cause TR and specifically the impact of ventricular dilatation on the severity of TR. It is hypothesized that ventricular dilatation can affect TR in three ways, by dilating the annulus, displacing the PMs and a combination of both. Specific aims 1 through 3 will help to understand how changes in ventricular dilatation lead to changes in PM position

and annulus size, which affect chordal forces, thus altering leaflet mobility and causing improper leaflet coaptation and finally resulting in TR.

This will be achieved by first identifying geometrical changes induced by dilatation of the ventricles *in vivo*. In ***specific aim 1*** the degree of PM displacement for each PM with respect to RV dilatation, LV dilatation and combined RV/LV dilatation will be determined. In addition to determining PM position the correlation between the degrees of ventricular dilatation to the severity of TR will be determined. The next step is to understand the underlying mechanisms involved in the development of TR due to annular and sub-valvular geometric alterations. In ***specific aim 2,*** isolated annular dilatation with normal PM position and isolated PM displacement with normal annular size *in vitro* will be investigated. The effects of these perturbations on chordal stresses, leaflet mobility, leaflet coaptation and severity of TR will be explored. In ***specific aim 3*** combined annular dilatation and PM displacement *in vitro* will be investigated. As in specific aim 2, the effect of dilating the annulus and PM displacement on chordal stresses, leaflet mobility, leaflet coaptation and finally severity of TR will be investigated. The information on the effects of isolated and combined annular dilatation and PM displacement from *specific aims 2 and 3* will be compared to help propose an integrated mechanism explaining the impact of ventricular dilatation on the severity of TR.

Although some information as to the impact of ventricular dilatation on the severity of TR can be provided by *in vivo* studies, *in vitro* studies allow detailed investigation into the underlying mechanisms. *In vitro* experimentation allows for precise

control over annular size and PM position, allowing for isolated cases and specific replication of disease etiologies.

CHAPTER 2

BACKGROUND

2.1 Tricuspid Valve (TV) Anatomy

The tricuspid valve is one of the two atrioventricular valves which separate the atrium from the ventricle. The tricuspid valve is located on the right side of the heart between the right atrium and right ventricle. The valve operates under much lower pressures than the left side of the heart with a peak systolic pressure of only 40 mmHg as compared to 120 mmHg. The valve consists of valvular, leaflets and an annulus, as well as subvalvular components, tendinous chords and papillary muscles (PM) (Fig 2.1).

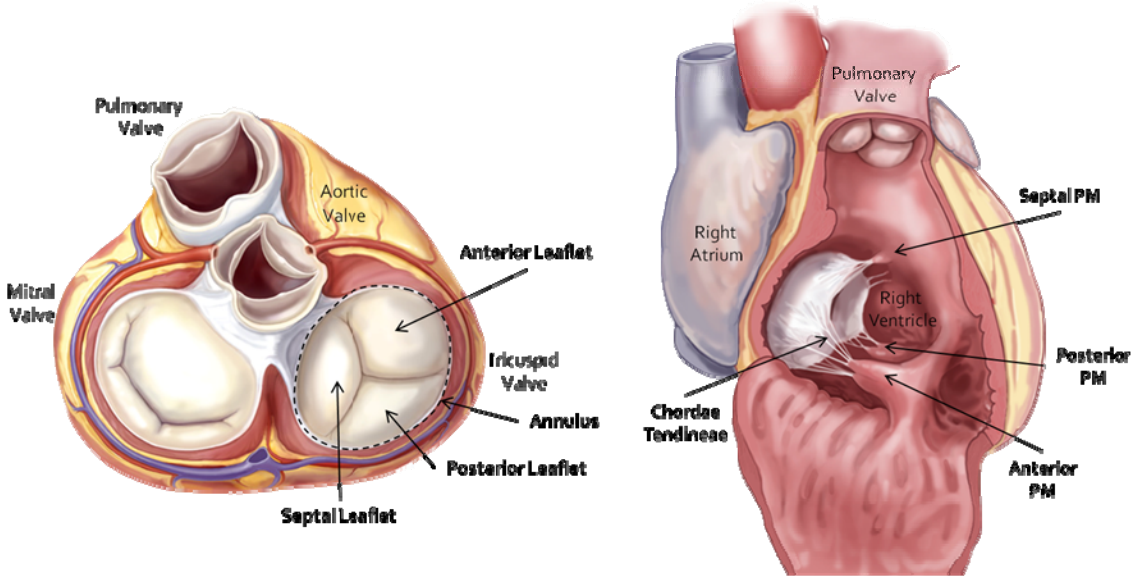

Figure 2.1: Right Heart Anatomy, showing location of tricuspid valve, annulus, leaflets, chordae tendineae and papillary muscles. (Modified from Carpentier's Reconstructive Valve Surgery)

The purpose of the TV is to prevent backflow of blood from the right ventricle to the right atrium during systole and also allow optimal ventricular filling during diastole. A normal functioning valve opens during diastole and allows the blood to flow from the

right atrium and fill the right ventricle. During systole the ventricle contracts and the pressure raises closing the valve and preventing backflow. Proper closure is obtained through coaptation of the leaflets, which is achieved through the combination of all the components of the valve working together. The PMs and chords work together to prevent the leaflets from prolapsing into the atrium during systole and thus proper coaptation geometry and position are achieved.

2.1.1 Annulus

The annulus is a fibrous ring located on the perimeter of the valve and connects the leaflets to the myocardial wall. The annulus has a complex 3D geometry as seen in figure 2.2 [29-36]. While some studies have reported the annulus to be oval [29, 37], others report that it is triangular [32]. Studies have shown this to be a dynamic structure which contracts during systole and expands during diastole [33, 34, 38]. Annulus areas range from 7.6 to 11.2 cm^2 during systole and 11.3 to 18.35 cm^2 during diastole [34, 37, 38].The tricuspid valve annulus area significantly increases from early to late systole in healthy subjects by 5.4 ± 1.6 % [34] and experiences differences ranging from 28% to 48% from its minimum to maximum area throughput the cardiac cycle [33, 36, 38]. The area of the TV annulus is at its maximum during diastole increasing the efficiency of filling by providing a larger orifice [36] and minimum during systole aiding coaptation of the leaflets. In addition to changes in area throughout the cardiac cycle, the annulus changes its shape as well. The annulus of the TV has a 3 dimensional saddle [33-35], as seen in Figure 2.2, with the annulus becoming more planar during diastole [35].

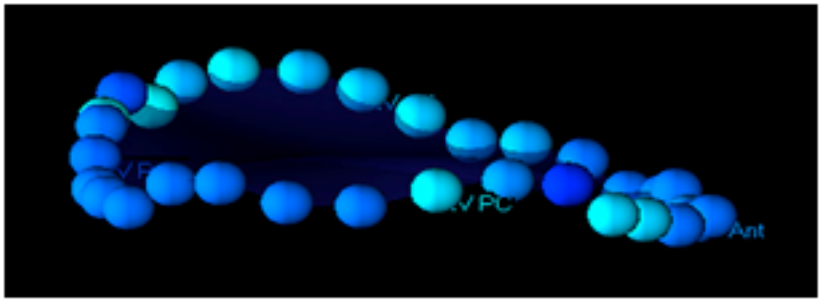

Figure 2.2: Results from an in vivo sonomicrometry study on sheep show the clockwise rotation motion of the papillary muscles over the cardiac cycle [36].

2.1.2 Leaflets

The three leaflets are named according to their position in the heart: anterior, posterior and septal leaflet. The septal leaflet is located along the septal wall and is attached to the wall with short chordae [32]. The anterior and posterior leaflets are located along the free wall with the anterior leaflet reported to be the largest [37, 39, 40]. While it is typically accepted that the TV has three main leaflets, numerous studies have reported there to be a variable number of leaflets ranging from 2 up to 7 leaflets [32, 41]. The septal leaflet is always present but the number of leaflets along the free wall can vary (Fig. 2.3).

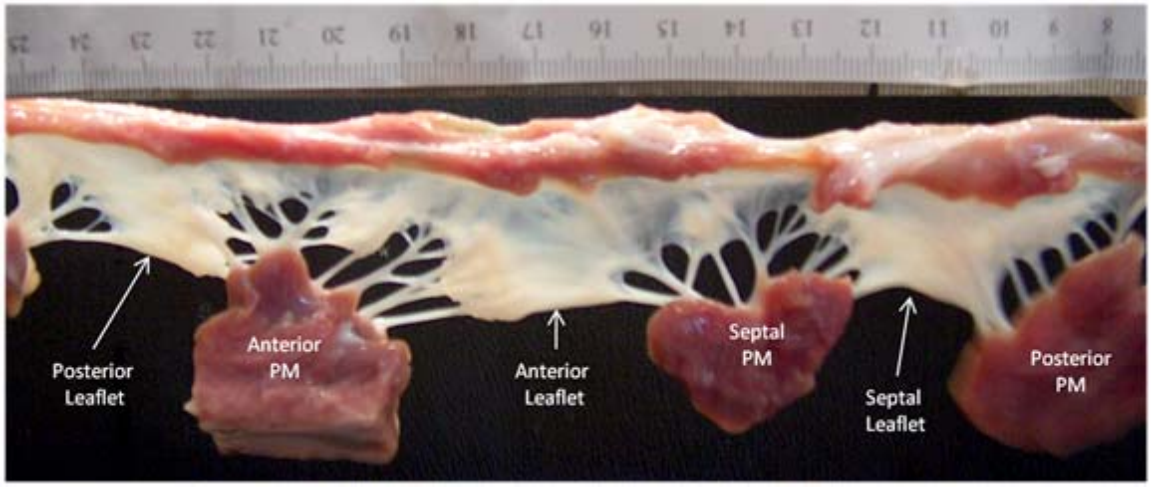

Figure 2.3: Explanted porcine valve, showing leaflet and PM locations relative to another.

2.1.3 Chords

The chords are made predominately of collagen [6] which attach the leaflets to the PMs. Each PM has several chords which attach to the two corresponding leaflets, for example the anterior PM has chords that insert into the anterior and posterior leaflets. Chords are classified based upon their insertion location into the leaflet with four categories: marginal/primary, inserting into the free edge of the leaflet, rough/supplemental, inserting between the marginal and intermediate chords, intermediate/secondary, inserting into the belly of the leaflet and basal chords, inserting near the annulus[32]. Silver et al report the deep/strut chordae to be the longest (1.7 ± 0.4 cm). All chords have similar thickness ranging from 0.8 ± 0.3 cm to 1.1 ± 0.4 cm [32].

2.1.4 Papillary Muscles (PM):

The PMs connect the leaflets to the ventricle wall through the chords and directly relate the TV to ventricle function. The PMs on the right side of the hearts are not as well

defined as those seen on the left side of the heart as with the mitral valve [42]. There are three main PM groups which are named according to their location in the ventricle: anterior, posterior and septal. The septal papillary muscle is located on the anterior side of the septum between the septal and anterior leaflets, while the posterior PM is located on the posterior side between the septal and posterior leaflets. The anterior PM is located on the free wall between the anterior and posterior leaflets. The anterior PM the most well defined with one main PM head [42, 43]. The posterior PM often has multiple heads, while the septal PM is often fused to the wall with no protruding PM head [42]. In human patients a moderator band has been reported which connects the septal wall to the free wall, but its function is unknown. The PMs are classified into three groups based upon structure: finger-like, with the muscle protruding, tethered, with the muscle imbedded in the wall, and vestigial with the chords attaching directly to the well [42] (Fig. 2.4).

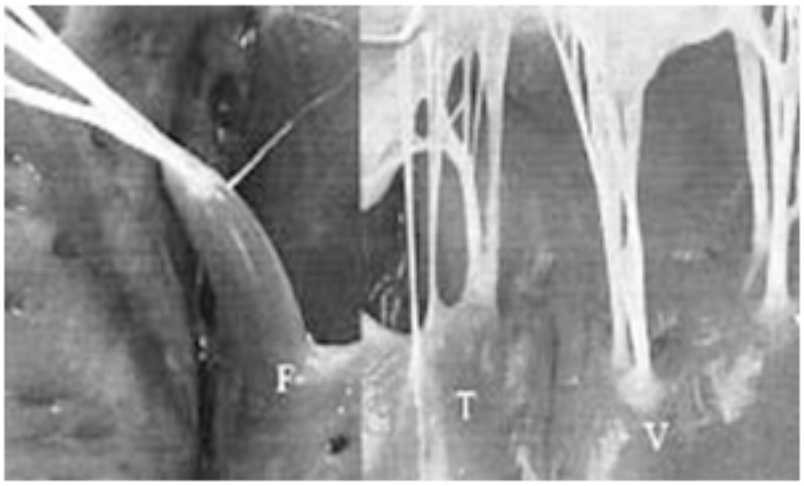

Figure 2.4: Classification of the three groups of papillary muscles: F-Finger-like, T-Tethered, and V-Vestigial. As classified using excised porcine hearts by Joudinaud in 2006 [42].

Juaon et. al. studied the dynamics of the three PMs of the right side of heart [36] during the cardiac cycle and found that the PMs move in a clockwise manner during

systole. The anterior PM experiences the greatest movement during the cardiac cycle, due to the contraction of the myocardium since the PM is located on the free wall. The motion of the PMs has been observed to twist, shift, and bend in relation to the annulus plane, while the distance from the PMs to the annulus plane remains relatively constant [36].

2.2 Disease of the Tricuspid Valve and Treatment

When the valve fails to coapt properly regurgitation of blood may occur. TR is the back flow of blood from the right atrium to the right ventricle. TR was initially thought of as benign, but has recently been shown to have a significant impact on morbidity and mortality [1]. Uncorrected significant TR can adversely affect durability of left heart repairs and is associated with poor survival in severe cases [24] [3]. Symptoms are often nonspecific, but may include fatigue and reduced exercise capacity [1, 2]. Additionally they may also experience symptoms associated with right heart failure such as ascites, congestive hepatopathy, peripheral edema, decreased appetite, and abdominal fullness[2].

If left untreated TR may become worse over time and eventually lead to death[11]. A retrospective study performed by Nath et al. in 5223 patients found there to be a worse outcome in patients with moderate to severe TR as compared with those without TR[44] (Fig.2.5).

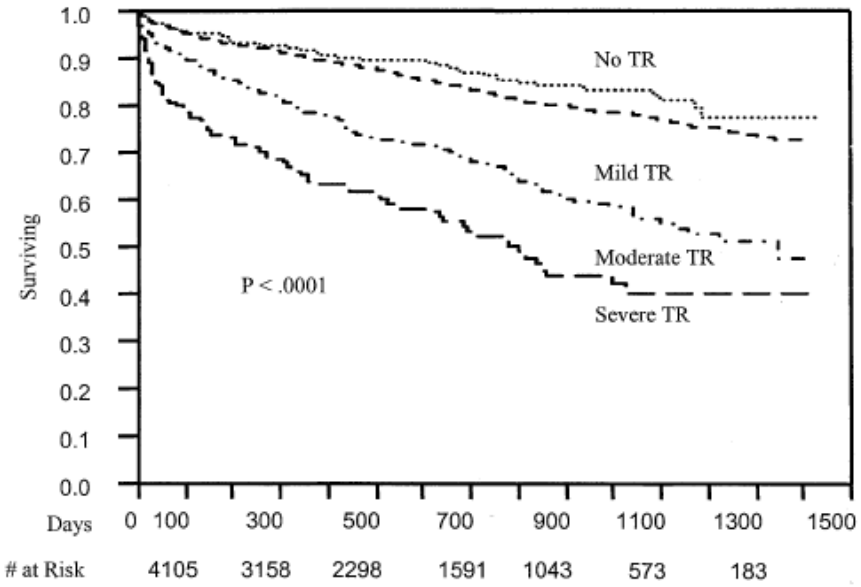

Figure 2.5: Kaplan-Meier survival curves for patients with and without tricuspid regurgitation. Patients with moderate and severe TR had significant worse survival rates (Nath et al. 2004).

In addition, patients with higher levels of TR also have worse outcomes after tricuspid valve repair. It is believed that if treatment for TR is to be preformed it should be conducted sooner rather than later[45, 46]. A recent study by Topilsky et al. analyzed 189 patients after tricuspid valve replacement and found late mortality to be associated with preoperative New York Heart Association Class[46] (Fig. 2.6).

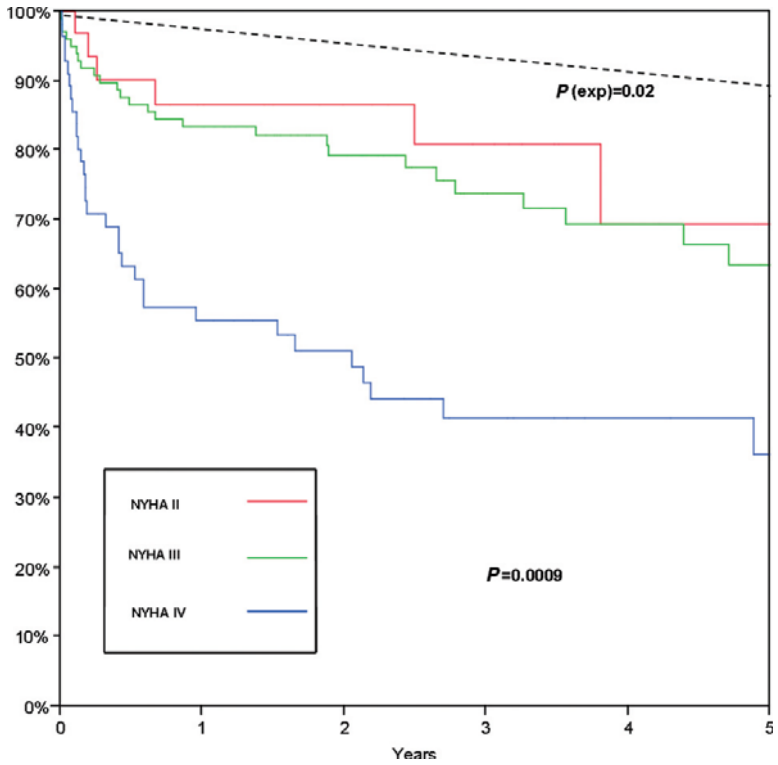

Figure 2.6: Observed postoperative survival for patients operated on for severe tricuspid regurgitation with minimal symptoms (New York Heart Association [NYHA] class II, red line), intermediate symptoms (NYHA class III, green line) or severe symptoms (NYHA class IV, blue line) before surgery. Compared with patients with preoperative NYHA class II or III, those with NYHA class IV heart failure incur considerable excess postoperative mortality. The dashed line represents the expected survival. Even those with minimal symptoms (NYHA class II) incurred excess long-term mortality compared with the expected mortality (Topilsky et al. 2011).

2.2.1 Diagnosis:

The amount of tricuspid regurgitation is classified similar to the mitral valve with the use of color Doppler visualization of the jet in the four chamber view. Quantitative measurements of the regurgitant volume are obtained with the proximal isovelocity surface area (PISA) method. There are four different grade classifications: trace (1+), mild (2+), moderate (3+) and severe. Images of the various TV regurgitation volumes have been measured using color Doppler [47] and are shown in figure 2.7. In addition,

echocardiographic studies typically report a central jet, as seen in the apical 4 chamber view [47].

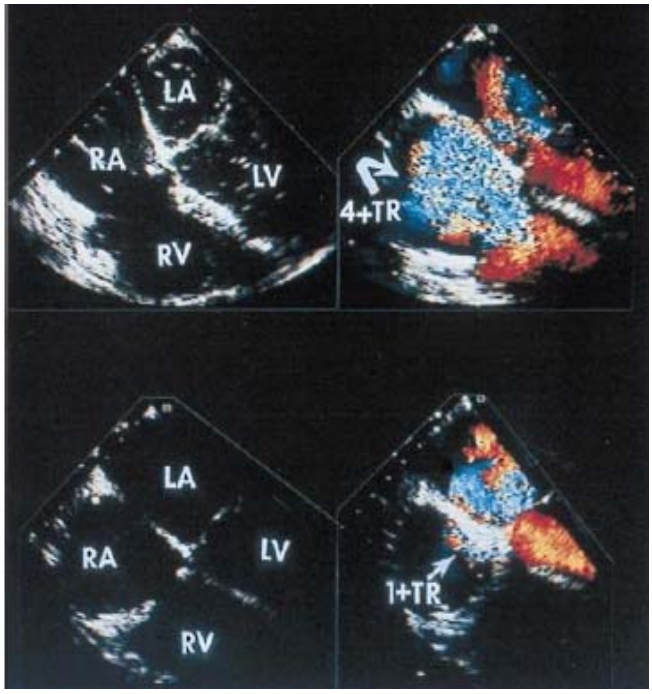

Figure 2.7: Color Doppler images of various degrees of tricuspid regurgitation. A clear increase in the jet can be seen from trace (1+) to severe (4+) (Bajzer et al. 2008).

2.2.2 Prevalence:

TR is typically found in 82% of men and 86% of women (US population), of which 15% of men and 19% of women have mild to severe TR , as was determined in a population-based cohort study of patients attending routine examination at the Framingham Study[48]. The prevalence of TR of more than or equal mild increases with age, independent of sex[48].

2.2.3 Cause:

TR is more commonly functional rather than organic[49, 50] in that the regurgitation is secondary to another mechanism and not due to disease of the leaflets. These other

mechanisms can include, but are not limited to changes in preload, after load and RV function [9, 16]. The amount of TR varies with the mechanisms. Although there are various indicators for TR, various arguments exist as to which is the key contributor. Dreyfus believes that the annulus and RV must be dilated in order to leak [9], while Matsuyama and Abe agree with RV dilatation, but also believe it to be associated with pulmonary hypertension [50, 51]. It is also believed that TR occurs in conjunction with left side heart disease and ventricular dysfunction [33]. Visualization of TR for various patient etiologies is shown in the below figure (2.8).

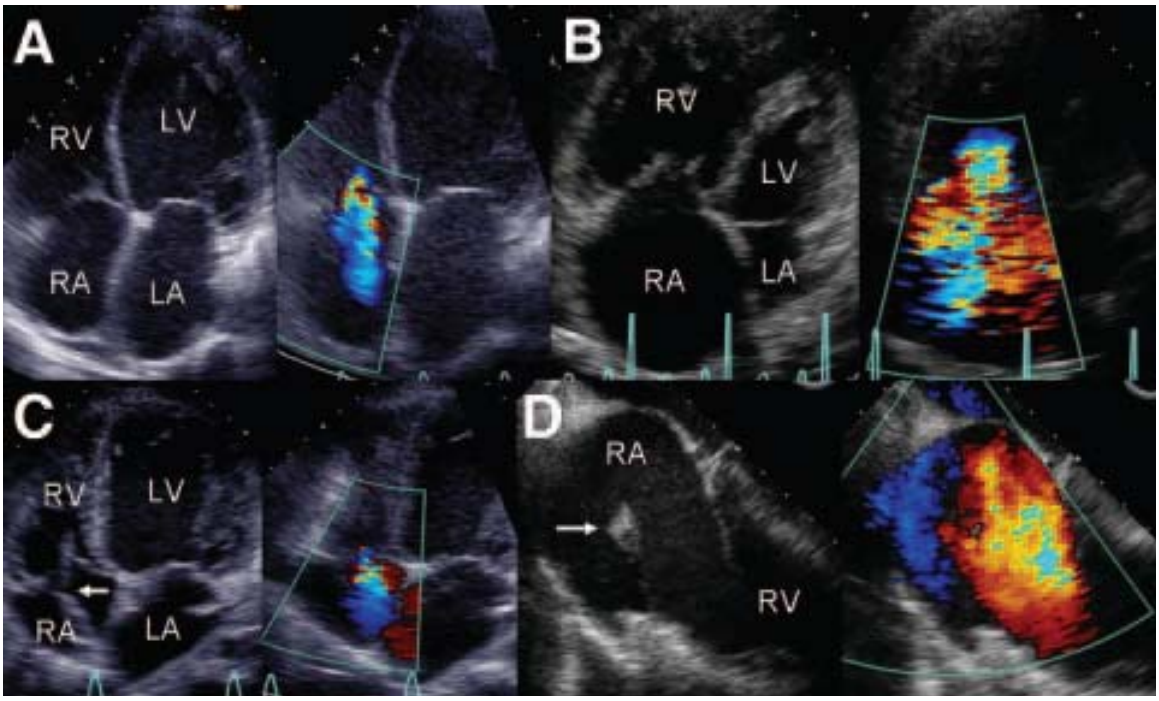

Figure 2.8: Echocardiographic appearance of tricuspid regurgitation (TR) from various pathologies. (A) Left ventricular (LV) dysfunction with mitral regurgitation and left atrial (LA) enlargement, with secondary right heart enlargement (mild TR). (B) An RV pacemaker lead present(arrow) (mild TR). (D) Cardiac contusion from motor vehicle accident with anterior papillary muscle rupture. The papillary muscle can be seen prolapsing into the RA with systole (arrow), resulting in torrential TR (Rogers and Bolling 2009).

2.2.3.1 Pacing Leads:

One of the most common causes of TR is the presence of a pacemaker or defibrillator lead, as the lead passes through the TV and attaches to the ventricle. The leads may restrict the motion of the leaflets by pressing the leaflet again the wall. The leads themselves may also puncture the leaflets or become entangled in chords. Many studies have shown pacing leads to be responsible for TR and if not removed at the time of tricuspid valve repair result in residual TR[11] (Fig 2.9). An echocardiograph study by Kim et al. of pre and post implantable pacemaker or defibrillator patients found the grade of TR to be worsened by a grade of 1 or more with lead placement through the TV[52].

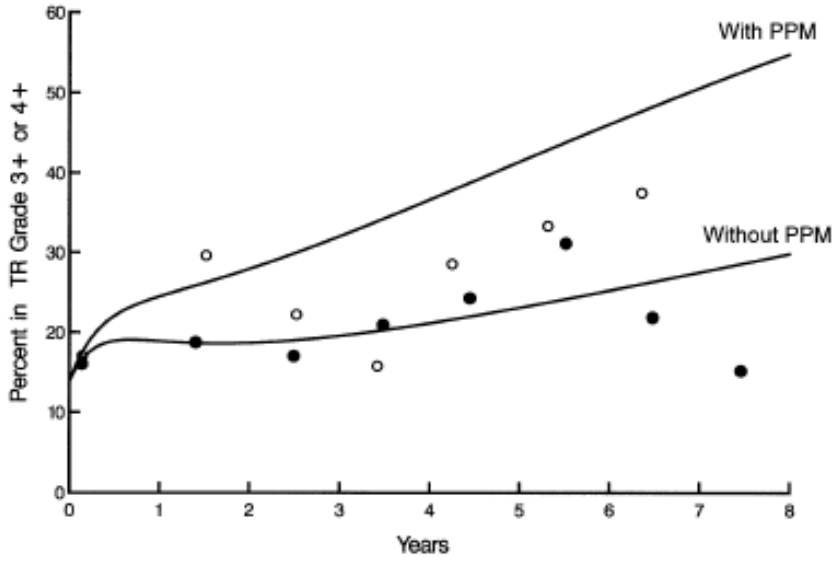

Figure 2.9: Influence of preoperative permanent pacemaker on evolution of postoperative 3_ and 4_ tricuspid regurgitation. *Open circles* _ pacemaker; *solid circles*_ no pacemaker. *PPM*, Permanent pacemaker; *TR*, tricuspid regurgitation (McCarthy et al. 2004).

2.2.3.2 Ventricle Dilatation:

One of the proposed mechanisms of TR is caused by dilation of the right ventricle. Since the valve apparatus is part of the ventricle with its PMs attached directly

to the ventricular wall and its annulus located in the wall between the atrium and ventricle, changes in the ventricle are directly transferred to the valve apparatus. The dilatation of the right ventricle has detrimental effects on the mechanics of the tricuspid valve. One of these includes less-than-normal systolic reduction in annulus [38] which is caused by the decrease in right ventricular function. This RV enlargement also causes tricuspid annulus deformations and displacement of PMs [17, 18, 28, 33, 38, 53, 54], which also play a role in TR. It has also been reported that with RV systolic "failure" diastolic pressure rises, increasing pulmonary pressure and moving the septum towards the left side [3]. In addition, dilatation of the left ventricle may affect proper closure of the valve. It is possible for the septal and posterior PMs to be affected by LV dilation since the two ventricles are connected, but has yet to be identified. Studies have shown that PM position effects TR, but the specifics of which PMs are displaced with specific etiologies, the direction of displacement, and how much they are displaced is speculative and controversial.

2.2.3.3 Annular Dilatation:

Recently most of the focus has been directed at investigating how the annulus dilates in the diseased condition. Many believe annular dilation to be the key contributor to TR. Human clinical studies have reported that the tricuspid annulus is significantly larger in patients with TR as compared to normal subjects [38] and found the diameter in fact to be two times the size, measuring 35 mm and 70 mm respectively. Studies may have focused on annular dilatation because it is believed to be a better indicator of TV pathology then TR [9] since patients with no TR initially and a dilated annulus developed TR. This same study also reports that annular dilatation may not always result in TR, and

may be dependent on other factors [9]. It is believed that without dilatation there is a low probability that the valve will leak [9]. It is important to note that it is believed that only the anterior and posterior segments of the annulus can dilate, since on they are the only segments on the free wall [9]. This is best illustrated in figure 2.10.

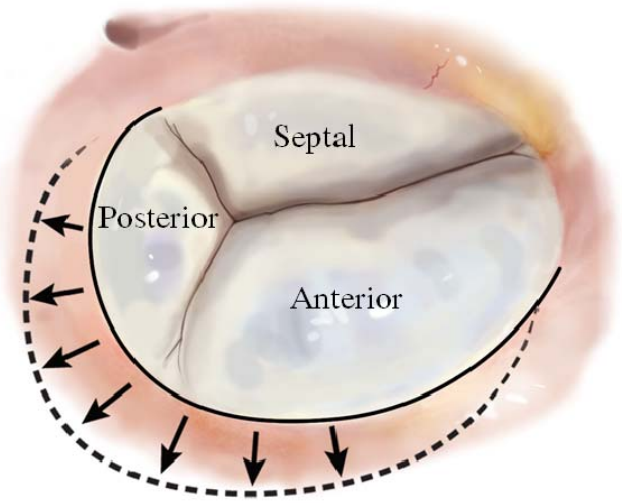

Figure 2.10: This figure demonstrates the free wall dilatation which results in an increase in annulus area along the anterior and posterior regions.

It is important to investigate this further and in more detail as this is essential to understanding the mechanics of TR and how to repair it. Once the annulus becomes dilated it cannot return to original size and may continue to dilate [9].

It is not just the increase in annulus size which is believed to cause TR, but the loss of the dynamic function of the annulus. The loss of systolic annular contraction in TR patients may be an important pathogenesis [38, 51]. In normal patients the annulus decreases in area during systole to further prevent regurgitation, but this change from diastole to systole is lost in patients with TR, and their annulus reflects a size more favorable to diastolic filling. Numerous studies have investigated the loss of dynamic annulus area during the cardiac cycle[38 33].

Although it is know that TR occurs with annular dilatation it is not know at which amount of dilatation TR begins. A clinical study reported by Ubago, reported this size to be between max diameter of rheumatic without TR and minimum with moderate to severe TR. This threshold is reported to be 27 mm/m^2 [17]. It is important to know this threshold as to determine a preferential annulus size for patients, so if a repair is to be performed there is a specific goal. Also it is important to understand why the threshold is what it is. It may be due to the geometry and excess leaflet tissue which can only overlap and coapt up to a certain point, or it may have to do with the change in 3D geometry of the annulus, or most likely a combination of the two.

2.2.3.4 PM Displacement and Leaflet Tethering:

Another effect of right ventricular dilation is papillary muscle displacement which leads to leaflet tethering [20] and possibly leaflet prolapse depending on the type of dilatation. Restoration of the annulus to its original size does not always eliminate TR completely after repair and may allow for TR to return[26, 33], thus reducing the annulus may not be enough to correct TR [26, 55]. Thus additional mechanisms have been investigated, specifically the effects of PM displacement. TV tethering has been shown to be an independent predictor of TR after TV annuloplasty [26, 55] and may indicate PM displacement as another factor in TR. A study by Min et al. repaired TR with the use of an annuloplasty and found preoperative tenting volume to be a predictor of residual TR. Additionally, the reported that will most geometric parameters were decreased with ring implantation leaflet tethering angle increased[56]. This shows that PM displacement may be responsible for TR and if the PM displacement is not corrected tethering will persist even in the presence of annuloplasty repair.

It may be a combination of these factors: annular dilatation and PM displacement in conjunction with nonspecific designed devices which do not adequately correct TR. It is our incomplete understanding of the normal and diseased anatomy of the valvular and subvalvular components of the tricuspid valve which do not allow us to completely repair the valve and remove all current and possibility for recurrent TR.

2.2.4 Treatment and Repair:

Current treatment includes repairs, such as an annuloplasty, which reduces the annulus to its original size, and complete valve replacement. Annular repairs include various rings, as well as a De Vega annuloplasty which uses a suture to cinch the size of the annulus. Annulus cinching has also been conducted by creating a bicuspidization in which the posterior annular section and leaflet are brought together by sutures. These techniques are shown below in figure 2.11.

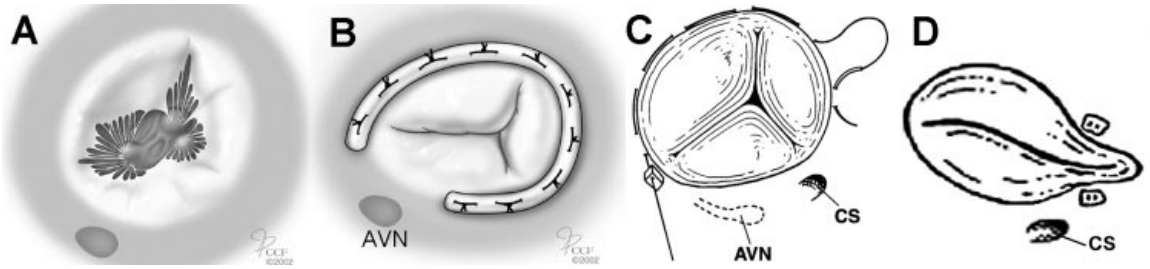

Figure 2.11: The main surgical approaches for correcting functional TR in the presence of a dilated annulus are shown. (A) Dilated tricuspid annulus (B) Rigid or flexible annular bands are used to restore a more normal annular size and shape (ovoid), thereby reducing or eliminating TR. The open ring shown spares the atrioventricular node (AVN), thus reducing the incidence of heart block. (C) DeVega–style suture annuloplasty in which a purse-string suture technique is used to partially plicate the annulus and reduce annular circumference and diameter. (D) Suture bicuspidization is performed by placement of a mattress suture from the anteroposterior to the posteroseptal commissures along the posterior annulus. CS indicates coronary sinus (Rogers and Bolling 2009).

Most current repair procedures focus solely on the annular apparatus, while numerous studies have suggested that repairing the annulus may not be enough [26, 33, 55]. As tethering of the leaflets are becoming a more widely accepted mechanism of TR and are a predictor of residual TR, methods have been developed to address this. Anterior leaflet augmentation, a recent surgical technique to reduce leaflet tethering has been introduced by Dreyfus et al. In addition to the placement of an annuloplasty ring, this technique uses a pericardial patch to extend the surface of the anterior leaflet and provide for addition leaflet for coaptation (Fig. 2.12)[57].

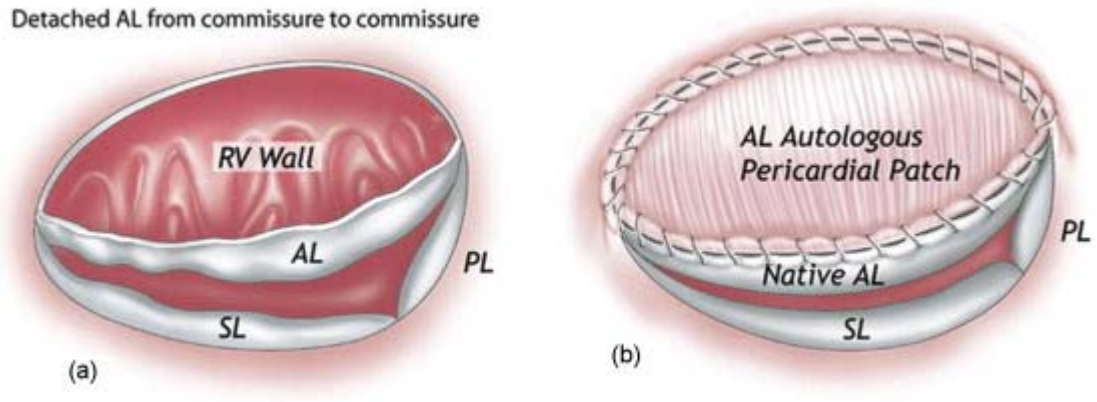

Figure 2.12: Schematic diagrams demonstrating tricuspid leaflet augmentation: (a) anterior leaflet detached from the tricuspid annulus; (b) autologous pericardial patch sewn onto the tricuspid annulus and the detached anterior leaflet. AL, anterior leaflet; PL, posterior leaflet; SL, septal leaflet (Dreyfus et al. 2008).

Although, recent trends are towards repairing the valve there are only a small number of devices and repairs are designed specifically for the TV, and operations to treat returning levels of TR are often required [33]. Until recently repair of TR was conservative as surgeons believed it would be relived with repair of the left side disease[7]. More recent studies have shown excellent results with repair of TR at the time of MV repair [8, 9, 49]. Many questions remain surrounding the repair of the tricuspid valve such as

the optimal timing of replacement, the choice of repair, and the prediction of TR after MV repair [3].

To provide solutions to annular and subvalvular problems associated with TR, we must first understand the mechanisms that lead to TR. If we can determine the independent and combined role of annular and subvalvular alterations, then specific devices and repairs can be developed to restore the valve back to its native geometry. This study will provide some of the missing scientific knowledge into how the tricuspid valve achieves proper coaptation and how it is affected by various diseases which result in dilatation of the right and left ventricle.

CHAPTER 3

HYPOTHESIS AND SPECIFIC AIMS

Tricuspid regurgitation (TR), back flow of blood from the right ventricle to the right atrium, has been reported in approximately 85% of the population, with 16% having clinically severe (mild or severe) TR[48]. Out of this population, 8,000 per year are treated [8, 58], either with complete valve replacement or with repair such as an annuloplasty, which reduces the size of the valve annulus to its physiological size. If left untreated, patients with moderate to severe TR have increased morbidity and mortality[16, 39, 50] and may experience decreased exercise capacity, thus affecting the patients' quality of life. It has also been shown that TR may affect the durability of mitral valve repairs[3, 24]. Though TR was previously thought to be benign, recent studies showing the role of correcting TR with an improved patient outcome have increased interest in TR[1, 2]. Although current practice repairs the valve and corrects the TR, there are a limited number of devices and procedures which are specific to the tricuspid valve (TV), and those that do exist are often adapted from the mitral valve. These current methods of repair offer limited success, with many patients requiring further operations due to reoccurrence of TR [47]. The presence of unsuccessful repairs may be due to incomplete understanding of the functional anatomy and mechanics of the TV and the underlying cause of TR. Although current scientific information is lacking, current studies have begun to provide insight into the cause of TR. While studies have associated TR with annular dilatation, they have found that repairing the annulus alone may not eliminate TR completely, and in many cases TR returns[26, 33]. Additional studies have pointed to annular dilatation combined

with papillary muscle (PM) displacement and have shown that TV tethering, or restriction of leaflet mobility caused by PM displacement, is an independent predictor of TR after tricuspid valve annuloplasty [26, 55]. These studies provide insight into a possible mechanism, but do not completely explain the role of the leaflets, chordae tendineae, and papillary muscles in providing proper coaptation, or how the valve and subvalvular apparatus are altered in disease. The amount of PM displacement in patients with TR has yet to be quantified nor related to the severity of TR. In addition, the independent and combined effects of annular dilatation and PM displacement on the severity of TR have not been investigated. This study seeks to understand how the valvular and subvalvular apparatus work together to provide proper coaptation and how alterations in the normal function of these components lead to regurgitation.

The overall hypothesis of this proposal is **alterations in the geometry of tricuspid valve annular and subvalvular apparatus induced by ventricular dilatation alter the function of the valve and impact the severity of TR**. The objective of this study is to clearly delineate the geometric alterations of the tricuspid valve that cause TR and correlate such alterations with different disease conditions which occur with tricuspid regurgitation. In addition to quantifying the relationship between annulus, papillary muscles, and the ventricles in healthy and diseased humans, the impact of each geometric change on tricuspid valve function will be understood in an in-vitro right heart simulator. The in-vitro methodology allows for precise control over the tricuspid valve geometry and allows for measurement of specific hemodynamic and mechanicistic parameters that could potentially aid in elucidating the underlying causes of TR in different disease etiologies. Insight to the underlying causes of TR will help both

physicians and biomedical engineers to make more educated decisions for repair strategies and device development.

Specific Aim 1: Measure the change of PM position and annular size due to ventricle dilatation *in vivo* and quantify the impact of ventricular size/shape on tricuspid valve function. These aim measures, *in vivo*, the effects of ventricular dilatation on PM position and annular size, and uses 3D echocardiography to quantify PM position inhuman patients. Both RV and LV size will be correlated with the severity of TR and alteration in valve geometry.

Specific Aim 2: Elucidate the effect of isolated annular dilatation and PM displacement on tricuspid valve function and mechanics. The impact of isolated annular dilatation and PM displacement on coaptation geometry and chordal forces of the tricuspid valve within a physiological *in vitro* environment will be investigated using porcine tricuspid valves. This aim should provide an in depth understanding of the independent mechanisms and their effect on TR.

Specific Aim 3: Determine the effect of combined annular dilatation and PM displacement on tricuspid valve function and mechanics. Changes in coaptation geometry and chordal forces of the tricuspid valve with combined annular dilatation and PM displacement within a physiological *in vitro* mechanical environment using porcine valves will be measured**.** By simulating combined annular dilatation and PM displacement we gain an understanding of these effects on the severity of TR. In addition, an understanding of the combined effects in comparison to isolated cases on alterations in valve function and mechanics is necessary.

CHAPTER 4

MATERIALS

4.1 *In Vivo*

3D echocardiography was used to make anatomical cardiac measurements *in vivo.* The following section describes in detail the machine and post processing software used to complete this.

4.1.1 GE Echo Machine

All images were acquired using a GE Vivid 7® (GE Healthcare, Wauwatosa, WI) ultrasound system with a 4V-D probe. Routine transthoracic exams were conducted on patients with the addition of 3D images of the right ventricle (RV). Views which were acquired for measurements included: 3D full volume, 4-chamber (black and white and color Doppler) and inferior vena cava (IVC). 3D full volume echo images were acquired with the probe positioned apically to focus on the RV. A 4-chamber view was used to determine end diastolic area (EDA) for both the RV and left ventricle (LV). The grade of TR was assessed using color Doppler, graded from trace to severe based upon the size of the jet area in relation to the area of the right atrium. Pulmonary arterial (PA) pressure was determined using a standard clinical method, that is using the modified Bernoulli's equation with TR jet velocity and the diameter of the IVC for right atrial pressure estimation.

4.1.2 GE EchoPAC

GE EchoPAC® (GE Healthcare, Wauwatosa, WI) was used to interrogate the 3D RV volume with 2D slices along the apical 4-chamber and parasternal short axis views (Fig. 1) to measure: Annular area, distance from the tricuspid valve annulus plane and each of the three RV PM tips, and the position of the PM tips with respect to the center of the annulus. The slice option in GE EchoPAC was used to manipulate the 2D planes within the 3D image with the caliper tool used to make distance and area measurements.

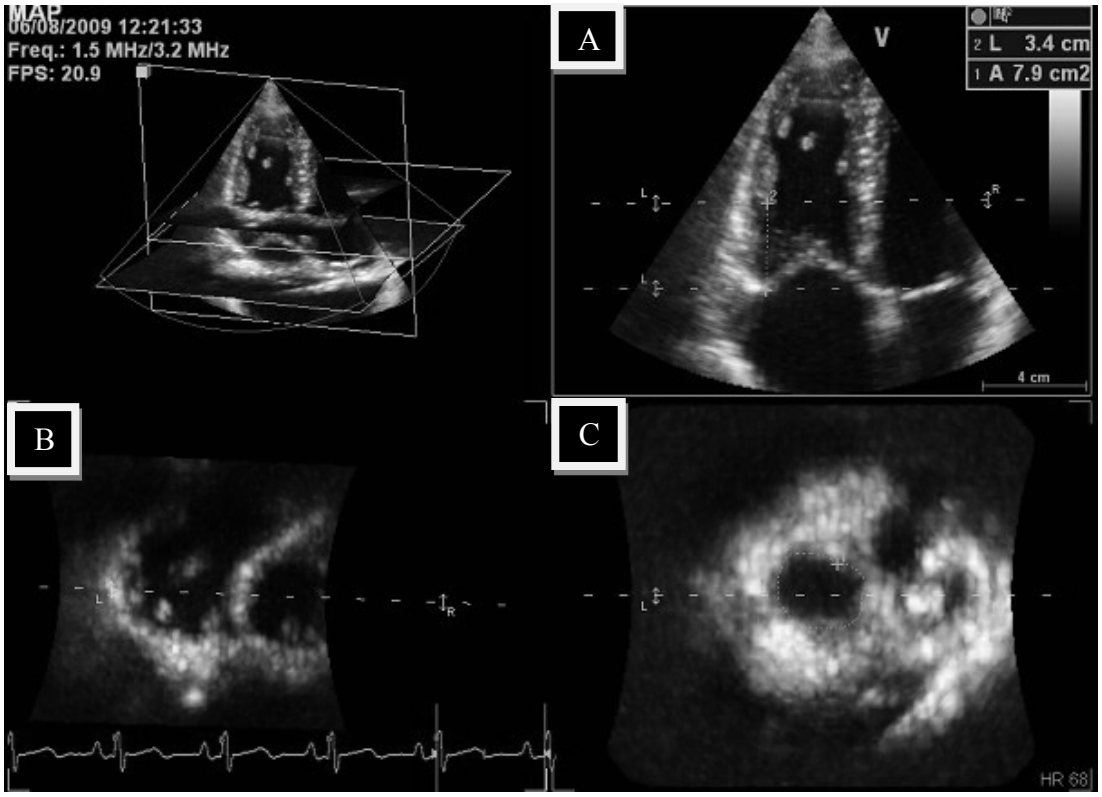

Figure 4.1: Screenshot of GE EchoPac in which three slices of the original 3D echo are shown. A) Four chamber view, B) short axis view and C) annulus plane view.

4.2 *In Vitro*

In this section the various components needed to investigate the effect of annular and subvalvular alteration on TR *in vitro* are presented. Including in this section is the model which was developed and used and measurement techniques.

4.2.1 Tricuspid Valve Selection

Due to the difficulty of obtaining numerous human TVs, porcine valves were used as they have been reported to have similar anatomy to humans[43]. A further detailed geometrical comparison between these two valve types can be found in Appendix A. Porcine hearts were acquired from a local abattoir (Holifield Farms, Covington, GA) and transported to the lab in a cooler. A selection criteria form was completed for each valve. A combination of qualitative and quantitative metrics was used for valve selection. Appropriate PMs and relative size of leaflets was identified using quantitative means. Annulus segments and leaflets lengths were measured and accepted if they fell within a specific range. See appendix B for specific values and selection form. Valves with an annular area of 6 cm^2 were selected by measuring the annulus of the pressurized heart[33, 38]. In addition the annular perimeter and segment length of the septal and combined anterior/posterior section was measured and compared to reported values for humans[33, 38]. The intact leaflet height and width were then measured with the use of a flexible ruler to confirm appropriate size, as previously reported for human valves[22, 32, 40]. The selection criteria for these measurements were determined from the average of the reported values in literature. Further selection criteria was based upon chordal insertions and three distinct PM groups (anterior, posterior and septal), to allow for placement in the simulator. Selected valves were excised with the annulus, leaflets, chords and PMs intact.

4.2.2 *In Vitro* Flow Loop

Experiments were conducted in an *in vitro* right heart simulator. The right heart simulator was designed based upon the Georgia Tech left heart simulator, which has been widely used to conduct studies on native mitral valves[59, 60]. Adjustments were made to accommodate for the lower pressures on the right side of the heart and the difference in valve anatomy: an additional PM holder and a TV specific annulus plate. In order to reduce the resistance to flow, a large compliance for the pulmonary chamber (42 x 28 x 28 cm) and larger diameter pipe and tubing of 3.8 cm were used. This allowed for an appropriate cardiac output with a much lower driving force as compared to the left heart simulator. The main components of the simulator consisted of a clear acrylic ventricle and atrial chamber, an outer pump chamber with a flexible bulb pump connected to solenoid valves and a compressor, a pulmonary reservoir, compliances, an adjustable annulus plate, adjustable PM holding rods, and a rigid pulmonic outflow with a mechanical valve. The atrial reservoir (30 x 28 x 8 cm) was contained within the pulmonary reservoir such as when the pulmonary reservoir filled it poured over the edge into the atrial reservoir. This assisted in maintaining the fluid volume of the system (Fig. 4.2).

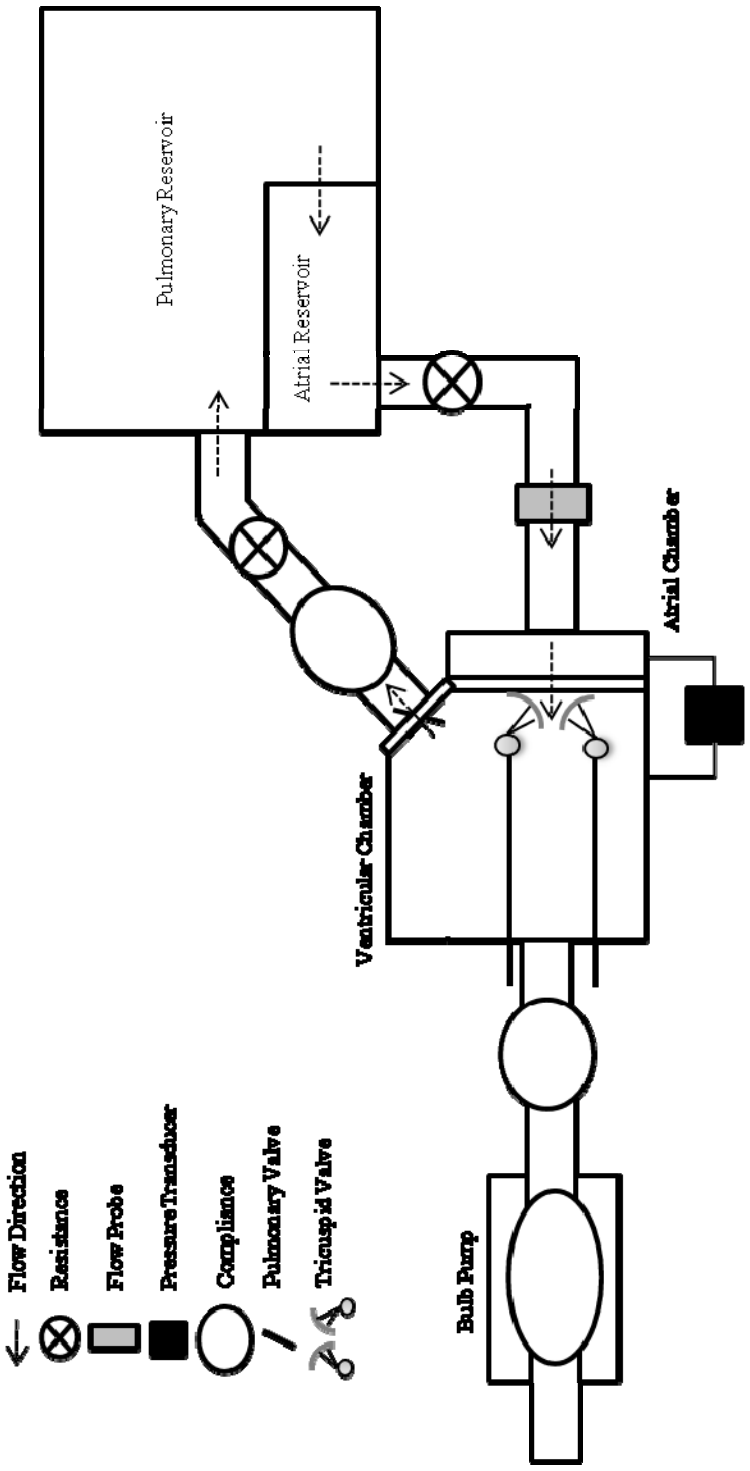

Figure 4.2: Right heart simulator, top view. Ventricular and atrial chamber, atrial and pulmonary reservior and all components including placement of valves are shown.

The triggered solenoid valves (pulse duplicator) controlled inflow of compressed air to expand and deflate the bulb pump, altering ventricle pressure and controlling the pulsatility of the system. Time durations of 220 milliseconds for systole and 640 milliseconds for diastole, a total of 860 milliseconds, was used to simulate a single cardiac cycle. Physiological conditions were maintained throughout experimentation: 5 L/min average cardiac output, 70 beats/min heart rate, and 40 mmHg peak transvalvular pressure as seen in figure 4.3.

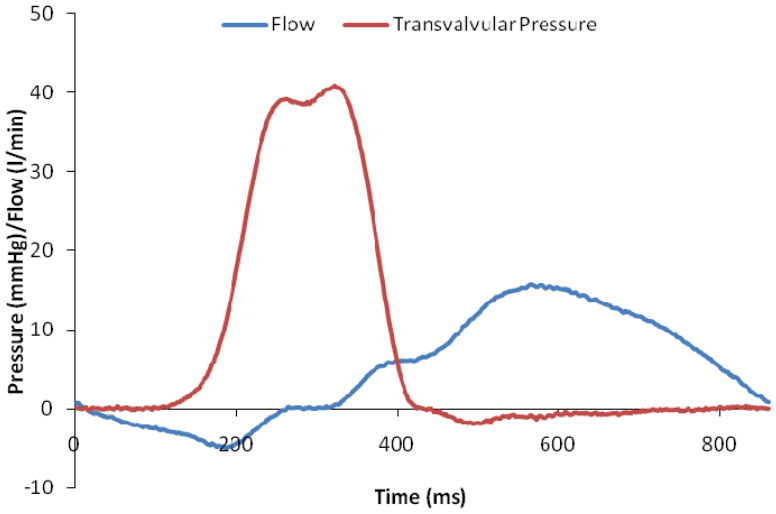

Figure 4.3: Representative transvalvular in vitro pressure and flow curves, averaged over 15 cardiac cycles.

Atrial and pulmonary pressures were maintained through the reservoir height. Cardiac output was controlled through resistances upstream of the TV and downstream of the pulmonary valve (Omniscience, tilting disc mechanical valve). 0.9% saline solution was used as a blood analog in the system. A flow probe (600 Series, Carolina Medical Electronics, North Bend, SC) and pressure transducer (DP9-30, Validyne Engineering Corp., Northridge, CA) allowed for real-time pressure and cardiac output monitoring using an in-house LabVIEW data acquisition program.

4.2.3 Chamber

The atrial and ventricle chambers were constructed of 0.5 inch thick clear acrylic. Engineering drawings for both chambers can be found in appendix C. The annulus plate was pressed between the two chambers and sealed with foam tape. The top plate of the ventricular chamber could be removed when necessary for easy access to the valve and PM rods. The three PM rods, which could be adjusted in all 3 dimensions, were attached to the ventricle chamber. Pressure ports were located on both the atrial and ventricular chambers at the same height. A mechanical pulmonary valve maintained pressure in the ventricular chamber during diastole and provided an outlet for the flow during systole.

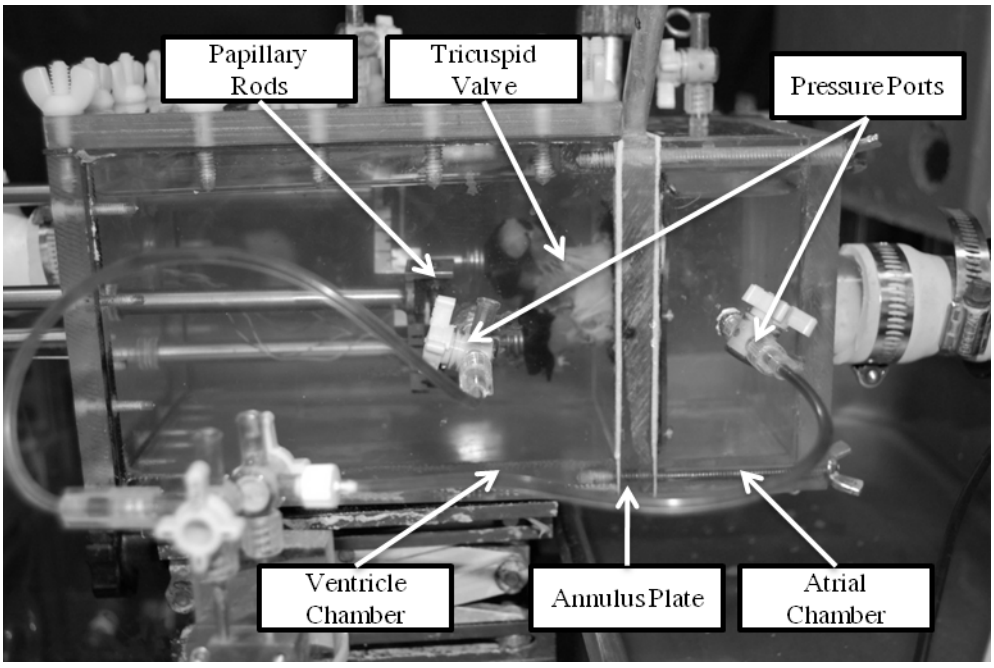

Figure 4.4: Side view of the chamber used to house native tricuspid valve. Annulus plate is mounted between the atrial and ventricular chambers.

4.2.4 Papillary Muscle Rods

Papillary muscle adjustments were achieved with three-dimensional adjustable rods using a system of gears, as used in previous studies[59, 61] (Fig 4.5).

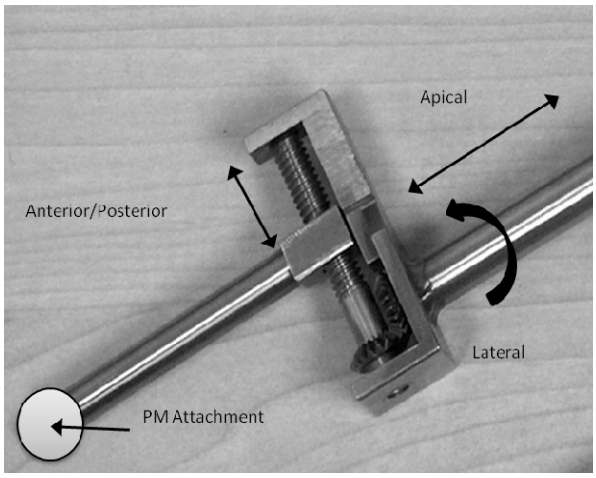

Figure 4.5: 3D adjustable papillary muscle rod, used for apical/basal, anterior/posterior and lateral/septal movement.

To displace the PMs apically, each rod was pulled in the apical direction away from the valve annulus. Anterior/posterior and lateral movement was achieved by rotating the angle of the rod as well as moving the extender rod up and down the threaded rod. Trigonometric ratios were used to calculate the angle and number of turns of the threaded rod as needed to achieve a specific displacement (Fig. 4.6). See appendix D for sheet used in experimentation to calculate adjustments needed to create PM displacements for specific disease conditions. These rods allowed for precise and repeatable positioning of papillary muscles between experiments.

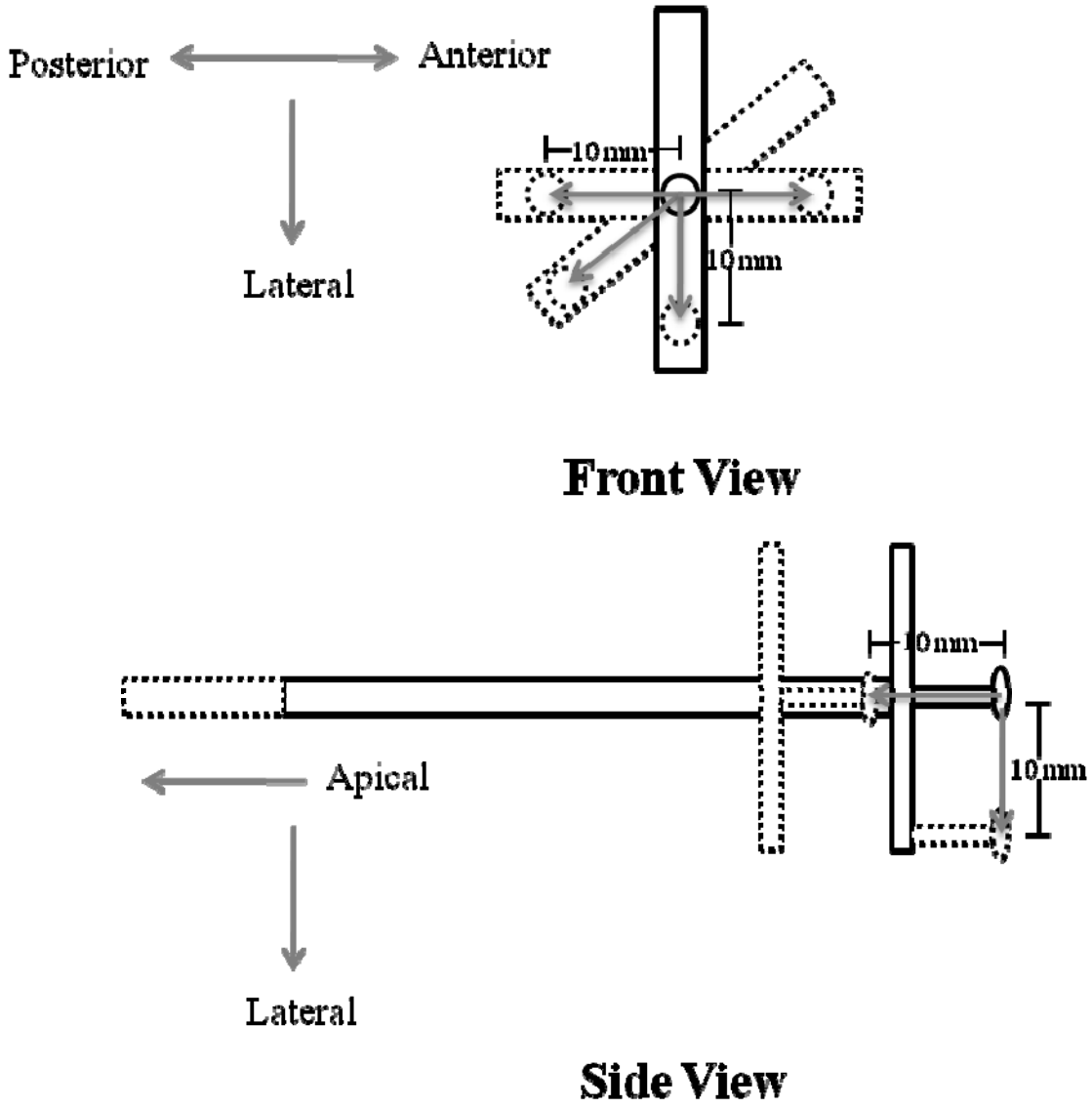

Figure 4.6: Repositioning of PMs as achieved with 3D rods. Front view depicts both isolated posterior/anterior and lateral as well as combined displacement. Side view depicts isolated anterior and apical displacement.

4.2.5 Annulus Plate

The plate consisted of an adjustable annulus that was sutured to a flexible membrane. The membrane was then sandwiched between two acrylic plates in which a section the size of the dilated annulus was removed. The sandwiched membrane and plates were attached to a larger acrylic plate. Image of assembled plate can be seen in

figure 4.7. Valves were sutured to the adjustable annulus plate with attachment points on the three commissures: septal/anterior, anterior/posterior, and posterior/septal. A running mattress suture (3-0, silk) was used attach the valve annulus to the plate.

4.2.5.1 Dilatation

Physiological dilatation was achieved through an adjustable anterior and posterior section, similar to reported physiological dilation that is associated with displacement of the free wall section[12, 13] (Fig. 4.7). The size of the annular area was adjusted from normal (6 cm^2) to 100% dilatation (12 cm^2) with septal/lateral (2.27 ± 0.05 to 3.53 ± 0.04 cm) and anterior/posterior (3.13 ± 0.04 to 4.10 ± 0.07 cm) diameters, replicating previously reported human measurements (area[33, 38], septal/lateral diameter[33, 62], anterior/posterior diameter[12, 33]) at normal and all levels of dilatation. The annulus was constructed out of a flexible spring (anterior/posterior section) which was attached to a hollow acrylic tube (septal section) on both ends and surrounded by silicone-lined Dacron cloth. A wire was inserted into the spring and pulled to adjust the size of the annulus. Physiological shape change from a triangle, in a normal state, to an oval, in a diseased state,[32, 37] was replicated in conjunction with annular dilatation.

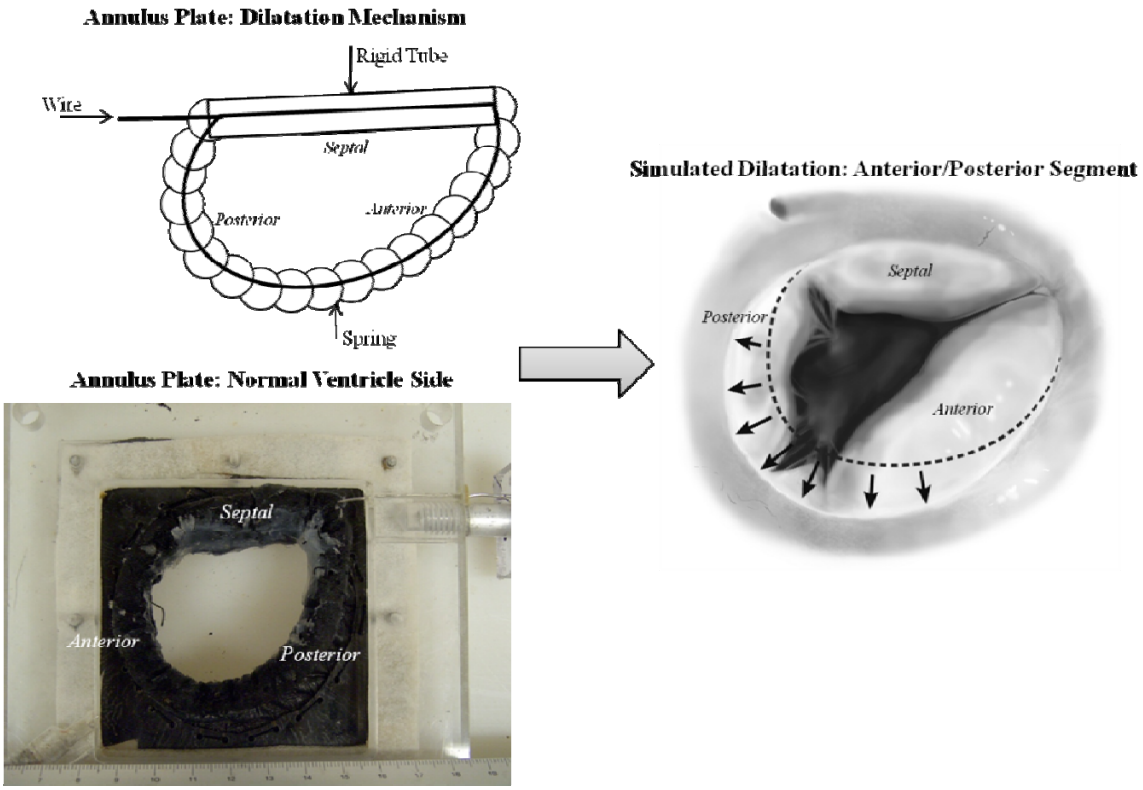

Figure 4.7: Dilating annulus plate used to simulate physiological dilatation. Dilatation was created with the use of a rigid rod for the septal section and a spring for the anterior and posterior sections.

4.2.5.2 Annular Saddle Shape

The saddle-shape was implemented based on the clinical data reported by Fukuda et. al and Ton-Nu et. al, with the posteroseptal and anterolateral segments (highlighted in blue, Fig. 4.8) of the annulus being pulled back into the ventricular chamber 6 mm each, resulting in saddle height of 3mm towards the atrium and 3mm into the ventricle[12, 33]. This resulted in an approximate annulus width to commissural height ration of 10%. Suture (1-0, silk) was attached at low points on the annulus and pulled through the back plate of the ventricular chamber when the creation of a saddle was necessary.

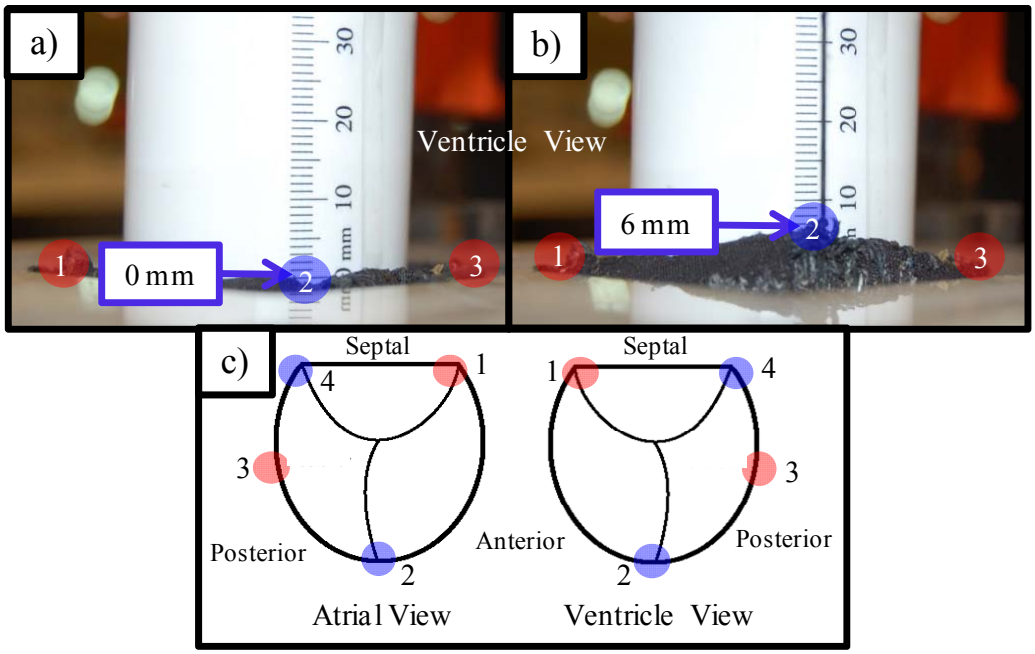

Figure 4.8: Implementation of a saddle shape on the annulus plate A) flat configuration, B) saddle configuration with saddle height of 6mm. C) Schematic of high (red) and low (blue) saddle points, with posteroseptal and anterolateral segments of the annulus low and the anteroseptal and posterolateral segments high.

4.2.6 Chordal Force Transducers

Miniature c-shaped force transducers were used to measure individual chordal force during experimentation. Strain gauges were bonded to the c-ring surface to measure deformation in the c-ring. C-ring transducer production was adapted from the previously published protocol[63].

First, the c-shaped brass frame was degreased, conditioned, neutralized, and coated with three coats of M-bond 43-B adhesive. Each adhesive layer was cured for an hour at 125° C (255° F). A strain gauge was mounted on the inner and outer curved surfaces of the c-ring frame. Resistance of the gauge was checked after each step in the manufacturing process to ensure a resistance of 350 ± 5 Ω. Thin triple conductor wires were then soldered to the strain gauge at terminals on both sides to create a Wheatstone

half bridge connection. The c-ring was then coated with M-bond 43-B adhesive and three Nitrile rubber coatings to create a moisture barrier and mechanical protection. The thin wire was soldered to thick triple conductor wire and then to a connector, which was plugged into the amplifier box. Each c-ring was calibrated after manufacturing and after each experiment. A final c-ring assembly can be seen in figure 4.9.

Figure 4.9: Completed c-ring used to measure chordal forces. Scale shown in cm.

An amplifier box was used to convert the resistance to voltage and adjust the gain for the signal. The amplifier was attached to the DAQ system to allow for force measurements.

4.2.7 Leaflets Markers

Tissue marking dye (Thermo Scientific, Pittsburgh, PA) was used to put markers on the leaflets to allow for measurement of RLL. A 2 mm × 2 mm grid was attached to a rubber sheet and placed behind the leaflet to allow for accurate leaflet marking. Image of marked leaflets can be seen in the methods section (Fig. 5.1).

4.2.8 Imaging

4.2.8.1 Video

Video of the marked leaflets was recorded from the atrial side, perpendicular to the leaflets, throughout the cardiac cycle for all conditions. The camera (Sony, DCR-TRV30, Japan) was mounted on a tripod with video captured for at least three cardiac cycles to ensure all leaflets were visible and in focus.

4.2.8.2 Echocardiography

3D echo images were acquired using a Phillips Intera (Philips iE33 system, Philips Healthcare, Andover, MA), with the probe (X7-1, Pediatric Probe) positioned on the front of the atrial chamber in the central region of the valve, perpendicular to the annulus. Full volume images were acquired for all conditions. Acquisition of echo measurements was triggered with the flow loop trigger system. Phillips QLAB software was used for all echo analysis.

CHAPTER 5

METHODS

5.1 *In Vivo*

As minimal data currently exists as to the location of the PMs in the right ventricle and how they are altered in disease, it was necessary to develop an in vivo study to obtain this information. The methods utilized to measure PM position and identify correlates to the grade of the TR are detailed in the following sections.

5.1.1 Patient Recruitment/Classification

64 subjects were prospectively recruited at Emory University Hospital, Atlanta, Georgia, and underwent a standard transthoracic echo analysis with an additional 3D echocardiographic image focusing on the RV. End-diastolic area (EDA) was measured and reviewed by a physician to classify ventricular geometry: Control (RVEDA $\leq$ 20 cm^2, LVEDA $\leq$ 33 cm^2, n = 21); Isolated RV Dilatation (RVEDA $\geq$ 20 cm^2, LVEDA $\leq$ 33cm^2, n = 17); Isolated LV Dilatation (RVEDA $\leq$ 20cm^2, LVEDA $\geq$ 33cm^2, n = 13); and both RV and LV Dilatation (RVEDA $\geq$ 20 cm^2, LVEDA $\geq$ 33 cm^2, n = 13)[64]. The control group included patients with no known heart disease (n = 12) and healthy volunteers (n = 9). The study was approved by the Emory University Institutional Review Board for human subjects, with all patient identifiers removed and patient privacy protected according to HIPAA regulations (Appendix E). Informed consent was obtained from all patients prior to enrollment in the study (Appendix F). Patients were excluded from the study if they had a congenital heart defect, pacemaker lead or AICD, tricuspid valve (TV) repair or prosthesis, or poor image quality. Exclusion criteria ensured TR was caused by

geometry alone and not influenced by congenital abnormality or presence of a device, as these are known to cause TR.

5.1.2 Image Acquisition and Analysis

EDA for both the RV and LV was determined by analyzing the 4-chamber view using the area tool and tracing the ventricular border in the echo image using EchoPAQ software. TR was assessed with color Doppler and graded from trace to severe, based upon the size of the jet area in relation to the area of the right atrium[65]. PA pressure was calculated from the TR velocity jet and right atrial pressure using standard clinical application of the modified Bernoulli's equation, shown in eq. (1).

$$P_{Pul} = 4V^2 + P_{RA} \qquad (1)$$

where P_{Pul} is pulmonary pressure, V is TR jet velocity and P_{RA} is estimated right atrial pressure. Right atrial pressure was estimated from the diameter of the inferior vena cava (IVC)[66]: 5 mmHg (IVC small and collapsed), 10 mmHg (IVC < 2 cm in size and collapses 50% with inspiration), and 15 mmHg (IVC > 2 cm in size and collapses 50% with inspiration), 20 mmHg (IVC > 2 cm in size and > 50% collapse or non-collapsing).

GE EchoPAC was used to interrogate the 3D image of the RV with 2D slices along the apical 4-chamber and parasternal short axis views. The use of EchoPAC for measurement of the annulus area and PM positions is detailed below. The video of the complete geometry was viewed and stopped at end systole, when the ventricle was fully contracted, and used to make measurements.

5.1.2.1 Annulus Area Measurements

The annulus plane was identified within the 4-chamber image by noting the location of leaflet attachment and increased image intensity. The border was determined

by distinction of low (blood) and high intensity (annulus) signals. The annulus area was measured in the annulus plane using the area tracing tool in GE EchoPAC (Fig. 5.1). This measurement was repeated three times by the same observer and then averaged.

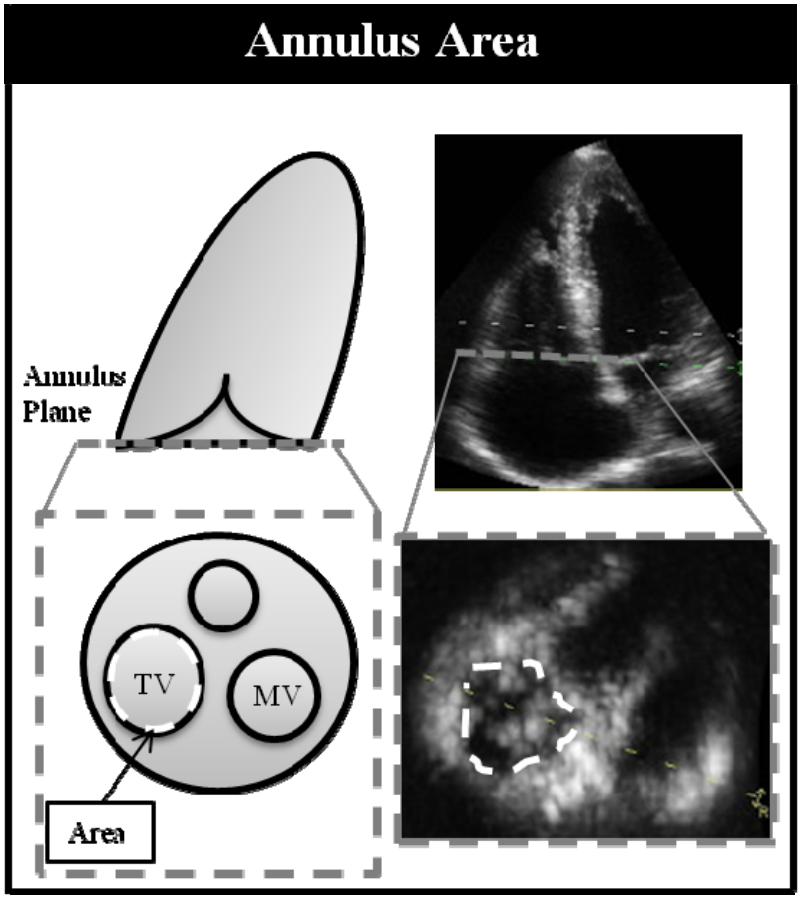

Figure 5.1: 4-chamber view schematic and echo image in which the annulus is identified. Measurement of the annulus area, within the annulus plane, is outlined in white.

5.1.2.2 Papillary Muscle Position Measurements

The apical, septal/lateral and anterior/posterior distances were measured on a single PM and then repeated for the additional two PMs. If three distinct PMs could not be identified, the PMs that were visible were measured and recorded. The slice option within GE EchoPAC provided the user with 3 slices that could be moved in three-

dimensional space. The 3 slices were used to visualize the PM (4-chamber view), identify the reference (short axis view), and intersection of the PM tip (short axis view) for measurement from the reference.

5.1.2.2.1 Distance of PMs from Annulus Plane (Apical)

Once the annulus plane was identified using a short axis slice, the long axis (4-chamber) view was then moved anteriorly and posteriorly throughout the RV until the PM/chordae could be seen. The PM was most easily identified by the location of chordae tendineae insertion, with the video playing throughout the cardiac cycle. The video was then stopped at peak systole and a third plane was moved parallel to the annulus to the PM tip within the 4-chamber view (Fig. 5.2A). The caliper tool was then used to measure the perpendicular distance between these two planes (annulus and PM tip) and recorded as the apical distance for the specific PM (Fig 5.2 A). This was repeated for all 3 PMs.

5.1.2.2.2 Distance of PMs from Center of Annulus (Septal/Lateral, Anterior/Posterior)

The short axis plane at the tip of the PM remained in position, while the annulus viewing plane was rotated to bisect the annulus, parallel to the septum. The distance from the PM tip to the reference was measured in the short axis plane (Fig 5.2 B). This distance was used to determine septal or lateral displacement from control, with positive displacement being towards the septum (septal) and negative being away from the septum (lateral).

The reference plane for calculating the septal/lateral distance was then rotated to bisect both the RV and LV, perpendicular to the septum. If necessary the PM plane was moved to the annulus plane to ensure that the reference plane bisected both the RV and

LV. The perpendicular distance was then measured from the PM tip to the reference plane, in the short axis plane (Fig. 5.2 C). This distance was used to determine anterior or posterior displacement from control, with positive displacement from the center of the RV being anterior and negative being posterior.

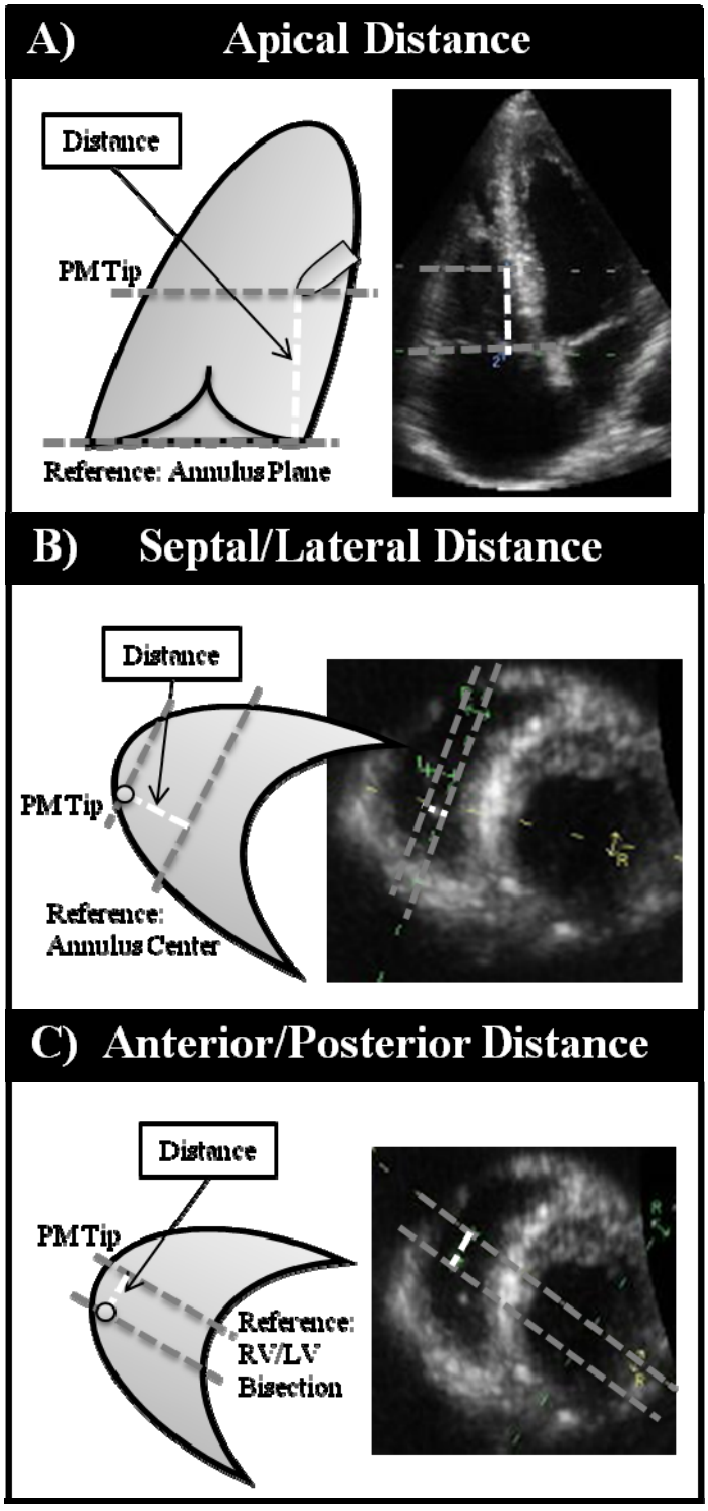

Figure 5.2: Schematic and echo image of distance measured from PM tip to A) annulus, B) annulus center, and C) bisection of the RV/LV. Reference plane and PM tip plane are shown in grey, with the measurement distance shown in white.

5.1.3 Statistical Analysis

All data was assessed for normality with an Anderson Darling and equal variance with a Levene's test prior to running an ANOVA. Statistical differences in annulus area, PM displacement and tethering, as compared to normal subjects, were determined using a One-Way ANOVA, with a Dunnett's post hoc test. If data were not normally distributed a Kruskal-Wallis test was used to test significance in the non normal group as compared to control and the ANOVA re ran with the non normal group removed. Significance was determined at $p \leq 0.05$. Distances were normalized by body surface area (BSA), as this is a standard technique to scale cardiac anatomy and account for variations in patient size. All measurements are expressed as mean ± standard deviation.

Correlates to the grade of TR were determined with a Spearman's test. All variables which were significantly correlated with the grade of TR were initially included in the multivariate regression model. Variables with the highest p value were incrementally removed until only variables with a p value ≤ 0.10 remained.

5.2 *In Vitro*

In vitro studies allow for simulation of specific diseases and investigation of incremental changes, with the measurement of detailed metrics. For this reason the following *in vitro* methods were utilized to determine the effect of alterations in the annular and subvalvular tricuspid valve apparatus on TR and valve mechanics. These include methods used to ensure an accurate disease model and measurement techniques used to quantify alterations.

5.2.1 Valve Instrumentation

Selected valves, as described in detail in the materials section and appendix A, were excised with the annulus, leaflets, chordae and PMs intact. Valves were then sutured to the adjustable annulus plate with a continuous mattress suture and attachment points at the three commissures corresponding to annulus segments. While ensuring no restriction of chordae, the papillary muscles were wrapped with Dacron cloth to prevent tearing the PMs. A button was then attached to the cloth, parallel to the tip on the base of the PM, to allow for attachment of the PMs to the adjustable PM rods in the simulator.

5.2.2 Loop Preparation and Tuning

Once the valves were placed in the simulator, the PMs were placed in a normal position. Normal position was defined with the septal PM (SPM) perpendicularly aligned to the septal and anterior commissure, anterior PM (APM) to the anterior and posterior commissure, and the posterior PM (PPM) to the septal and posterior commissure. The APM was positioned furthest from the annulus plane and the SPM closest, as reported for normal subjects using MRI[25]. This was achieved with three-dimensional adjustable rods using a system of gears, as used in previous studies as described in chapter 4[59, 61]. Finally, the PMs were adjusted apically to ensure the chordae were neither taut nor slack. Slight anterior/posterior and septal/lateral adjustments were made once the simulator was running to account for valve to valve variability and to ensure proper leaflet coaptation. This is the same method used for previous in vitro MV experiments[61, 67, 68]. Once proper coaptation was ensured, the resistance and compliance of the right heart simulator were adjusted for each valve as well as each experimental condition to ensure that pressure and flow were maintained at 5 L/min and 40 mmHg peak systolic transvalvular pressure.

5.2.3 Hemodynamics

Flow and pressure data acquired using the custom Labview program was averaged over 15 cardiac cycles. Tricuspid regurgitation (TR) volume was calculated by subtracting the closing volume, as determined from negative volume in the control condition, and normalized by the stroke volume, as shown in the representative image (Fig. 5.3).

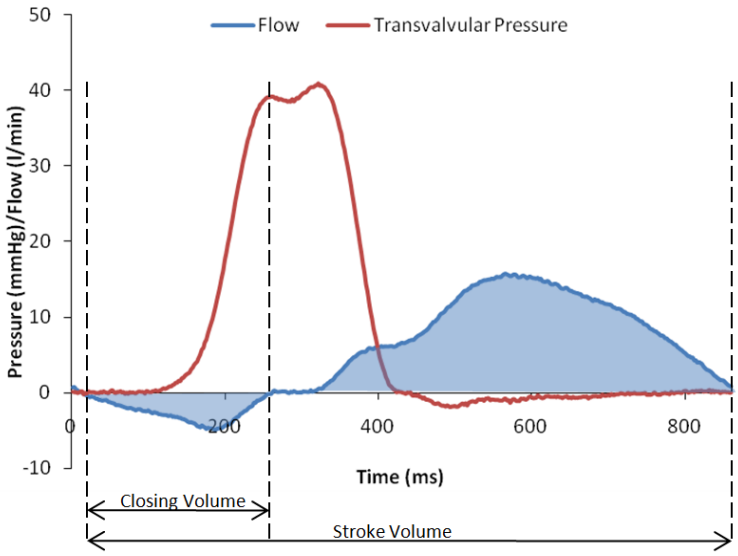

Figure 5.3: Depiction of closing volume and stroke volume as measured from the integration of the average flow curve.

5.2.4 Residual Leaflet Length

5.2.4.1 Preparation

Markers were placed in a 2 mm × 2 mm grid on the entire surface of each leaflet with tissue marking dye (Thermo Scientific, Pittsburgh, PA). The leaflet was first patted dry with a cloth and then attached to a rubber marker grid with pins. The leaflet and rubber surface was again patted dry prior to placing markers. The dull end of a needle

was dipped into marker dye and then dotted on the leaflet surface following the grid which was visible through the transparent leaflets. Both cross and box references were dispersed throughout the marker grid to aid in analysis of peak systolic images (Fig. 5.4). Once the entire leaflet surface was marked it was left to dry and allow the ink to soak into the tissue for approximately 5 minutes. The leaflet surface was then dabbed with a dry cloth to remove any access dye which was not absorbed into the tissue. An image was taken prior to placement in the simulator to serve as a baseline and to determine the original length of the leaflets along lines of interest. This was completed for each leaflet individually.

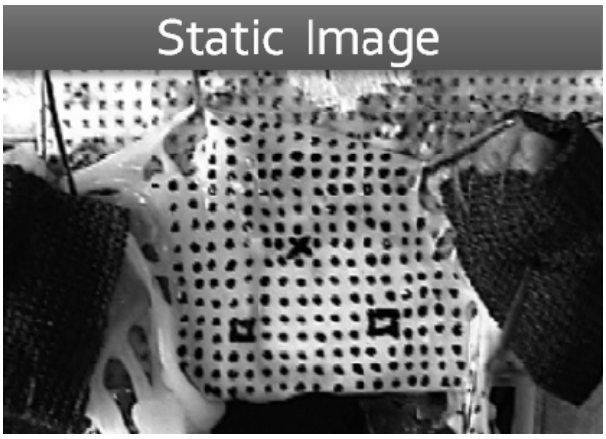

Figure 5.4: Image of leaflet with grid (shown as dot) and reference markers (shown as x and □), which is used as a baseline measurement for RLL.

5.2.4.2 Data Acquisition

Video images (Sony, DCR-TRV30, Japan) of the marked leaflets were recorded from the atrial side, perpendicular to the leaflets, throughout the cardiac cycle for all conditions. Approximately four cardiac cycles were acquired to ensure images were in focus for at least one complete cycle.

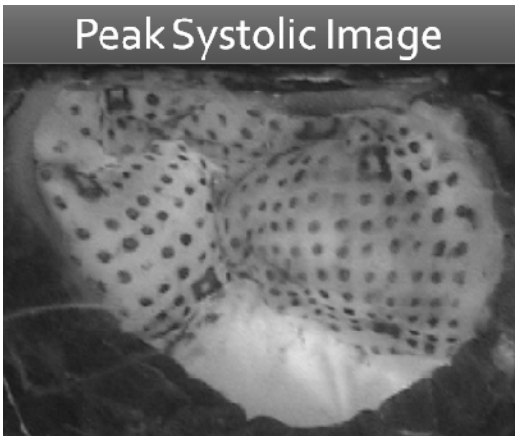

Figure 5.5: Peak systolic image of valve leaflets from the atrial view as visulized with the video camera.

5.2.4.3 Data Analysis

RLL is defined as the amount of leaflet available for coaptation (Fig. 5.6). While coaptation length is typically measured clinically it does not give coaptation information about each individual leaflet. As this thesis aimed to provide a more detailed mechanistic understanding of the valve RLL was measured.

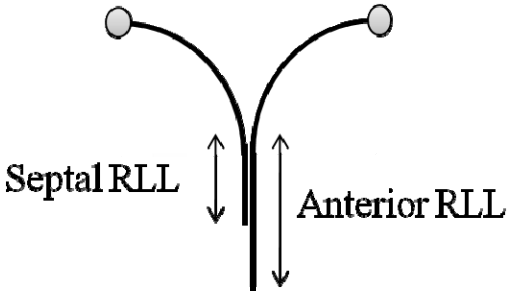

Figure 5.6: Individual residual leaflet length for the septal and anterior leaflets.

There were three major steps in the analysis of the RLL data. Step one was to extract images from the video, step 2 was to convert the leaflet markers to a matrix and step 3 was to measure the RLL.

To analyze the acquired images for RLL, static (reference) images were downloaded from the camera. The peak systolic image was identified from the video file.

Peak systole was determined as the first frame in which the valve was fully closed and did not move in the following frames. While multiple cardiac cycles were taken, the peak systolic image was chosen from the first cycle in which the image was clear enough to identify all dots in a single frame for all leaflets. Each peak systolic image was then saved and labeled accordingly. This step was repeated for all conditions and for all valves.

Following image identification, a matrix of the leaflet markers was constructed using Matlab (7.10.0, MathWorks Inc., Natick MA). The Matlab code which was used to generate the matrix and plots can be found in appendix G. First, the dots in each row as well as the number of rows were manually counted. This was simplified by printing images of both static and peak systolic images. For the static image, all dots were counted. For systolic images, only visible dots were counted. Additional dots were added in some cases where there were dots located in wrinkles or close to the annulus and could not be seen in coaptation. A matrix was created with this information. The row and column in which the references were located was identified within the matrix for all conditions (Fig 5.7), and is displayed as an x in the below image.

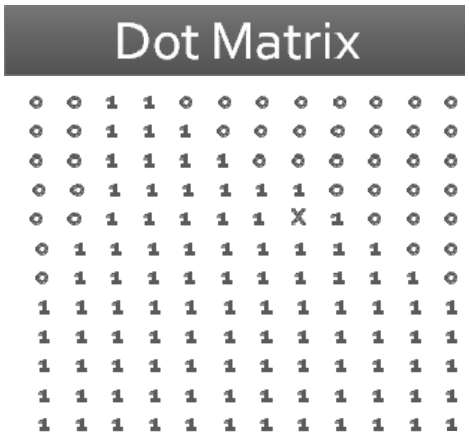

Figure 5.7: Matrix representation of the leaflet markers. Reference denoted as an X, leaflet markers as 1, and spacers (no leaflet) as 0s.

The static image was overlaid on each condition and plotted by aligning the matrices with the reference. An example plot is shown below (Fig. 5.8). This was repeated for each leaflet, experimental condition, and valve.

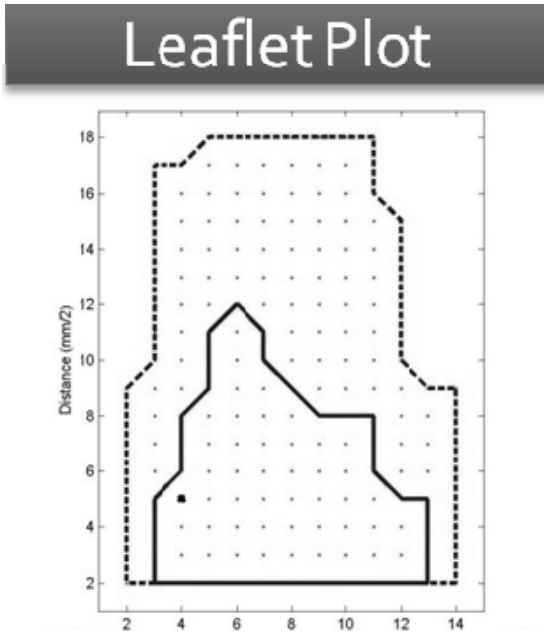

Figure 5.8: Plot generated in Matlab of the reference leaflet (hashed line) overlayed on the area visible at peak systole (solid line). Axes represent the spacing of the markers and are spaced 2mm apart.

To compute RLL, the line of interest was identified as the line of markers that intersected the central point of coaptation, as this is where malcoaptation occurs. The following image shows the line of interest for determining RLL for the posterior leaflet.

Figure 5.9: Markers of interest identified on the posterior leaflet (blue line) with reference (blue dot), anterior leaflet (red line) with reference (red dot), and septal leaflet (green line) with reference (green dot) for the central coaptation region.

Next, locating the line of interest on the leaflet plot was aided by using the reference as a landmark. Once the line of interest and reference were identified on the image the line of interest was identified on the plot of the leaflet. The distance from the reference to the line of interest was identified by counting the number of columns of dots between the two. For example with the posterior leaflet (blue) the line of interest is adjacent to the reference mark. The corresponding adjacent line on the plot is found in the below image (Fig. 5.10) and repeated for the septal and anterior leaflets.

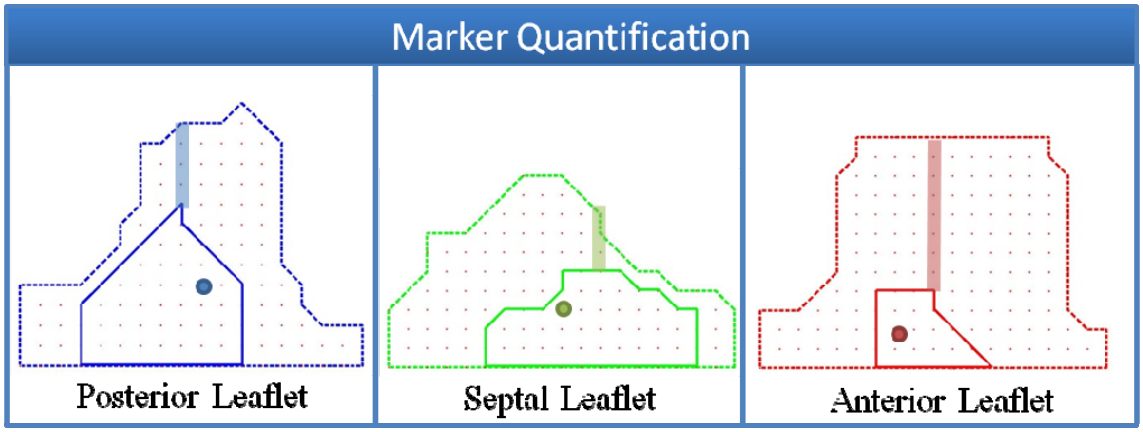

Figure 5.10: RLL visualization (bar) as determined by subtracting static markers from peak systolic markers.

RLL was defined as the number of markers on the line of interest in the static image minus the number of visible markers along the same line in the peak systolic image, times the marker spacing. For Figure 5.10 above, 16 markers were seen on the static image and 7 markers were observed at peak systole for the posterior leaflet. Since the markers are spaced at 0.2 cm, the RLL was calculated as 1.8 cm. RLL were then determined for all leaflets, for all conditions for all valves.

5.2.5 Leaflet Mobility

5.2.5.1 Data Acquisition

3D echo image acquisition was triggered with by the pulse duplicator by attachment of a BNC cable to the ECG leads of the echo machine. Once the signal registered on the machine it was adjusted to ensure there was only one distinct rising edge, as this was when the machine acquired an image. The following machine settings were used: full volume, Xres, high density, Pen, FV Opt (Frame Rate), resulting in a frame rate of 43 Hz. The gain was typically set to 50% but was altered ± 5% as needed

for each individual experiment. This method was used to acquire images for a total of 8 valves.

5.2.5.2 Data Analysis

Acquisition of a 3D data set allowed examination of any 2D slice within the 3D volume using Philips Qlab software (Philips Healthcare, Andover, MA). Thus, leaflet mobility was assessed with 2D slices which were interrogated across all three coaptation lines: anterior/posterior, posterior/septal and septal/anterior (Fig. 5.8a). For slices of interest, tenting height (TH) was measured as the perpendicular distance from the point of coaptation to the annulus plane and tenting area (TA) was measured as the area enclosed by tracing the annulus plane and leaflet surfaces (Fig. 5.11b). Measurements were conducted at peak systole, defined as the first image in which the valve was completely closed. Echocardiographic data was evaluated for 8 valves.

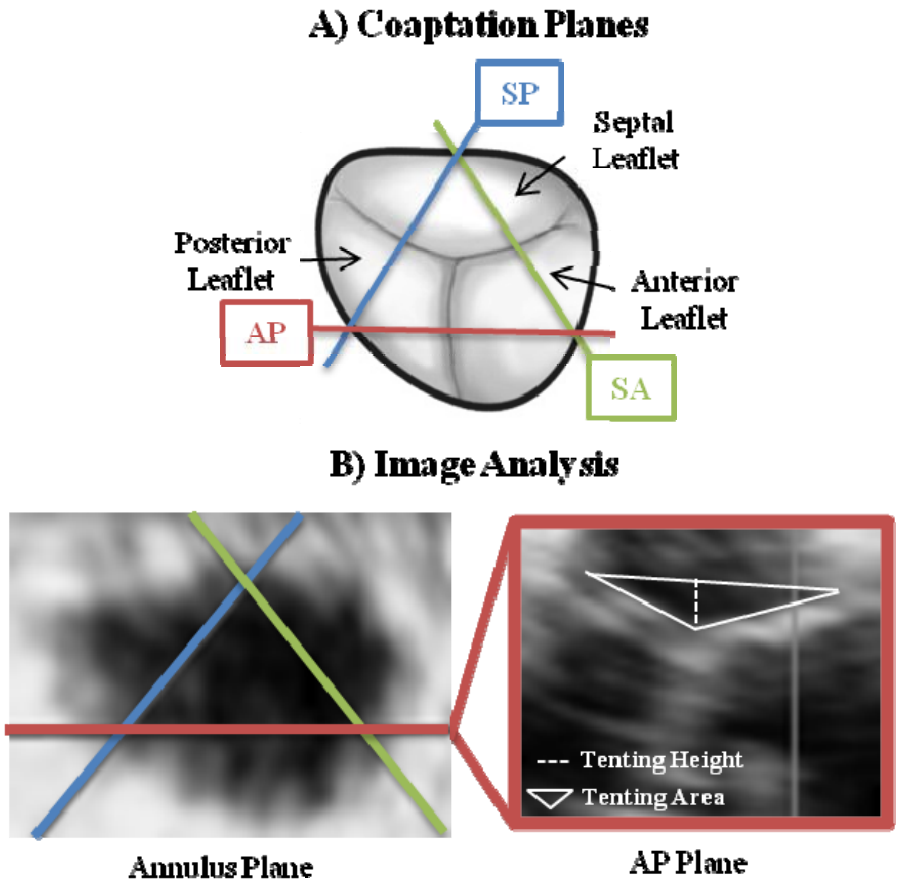

Figure 5.11 A) Imaging plane of the valve as viewed from the atrium. Anterior/posterior (AP, red), septal/anterior (SA, green) and septal/posterior (SP, blue) coaptation line are shown in which the B) tenting height and tenting area were measured in the resulting anterior/posterior plane.

5.2.6 Chordal Forces

5.2.6.1 C-ring Instrumentation

Force transducers were implemented on individual chordae originating from the APM and inserting into both the anterior and posterior leaflets. C-rings were implemented on a single PM to investigate the main chordae: marginal, intermediate and strut chordae as shown in figure 5.12. Only chordae originating from the APM were instrumented with transducers, which allowed for identification of the difference between

the forces on individual types of chords. The APM was selected as it was expected that chords inserting into the APM would be most affected by the conditions simulated. As annular dilatation displaces the anterior and posterior segments of the annulus in which the measured chords insert into would indirectly affect the chords, various displacements of the APM would directly affect the chords. It was not always feasible to instrument a single valve with 6 c-rings to measure each chordae from the APM and hence a total of 14 valves were used to achieve a minimum sample size of 8 for each type of chord.

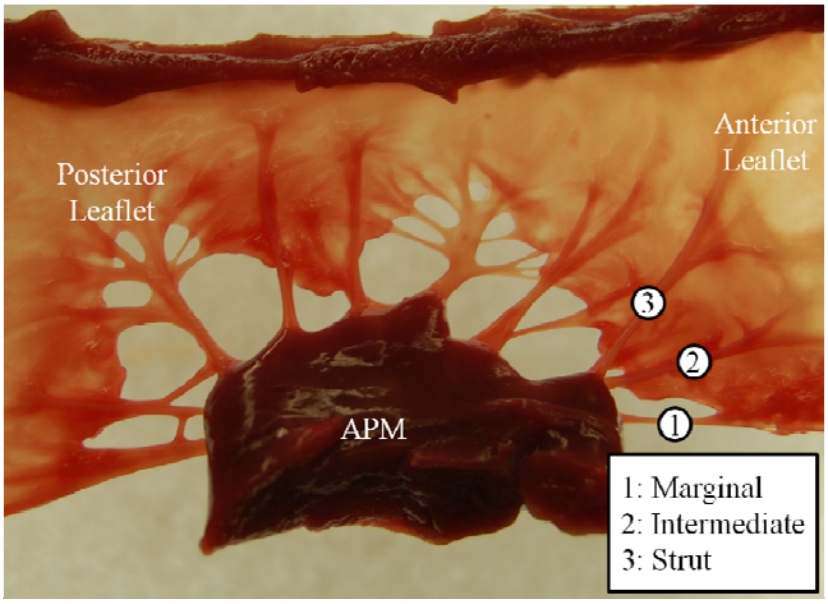

Figure 5.12: Chordae selected for c-ring attachment: 1-marginal, 2-intermediate, 3-strut.

Chordae were selected based upon the following criteria: no branching, adequate length (> 0.5cm), and diameter (< 0.06 cm), which fit within c-ring grooves. Chords were attached using 5-0 silk sutures on either end of the c-ring. The chord was then cut between the two ends of the transducer to allow for force transmission to the gauge. Attachment of c-rings to main chordae can be seen in figure 5.13.

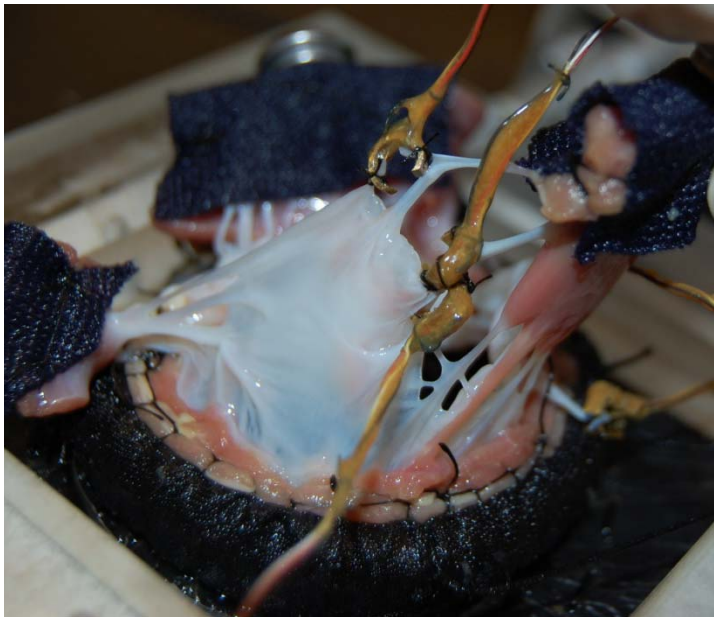

Figure 5.13: Image of attachment of c-ring to chordae. Image shows attachment of c-rings to marginal, intermediate and strut chords from the APM into the anterior leaflet.

5.2.6.2 Data Acquisition

Each c-ring was set to read zero voltage once the valve was in a normal position and prior to initialization of the simulator. The signal from each c-ring was sent to an in-house data acquisition and analysis program based on the LabVIEW platform (LabVIEW 5.1, National Instruments, Austin, TX) and measured throughout the cardiac cycle. Chordal force was acquired using separate valves as those for echo and RLL measurements, as it was not experimentally feasible to run both experiments simultaneously: avoiding interference in echo imaging due to the metallic c-rings and potential fading of leaflet markers.

5.2.6.3 Data Analysis

Differential force, the difference between diastolic and peak systolic force, were measured for each condition (Fig. 5.14). This information aimed at providing an

understanding of the combined geometric and hemodynamic influence on chordal force distribution. Chordal force measurements were ensemble averaged over 15 cardiac cycles.

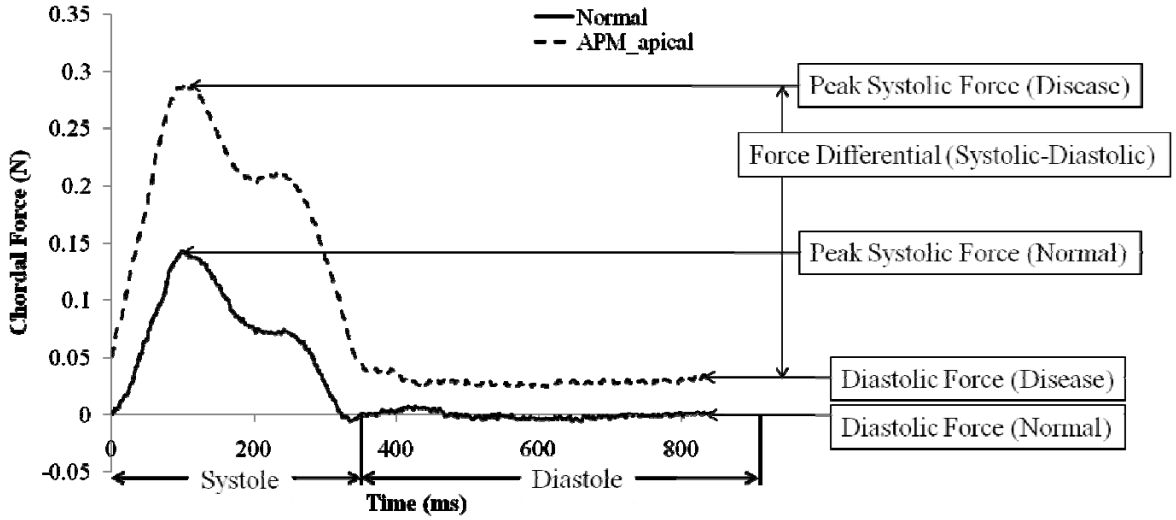

Figure 5.14: Representative chordal force measurement results. Both normal (solid line) and apical displacement of the APM (dashed line) chordal force measurements are shown for the anterior strut chord as an average over 15 cardiac cycles. Determination of the diastolic and differential forces are shown.

5.2.7 Experimental Conditions

Valve dynamics were quantified with isolated annular dilatation starting at a normal annular size (6 cm^2) and dilated to 100% by increments of 20%. Isolated displacement of the PMs was achieved by repositioning the PMs on the septal wall simultaneously (PPM/SPM), which simulated left ventricle (LV) dilatation[69]. The sole displacement of the APM simulated right ventricle (RV) dilatation[23, 24]. Combined RV and LV dilatation was investigated for normal, 40% and 100% dilated annulus sizes with all PM displacements. The APM was displaced both laterally and apically, individually and combined. Anterior/posterior displacement was disregarded early on in experimentation as it showed no difference and was not physiological, as confirmed by in

vivo echo images. The SPM and PPM were displaced anteriorly/posteriorly, (SPM/PPM), laterally and apically, as isolated and combined conditions. For combined RV/LV dilatation all PMs were displaced in all directions. All PMs were displaced by 10 mm for each displacement condition. All experimental conditions both isolated and combined are schematically summarized in Table 5.1.

Table 5.1: Conditions simulated during experimentation. Dashed lines indicates alteration from control. Apical displacment is shown as a smaller circle.

Condition	Dilatation	PM Displacement		Schematic	3D PM Position
Control	None	None			
Isolated Annular Dilatation	20, 40, 60, 80, 100	None		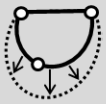	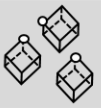
Isolated PM Displacement	None	APM	Lateral		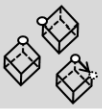
			Apical		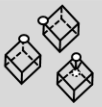
			Lateral+Apical		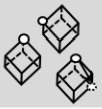
		SPM PPM	Anterior Posterior		
			Lateral		
			Apical		
			Anterior+Lateral+Apical Posterior+Lateral+Apical		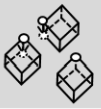
		APM SPM PPM	Lateral+Apical Anterior+Lateral+Apical Posterior+Lateral+Apical	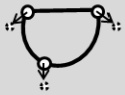	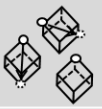
Combined Annular Dilatation and PM Displacement	40, 100	APM SPM PPM	Lateral+Apical Anterior+Lateral+Apical Posterior+Lateral+Apical	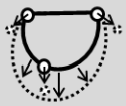	

Hemodynamics, leaflet coaptation, leaflet mobility and chordae forces were investigated for the previously mentioned conditions. While all conditions were simulated, not all measurement techniques were used for each condition. Hemodynamics

and RLL was quantified for every condition, including isolated and combined disease conditions. Echocardiographic images were acquired for all PM displacements, but only for dilatations of 40% and 100% for both isolated and combined conditions. Since significant TR was first seen at 40%, this amount of dilatation and an extreme case of 100% were investigated to see if alterations occurred in leaflet mobility which could give more information as to why TR occurred. Force measurements were only acquired for extreme dilatation of 100%, and displacement of the anterior PM both in the isolated and combined cases. Measurement techniques which were used for specific disease conditions can be seen in the table 5.2.

Table 5.2: Measurement techniques used for specific disease conditions. X identifies conditions which were measured with specific technique, with – denoting technique which were not utilized for the specific condition. Note (*): Force was only investigated for 100% dilatation and combined PM displacement.

Disease			Measurement			
	Dilatation	PM Displacement	TR	RLL	Echo	Force
Control	None	None	X	X	X	X
Isolated Annular Dilatation	20	None	X	X	-	-
	40	None	X	X	X	-
	60	None	X	X	-	-
	80	None	X	X	-	-
	100	None	X	X	X	X
Isolated PM Displacement	None	APM (Lateral)	X	X	X	X
	None	APM (Apical)	X	X	X	X
	None	APM (Lateral+Apical)	X	X	X	X
	None	SPM/PPM (Anterior/Posterior)	X	X	X	-
	None	SPM/PPM (Lateral)	X	X	X	-
	None	SPM/PPM (Apical)	X	X	X	-
	None	SPM/PPM (Anterior/Posterior+Lateral+Apical)	X	X	X	-
	None	APM (Lateral+Apical) + SPM/PPM (Anterior/Posterior+Lateral+Apical)	X	X	X	X
Combined Annular Dilatation and PM Displacement	40, 100	APM (Lateral)	X	X	X	-
		APM (Apical)	X	X	X	-
		APM (Lateral+Apical)	X	X	X	-
		SPM/PPM (Anterior/Posterior)	X	X	X	-
		SPM/PPM (Lateral)	X	X	X	-
		SPM/PPM (Apical)	X	X	X	-
		SPM/PPM (Anterior/Posterior+Lateral+Apical)	X	X	X	-
		APM (Lateral+Apical) + SPM/PPM (Anterior/Posterior+Lateral+Apical)	X	X	X	X*

5.2.8 Statistical Analysis

All statistical analysis was completed using Minitab 15 (Minitab Inc, State College, PA) and expressed as mean ± standard deviation. An Anderson Darling test was first performed to assess data normality. Each valve served as its own control, such that measurements of disease conditions were compared to those made on the same valve for

the normal position. A General Linear Model (GLM) was used for the analysis of all in vitro data as the samples were not independent, and involved repeated measures. For this reason a standard One Way ANOVA or student's t-test could not be used. While these two tests are a form of GLM, the use of the standard GLM allows for pairing of samples on multiple measurements[70].

A GLM was used to investigate the effect of individual and combined annular dilatation and PM displacement on TR, RLL, leaflet mobility and chordal force. Pairing of repeated measurements on the same valve was implemented in the model by including the valve as a random factor. Significance was determined at $p \leq 0.05$. If a significant difference was present; a Dunnett's post hoc was used to asses which groups varied from control.

A GLM was also used to assess the difference in RLL across leaflets with various disease conditions, with significance at $p \leq 0.05$. A Dunnett's post hoc was used to assess which groups were significantly different from control RLL for each leaflet. Additionally, a Tukey's post hoc was used to assess differences within PM displacements which resulted in significant TR across leaflets. A Spearman's test was used to determine correlation between RLL of an individual leaflet and TR.

5.2.9 Calibration

Calibrations were conducted for the flow probe, pressure transducer, and c-rings. Flow probe and pressure transducer calibrations were conducted approximately every 3 months, with the c-rings being calibrated before and after every experiment.

A flow probe (600 Series, Carolina Medical Electronics, North Bend, SC) was connected to a flow meter and calibrated with the use of a variable voltage transformer,

steady centrifugal pump, a graduated cylinder and a stopwatch using saline solution. The ground was placed at the inlet flow of the flow probe. A range of flow rates was created by changing the pump voltage via the transformer. Flow was calculated as the total volume emptied into a graduated cylinder for a given time period and calculated in both directions. This was repeated three times and averaged, with a linear regression fit providing the calibration factor. A sample data set is plotted below.

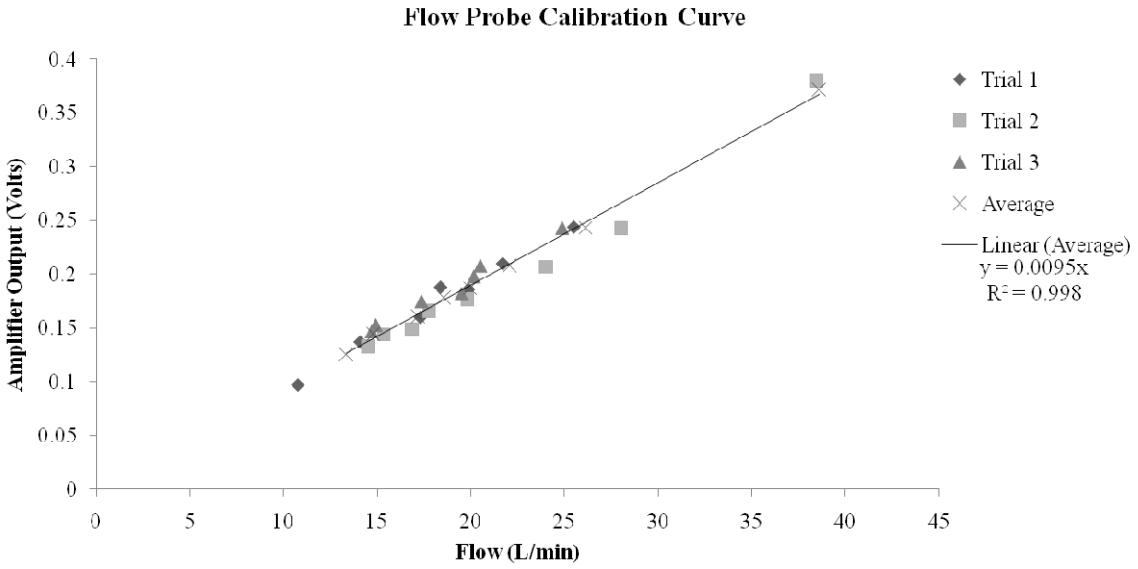

Figure 5.16: Representative calibration curve for the flow probe.

The pressure transducer (DP9-30, Validyne Engineering Corp., Northridge, CA), a dual chamber transducer with an interchangeable diaphragm, was connected to an amplifier box, and was calibrated from 0 to 70 mmHg for each chamber with the use of a differential water column. A voltmeter was attached to the pressure transducer amplifier box to measure voltage for each pressure. Each chamber was exposed to a range of water column pressures individually and this was repeated three times and averaged. Pressure was converted from cmH_2O to mmHg and plotted against the voltage measured, with a linear regression fit providing the calibration factor. A sample plot is shown below.

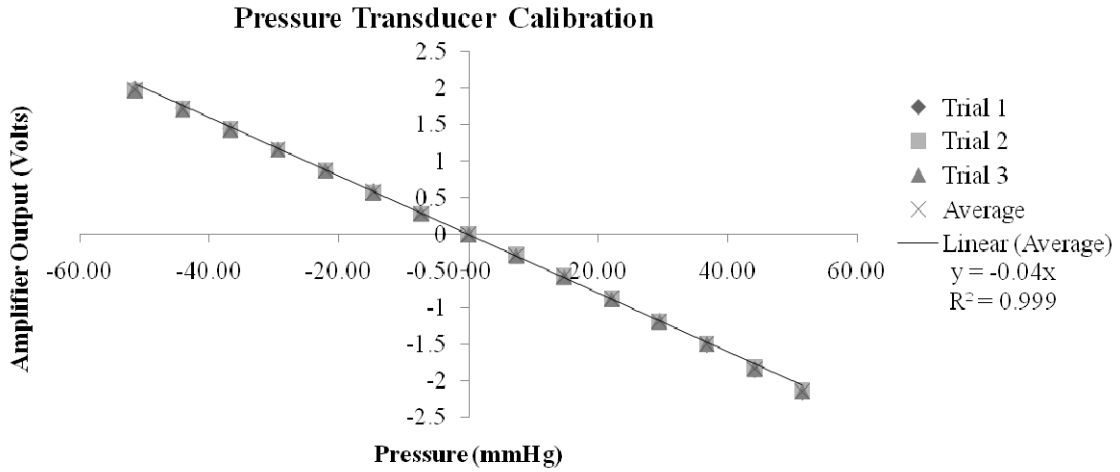

Figure 5.17: Typical calibration curve for the pressure transducer.

C-rings were calibrated in room temperature saline solution and were zeroed prior to calibration. Force transducers were connected to a Wheatstone bridge amplifier to complete the circuit. Known weights, ranging from 10g to 1000g were hung from one end of the gauge while the other end was anchored. Weights were used to induce deformation causing a variation in voltage. Force was plotted against voltage to determine the sensitivity of each c-ring. Calibration was conducted after manufacturing and before and after each experiment to assess functionality. A sample plot is shown below.

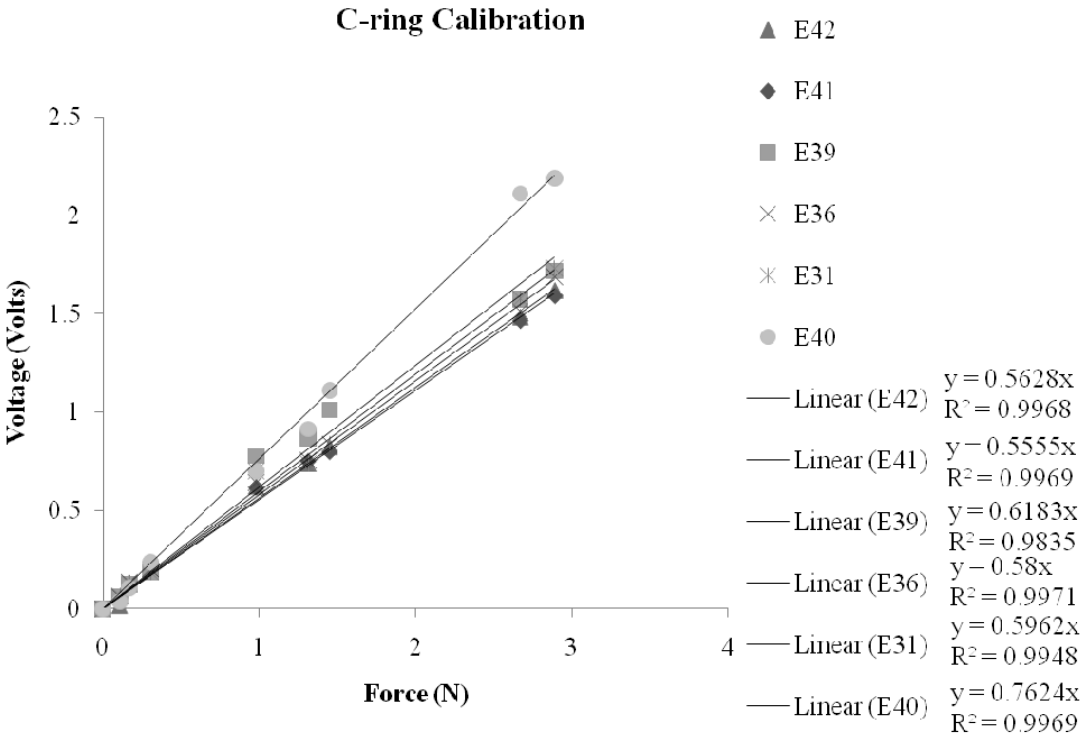

Figure 5.18: Typical calibration curve for 6 individual c-ring transducers.

CHAPTER 6

RESULTS

This chapter is divided into *in vivo* and *in vitro* results. For the *in vivo* results, the characteristics of enrolled patients are presented followed by the comparison of PM positions of dilated ventricular patients and control subjects. Measured parameters were then assessed for their correlation to TR. For the *in vitro* section, results have been divided into sections based upon disease conditions simulated: a) isolated annular dilatation b) isolated PM displacement and c) combined annular dilatation and PM displacement. Hemodynamics, residual leaflet length (RLL), chordal forces and leaflet mobility data are presented for all conditions. Absolute RLL measurements were investigated for isolated annular dilatation demonstrating incremental changes with dilatation. For both isolated and combined, percent change in RLL was determined to demonstrate relative changes from control. Chordal force data were quantified for both diastole and the differential of force between peak systole to diastole for all disease conditions simulated.

6.1 *In Vivo*

6.1.1 Patient Characteristics

A total of 64 subjects were enrolled and included both volunteers and Emory University Hospital patients. All patient data can be found in the raw data section A. The demographics of the subject group consisted of a mean age of 51 ± 18 years with 58% male and 42% females (Table 6.1).

TABLE 6.1: Patient Characteristics

	Study Patients (n = 64)
Age	51 ± 18 years
Male	37 (58%)
Female	27 (42%)
Primary Etiology	
Pulmonary Arterial Hypertension	19 (30%)
Congestive Heart Failure	8 (13%)
Atrial Fibrillation	6 (9%)
Cardiomyopathy	7 (11%)
Coronary Artery Disease	5 (8%)
Aortic Stenosis	3 (5%)
Endocarditis	2 (3%)
Other (Non-Cardiac Related)	5 (8%)
Normal Volunteer	9 (14%)
Tricuspid Regurgitation	
Trace	20 (31%)
Mild	13 (20%)
Moderate	17 (27%)
Severe	14 (22%)

The right ventricular end diastolic area (RVEDA) of patients was plotted against left ventricular end diastolic area (LVEDA) to assess appropriate classification of patients. These values were used to classify patients based upon normal clinical 4 chamber echo measurements, RVEDA of 20.1 ± 4.0 cm^2 and LVEDA of 32.2 ± 7.7 cm^2 [71], with values greater than one standard deviation considered dilated (Fig. 6.1). With blinded clinical assessment used to verify classification from measurements, three patients were reclassified from their original size classification. Thus while most patients fell within one deviation of the size classification, the three reclassified patients were placed into the normal, dilated RV and dilated RV/LV groups. As the control group was defined by normal ventricular geometry, the group consisted of both healthy volunteers (n = 9) and patients (n = 12).

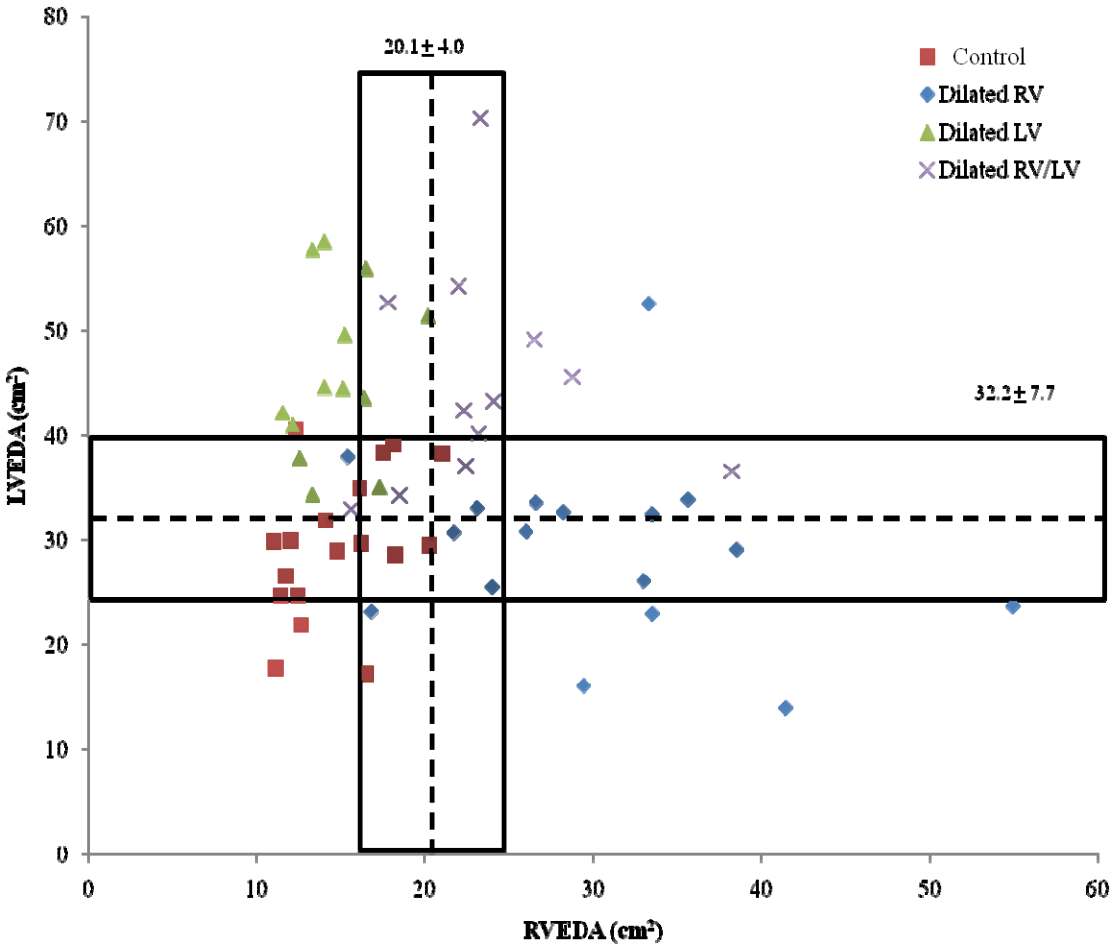

Figure 6.1: Assessment of patient classification. RVEDA is plotted against LVEDA for each patient, with their classification designated by color and shape of marker. Clinically accepted normal values are designated by the dashed line with one standard deviation, as shown with a gray bar.

Assessment of patient group characteristics, as compared to control (ie. subjects with a normal sized RV and LV), found the highest levels of clinically significant TR (moderate to severe) in patients with RV dilatation, either in isolation (81%) or combined with LV dilatation (79%). Only 31% of patients with isolated LV dilatation had clinically significant TR (Fig. 6.2). It is interesting to note that 14% (3 patients) of the control group presented with clinically significant TR. While these patients did have normal sized RV and LVs, one had aortic stenosis, a second had atrial fibrillation, and a third had

pulmonary hypertension. The explanation for the presence of severe and moderate TR in the control group, can be explained by the aforementioned etiologies as they are know correlates of TR, irrespective of ventricle size.

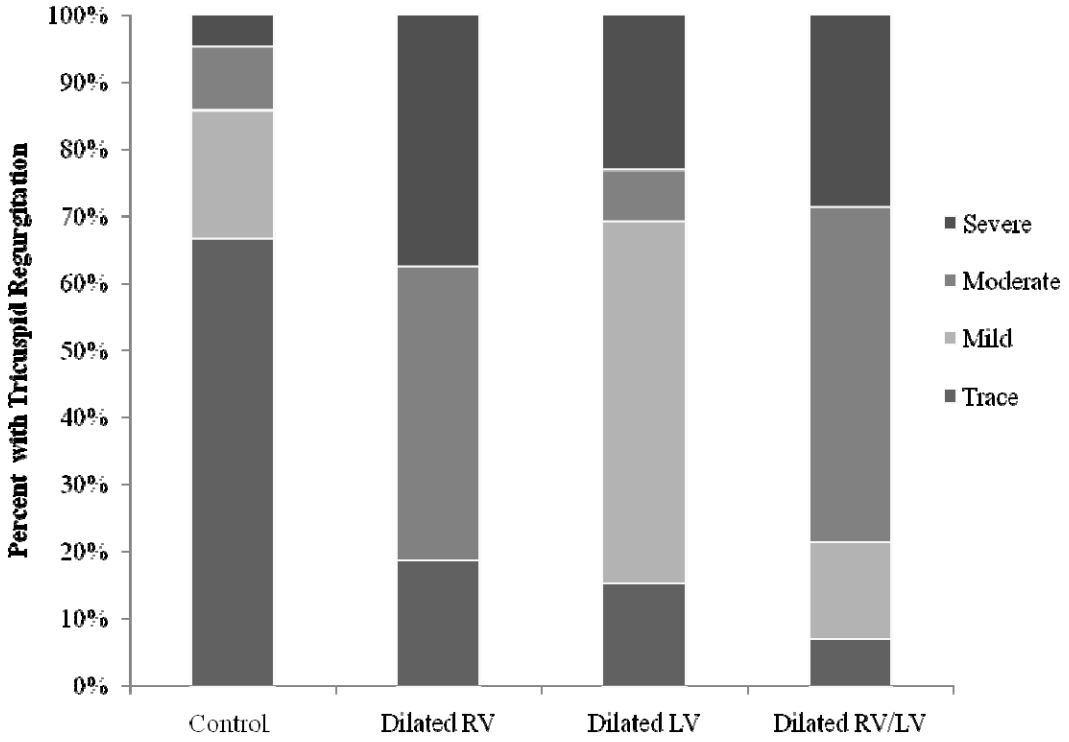

Figure 6.2: Prevalence of the percentage of patients with TR within the classifications: control, dilated RV, dilated LV, dilated RV/LV. The largest percentage of clinically significant TR was present patients with isolated RV or both RV/LV dilatation. Note that no patients with a dilated RV presented with mild TR.

A significantly higher ($p \leq 0.05$) pulmonary arterial (PA) pressure compared to normal was observed in patients with a dilated RV and both RV and LV dilation (Fig. 6.3). These were the same groups which were observed to have the highest levels of clinically significant TR.

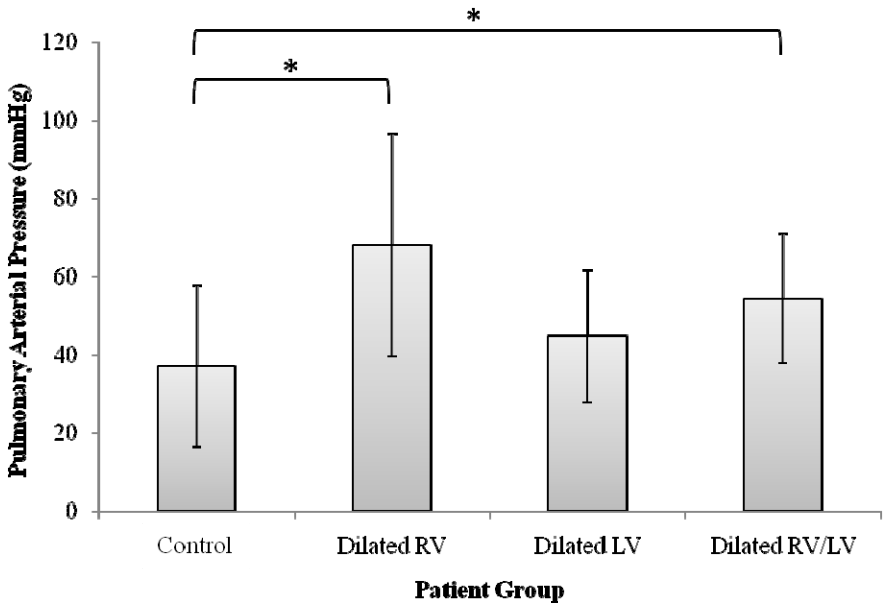

Figure 6.3: Peak systolic pulmonary arterial pressure for all patient groups. Significance (*) defined at $p \leq 0.05$ using a One Way ANOVA with Dunnett's post hoc.

Patients with a dilated RV and those with both ventricles dilated had a significantly larger ($p \leq 0.05$) normalized annulus area as compared to control when normalized by BSA (Fig 6.4).

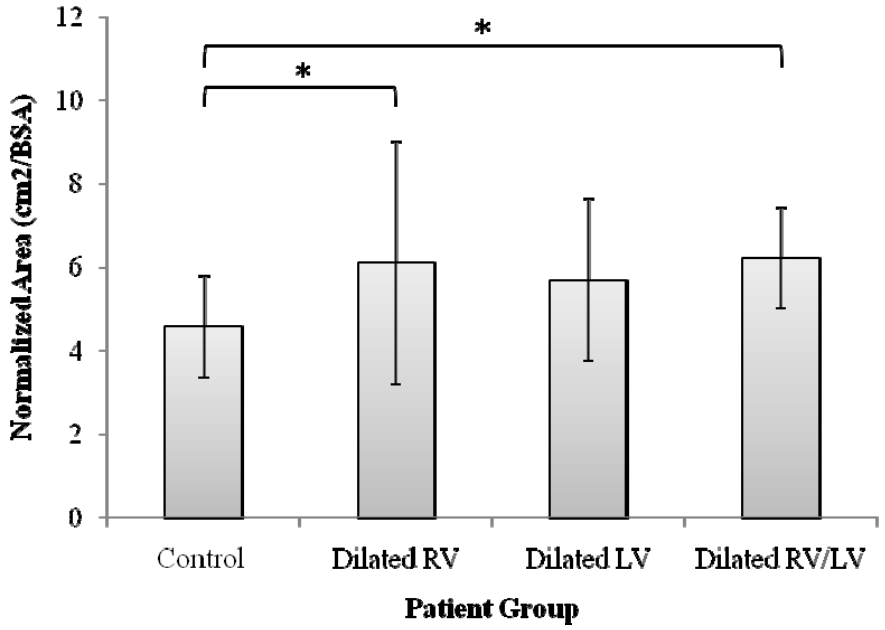

Figure 6.4: Annulus area normalized by body surface area, as measured from peak systole, for all patient groups. Significance (*) defined at $p \leq 0.05$ using a One Way ANOVA with Dunnett's post hoc.

Additional analysis was conducted to better understand the variation in annulus area within both patients groups (Fig. 6.5) and the severity of TR (Fig. 6.6). Similar annulus area was seen with both trace and mild TR with 8.7 cm^2 and 8.9 cm^2. Patients with moderate TR had an average annulus size of 11.4 cm^2, with patients with severe TR having the largest annulus area of 13.2 cm^2.

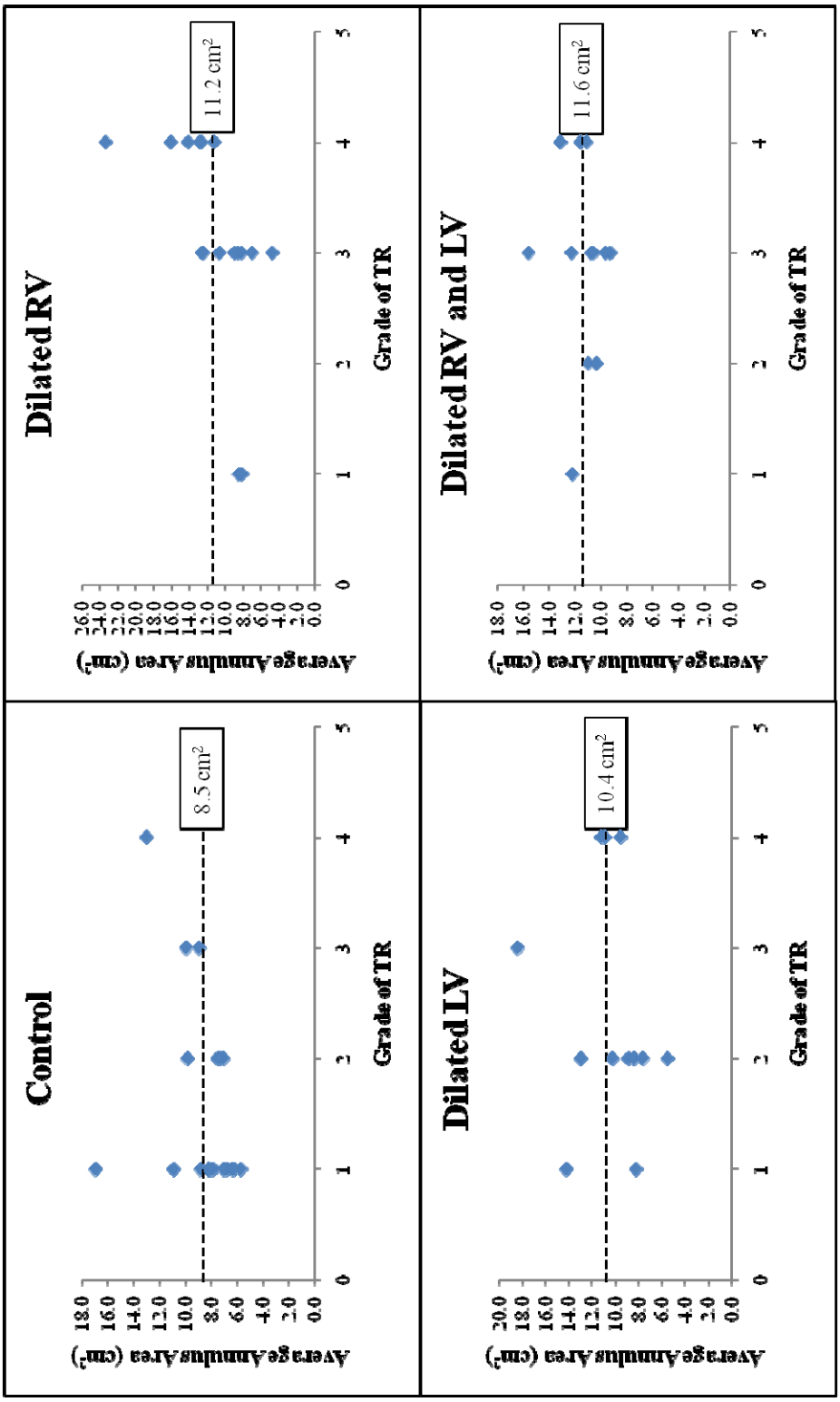

Figure 6.5: Annulus area of patient groups, within the severity of TR. Average TR shown for patient group with dotted line.

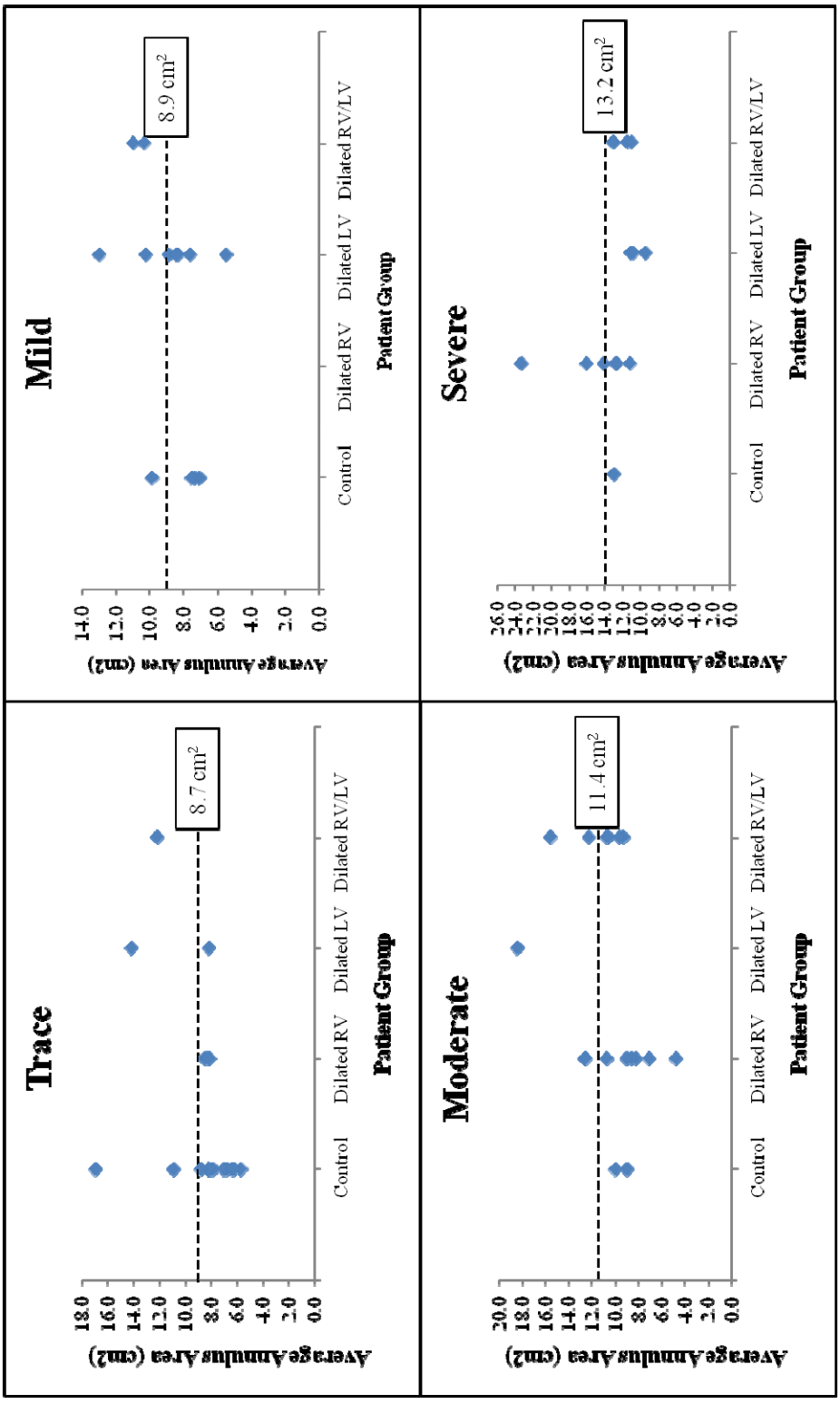

Figure 6.6: Annulus area per severity of TR, within each patient group. Average TR shown for severity of TR with dotted line.

6.1.2 Papillary Muscle Position and Leaflet Tethering

PA pressure, annulus area, PM positions and leaflet tethering data according to patient ventricular dilatation grouping are shown in Table 6.1. Schematics depicting significant PM displacement from control are shown in each classification section (6.1.2.1-6.1.2.4). Raw data measurements for all patients are located in the raw data section B. All patients with single or biventricular dilatation had significant ($p \leq 0.05$) PM displacement, when normalized by BSA and compared to PM position in control subjects.

TABLE 6.1: Patient Measurements: Pulmonary Artery Pressure, Annulus Area, Papillary Muscle Positions. Annulus area and papillary muscle position normalized by BSA. Abbreviations: Setpal/Lateral (sept./lat.), Anterior/Posterior (ant./post.), Apical (api.) 4-chamber (4ch), Tenting Area (TA), Tenting Height (TH).

	Control	Dilated RV	Dilated LV	Dilated RV/LV
Peak Systolic PA Pressure (mmHg)	36.96 ± 20.77	68.98 ± 27.85*	44.68 ± 16.82	52.11 ± 14.84
Annulus Area (cm^2/m^2)	4.6 ± 1.2	6.2 ± 3.0 #	5.7 ± 2.0	6.1 ± 1.0*
APM (sept./lat.) (cm/m^2)	-0.2 ± 0.5	-0.5 ± 0.6 #	-0.1 ± 0.7	-0.5 ± 0.5
APM (ant./post.) (cm/m^2)	-0.4 ± 0.3	0.3 ± 0.5	-0.2 ± 0.5	-0.3 ± 0.6
APM (api.) (cm/m^2)	1.5 ± 0.3	1.9 ± 0.8 #	2.0 ± 0.6*	2.0 ± 0.4*
SPM (sept./lat.) (cm/m^2)	0.6 ± 0.2	1.0 ± 0.5 #	0.6 ± 0.3	0.7 ± 0.2
SPM (ant./post.) (cm/m^2)	0.2 ± 0.3	0.3 ± 0.2	0.3 ± 0.3	0.2 ± 0.2
SPM (api.) (cm/m^2)	0.7 ± 0.2	1.1 ± 0.3*	0.8 ± 0.2	1.0 ± 0.2*
PPM (sept./lat.) (cm/m^2)	0.5 ± 0.2	0.9 ± 0.5 #	0.6 ± 0.2	0.7 ± 0.2
PPM (ant./post.) (cm/m^2)	-0.6 ± 0.3	0.4 ± 0.5	-0.5 ± 0.5	-0.7 ± 0.4
PPM (api.) (cm/m^2)	0.8 ± 0.3	1.3 ± 0.4*	0.9 ± 0.2	1.0 ± 0.4
4ch TA (cm^2)	0.6 ± 0.2	1.4 ± 0.5*	1.1 ± 0.6*	1.4 ± 0.5*
4ch TH (cm)	0.3 ± 0.1	0.6 ± 0.2*	0.5 ± 0.2*	0.5 ± 0.1*

* = $p \leq 0.05$, as compared to control group, ANOVA
# = $p \leq 0.05$, as compared to normal, Kruskal-Wallis

6.1.2.1 Control (Normal Right and Left Ventricle)

Of the 64 subjects, 21 were classified as control by measurement of a normal RV and LV area. These subjects were imaged as either volunteers (n = 9) or as requested by their physician (n=12). Positions of control PMs were consistent with previously reported locations as identified in normal subjects using MRI [72]. The findings of the MRI study can be found in appendix H, with the measurements in the raw data section C. The anterior PM was the most apical of all three PMs and the only PM located on the free

wall and was typically more posterior as denoted with the negative measurement of -0.40 ± 0.29 cm/m^2. Both the SPM and PPM were located on the septum and were located at a similar distance from the annulus, with the SPM located more anterior and the PPM located in the posterior direction.

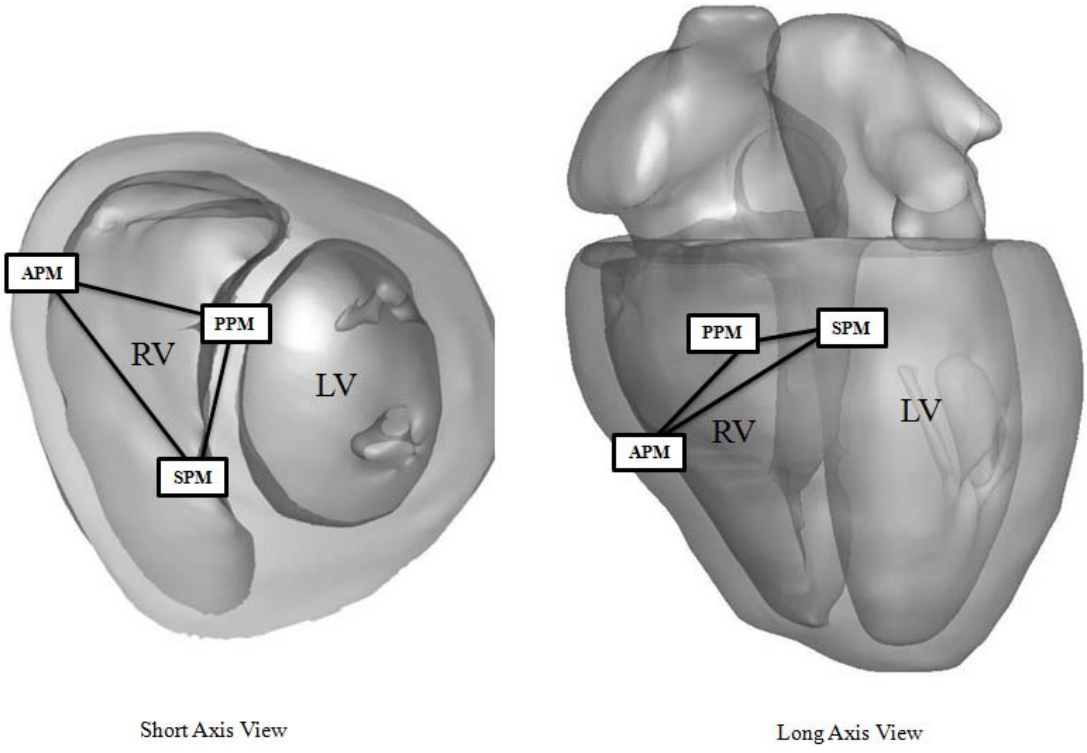

Figure 6.7: Relative location of papillary muscles. SPM: septal papillary muscle, PPM: posterior papillary muscle, APM: anterior papillary muscle.

6.1.2.2 Dilated Right Ventricle

16 of the 64 patients in the study were classified as having only RV dilatation. Patients with a dilated RV had significant displacement of all PMs away from the center of the annulus, with the APM displaced septally (-0.5 ± 0.6 cm/m^2) and the septal and posterior PMs displaced laterally, towards the LV. All PMs were also displaced apically

in these patients (APM: 1.9 ± 0.8 cm/m^2, SPM: 1.1 ± 0.3 cm/m^2, PPM: 1.3 ± 0.4 cm/m^2). Directions of statistically significant displacement are shown in the figure 6.8.

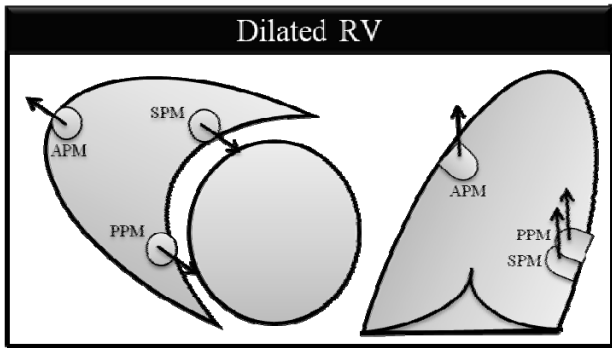

Figure 6.8: Depiction of significant displacement for patients with a dilated RV, as compared to control subjects. Both short and long axis views are shown.

Tethering, as measured as both tenting area (TA) and tenting height (TH) was significantly ($p \leq 0.05$) increased in patients with a dilated RV as compared to control. While TH was consistent amongst patient groups, TA was highest with isolated RV dilatation (1.4 ± 0.5 cm/m^2).

6.1.2.3 Dilated Left Ventricle

It was difficult to find patients with isolated LV dilatation as most had a pacemaker lead through the tricuspid valve; these patients were excluded from the study as this is a known cause of TR [11, 73]. Thus, 13 of the 64 patients were classified as having only LV dilatation. The only significant PM displacement in these patients was apical displacement of the APM (2.0 ± 0.6 cm/m^2).

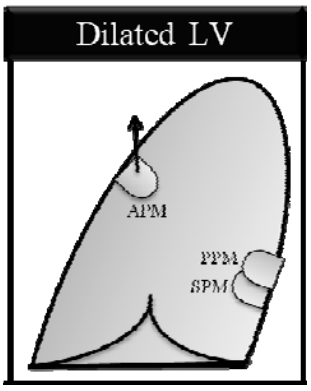

Figure 6.9: Depiction of signficant displacement for patients with a dilated LV, as compared to normal subjects. A long axis view is shown.

Tethering, as measured as both TA and TH was significantly ($p \leq 0.05$) increased in patients with a dilated LV as compared to control. While TH was consistent amongst groups, patients with a dilated LV did not have the highest levels of TA.

6.1.2.4 Dilated Right and Left Ventricle

Of the 64 patents enrolled for this study, 14 had dilatation of both the RV and LV. Patients with both ventricles dilated had significant apical displacement of both the APM (2.0 ± 0.4 cm/m^2) and SPM (1.0 ± 0.1 cm/m^2).

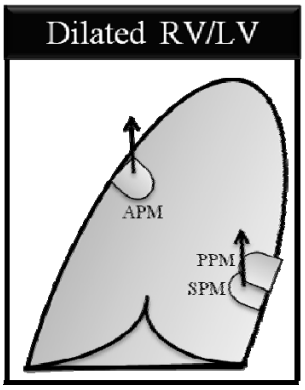

Figure 6.10: Depiction of significant displacement for patients with both a dilated RV and LV, as compared to normal subjects. A long axis view is shown.

Tethering, as measured as both tenting area (TA) and tenting height (TH) was significantly ($p \leq 0.05$) increased in patients with combined RV and LV dilatation as compared to control. While TH was consistent amongst patient groups, in addition to isolated RV dilatation, the combination of RV and LV dilatation also resulted in the highest TA (1.4 ± 0.5 cm/m^2).

6.1.3 Determinants of Tricuspid Regurgitation

Once the displacement of the PMs was defined, a more in depth investigation of the variables measured was conducted to determine which, if any, of the measurements were correlated to the severity of TR of the patients. All measured parameters, as listed in the table, were assessed for correlation of the grade of TR. A variable was considered to be clinically correlated to TR with a p value greater than or equal to 0.05. Investigated variables and their correlation associated with the severity of TR are shown in table 6.2.

TABLE 6.2: Determinants of the Grade of Tricuspid Regurgitation. Abbreviations: Septal/Lateral (sept./lat.), Anterior/Posterior (ant./post.), Apical (api.) 4-chamber (4ch), Tenting Area (TA), Tenting Height (TH), Coefficient (Coeff.).

		Correlation		Multivariate	
		r	p	Coeff.	p
Age	(n=57)	0.14	0.293		
PA Pressure	(n=62)	0.66	0.000	0.28	0.000
MR Grade	(n=62)	0.21	0.102		
Classification	(n=64)	0.46	0.000	0.26	0.001
RVEDA	(n=64)	0.48	0.000		
LVEDA	(n=64)	0.24	0.059		
Annulus Area	(n=64)	0.51	0.000	1.60	0.027
APM (sept./lat.)	(n=63)	-0.11	0.376		
APM (ant./post)	(n=63)	0.06	0.656		
APM (api.)	(n=63)	0.26	0.038	-4.52	0.061
SPM (ant./post)	(n=58)	-0.02	0.867		
SPM (sept./lat.)	(n=58)	0.37	0.004		
SPM (api.)	(n=58)	0.40	0.002		
PPM (sept./lat.)	(n=59)	0.40	0.001		
PPM (ant./post)	(n=59)	-0.01	0.951		
PPM (api.)	(n=59)	0.49	0.000		
4ch TA	(n=58)	0.54	0.000		
4ch TH	(n=58)	0.49	0.000		

PA Pressure ($r = 0.66$, $p = 0.000$) was an independent predictor of the grade of TR. When the geometry of the ventricles was investigated, all parameters (Classification: $r = 0.46$, $p = 0.000$, RVEDA: $r = 0.48$, $p = 0.000$) were significantly correlated, with the exception of LVEDA ($r = 0.24$, $p = 0.059$). Changes in the annular and subvalvular apparatus were significantly correlated with the grade of TR, specifically annulus area ($r = 0.51$, $p = 0.000$) and apical PM displacement of the APM ($r = 0.26$, $p=0.038$), SPM ($r = 0.40$, $p = 0.002$) and PPM ($r=0.49$, $p=0.000$). Additionally, displacement of the SPM ($r = 0.37$. $p = 0.004$) and PPM ($r = 0.40$, $p = 0.001$) away from the center of the RV towards the LV were correlated with the grade of TR. Both measurements of tethering, TA and TH, were correlated with the grade of TR, ($r = 0.54$, $p = 0.000$) and ($r = 0.49$,

p =0.000), respectively. It is important to note that PM position and tenting measurements could not be obtained for all patients, explaining why the sample size for the measurements is less than 64 in all cases.

Once correlations of individual parameters were determined a multivariate analysis was then conducted, to determine if the combination of multiple variables could better predict TR. Those variables which had a significant correlation to TR were included in the original model: PA pressure, classification, RVEDA, annulus area, APM (apical), SPM (anterior/posterior, apical), PPM (septal/lateral, apical), tenting height and area. The test was run with all variables and then again with the highest p value eliminated. This was repeated until all remaining variables had $p \leq 0.10$. While tethering area was highly correlated with TR, it dropped out on the 6^{th} step, with a p-value of 0.794. Two additional steps were completed before all variables in the multivariate regression where $p \leq 0.10$, leaving four variables. PA pressure ($p = 0.000$), classification ($p = 0.001$), annulus area ($p = 0.027$) and apical displacement of the APM ($p = 0.061$) were predictors of the grade of TR in a multivariate regression analysis.

6.2 *In Vitro*

The results for the in vitro work are divided into results from experiments with isolated annular dilatation, isolated PM displacement, and combined annular dilatation and PM displacement. The isolated PM displacement and combined sections are further divided by the PM which was displaced in the experiments. Results from isolated anterior and septal/posterior PM displacements are first presented and then results for the displacement of all three PMs together. Hemodynamic results are presented first followed by RLL, chordal force and leaflet mobility data, to assist in explaining differences

observed in the amount of TR. All data are shown as mean ± standard deviation, with the exception of the RLL data which are expressed as mean ± standard error, to ease visualization of data on graphs.

6.2.1 Isolated Annular Dilatation

6.2.1.1 Hemodynamics

When the isolated effect of annular dilatation was investigated on the amount of TR, a significant effect ($p = 0.000$) was found. A significant increase ($p \leq 0.05$) in regurgitation could be seen with 40% annular dilatation as compared to the control (7.9±3.4 mL, $n = 8$). Further dilatation in excess of 40% resulted in a significant ($p \leq 0.05$) increase in TR from control. The largest amount of TR (20.1 ± 6.2 l) was seen with 100% dilatation (Fig. 6.11).

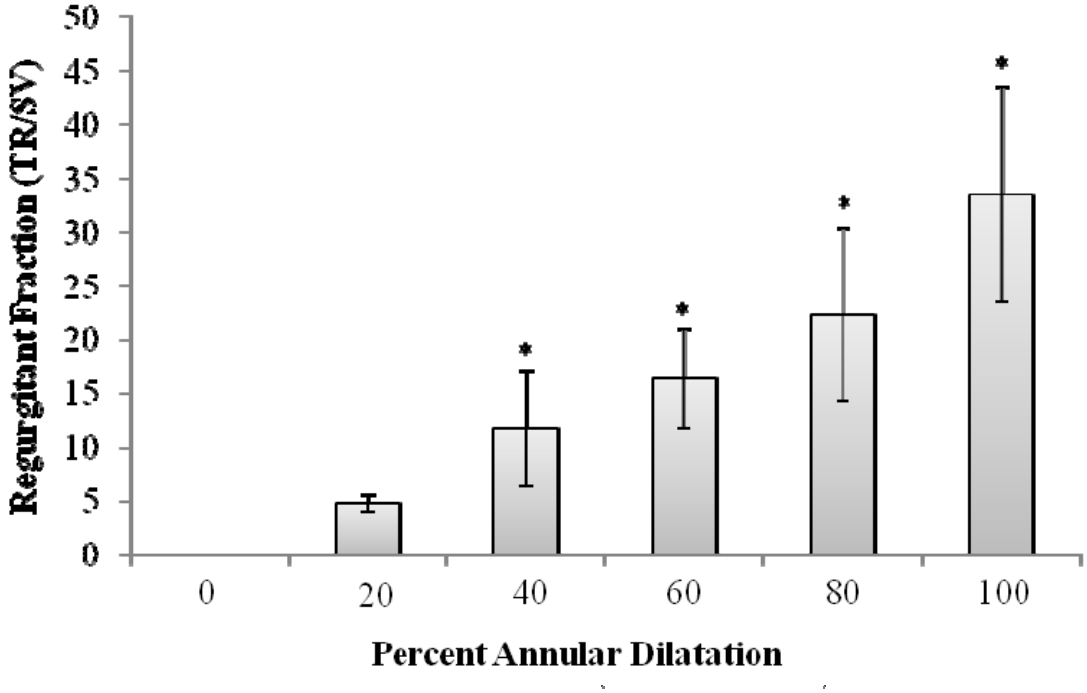

Figure 6.11: Tricuspid regurgitation volume as an effect of annulus area times normal with significance (* = $p \leq 0.05$), as compared to control (0), n = 8.

Malcoaptation, as visualized by a hole, first appeared at 40% dilatation of the normal annulus area and increased in size with further dilatation. In all cases the orifice was in the central region of the three leaflets, towards the septum. This can be seen in the below figure which shows the tricuspid valve from the atrial view (Fig. 6.12).

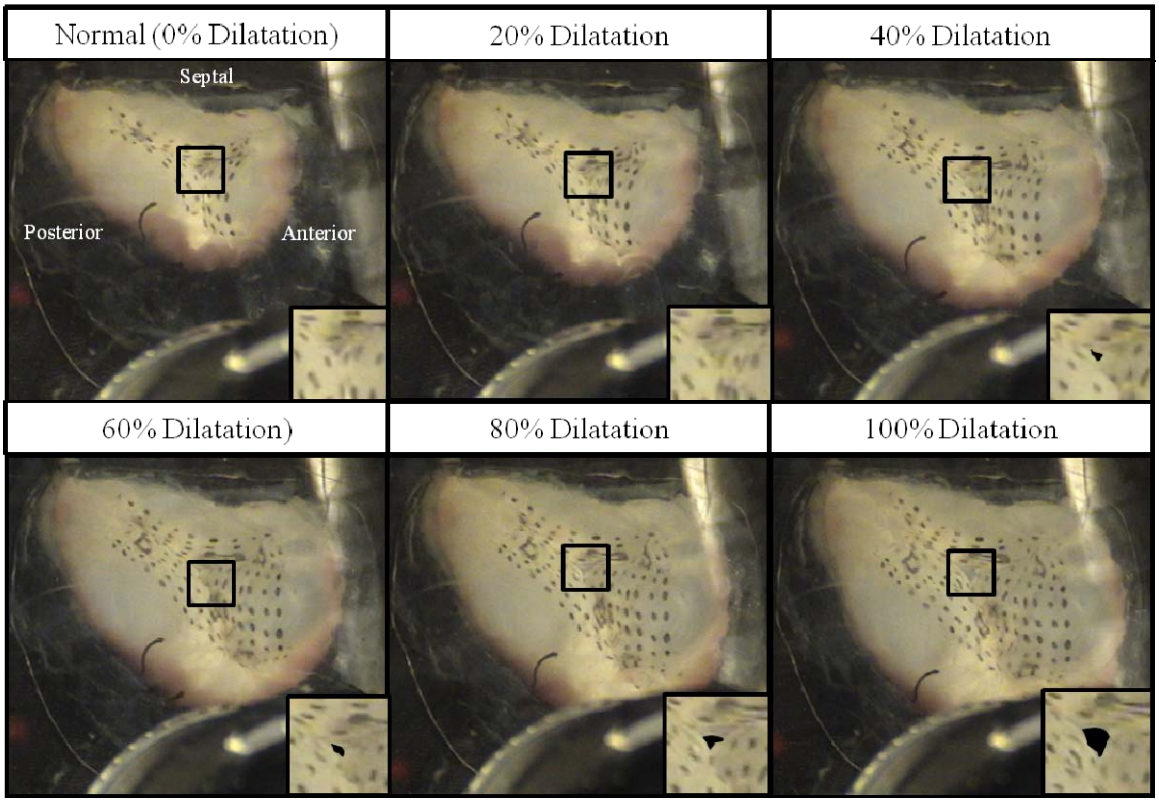

Figure 6.12: Image of representative valve (Expt8_040609) with isolated annular dilatation from 0-100%. Central malcoaptation is highlighted with black. Video is provided through the link (click image for video).

In addition to measurement of an increase in TR and visualization of a central hole in valve images, a regurgitant jet could be seen with color Doppler imaging using 3D echo. Peak systolic images of the same valve can be seen for both a normal annulus size and 100% dilated annulus. No jet is present with the normal annulus, while a distinct central jet is present with 100% dilatation (Fig. 6.13).

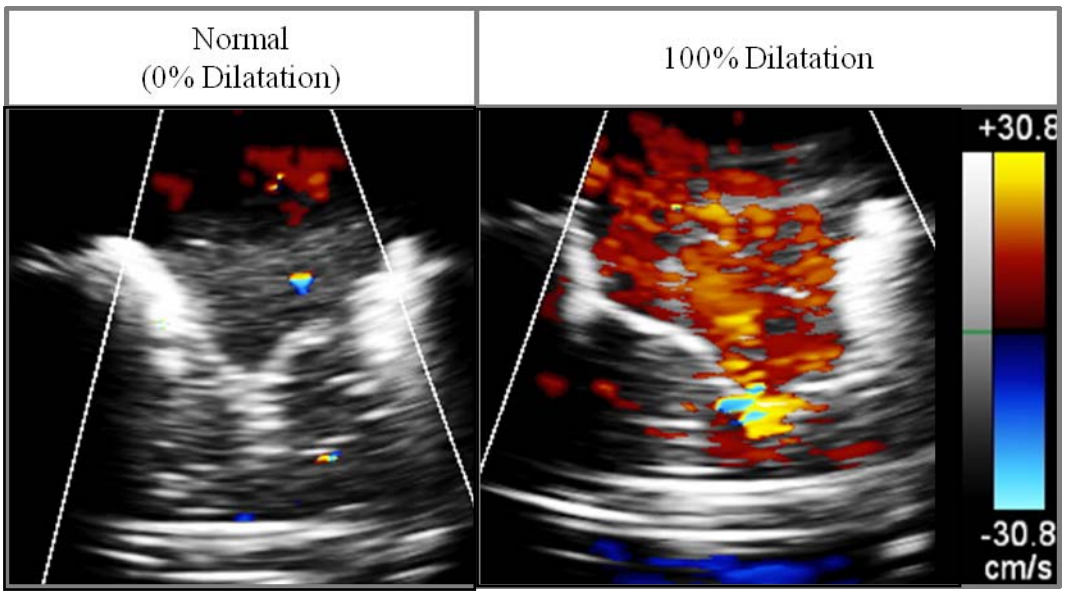

Figure 6.13: Color Doppler images of a valve with a normal annulus area and 100% dilated annulus. A central regurgitant jet is visible with 100% dilatation (click images for videos).

In addition to showing that dilatation of the annulus had a significant effect on TR, it was of interest to determine if the presence of a 3D saddle shape reduced TR. No significant difference was seen in the amount of TR when saddle and no saddle were compared for 100% annular dilatation (Fig. 6.14). Thus, the presence or absence of a saddle had no impact on the amount of TR.

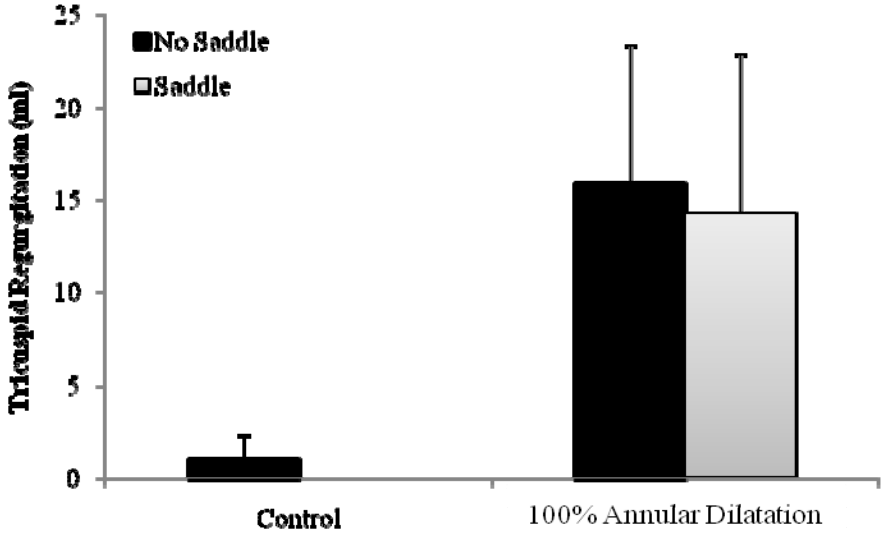

Figure 6.14: Plot of TR for control and 100% dilatation with and without a saddle. No significance was found between saddle and no saddle conditions. Note: Negative volume of control with a saddle was assumed as closing volume and subtracted from all measurements.

6.2.1.2 Residual Leaflet Length

Next, the effect of annular dilatation on RLL was investigated to provide a better understanding of the mechanism responsible for TR, by measuring the amount of leaflet available for coaptation on each individual leaflet. The individual leaflet, whether anterior, septal or posterior in which RLL was measured had a significant ($p = 0.000$) effect on RLL. Likewise, the amount of annular dilatation ($p = 0.000$) had a significant effect on RLL. When the impact of leaflet was investigated further it was found that there was an inverse relation of RLL to dilatation, with RLL decreasing with increasing annular dilatation, for all leaflets ($n = 8$) (Fig. 6.15). A significant difference ($p \leq 0.05$) was seen in RLL of the posterior leaflet as compared to both the anterior and septal

leaflets, with the posterior having the largest RLL throughout. No difference was seen in RLL between the anterior and septal leaflets for any annulus area measured. Next, when determining which leaflet was most affected by dilatation, it was found that anterior leaflet RLL was most affected, as it decreased from an initial RLL of 1.1 ± 0.4 to 0.2 ± 0.2 cm. The loss of valve competence and significant TR coincided with a minimum RLL of 0.5 ± 0.2 cm, as measured on the anterior leaflet. A negative correlation could be seen between RLL and TR for the posterior (r = -0.303) and anterior (r = -0.685) leaflets, but not with the septal leaflet (r = -0.423), demonstrating the decrease in RLL as the amount of TR increases.

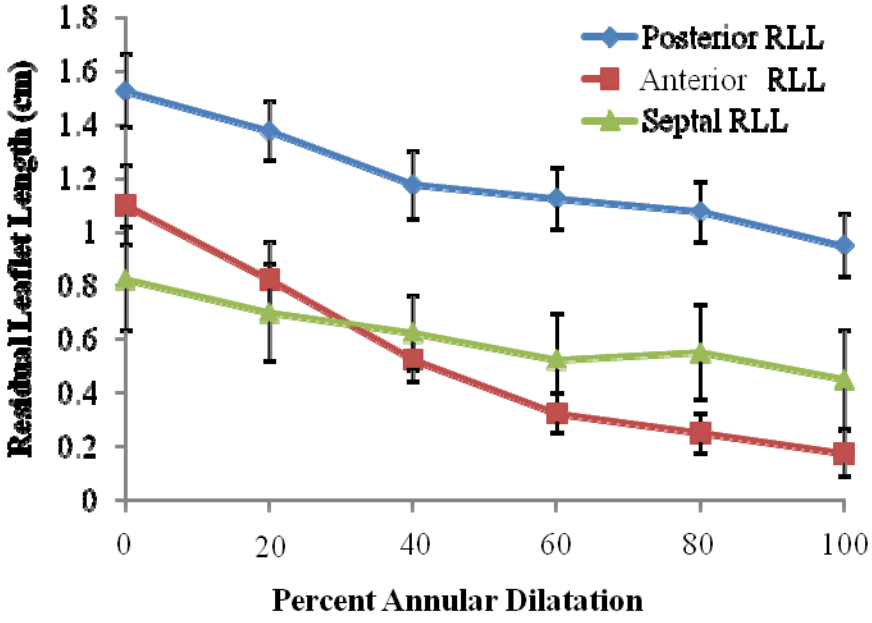

Figure 6.15: RLL as an effect of annulus area times normal, as shown for each individual leaflet: posterior (blue), anterior (red), and septal (green). Standard error is shown.

6.2.1.3 Chordal Forces

The force on the chords connecting from the anterior PM to the anterior and posterior leaflets was investigated to see if annular dilatation resulted in redistribution of the forces. 100%

dilatation of the annulus had a significant effect on all chordae inserting into the anterior (marginal: $p = 0.005$, intermediate: $p = 0.027$, strut: $p = 0.008$) and posterior leaflets (marginal: $p = 0.039$, intermediate: $p = 0.014$, strut: $p = 0.021$). Both anterior and posterior marginal chords experienced the highest percent increase in force from control with 147 ± 34%and 96 ± 52%, respectively. Percent increases in force of the intermediate chords were 91±41% for the posterior leaflet and 80±43% for the anterior leaflet. While strut chordae tensions were significantly increased, they were the least impacted by dilatation with the lowest level (43±26% and 25±22% anterior and posterior) of increase, as compared to marginal and intermediate chordae. Typically, the chordae inserting into the anterior leaflet experienced higher percent increases in differential force from normal as compared to chordae inserting into the posterior leaflet (Fig. 6.16). Only the APM was instrumented with c-rings, as the anterior and posterior leaflets were expected to be most affected by dilatation as the anterior and posterior sections of the annulus are dilated.

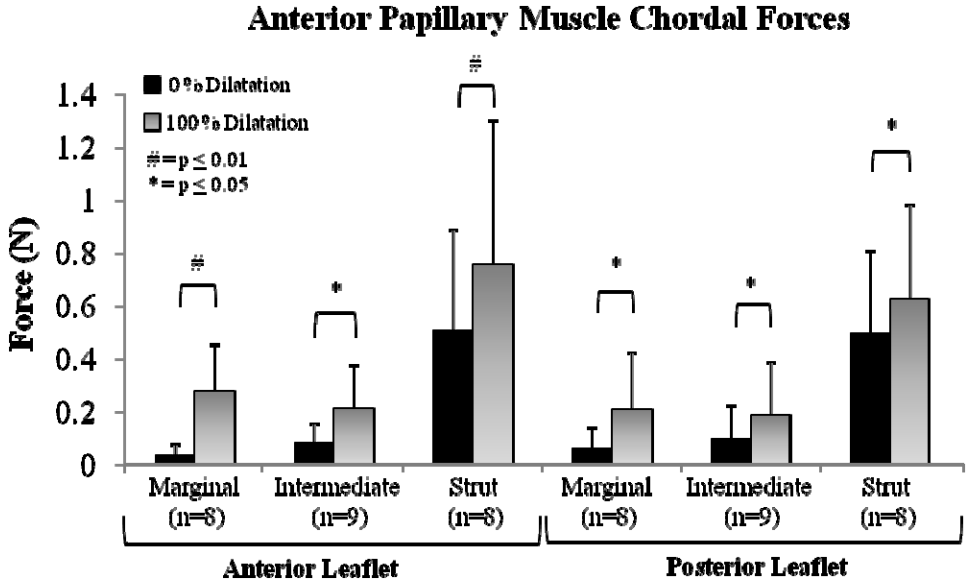

Figure 6.16: Peak systolic chordal force measurements for chords originating from the APM. Significance (* = $p \leq 0.05$, # = $p \leq 0.01$) as determined with a GLM as compared to 0% dilatation for the same valve.

6.2.1.4 Leaflet Mobility

Finally, the impact of annular dilatation on leaflet mobility was assessed through measurement of tenting height and tenting area along the three coaptation zones. No significant difference was seen with tenting height as an effect of annular dilatation for the septal/anterior ($p = 0.752$), anterior/posterior ($p = 0.150$), and posterior/septal ($p = 0.536$) coaptation lines. Additionally, no significant difference in tenting area could be seen with increased levels of dilatation at any coaptation line: SA ($p = 0.254$), AP ($p = 0.173$), and PS ($p = 0.276$). While the values for 100% tended to be larger, especially with TA, the difference was not statistically significant (Fig. 6.17).

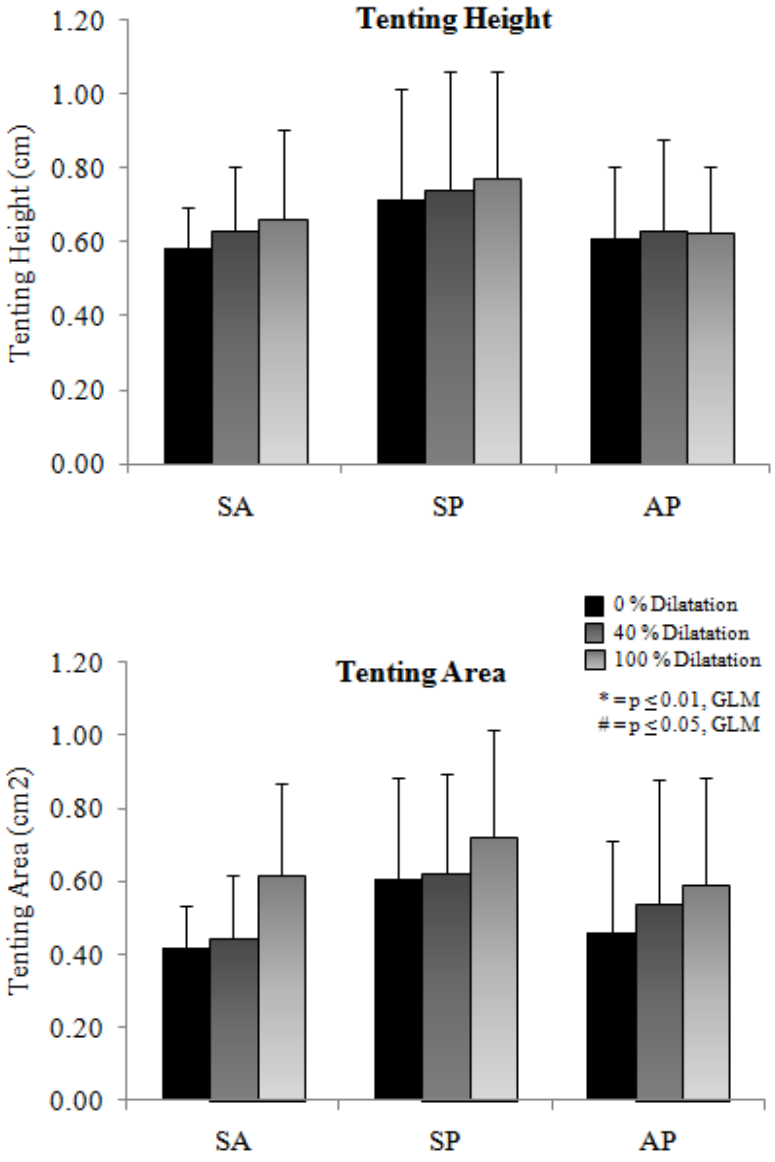

Figure 6.17: Peak systolic tenting height and area measurements are shown as an effect of annular dilatation, along the coaptation lines: septal/anterior (SA), septal/posterior (SP), anterior/posterior (AP).

6.2.2 Isolated Papillary Muscle Displacement

The effect of PM displacement was investigated through sole displacement of the anterior PM and combined displacement of the septal and posterior PM, as these PMs would be expected to move together as they are both located on the septum. Combined PM displacement was then

simulated in which all three PMs were displaced. Each PM was displaced in multiple directions and is described in further detail in each section.

6.2.2.1 Anterior Papillary Muscle Displacement

The anterior PM was displaced from a control position laterally and apically, both separately and combined (Fig. 6.18). Each PM was displaced by 10 mm from its control position in each direction.

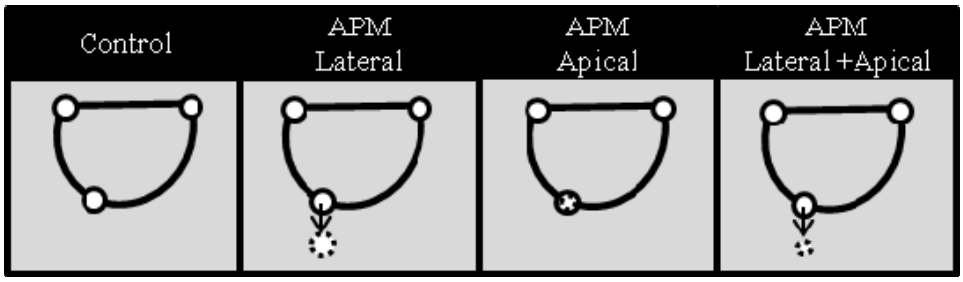

Figure 6.18: Control position of PMs along with directions of APM displacement. Control position is shown with a solid line with displaced positions is shown with a dashed line. Note: Apical displacement is shown as displaced into the image, away from the annulus, as a smaller circle.

6.2.2.1.1 Hemodynamics

TR was significantly ($p = 0.001$) impacted by PM displacement, when annular size was maintained at a normal size. Individual APM displacement in the lateral (1.76 ± 1.89 mL) and apical (4.13 ± 4.35 mL) directions did not result in significant increases in TR from control. A significant increase in TR was seen with displacement of the APM alone (Fig.6.19). Only combined displacement in the apical and lateral directions resulted in significantly increased TR (4.64 ± 3.91 mL) from control.

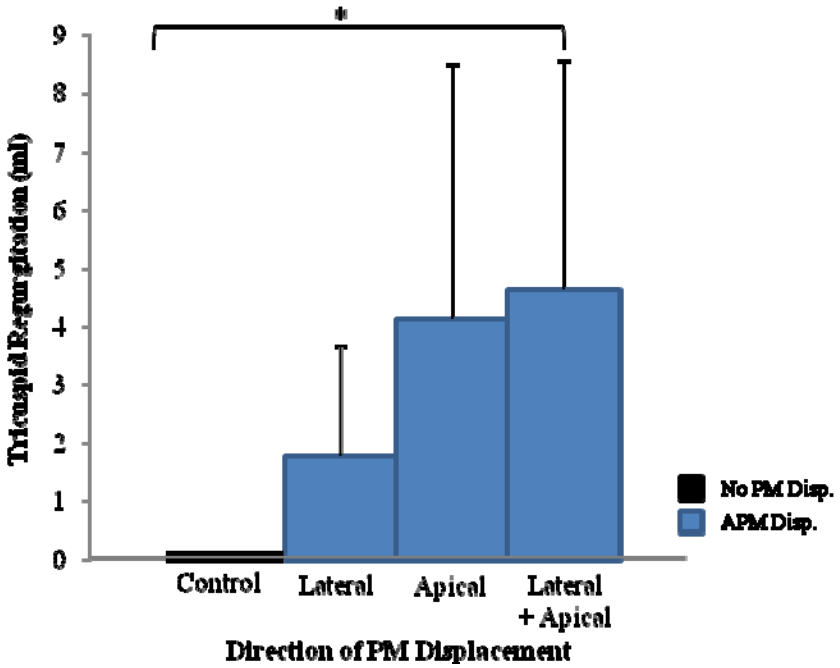

Figure 6.19: Tricuspid regurgitation as an effect of APM displacement with significance (* = $p \leq 0.05$), as compared to control, n = 8. Bar colors correspond to PM which was displaced: black (no displacement), blue (APM).

Malcoaptation, defined as the absence of leaflet coaptation, was visibly present in the center of the three leaflets with displacement of the APM with combined lateral and apical displacement. Lateral displacement of the APM resulted in valve coaptation similar to that in the normal valve, with coaptation towards the septal annulus segment. Apical displacement of the APM either isolated or combined with lateral displacement resulted in a coaptation of the leaflets that was more central as compared to control, which was closer to the septal segment of the annulus (Fig. 6.20).

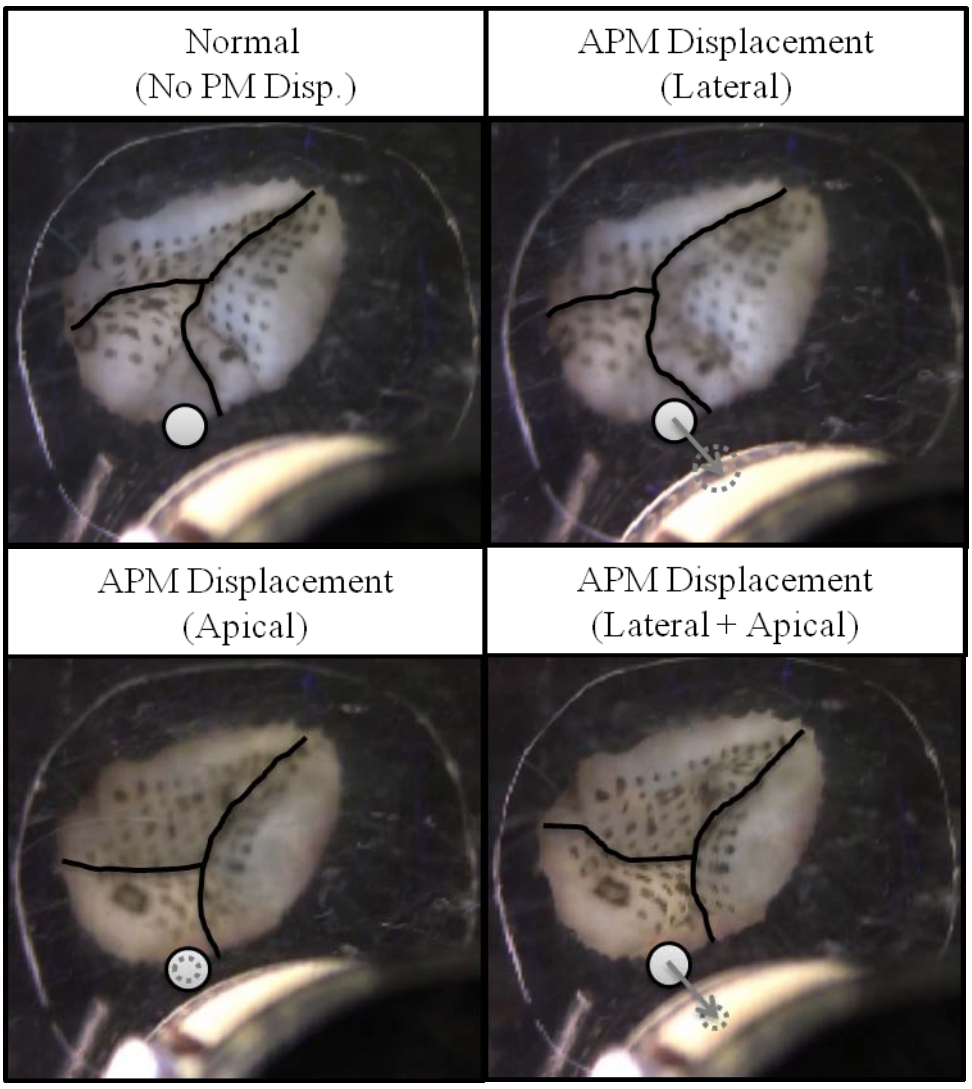

Figure 6.20: Image of valve with isolated APM displacement. PM displacement shown with a dashed line, as compared to control position solid line.

6.2.2.1.2 Residual Leaflet Length

With significant TR measured in the presence of APM displacement in a combined direction (lateral and apical), the effect of APM displacement on RLL was then investigated. RLL was measured for all three leaflets as an effect of APM displacement in individual apical and lateral and combined directions. When the difference in RLL for each leaflet was investigated across all PM displacements, RLL was found to vary

significantly on the anterior leaflet ($p = 0.004$), but not for the posterior ($p = 0.342$) or septal ($p = 0.110$) leaflets. Anterior RLL was significantly different ($p \leq 0.05$, denoted in Fig 6.21,#) from control with apical and combined lateral and apical displacement of the APM. Percent change in RLL varied significantly by leaflet ($p = 0.000$). The septal leaflet was significantly different than both anterior and posterior RLL. This is observed in figure 6.21 with septal RLL consistently decreasing and anterior and posterior RLL increasing. Further investigation was conducted with combined lateral and apical displacement of the APM, as this was the condition which resulted in significant TR. RLL was significantly different across the three leaflets ($p = 0.002$) with the septal leaflet having significantly ($p \leq 0.05$,*) less leaflet available for coaptation as compared to the anterior and posterior leaflets.

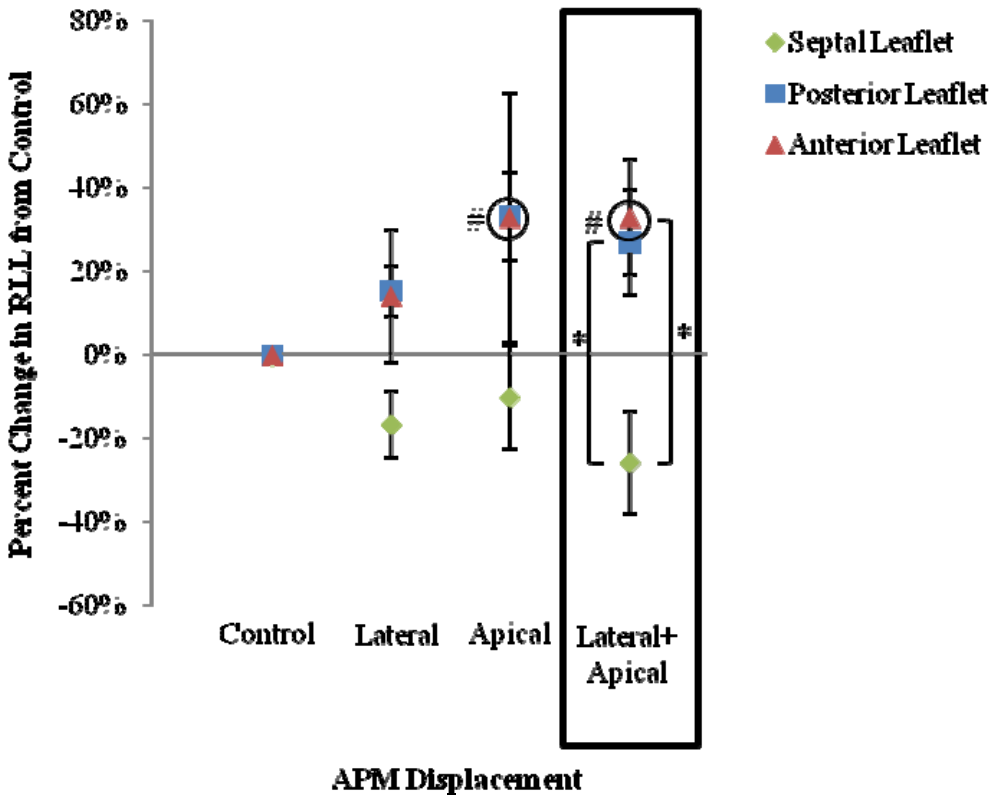

Figure 6.21: Percent change in RLL from control as an effect of APM displacement as shown for each individual leaflet: posterior (blue), anterior (red), and septal (green). Standard error is shown. Significance shown as *, $p \leq 0.05$ compared within PM displacement, #, $p \leq 0.05$ compared to control for the same leaflet. Grey box highlights condition with significant TR.

6.2.2.1.3 Chordal Force

With an understanding of the changes in RLL, the effect of APM displacement on forces of the chords branching from the APM and inserting into the anterior and posterior PM was investigated. Chordal force was not affected by APM displacement for any of the chords measured: Anterior marginal ($p = 0.358$), anterior intermediate ($p = 0.862$), anterior strut ($p = 0.695$), posterior marginal ($p = 0.360$), posterior intermediate ($p = 0.956$) and posterior strut ($p = 0.072$). Force measurements for chordae measured are shown in the below figure 6.22.

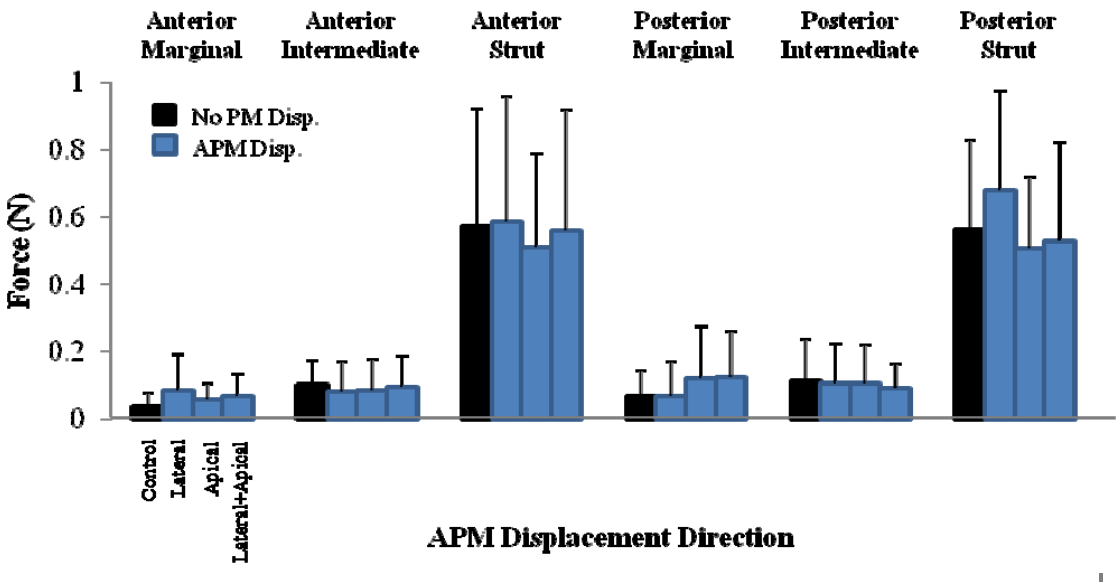

Figure 6.22: Differential chordal force measurements for chordae originating from the APM. Bar colors correspond to PM which was displaced: black (no displacement), blue (APM).

6.2.2.1.4 Leaflet Mobility

Finally, the impact of APM displacement on leaflet mobility was assessed through measurement of tenting height and tenting area on the septal/anterior, septal/posterior, and anterior/posterior coaptation lines. APM displacement had a significant impact on tenting height ($p = 0.016$) and tenting area ($p = 0.009$) across the anterior and posterior leaflets. There was no difference in tenting height ($p = 0.334$) or tenting area ($p = 0.080$) at the coaptation of the septal and anterior leaflets. Likewise no difference was seen for the septal and posterior coaptation line for tenting height ($p = 0.179$) or tenting area ($p = 0.803$). Investigation into which direction of APM displacement was responsible for alterations in leaflet mobility at the anterior/posterior coaptation line found differences in both tenting height and tenting area with combined lateral and apical displacement (Fig. 6.23). It is interesting to note that this is the same condition in which a significant increase was reported for TR.

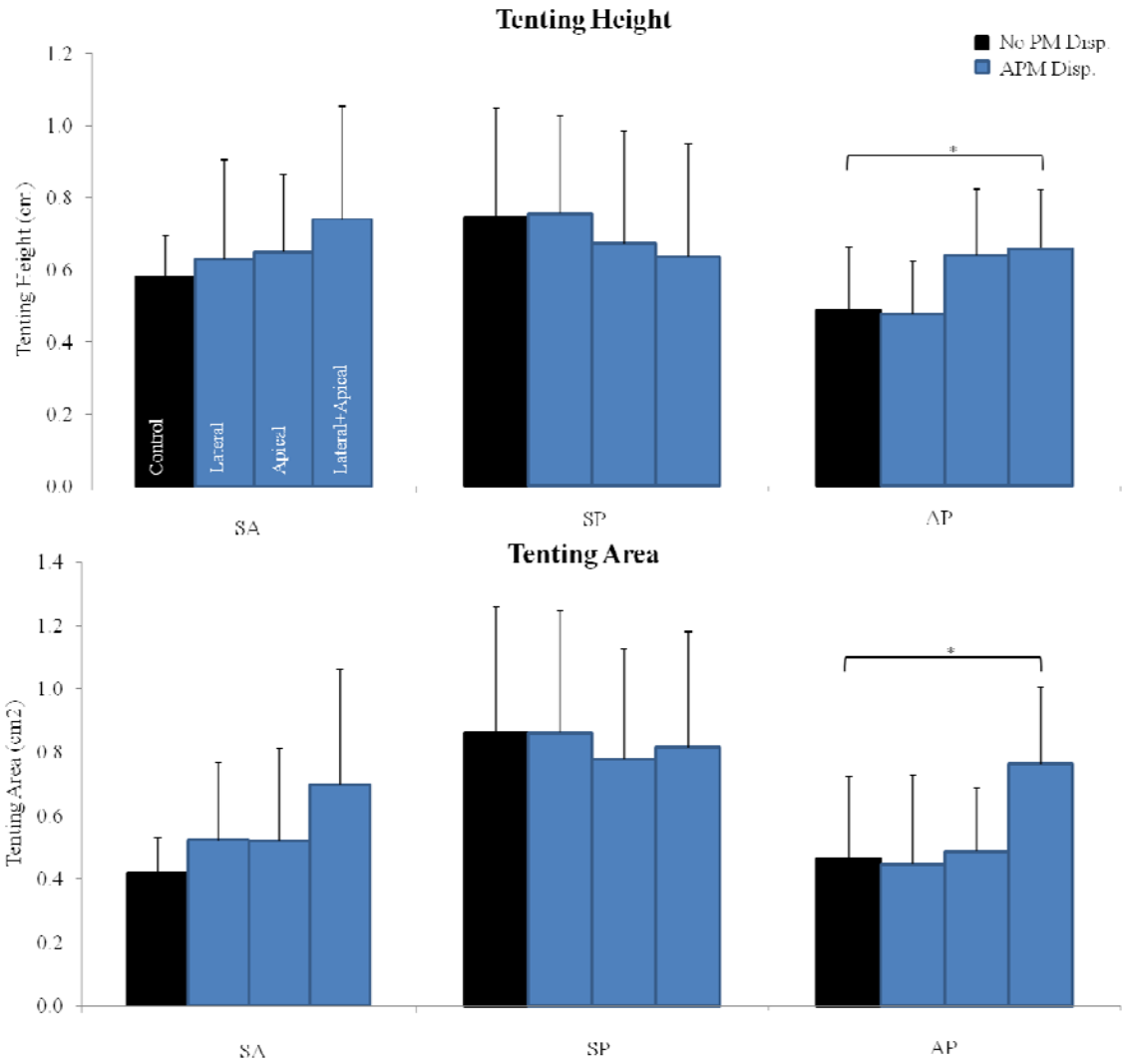

Figure 6.23: Peak systolic tenting height and area measurements are shown as an effect of APM displacement, along the coaptation lines: septal/anterior (SA), septal/posterior (SP), anterior/posterior (AP). Significance shown as *, $p \leq 0.05$.

6.2.2.2 Septal and Posterior Papillary Muscle Displacement

The septal and posterior PM were displaced simultaneously as they are both located on the septum and would be expected to move together in a similar direction. The septal PM was displaced from a control position anteriorly, laterally and apically, both separately and combined. Likewise the posterior PM was displaced from a control

position posteriorly, laterally and apically, both separately and combined (Fig. 6.24). Each PM was displaced by 10 mm from its control position.

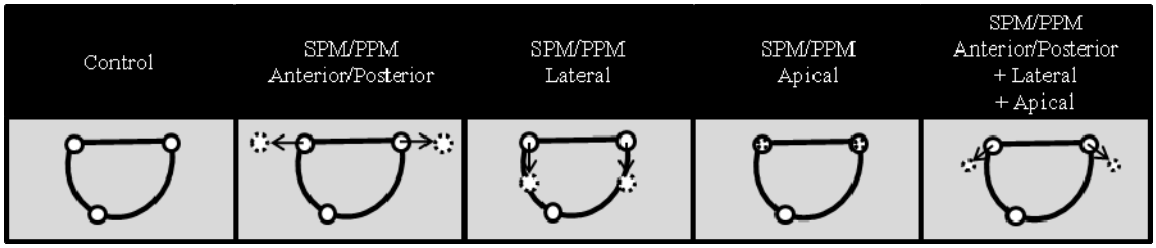

Figure 6.24: Control position of PMs along with directions of SPM/PPM displacement. Control position is shown with a solid line with displaced positions shown with a dashed line. Note: Apical displacement is shown as displaced into the image, away from the annulus, as a smaller circle.

6.2.2.2.1 Hemodynamics

TR was significantly ($p = 0.001$) impacted by PM displacement, when annular size was maintained at a normal size. Specifically, displacement of the septal and posterior PMs in the combined direction (anterior/posterior, lateral and apical) resulted in significant ($p \leq 0.05$) TR when compared to control (Fig.6.25). Additionally, when looking at the hemodynamic results one might suspect that lateral displacement of the septal and posterior PMs resulted in significant TR, but this cannot be shown statistically. The reason for this is due to the high variability in the measurements which resulted in a non-normal distribution of the data. When a detailed analysis was conducted of the measurements for this condition it was seen that the data fell into two groups, valves ($n = 3$) with high levels of TR (11.4 ± 5.4 mL) and valves ($n = 5$) with insignificant levels (1.7 ± 0.3 mL). Thus, the resulting two groupings of data could not be assessed with statistical comparisons, because even the use of a non normal test would rank the data, and result in two distinct groups without a distribution.

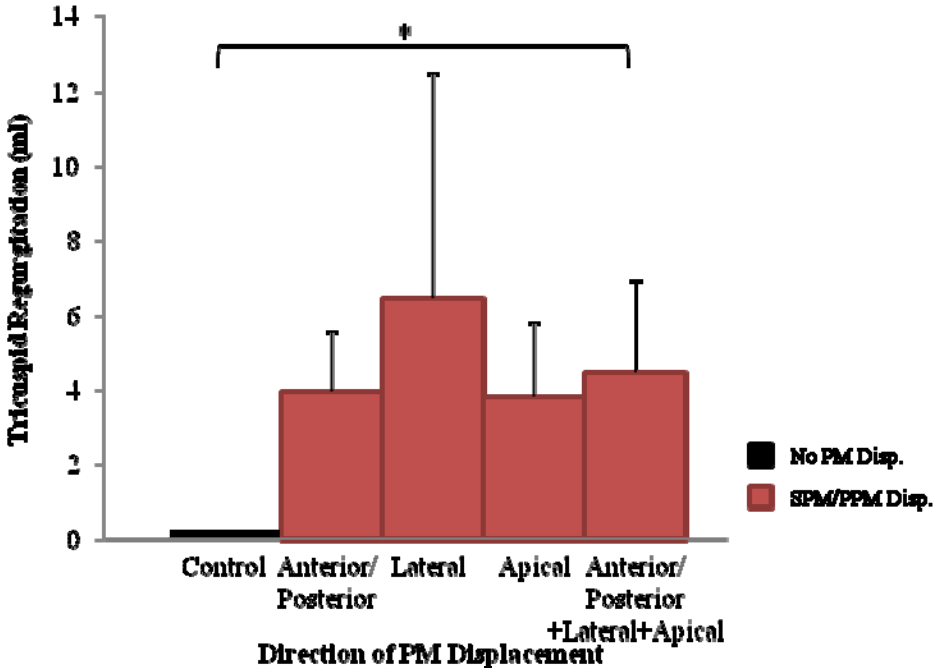

Figure 6.25: Tricuspid regurgitation as an effect of SPM/PPM displacement with significance (* = $p \leq 0.05$), as compared to control, n = 8. Bar colors correspond to PM which was displaced: black (no displacement), red (SPM/PPM).

Observations were next made as to the effect of septal and posterior PM displacement on leaflet coaptation. Differences in leaflet coaptation, as viewed from the atrium, were only visible with lateral displacement either isolated or combined, of the septal and posterior PMs. When the PMs were displaced only laterally the coaptation line was towards the anterior/posterior sections of the annulus, thus the septal leaflet covered the majority of the orifice (6.26). With lateral displacement of the SPM/PPMs was combined with apical displacement the coaptation line of the three leaflets was more central.

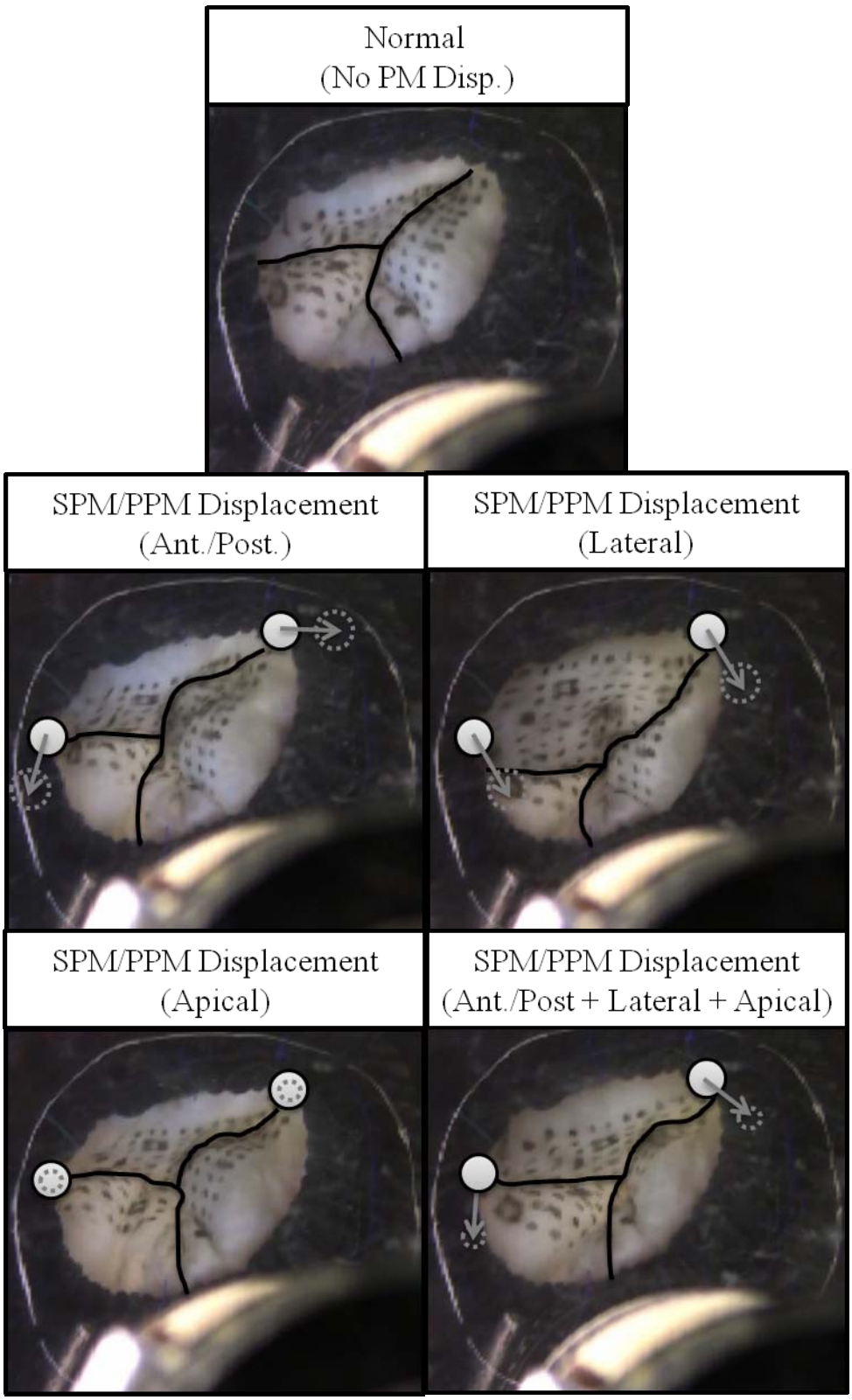

Figure 6.26: Image of valve with isolated SPM/PPM displacement. PM displacement shown with a dashed line, as compared to control position with a solid line.

6.2.2.2.2 Residual Leaflet Length

The effect of SPM and PPM displacement on RLL was investigated as this condition resulted in a significant increase in TR when displaced in the combined direction (anterior/posterior, lateral and apical) direction. RLL was measured for all three leaflets as an effect of SPM/PPM displacement in individual (anterior/posterior, lateral and apical) and combined directions. When the difference in RLL for each leaflet was investigated across all PM displacements, RLL did not vary significantly across any leaflet: anterior ($p = 0.229$), posterior ($p = 0.352$) and septal ($p = 0.343$) (Fig. 6.27). Percent change in RLL varied significantly by leaflet ($p = 0.006$) with the septal leaflet being significantly different than the posterior RLL. This is observed in figure 6.19 with the septal leaflet RLL consistently decreasing while posterior RLL was increasing. Further investigation was conducted with combined anterior/posterior, lateral and apical displacement of the SPM/PPM, as this was the condition which resulted in significant TR. RLL was not significantly different across the three leaflets ($p = 0.247$). Additional analysis was conducted to determine if there was a difference between RLL across the leaflets when the SPM/PPM was displaced laterally as this condition resulted in high levels of TR in some valves. However, individual leaflet RLL was not affected ($p = 0.108$) by displacement of the septal and posterior PM in the lateral direction.

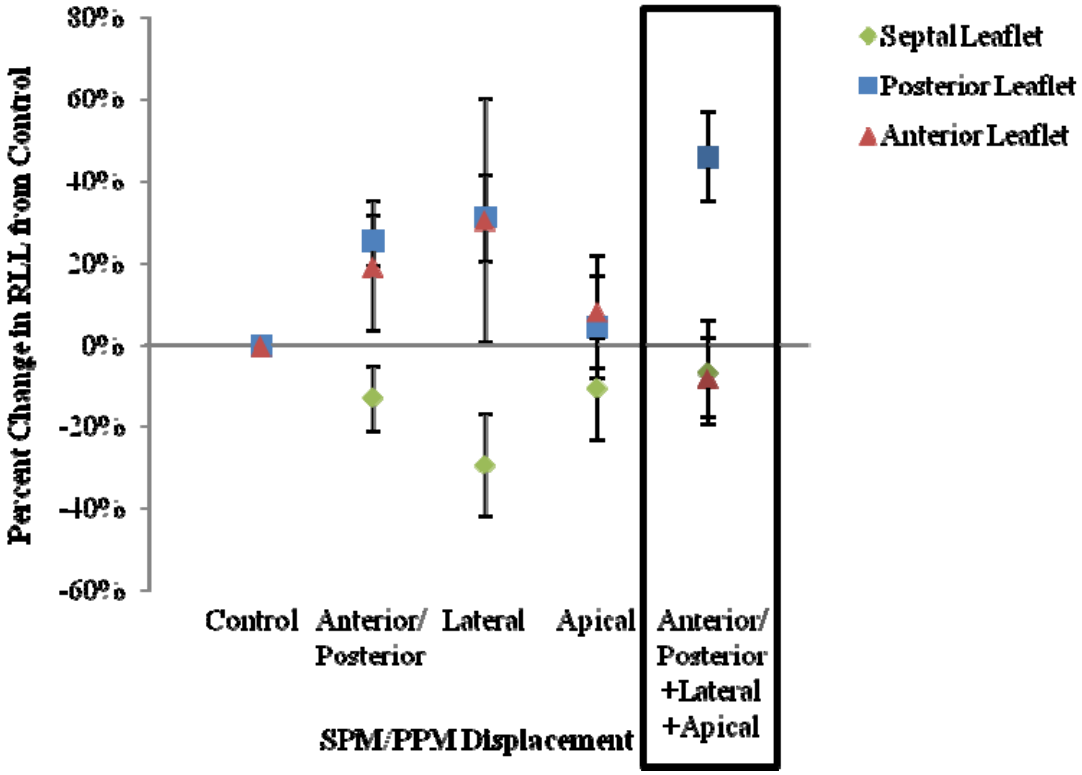

Figure 6.27: Percent change in RLL from control as an effect of SPM/PPM displacement as shown for each individual leaflet: posterior (blue), anterior (red), and septal (green). Standard error is shown. Grey box highlights condition with significant TR.

6.2.2.2.3 Chordal Force

Chordal force was not measured with isolated displacement of the septal and posterior PMs in any direction. It was assumed that displacement of the SPM and PPM would not significantly alter forces on chords originating from the APM hence the force transducers were mounted on the APM only. However, displacement of the SPM and PPM was investigated in conjunction with APM displacement, with all three PMs displaced in the combined directions. See section 6.2.2.3.3 for detailed results.

6.2.2.2.4 Leaflet Mobility

Lastly, the impact of septal and posterior PM displacement on leaflet mobility was assessed through measurement of tenting height and tenting area on the three coaptation lines. No difference was seen in tenting height ($p = 0.109$) or tenting area ($p = 0.166$) across the septal and anterior coaptation line. Similarly no difference was seen in either tenting height ($p = 0.057$) or tenting area ($p = 0.206$) across the septal and posterior coaptation line. Finally when leaflet mobility was assessed for the anterior and posterior coaptation line, no difference was seen in either tenting height ($p = 0.527$) or tenting area ($p = 0.713$). Results for leaflet mobility measurements can been seen in the below figure (Fig. 6.28). While displacement of the septal and posterior PMs in the combined directions (posterior/anterior, lateral and apical) seems to decrease leaflet mobility, as seen with an increase in tenting height and tenting area in the septal/posterior and septal/anterior, the difference was not statistically significant.

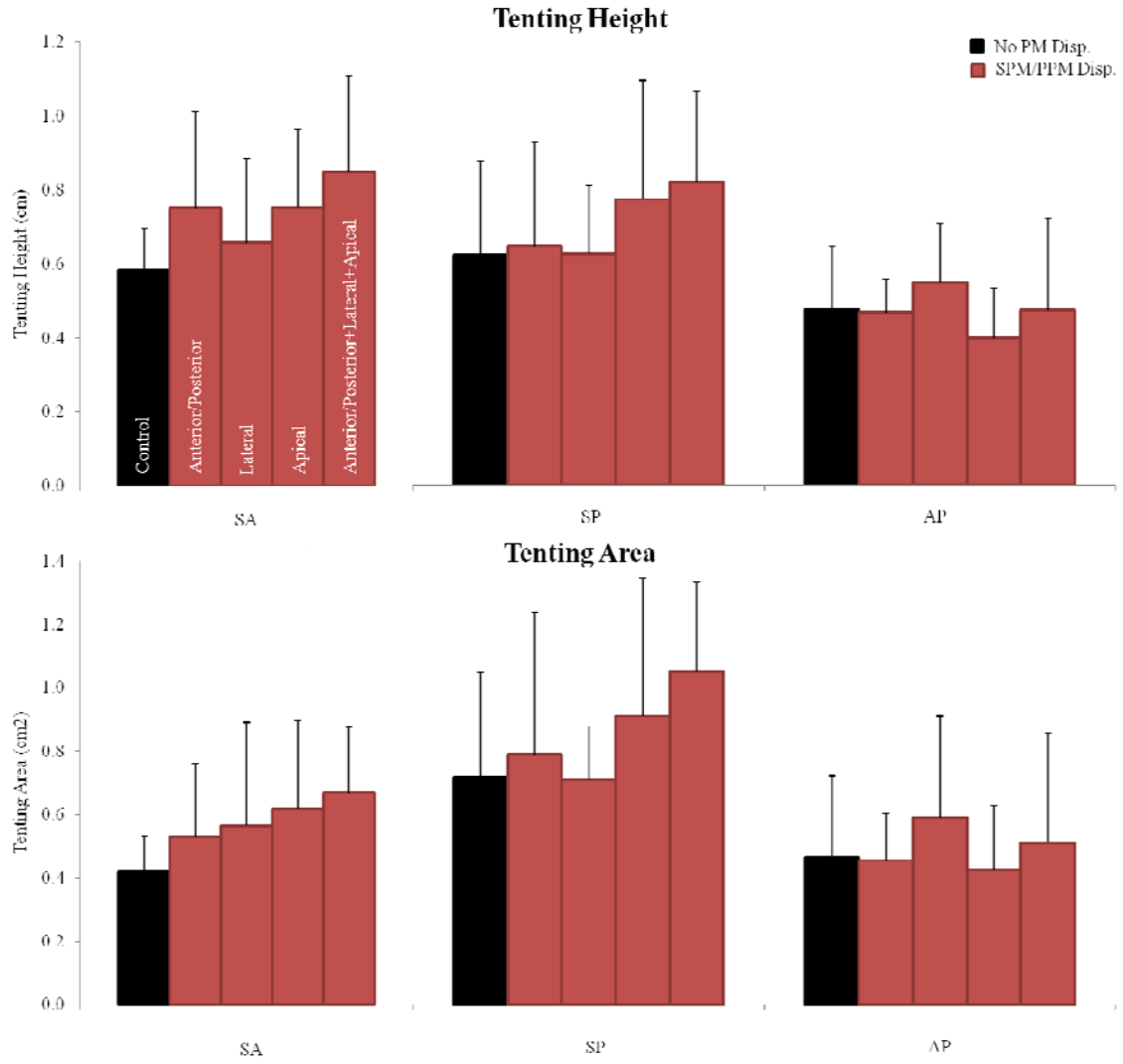

Figure 6.28: Peak systolic tenting height and area measurements are shown as an effect of SPM/PPM displacement, along the coaptation lines: septal/anterior (SA), septal/posterior (SP), anterior/posterior (AP).

6.2.2.3 Combined Anterior, Septal and Posterior Papillary Muscle Displacement

Finally, a severe PM displacement condition was created in which all three PMs were displaced simultaneously with combined directions. The anterior PM was displaced with combined lateral and apical directions. This was simulated in conjunction with displacement of the septal PM in an anterior, lateral and apical direction while the

posterior PM was displaced in a posterior, lateral and apical direction (Fig. 6.29). Each PM was displaced by 10 mm from its control position.

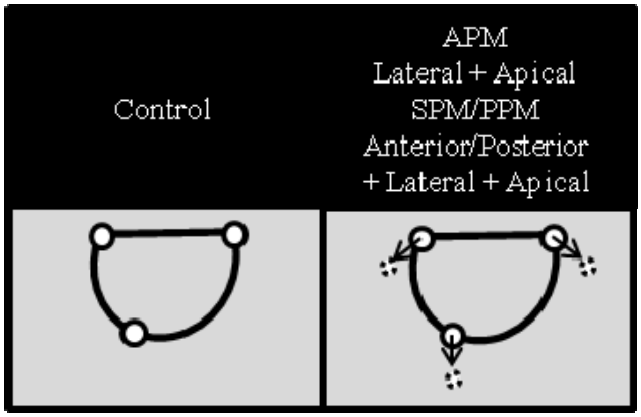

Figure 6.29: Control position of PMs along with directions of APM/SPM/PPM displacement. Control position is shown with a solid line with displaced positions is shown with a dashed line. Note: Apical displacement is shown as displaced into the image, away from the annulus, as a smaller circle.

6.2.2.3.1 Hemodynamics

TR was significantly ($p = 0.001$) impacted by PM displacement, when annular size was maintained at a normal size. A significant increase ($p \leq 0.05$) in TR was seen with severe displacement of all three PMs (Fig.6.30). Combined displacement of the anterior, septal and posterior PMs resulted in regurgitation of 7.3 ± 3.0 mL.

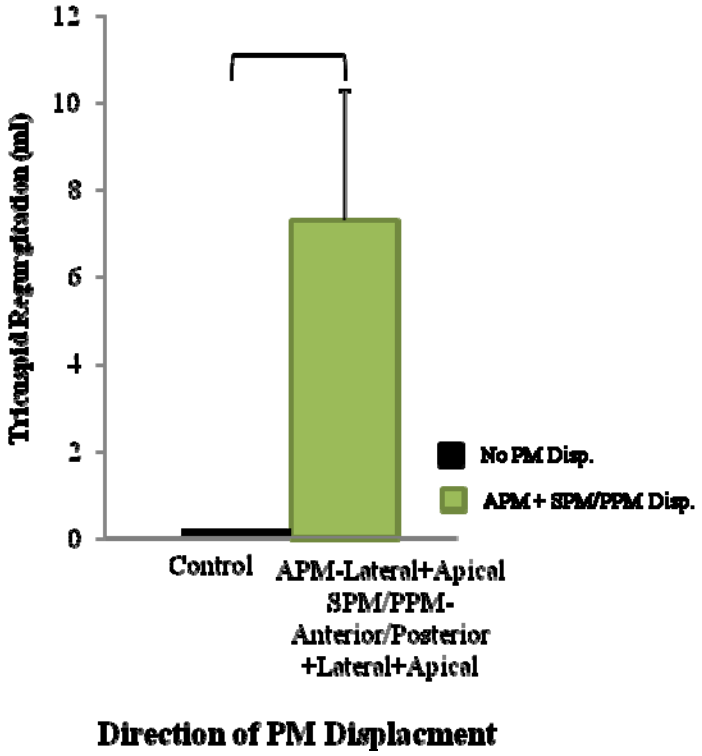

Figure 6.30: Tricuspid regurgitation as an effect of combined APM/SPM/PPM displacement with significance (* = $p \leq 0.05$), as compared to control, n = 8. Bar colors correspond to PM which was displaced: black (no displacement), green (APM/PPM/PPM).

With significant levels of TR observed with combined PM displacement, observations were made as to the effect on leaflet coaptation. A difference could be seen in the location of leaflet coaptation with the leaflets coapting more towards the anterior and posterior section of the annulus, away from the septal segment. This can be seen in the below images when compared to the control case (Fig. 6.31). Displacement of all PMs results in the septal leaflet covering more of the orifice. This is due to a restriction in the anterior and posterior leaflets, with anterior PM displacement and increased septal leaflet mobility towards the center of the annulus with septal and anterior PM displacement.

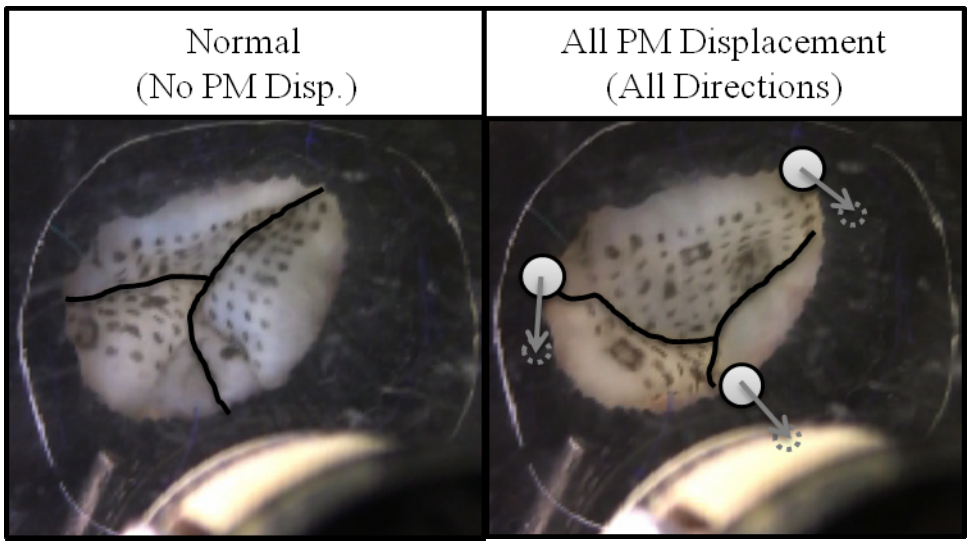

Figure 6.31: Image of valve with combined APM/SPM/PPM displacement. PM displacement shown with a dashed line, as compared to control position with a solid line.

While it could be shown that combined displacement of the APM (lateral and apical), SPM (anterior, lateral, apical) and PPM (posterior, lateral apical) resulted in significant TR, it was of interest to determine the role of a 3D saddle shape on TR. A significant difference ($p = 0.024$) was seen in the amount of TR when saddle and no saddle was compared with severe PM displacement (Fig. 6.32). In the case of severe PM displacement the presence of a 3D saddle resulted in a reduction in TR from 6.32 ± 7.28 with a flat saddle to 4.48 ± 7.12 mL with a saddle, for an approximate reduction of 1.40 ± 0.68 mL.

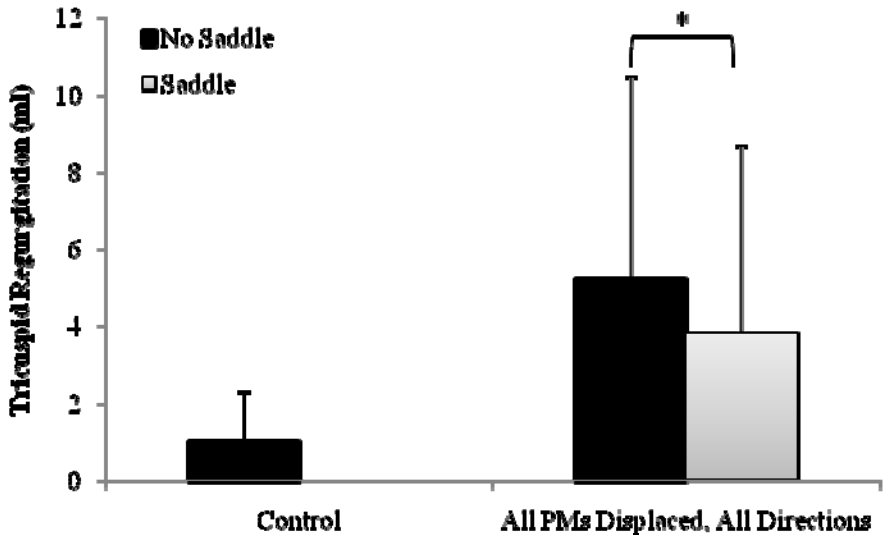

Figure 6.32: Plot of TR for control and all PMs displaced in all directions with (grey bar) and without a saddle (black bar). Significance shown as * = p ≤ 0.05.

6.2.2.3.2 Residual Leaflet Length

Next, RLL was then investigated to determine if the increase in TR could be explained with alterations in the leaflet mechanics. RLL was measured for all three leaflets as an effect of APM/SPM/PPM displacement in combined directions. Posterior RLL was the only leaflet which had a significant difference (p = 0.049, #) from control with PM displacement. Neither anterior (p = 0.087) nor septal (p = 0.147) RLL was affected by severe PM displacement (Fig. 6.33). Further investigation of RLL across leaflets with displacement of the APM (laterally and apically), SPM (anteriorlly, laterally and apically) and the PPM (posteriorlly, laterally, and apically) was conducted as this condition resulted in significant TR. RLL was significantly different across the three leaflets (p = 0.043). Specifically, septal leaflet RLL was significantly (p ≤ 0.05, *) different from the posterior leaflet with severe displacement of all PMs.

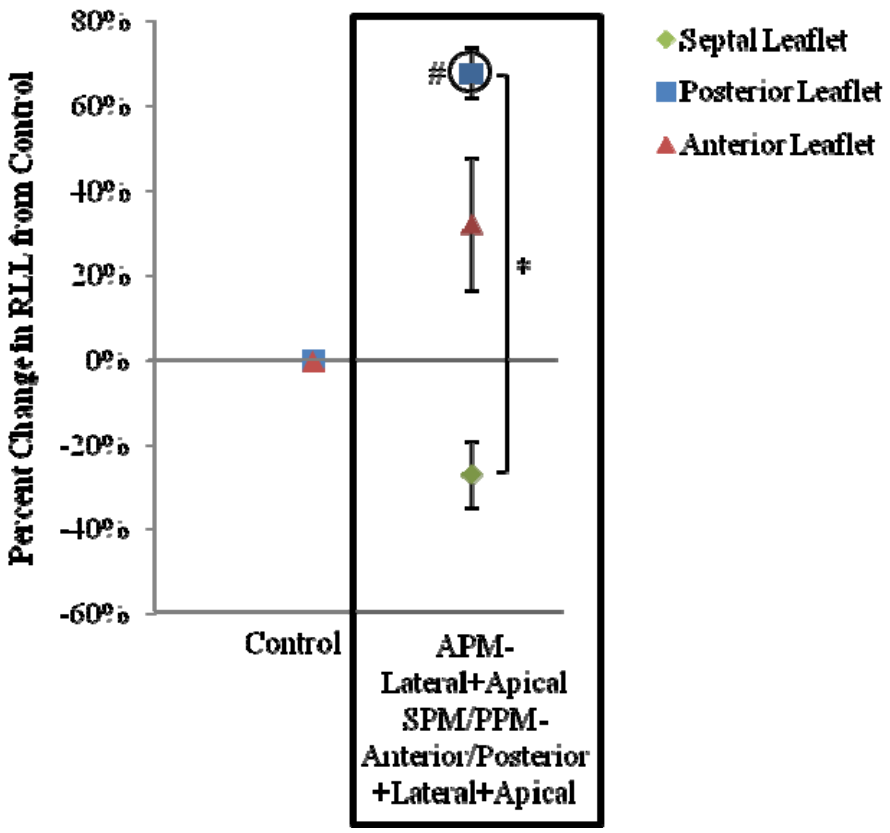

Figure 6.33: Percent change in RLL from control as an effect of APM/SPM/PPM displacement as shown for each individual leaflet: posterior (blue), anterior (red), and septal (green). Standard error is shown. Significance shown as *, $p \leq 0.05$ compared within PM displacement, #, $p \leq 0.05$ compared to control. Grey box highlights condition with significant TR.

6.2.2.3.3 Chordal Force

Next, the impact of multidirectional displacement of the anterior, septal and posterior PMs was investigated for the main chords originating from the APM and inserting into the anterior and posterior leaflets. Severe PM displacement resulted in a significant increase ($p = 0.020$) of force in the strut chord inserting into the posterior leaflet. No additional increases in forces were seen in chords inserting into the posterior leaflet: marginal ($p = 0.510$) and intermediate ($p = 0.824$). An increase in chordal force with severe displacement was not observed for any chords inserting into the anterior

leaflet: strut (p = 0.268), marginal (p = 0.430) and intermediate (p = 0.156). Results for chordal forces measurements are shown in figure 6.34.

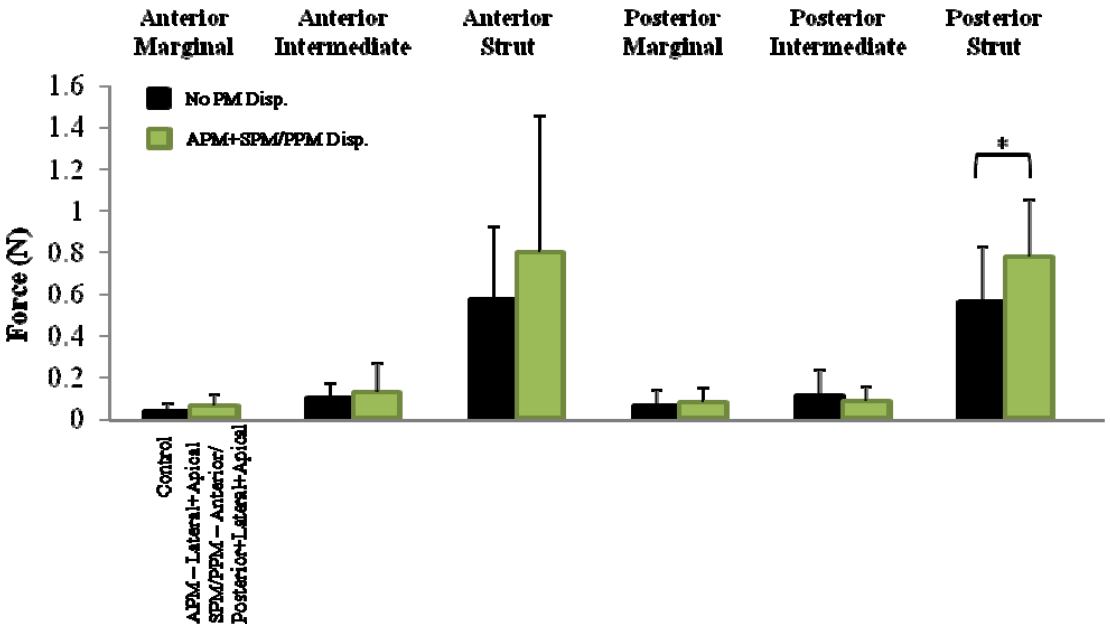

Figure 6.34: Differential chordal force measurements for chords originating from the APM/SPM/PPM. Bar colors correspond to PM which was displaced: black (no displacement), green (APM/SPM/PPM).

6.2.2.3.4 Leaflet Mobility

This final step for assessing the impact of isolated PM displacement on the tricuspid valve was to investigate changes in leaflet mobility with multidirectional displacement of the anterior, posterior and septal PM. Leaflet mobility was assessed through measurement of tenting height and tenting area on the septal/anterior, septal/posterior and anterior/posterior coaptation lines. A decrease in leaflet mobility was observed at the septal and anterior leaflet coaptation line as measured as a significant increase in tenting height (p = 0.017) and tenting area (p = 0.013). Additionally, a significant increase in tenting height (p = 0.013) and tenting area (p = 0.006) was observed across the septal and posterior leaflet coaptation line. While a decrease in leaflet

mobility was seen with coaptation lines of the septal leaflet, no change was seen the anterior and posterior leaflet coaptation line: tenting height ($p = 0.091$) and tenting area ($p = 0.088$) (Fig. 6.35). These results indicate that displacement of the APM (lateral and apical), SPM (anterior, lateral, apical) and PPM (posterior, lateral apical) affect only the mobility of the septal leaflet, while the anterior and posterior leaflets were unaffected.

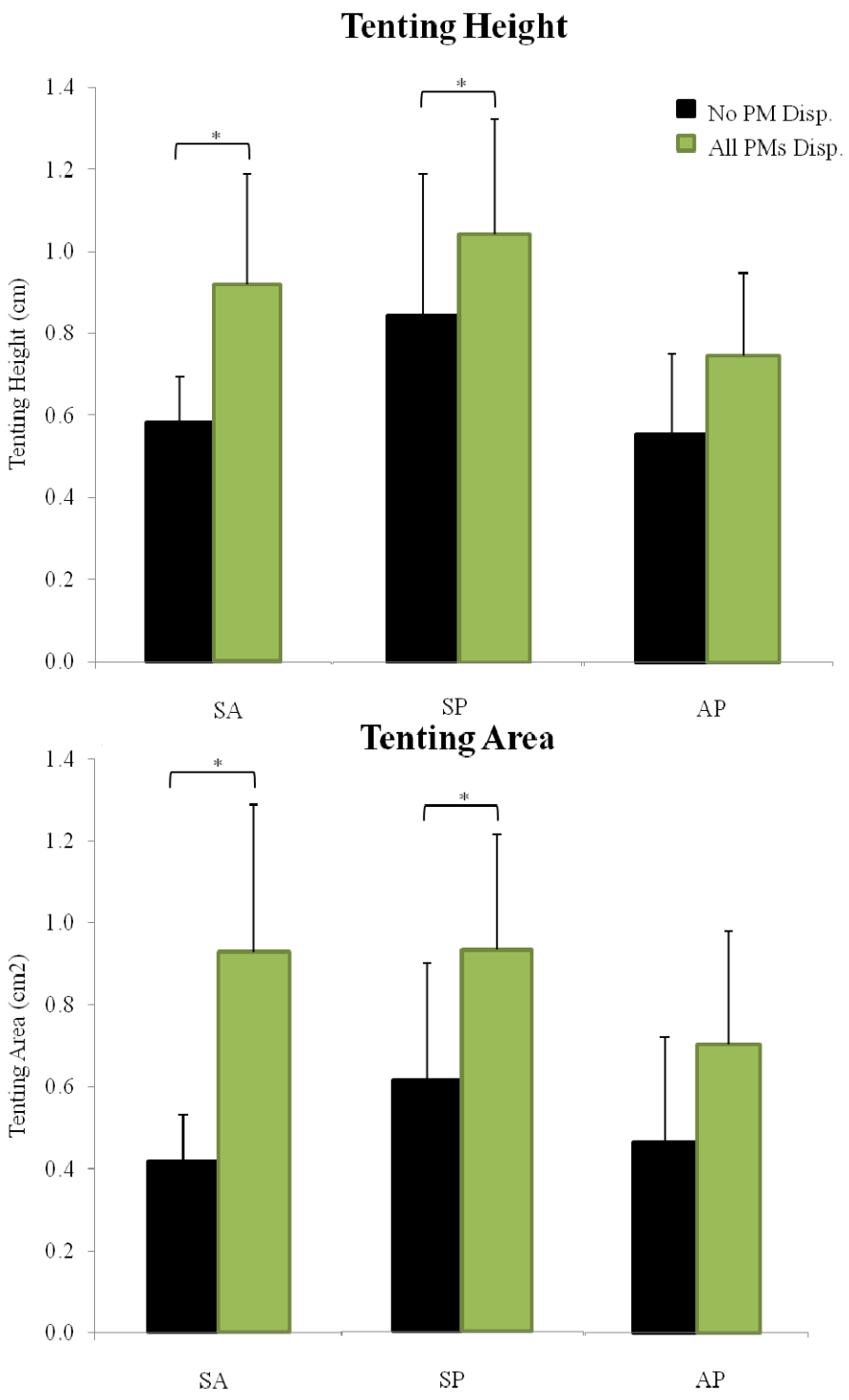

Figure 6.35: Peak systolic tenting height and area measurements are shown as an effect of APM/SPM/PPM displacement, along the coaptation lines: septal/anterior (SA), septal/posterior (SP), anterior/posterior (AP). Significance shown as *, $p \leq 0.05$.

6.2.3 Combined Annular Dilatation and Papillary Muscle Displacement

With investigation of isolated annular dilatation and PM displacement complete, the logical next step was to determine the impact of the combined effect of these alterations on the mechanics of the tricuspid valve. The next section will be divided in the same manner as the isolated PM displacement section, with annular dilatation combined with displacement of the anterior PM presented followed by combined septal and posterior PM displacement, and finally with the combination of all three PMs displaced.

6.2.3.1 Anterior Papillary Muscle Displacement

Annular dilatation was combined with displacement of the anterior PM from a control position laterally and apically, both separately and combined (Fig. 6.36). The APM was displaced by 10 mm in each direction from its control position.

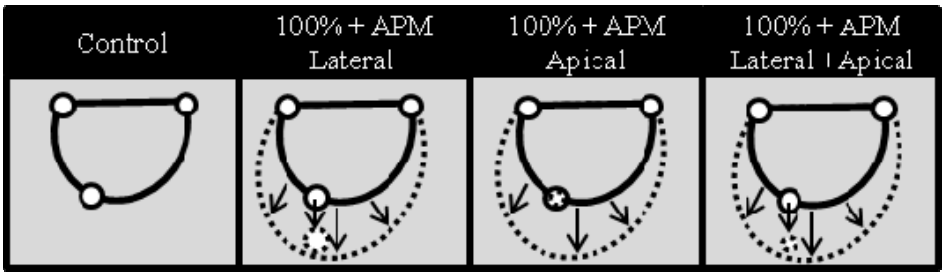

Figure 6.36: Control position of PMs along with directions of APM displacement. Control position is shown with a solid line with displaced and dilated positions shown with a dashed line. Note: Apical displacement is shown as displaced into the image, away from the annulus, as a smaller circle.

6.2.3.1.1 Hemodynamics

As dilatation alone resulted in significant TR beyond 40% dilatation, it was of interest to determine if PM displacement further increased the amount of TR. No significant increase in TR from isolated annular dilatation when combined with APM displacement (laterally, apically or combined) were observed (Fig. 6.37). APM

displacement only played a role in the creation of TR without the presence of annular dilatation as reported previously.

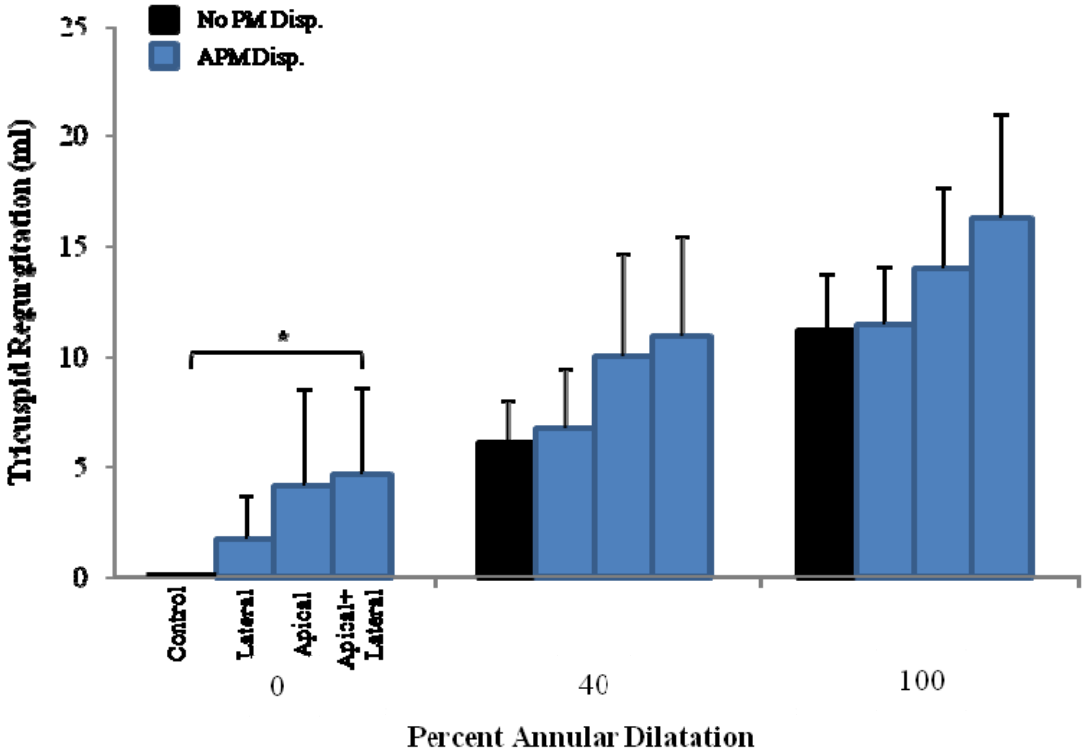

Figure 6.37: Tricuspid regurgitation as an effect of APM displacement with significance (* = $p \leq 0.05$), as compared to control, n = 8. Bar colors correspond to PM which was displaced: black (no displacement), blue (APM).

As was seen with isolated dilatation, in the combined case, the anterior and posterior leaflets covered a majority of the orifice as they attached to the sections of the annulus which were dilated. Similar coaptation characteristics as observed with isolated APM displacement were seen in the combined case, with apical displacement restricting leaflet mobility and resulting in a more central coaptation region (Fig. 6.38).

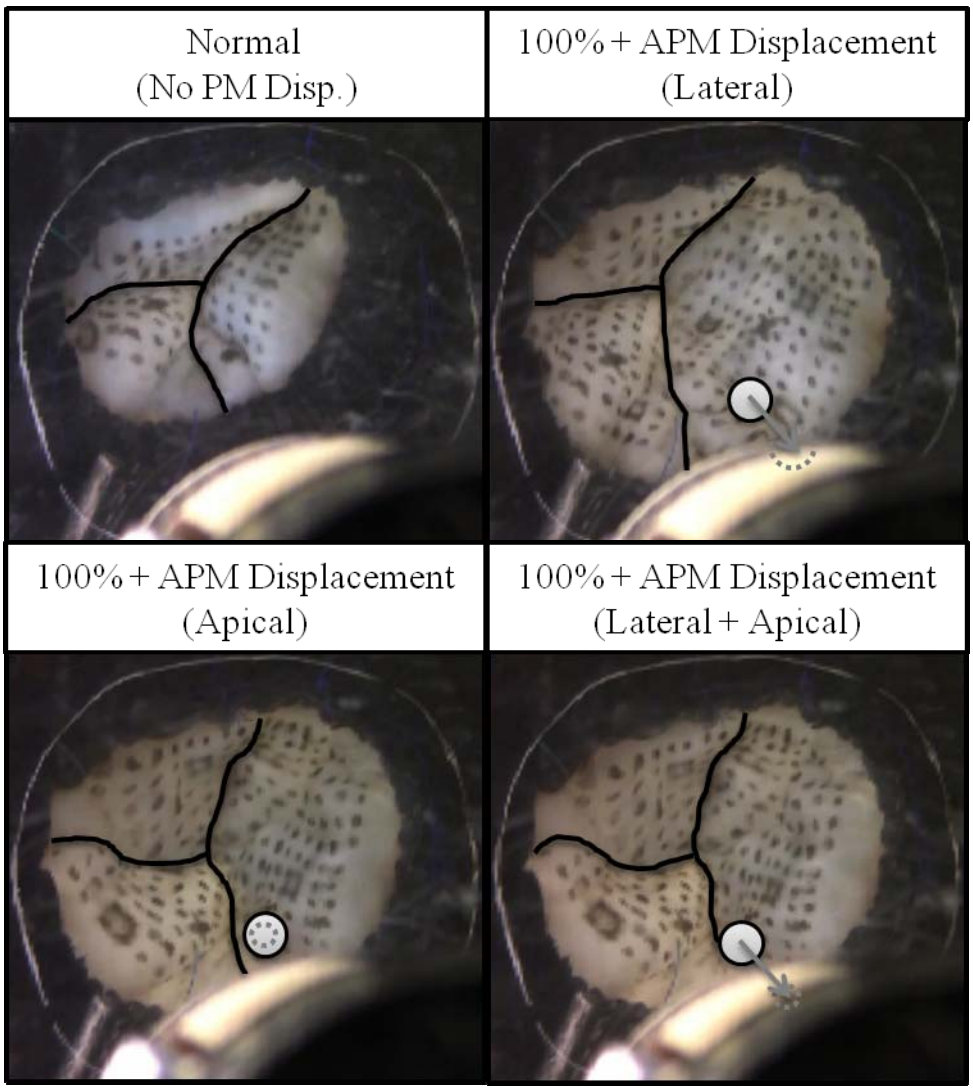

Figure 6.38: Image of valve with combined 100% annular dilatation and APM displacement. PM displacement shown with a dashed line, as compared to control position solid line.

6.2.3.1.2 Residual Leaflet Length

With no significant change in TR with combined annular dilatation and APM displacement, it was not expected that there would be significant alterations in RLL. A combination of 40% dilatation and displacement of the APM did not have a significant impact on RLL for any leaflet: anterior leaflet ($p = 0.051$), posterior ($p = 0.566$) or septal ($p = 0.506$) leaflets (Fig. 6.39). However, investigation of combined 100% annular

dilatation and APM displacement had a significant impact on anterior RLL ($p = 0.002$) for all directions displaced. This was not significant for the posterior ($p = 0.487$) and the septal ($p = 0.320$) leaflets. A difference in RLL was observed with APM displacement and combined annular dilatation, however, it was found to have less of a reduction in RLL as compared to dilatation alone.

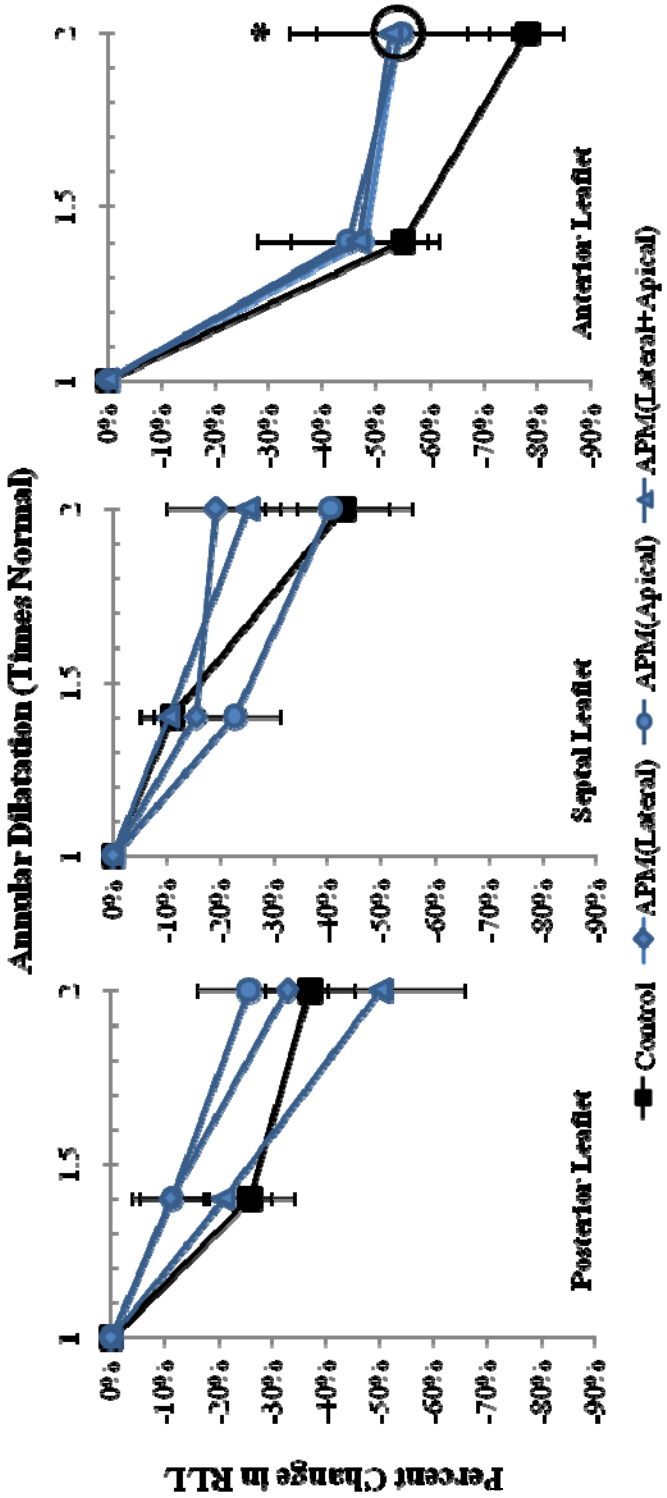

Figure 6.39: Percent change in RLL from control (y axis) as an effect of annular dilatation (x axis) for APM displacement for all individual leaflets. Standard error is shown. * = $p \leq 0.05$ as compared to control for same level of dilatation.

6.2.3.1.3 Chordal Force

Next, it was of interest to determine if chordal forces were redistributed with combined annular dilatation and APM displacement. As the forces were increased on all chords with isolated annular dilatation but not with isolated APM displacement it was of interest to see the results of the combined case. Combined annular dilatation of 100% and APM displacement had a significant impact on forces measured on all main APM chords inserting into the anterior leaflet: marginal ($p = 0.016$), intermediate ($p = 0.006$), strut ($p = 0.010$). Both isolated lateral and combined apical/lateral directional displacement of the APM resulted in significant increases ($p \leq 0.05$) in chordal force as compared to normal for the anterior chords. APM displacement had a significant impact on the posterior strut ($p = 0.032$) chord, but not for the posterior marginal ($p = 0.063$) or intermediate ($p = 0.210$) chords. Forces measured on strut chords inserting into the posterior leaflet had a significant increase in force only with apical displacement of the APM with 100% annular dilatation. Thus, combined annular dilatation and apical displacement of the APM only affected strut chords. Additionally, lateral displacement both isolated and combined with apical displacement affected only the chords inserting into the anterior leaflet. Chordal force measurements are shown in the below figure 6.40.

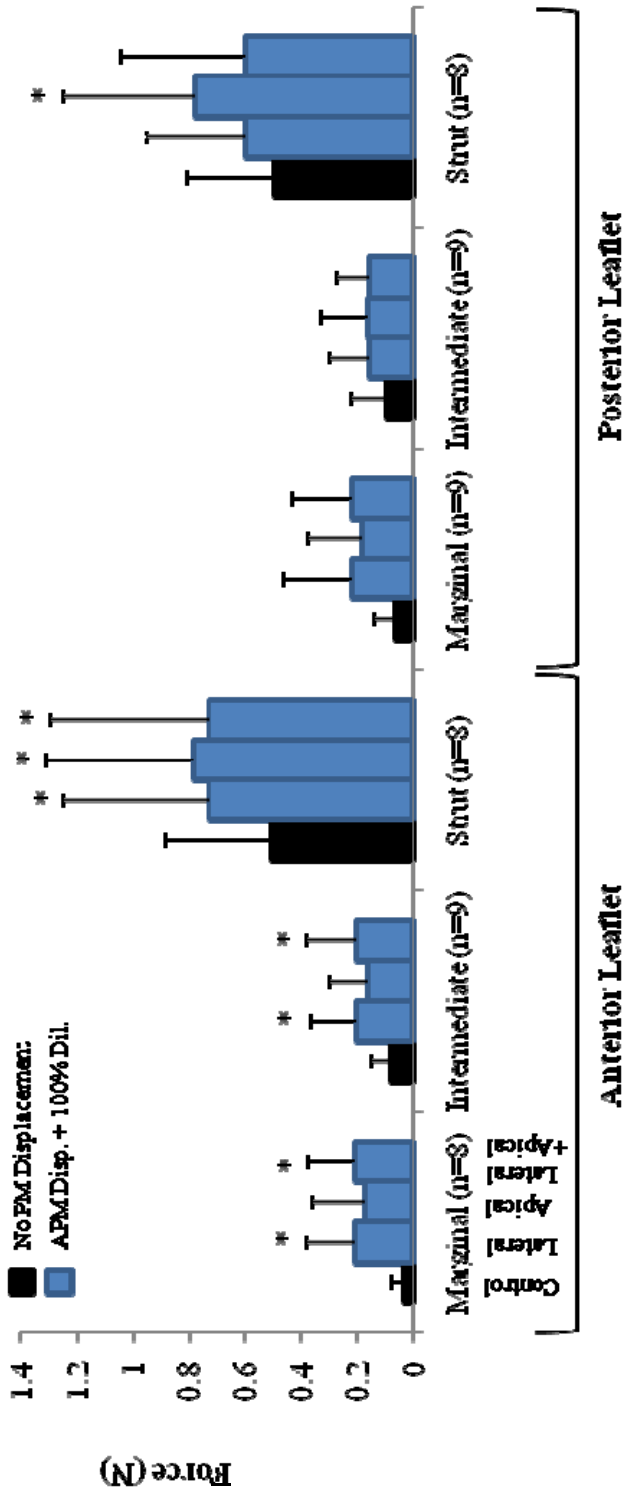

Figure 6.40: Differential chordal force measurements for chordae originating from the APM. Bar colors correspond to PM which was displaced: black (no displacement), blue (APM).

6.2.3.1.4 Leaflet Mobility

Tenting height and tenting area were then measured to assess the impact of combined annular dilatation of 100% and APM displacement on leaflet mobility. Leaflet mobility was measured across the coaptation of the leaflets: septal/anterior, septal/posterior and anterior posterior. Combined dilatation and APM displacement had a significant impact on tenting height ($p = 0.000$) and tenting area ($p = 0.000$) on the coaptation line of the anterior and posterior leaflets. There was no difference seen at the SA coaptation line in tenting height ($p = 0.619$) or tenting area ($p = 0.128$). Additionally, no difference was seen at the SP coaptation line for tenting height ($p = 0.935$) or tenting area ($p = 0.265$). It was found that combined annular dilatation and displacement of the APM apically, both isolated and combined with lateral displacement, resulted in significant increase ($p \leq 0.05$) in tenting height and area at the AP coaptation line (Fig. 6.41). Thus it can be stated that the mobility of the anterior and posterior leaflets was restricted in this case.

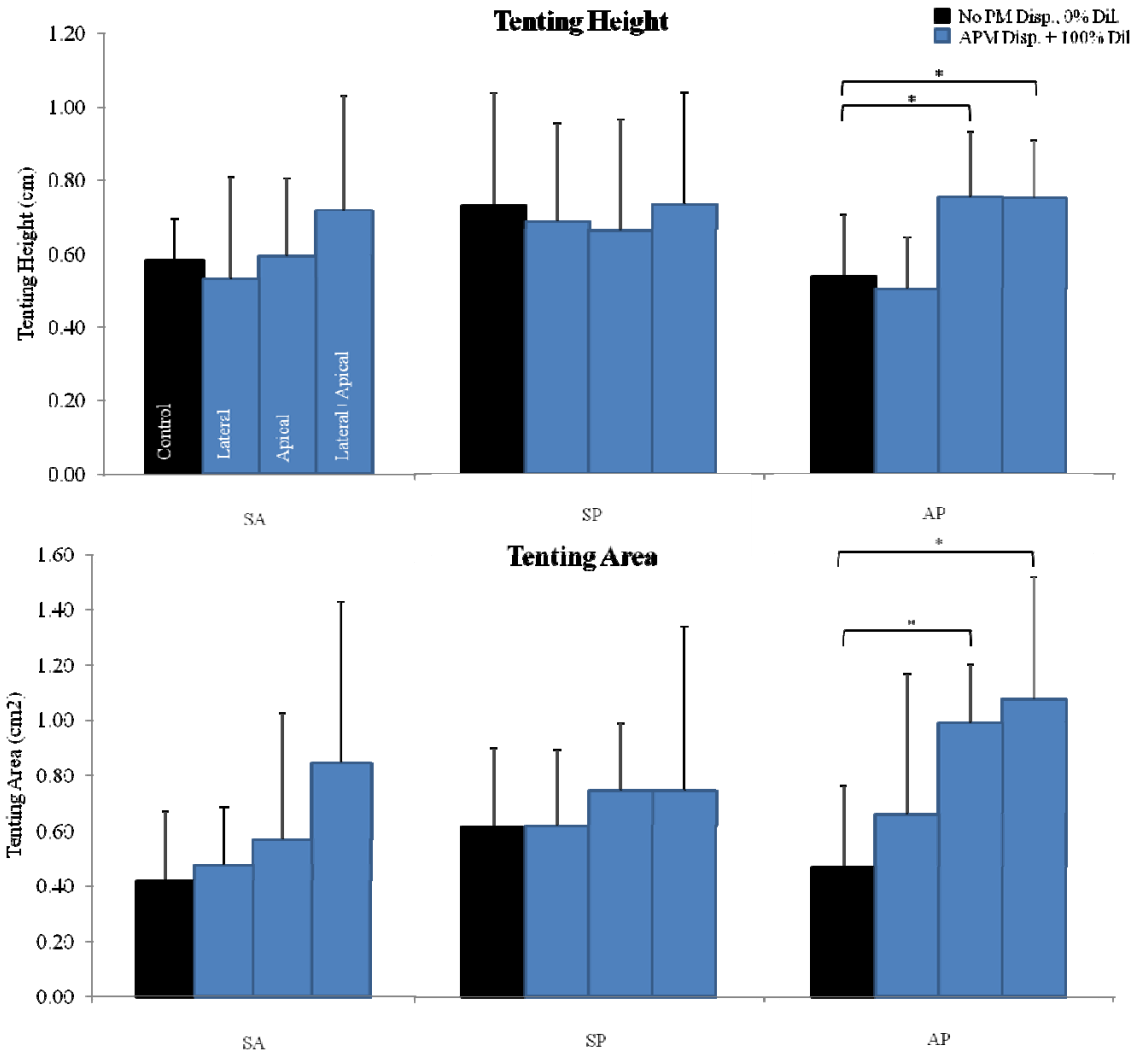

Figure 6.41: Peak systolic tenting height and area measurements are shown as an effect of APM displacement, along the coaptation lines: septal/anterior (SA), septal/posterior (SP), anterior/posterior (AP). Significance shown as *, $p \leq 0.05$.

6.2.3.2 Septal and Posterior Papillary Muscle Displacement

The septal and posterior PM were displaced together as they are both located on the septum and would be expected to move together in a similar direction. The septal PM was displaced from a control position anteriorly, laterally and apically, both separately and combined. Likewise the posterior PM was displaced from a control position

posteriorly, laterally and apically, both separately and combined (Fig. 6.42). Each PM was displaced by 10 mm from its control position.

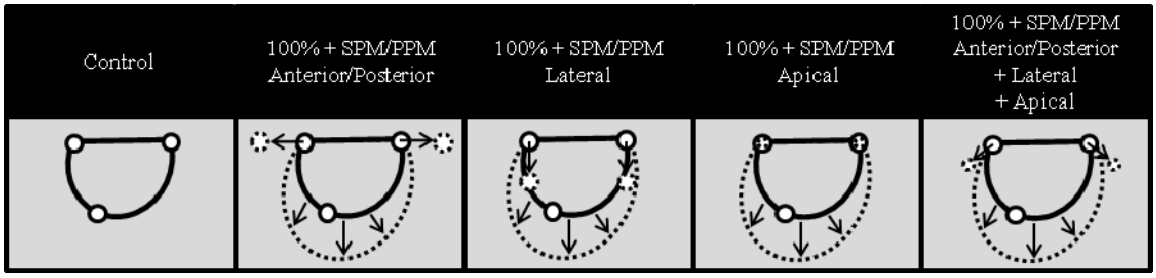

Figure 6.42: Control position of PMs along with directions of SPM/PPM displacement. Control position is shown with a solid line with annular dilatation and displaced positions shown with a dashed line. Note: Apical displacement is shown as displaced into the image, away from the annulus, as a smaller circle.

6.2.3.2.1 Hemodynamics

Once again, as dilatation alone resulted in significant TR beyond 40% dilatation, it was of interest to determine if displacement of PMs on the septum further increased the amount of TR. No significant increase from TR levels as observed with dilation was seen with the addition of simultaneous displacement of the SPM (anteriorly, laterally, apically or combined) and PPM (posteriorly, laterally, apically or combined) (Fig. 6.43). Displacement of the septal and posterior PMs only played a role in the creation of TR without the presence of annular dilatation as discussed previously. As was discussed in section 6.2.2.2.1, a statistical analysis could not be performed for the case of lateral displacement when combined with 40% dilatation as the data were not normally distributed and resulted in two distinct groups, valves ($n = 3$) with high levels TR (22.5 ± 5.6 mL) and valves($n = 5$) with insignificant levels (1.9 ± 1.9 mL). However, 100% dilated condition was normally distributed. Thus, lateral displacement was statistically assessed when combined with 100% but was not significant ($p \geq 0.05$).

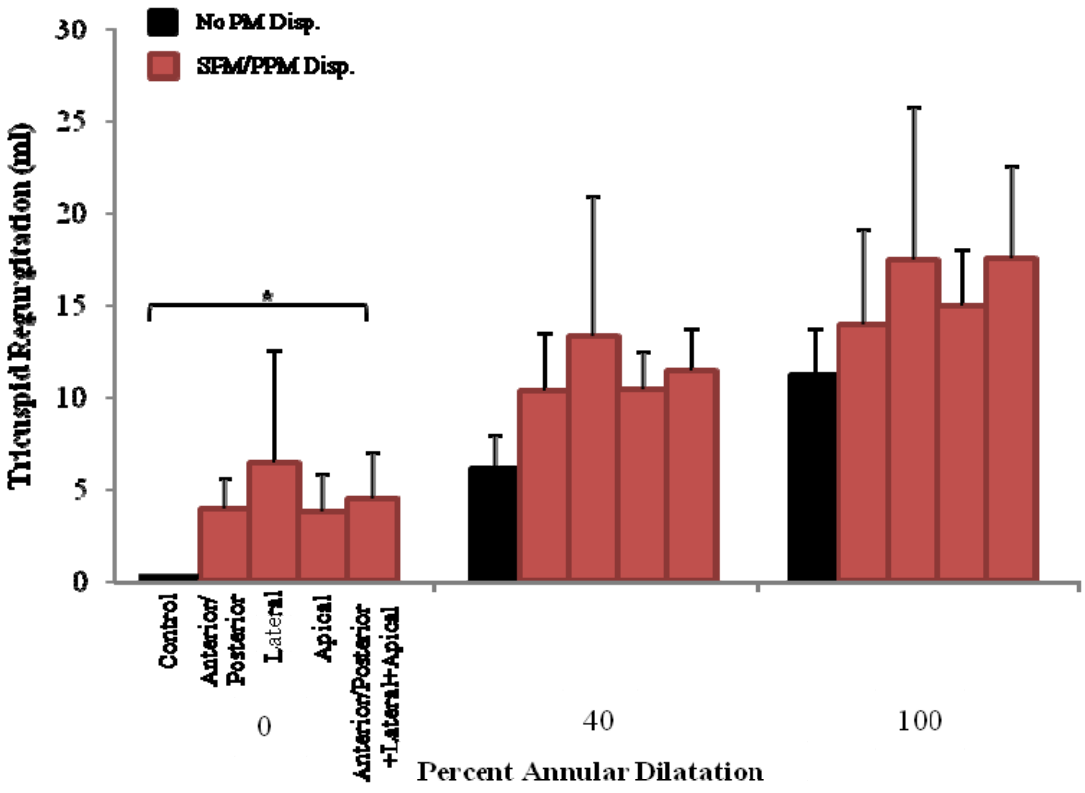

Figure 6.43: Tricuspid regurgitation as an effect of SPM/PPM displacement with significance (* = $p \leq 0.05$), as compared to control, n = 8. Bar colors correspond to PM which was displaced: black (no displacement), red (SPM/PPM).

As with all other conditions tested, observations were made as to the effect of combined annular dilatation and septal and posterior PM displacement on leaflet coaptation. Aside from the increase in surface area of the anterior and posterior leaflets with annular dilatation, differences in leaflet coaptation were only visible with lateral displacement of the septal and posterior PMs. When the PMs were displaced only laterally, the coaptation line was towards the anterior/posterior sections of the annulus, thus the septal leaflet covered the majority of the orifice. When the septal and posterior PMs were displaced in a combined direction (anterior/posterior, lateral, apical) coaptation was more towards the center of the annulus as compared to the normal and annular dilated conditions (6.44). The coaptation mimicked a combination of the isolated cases,

with lateral displacement of the anterior and posterior PMs moving the coaptation line away from the septum and dilatation increasing the surface area of the anterior and posterior leaflets.

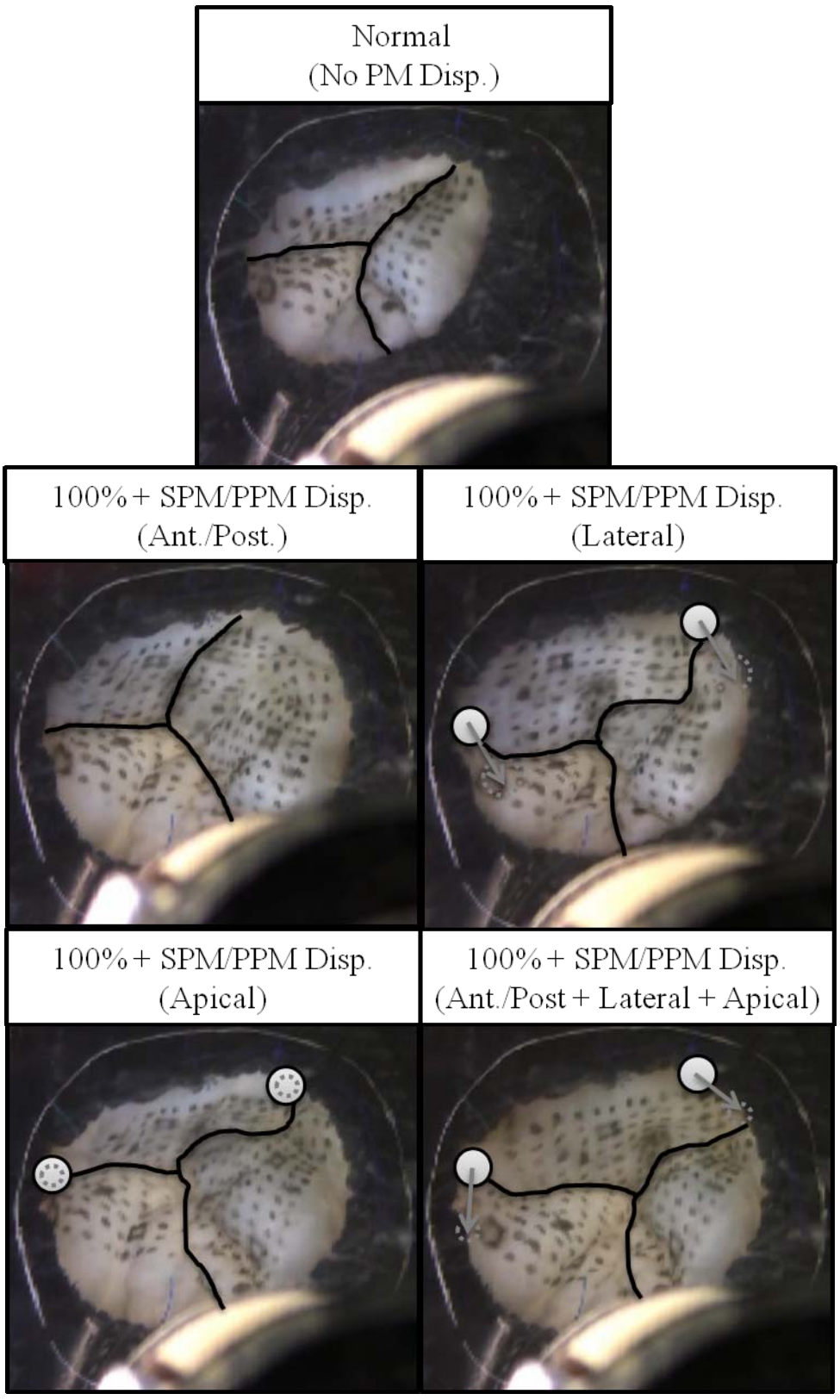

Figure 6.44: Image of valve with isolated SPM/PPM displacement. PM displacement shown with a dashed line, as compared to control position with a solid line.

6.2.3.2.2 Residual Leaflet Length

While no significant increases were observed with the addition of septal and posterior PM displacement to annular dilatation, it was still necessary to assess RLL as changes were observed in leaflet coaptation. RLL was measured for all three leaflets as an effect combined annular dilatation and SPM/PPM displacement in individual (anterior/posterior, lateral and apical) and combined directions. A combination of 40% dilatation and displacement of the SPM/PPM did not have a significant impact on RLL for any leaflet: anterior leaflet ($p = 0.051$), posterior ($p = 0.497$) leaflet. While SPM/PPM displacement had a significant effect on the septal ($p = 0.031$) leaflet mobility, further investigation showed there was no difference when disease conditions where compared to control, thus the difference was between the disease conditions. This is evident in the below figure where the RLL is much different with apical displacement as compared to control and the other disease conditions. Additionally, investigation of the combination of 100% annular dilatation and SPM/PPM displacement did not have a significant impact on RLL for any of the leaflets: anterior ($p = 0.126$), posterior ($p = 0.227$) and septal ($p = 0.139$) (Fig. 6.45).

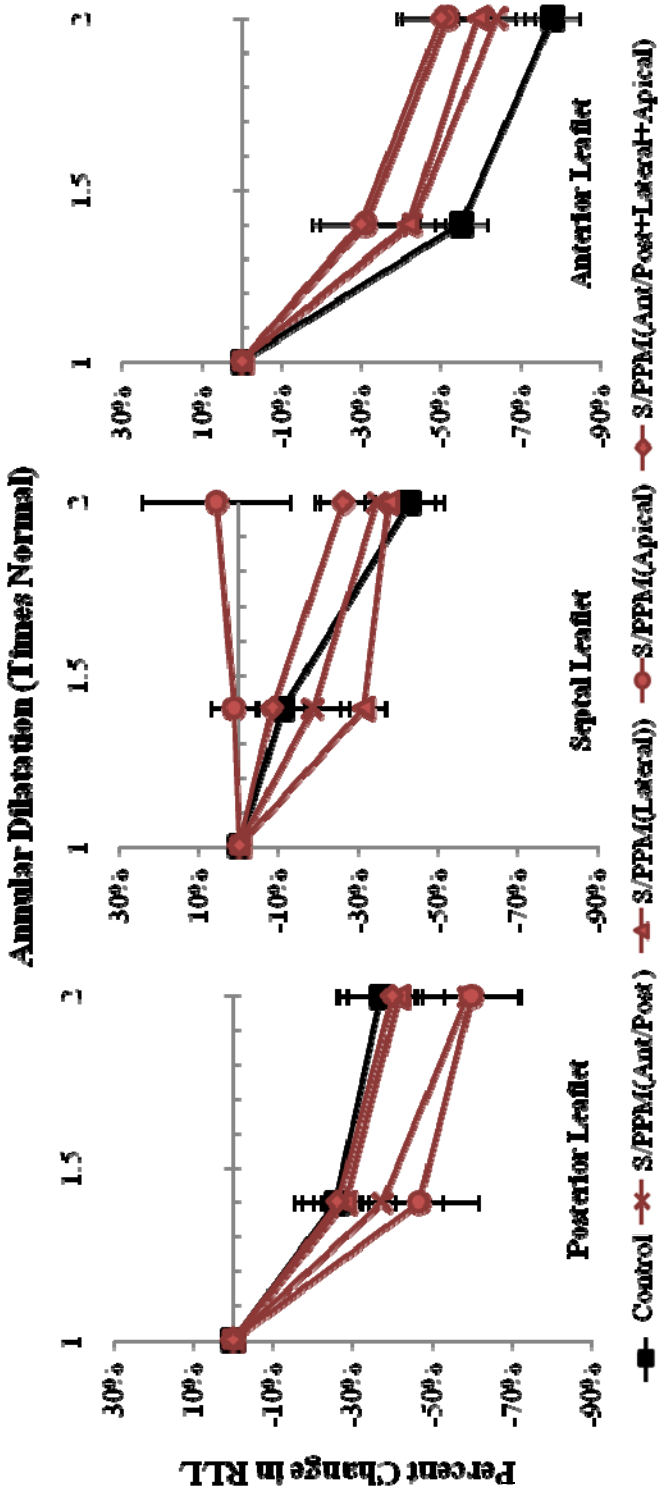

Figure 6.45: Percent change in RLL from control (y axis) as an effect of annular dilatation (x axis) for S/PPM displacement for all individual leaflets. Standard error is shown.

6.2.3.2.3 Chordal Force

Chordal force was not measured with combined annular dilatation and displacement of the septal and posterior PMs in any direction. The rational is the same as stated for isolated displacement of the septal and posterior PM, that since the force transducers were mounted on the APM, it was assumed that displacement of the SPM and PPM would not affect forces on chords originating from the APM. However, displacement of the SPM and PPM was investigated in conjunction with APM displacement, with all three PMs displaced in the combined directions with combined annular dilatation. See section 6.2.2.3.3 for detailed results.

6.2.3.2.4 Leaflet Mobility

Lastly, the impact of combined annular dilatation and septal and posterior PM displacement on leaflet mobility was assessed through measurement of tenting height and tenting area on the three coaptation lines: septal/anterior, septal/posterior, and anterior/posterior. A significant difference was observed at the septal/anterior coaptation line for both tenting height ($p = 0.004$) and tenting area ($p = 0.002$). It was determined that apical and combined (anterior/posterior, lateral, apical) directional displacement resulted in significant increases ($p \leq 0.05$) in both tenting height and area. No difference was seen in either tenting height ($p = 0.433$) or tenting area ($p = 0.834$) across the anterior and posterior coaptation line. While septal and posterior PM displacement had a significant impact on both tenting height ($p = 0.034$) and tenting area ($p = 0.013$), further investigation showed there was no difference when disease conditions where compared to control, thus the difference was between the disease conditions. This is better understood by visualizing the data in figure 6.46. It is evident that while the directions

measured in the S/A line did not vary from control they may have varied between the different directions of PM displacement, with lateral displacement appearing to be smallest. Results for leaflet mobility measurements can been seen in the below figure (Fig. 6.46). Displacement of the septal and posterior PMs in both apical and combined (posterior/anterior, lateral and apical) directions decrease leaflet mobility, at the coaptation line of the septal and anterior leaflets.

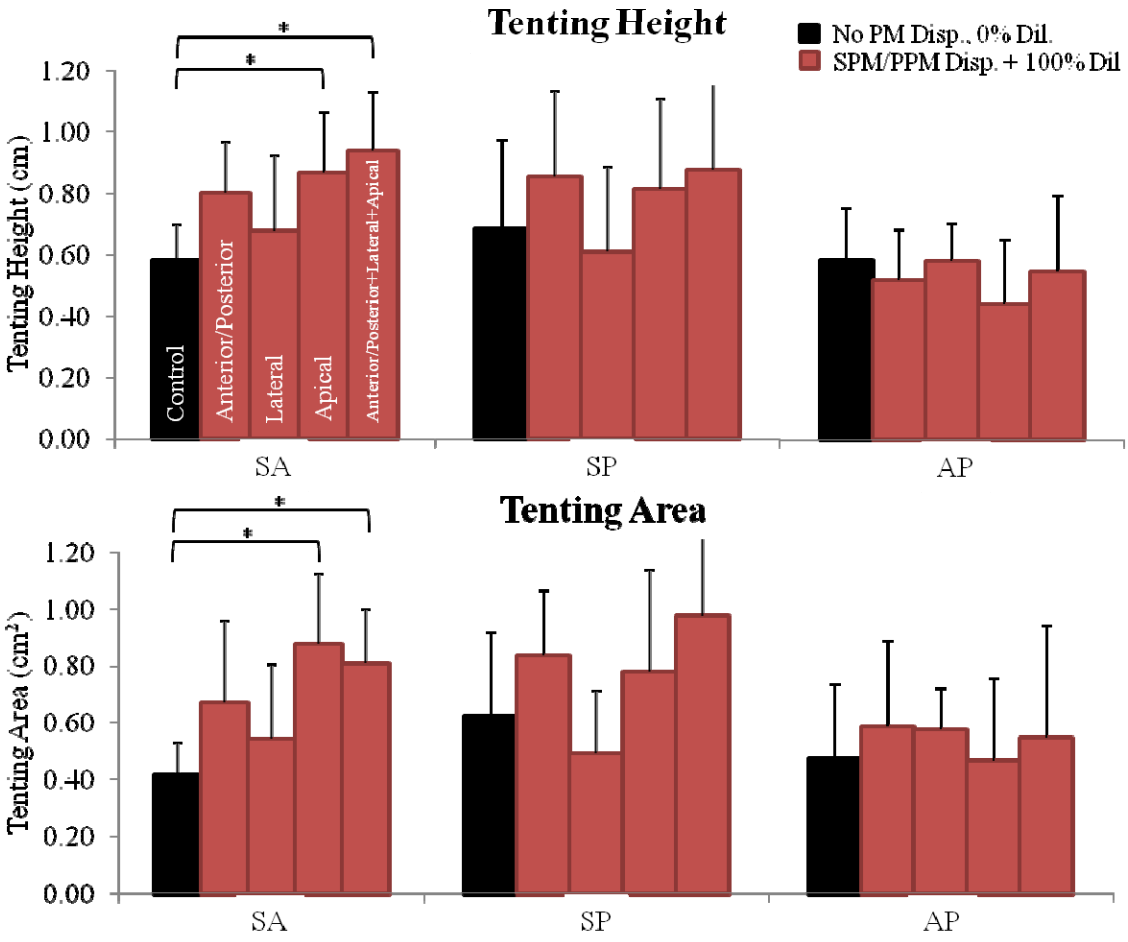

Figure 6.46: Peak systolic tenting height and area measurements are shown as an effect of combined 100% annular dilatation and SPM/PPM displacement, along the coaptation lines: septal/anterior (SA), septal/posterior (SP), anterior/posterior (AP).

6.2.3.3 Combined Anterior, Septal and Posterior Papillary Muscle Displacement

Finally, a severe PM displacement condition was created in which all three PMs were displaced simultaneously with combined directions and implemented in conjunction with annular dilatation. This condition was the most severe simulation of disease in the model. For combined PM displacement, the APM was displaced with combined lateral and apical directions with the SPM in an anterior, lateral and apical direction while the PPM was displaced in a posterior, lateral and apical direction (Fig. 6.47). Each PM was displaced by 10 mm from its control position.

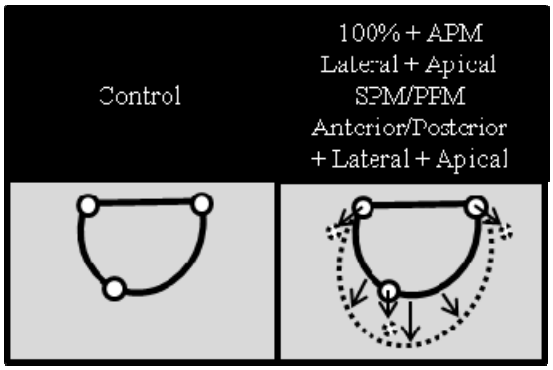

Figure 6.47: Control position of PMs along with directions of APM/SPM/PPM displacement. Control position is shown with a solid line with annular dilatation and displaced positions shown with a dashed line. Note: Apical displacement is shown as displaced into the image, away from the annulus, as a smaller circle.

6.2.3.3.1 Hemodynamics

When combined, both annular dilatation ($p = 0.000$) and PM displacement ($p = 0.000$) had a significant effect on TR as compared to annular dilatation alone. Severe PM displacement, all PMs displaced in all directions, was the only displacement which resulted in further increases ($p \leq 0.05$) in TR from annular dilatation, of 40% and 100%. The largest levels of TR were reached at 100% dilatation with all PMs displaced in all directions (19.6±5.7 mL, n = 8) (Fig. 6.48).

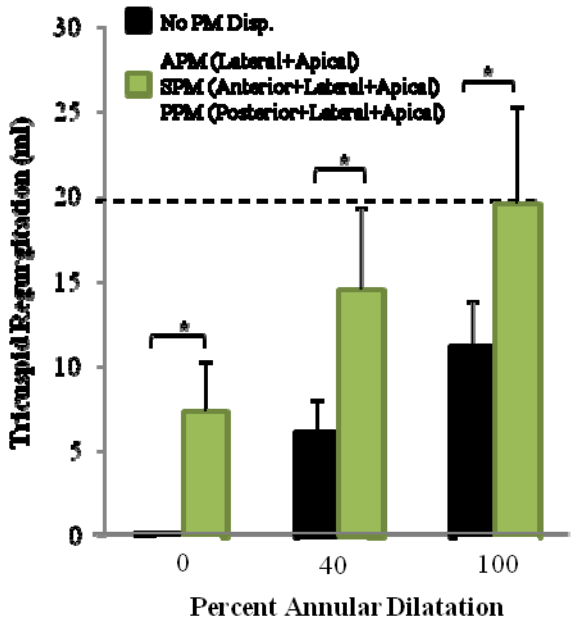

Figure 6.48: Tricuspid regurgitation as an effect of combined APM/SPM/PPM displacement with significance (* = $p \leq 0.05$), as compared to control, n = 8. Bar colors correspond to PM which was displaced: black (no displacement), green (APM/PPM/PPM).

While it could be shown that annular dilatation of 40% and 100% and combined displacement of the APM (lateral and apical), SPM (anterior, lateral, apical) and PPM (posterior, lateral apical) resulted in significant TR, it was unknown as to the role of a 3D saddle shape on TR in this disease state. No significant difference was seen in the amount of TR when saddle and no saddle were compared with combined annular dilatation and severe PM displacement (Fig. 6.49).

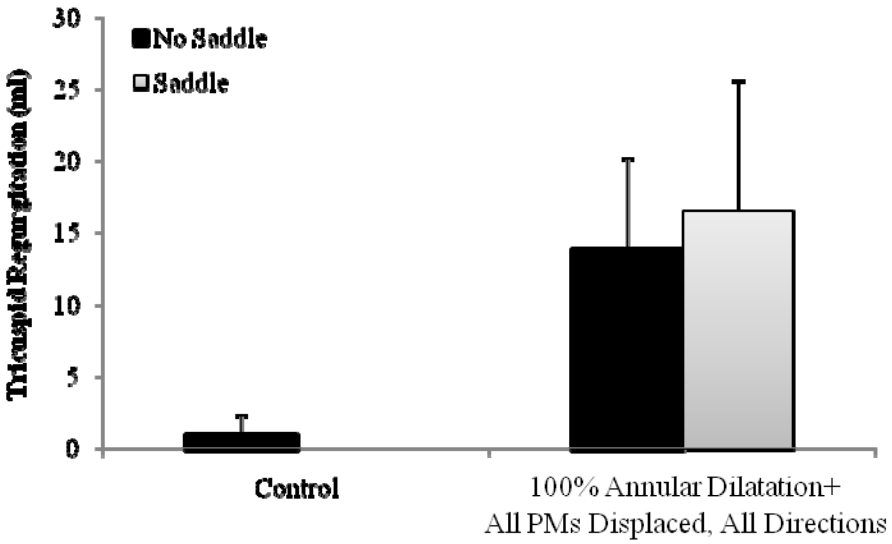

Figure 6.49: Plot of TR for control and 100% dilatation with all PMs displaced in all directions with and without a saddle. No significance was found between saddle and no saddle.

Malcoaptation occurred at the junction of the three leaflets for all combined disease conditions, as was expected as annular dilatation alone resulted in malcoaptation. The largest levels of TR, where seen when the annulus was dilated by 100% and all PMs were displaced in all directions. In this condition, the area of no coaptation was located more towards the anterior and posterior annulus segments. A large hole can be seen where the three leaflets join in the control case for the diseased case (Fig. 6.50).

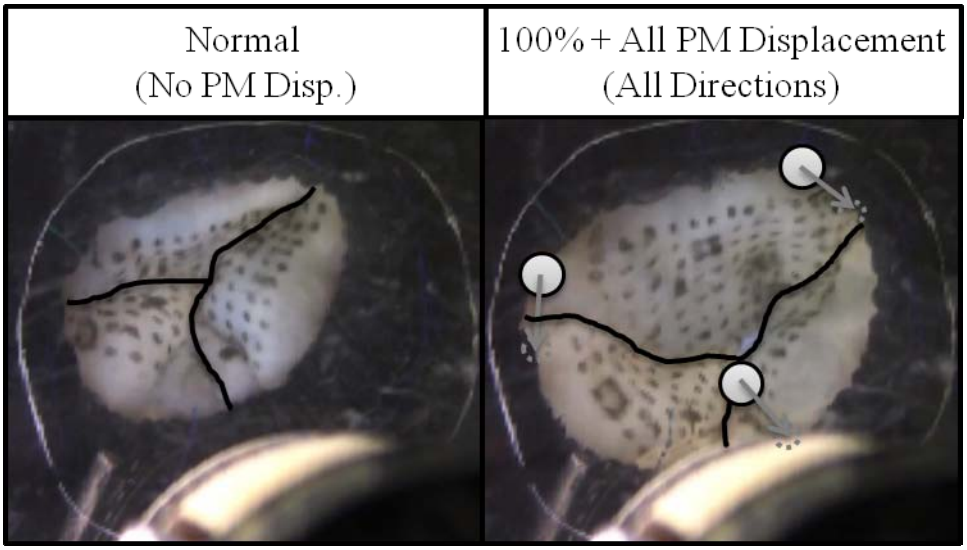

Figure 6.50: Image of valve with 100% dilatation and combined APM/SPM/PPM displacement. PM displacement shown with a dashed line, as compared to control position with a solid line.

6.2.3.3.2 Residual Leaflet Length

Next, RLL was assessed to determine if any information could be gained from the assessment in changes in the amount of leaflet available for coaptation, as to why significant TR occurred. RLL was measured for all three leaflets as an effect of combined annular dilatation and APM/SPM/PPM displacement in combined directions. It was first determined if RLL for an individual leaflet varied with disease as compared to control. Next, within a given dilatation, 40% and 100%, RLL of the disease case was compared to control. A significant difference in RLL was only observed for the anterior leaflet with 40% ($p = 0.004$) and 100% ($p = 0.012$) dilatation. No significance difference was seen for 40% dilatation for the posterior ($p = 0.629$) and septal ($p = 0.361$) with the same observations for 100% dilatation for the posterior ($p = 0.531$) and septal ($p = 0.519$) leaflets (Fig. 6.51).

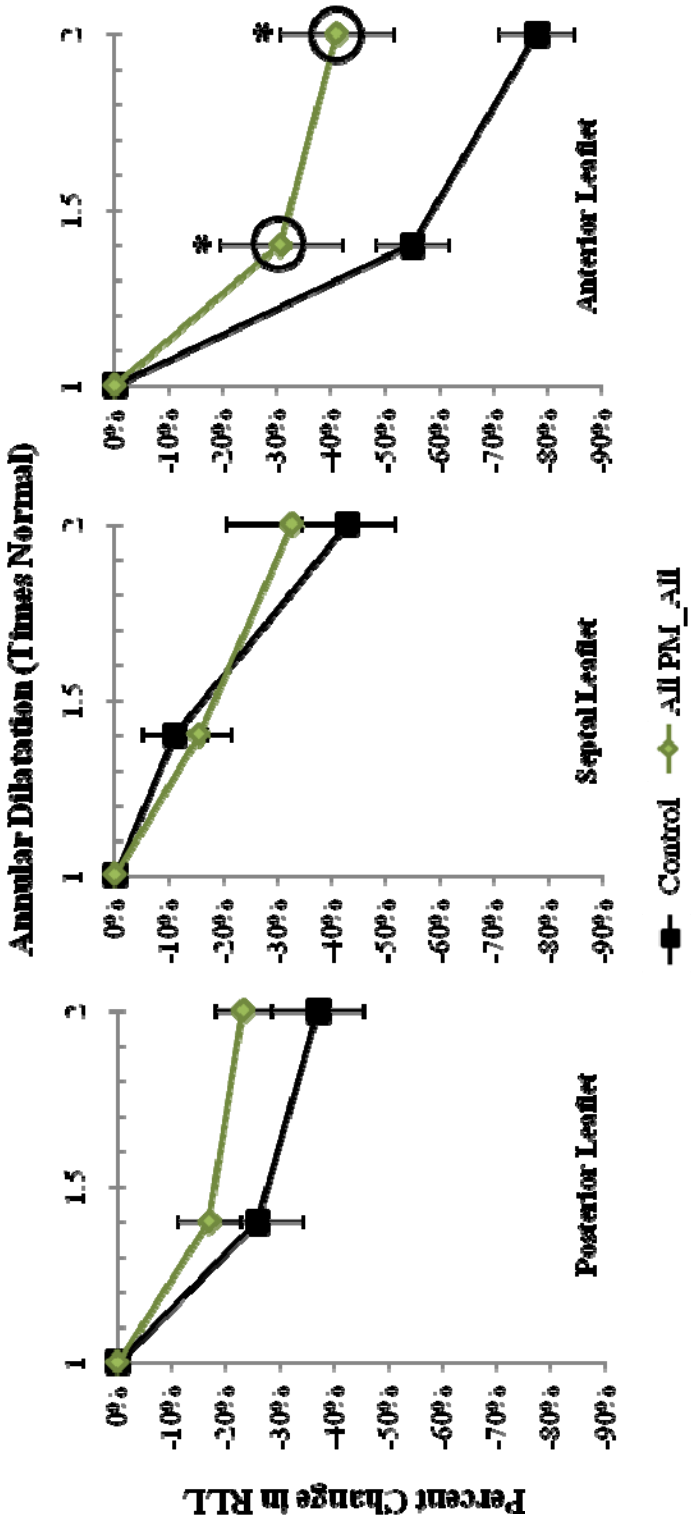

Figure 6.51: Percent change in RLL from control (y axis) as an effect of annular dilatation (x axis) for All PM displacement for all individual leaflets. Standard error is shown. * = $p \leq 0.05$ as compared to control for same level of dilatation.

6.2.3.3.3 Chordal Force

Next, the impact of combined annular dilatation and displacement of the anterior (lateral and apical), septal (anterior, lateral and apical) and posterior (posterior, lateral, apical) PMs was investigated for the main chords originating from the APM and inserting into the anterior and posterior leaflets. Combined annular dilatation and severe PM displacement resulted in a significant increase in force for strut chords inserting into the anterior ($p = 0.047$) and posterior ($p = 0.013$) leaflets. Displacement of all PMs and combined annular dilatation did not have an impact on chordal force for the anterior marginal ($p = 0.0.68$), anterior intermediate ($p = 0.103$), posterior marginal ($p = 0.117$), and posterior intermediate ($p = 0.209$) chords. Results for chordal forces measurements are shown in figure 6.52.

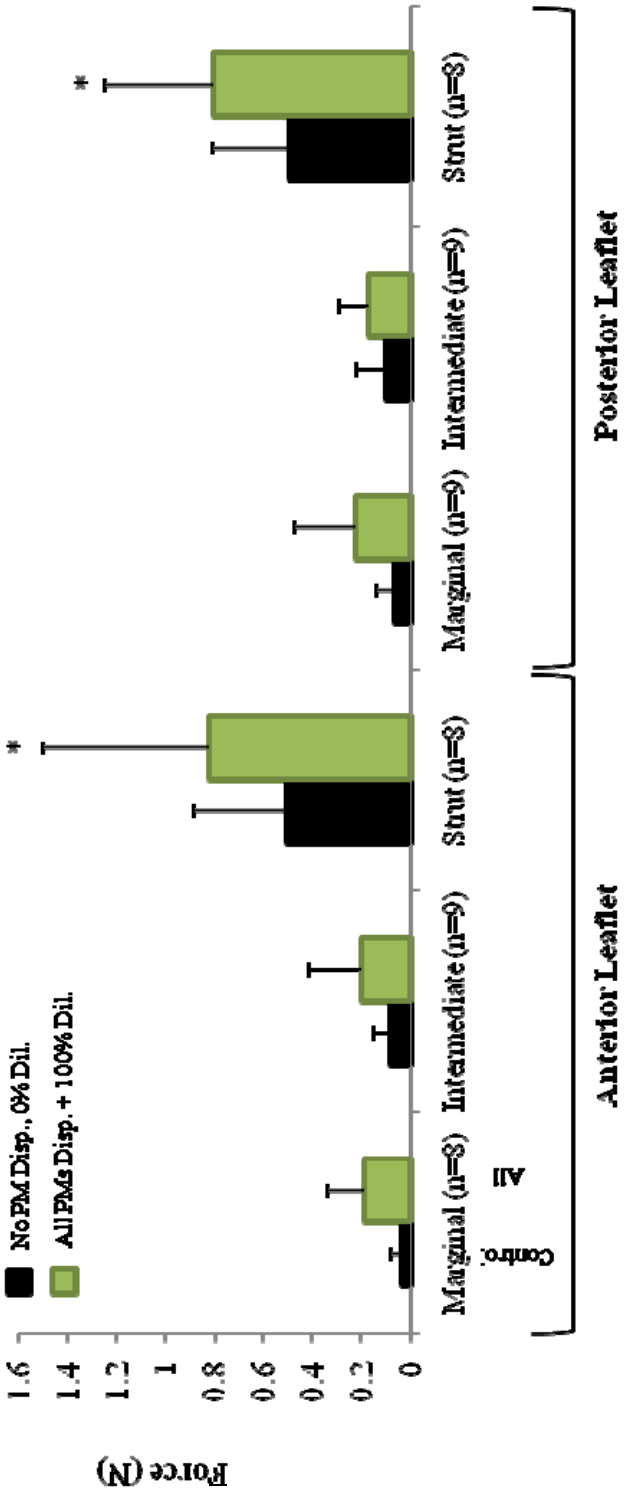

Figure 6.52: Differential chordal force measurements for chordae originating from the APM/SPM/PPM. Bar colors correspond to PM which was displaced: black (no displacement), green (APM/SPM/PPM).

6.2.3.3.4 Leaflet Mobility

This final step for assessing the impact of combined annular dilatation and PM displacement on the tricuspid valve was to investigate changes in leaflet mobility with multidirectional displacement of the anterior, posterior and septal PMs. This was completed through measurement of the tenting height and tenting area on the septal/anterior, septal/posterior and anterior/posterior coaptation lines. Tenting height was significantly increased across the septal/anterior ($p = 0.001$), septal/posterior ($p = 0.036$) and anterior/posterior ($p = 0.001$) coaptation lines. The same trends were seen with tenting area across the septal/anterior ($p = 0.000$), septal/posterior ($p = 0.007$) and anterior/posterior ($p = 0.001$) coaptation lines (Fig. 6.53). These results demonstrate that combined annular dilatation (100%) and displacement of the APM (lateral and apical), SPM (anterior, lateral, apical) and PPM (posterior, lateral apical) severely affects the mobility of all three leaflets, resulting in drastic alterations in leaflet coaptation geometry.

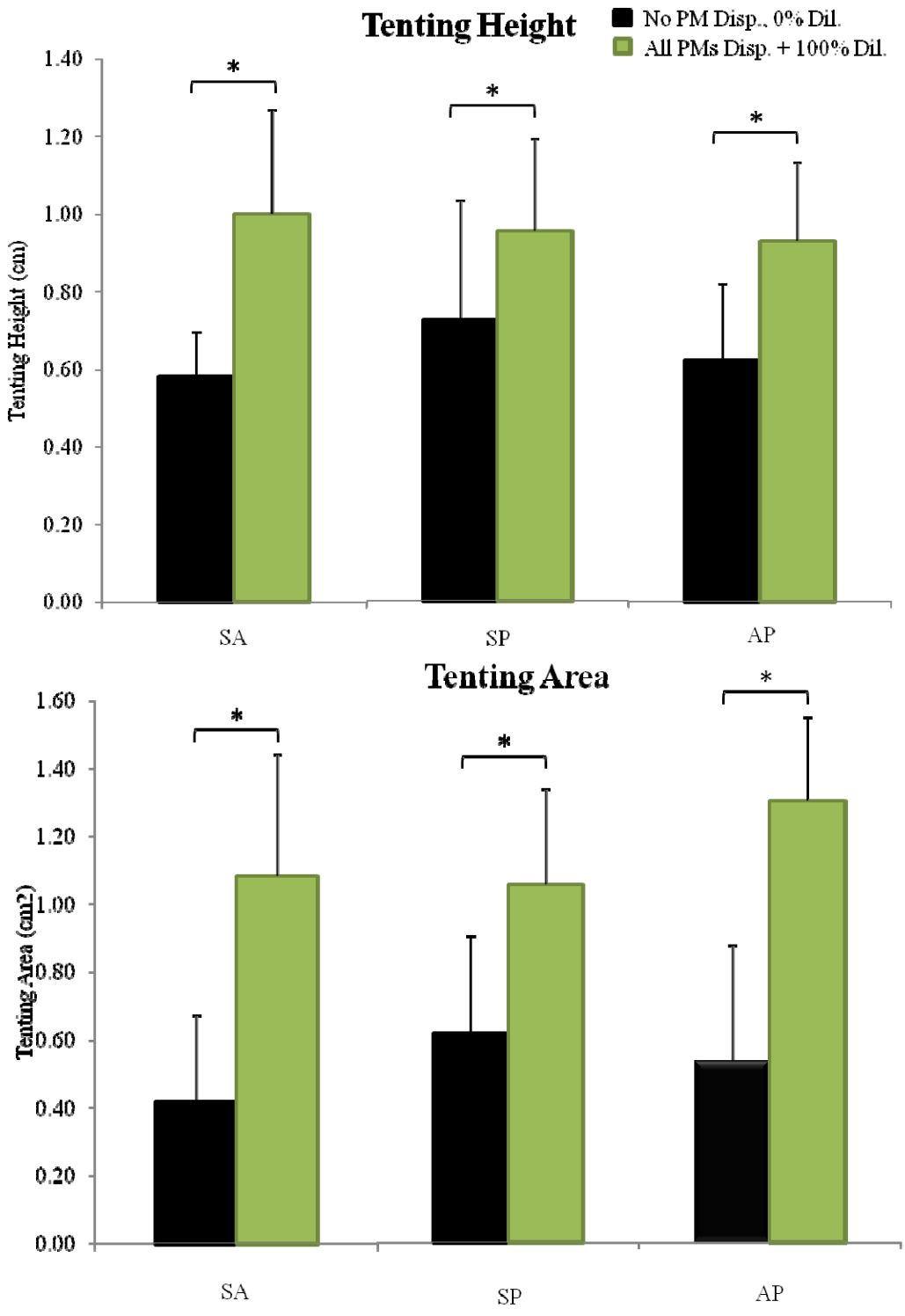

Figure 6.53: Peak systolic tenting height and area measurements are shown as an effect of APM/SPM/PPM displacement, along the coaptation lines: septal/anterior (SA), septal/posterior (SP), anterior/posterior (AP). Significance shown as *, $p \leq 0.05$.

The implication of these results and how they are used to explain the impact of alterations in the annular and subvalvular apparatus on tricuspid valve mechanics will be discussed in detail in the following chapter. Additionally, the clinical implications of this work along with the limitation will be discussed.

CHAPTER 7

DISCUSSION

This thesis provides a detailed understanding of the mechanics of the normal tricuspid valve, as well as insights into how the valve is altered in a diseased state. Details of these mechanisms are provided through both *in vivo* and *in vitro* investigations. This work is supported by the belief that providing a better understanding of how the tricuspid valve is altered from normal to disease, may provide valuable knowledge to the clinical community target and improve TV repairs.

The first specific aim used 3D echo imaging *in vivo* to determine if the RV papillary muscles were displaced with ventricular dilatation as has been theorized [13, 24, 45, 69] and as is seen in the MV [74, 75]. It was seen that both RV and LV dilatation result in PM displacement. The analysis was extended to determine correlation to the severity of TR to the geometry of the ventricle, specifically annular area and various PM displacements. In addition, PA pressure was seen to be a predictor of the severity of TR.

The *in vitro* set up allowed a precise determination of the specific geometric mechanisms responsible for TR, through investigation of RLL, leaflet mobility, and chordal forces. It was determined that with annular dilatation, the anterior leaflet extends to compensate for the larger orifice area, and reduced mobility of the septal and posterior leaflets. However, it can only successfully do so up to a 40% increase in annular area. Interestingly, it was shown that TR can be present with isolated PM displacement. More specifically, multidirectional displacement of a single or multiple PMs, results in extreme changes in leaflet mobility and loss of coaptation. A combination of annular dilatation

and PM displacement showed the highest levels of TR. This combined increase in annular orifice area and PM restriction, drastically alters leaflet mobility, coaptation, and chordal force distribution.

Unfortunately, it was not possible to investigate the specific PM displacements found in patients using the *in vitro* set up as these studies were done in parallel. However, information from both studies remains essential. *In vivo* studies were used to determine of pathological PM displacement, while *in vitro* studies provided a controlled environment to investigate specific disease conditions and their resulting mechanics. The development of a tool to measure PM position *in vivo* using 3D echocardiography will enable future studies to investigate more specific patient populations. In addition, the development of the *in vitro* model provides a test bed for further investigation into the mechanics of disease and eventually assessment of TV specific repairs.

7.1 *In vivo*

Prior to initiating the 3D echo measurements for specific aim one, it was first determined if RV PMs could be identified using MRI [76]. This study was the first report describing the specific locations of all three RV PMs. This was done in control subjects and patients with a dilated LV using cardiac MRI. While all three PMs could be identified, a difference was only seen in the septal PM when compared between RV PM position in normal patients and patients with a dilated left ventricle. These data showed that left ventricular dilatation resulted in the inward displacement of the septal PM towards the centroid of the three PMs. This may be due to the displacement of the septal wall into the RV with the increased left ventricular volume (Appendix H). While LV dysfunction has typically been related to RV dysfunction through pulmonary

hypertension [16, 18, 77], others believe changes in the LV geometry may be directly linked to the RV though the interventricular septum [2]. Additionally, Anyanwu et al. proposed LV dysfunction or dilatation as a mechanism of TR with normal pulmonary hypertension [24]. Weber and Janicki discuss in detail interventricular septum effects and the displacement of the septum into the RV with acute LV distention [69]. These results clearly show the interplay of the dilated left ventricular volume and the right ventricle and the effect of the resulting septum displacement into the RV on the PMs. This motion of the septal wall into the RV may affect the septal leaflet as it is attached to the septal and posterior PMs located on the septum through chordae tendineae. It is speculated that the PM displacement observed in the diseased group may have contributed to the TR present in five of the 7 patients. With this in mind the echo study was developed to specifically look at the effect of ventricular geometry on the TV apparatus and its relation to the grade of TR.

With the findings using MRI, 3D echo was then investigated as it is more widely used in clinical practice as opposed to MRI. Overall, 3D echo proved to be useful in this study to identify the PMs, as it allowed for offline analysis of the entire TV geometry. Previous methods used to identify TV PM position include, MRI[25], 2D echocardiography[78, 79] and sonomicrometry[35, 36]. While MRI may provide a more detailed geometrical description of the TV apparatus, it is not typically acquired in standard of care procedures, as it is a more expensive and longer procedure. Sonomicrometry is a useful tool but has only been used in *in vivo* animal studies and is not suitable for patient care. While 2D echo is the most commonly used modality for patient imaging, it requires the technician to identify the three PMs at the time of image acquisition. With recent

advancements and greater availability, 3D echocardiography is becoming more widely used clinically. 3D acquisition allows the offline interrogation of the entire TV geometry as the entire 3D volume is captured during the patient scan. Additionally, 3D echocardiography can be very useful in identifying leaflet motion, PM locations and presence of malcoaptation (Appendix I). Patients with a dilated RV were the easiest to image, with the viewing window adjusted to focus on the RV. The same adjustments were made for patients with both RV and LV dilation. The APM was the easiest to visualize in all patients, as it is the most well defined because of its protrusion from the free wall [43].

In vivo 3D echocardiography provided a unique investigation of the determinates of TR by utilization of an increasingly relevant clinical technique. Knowledge of the changes in ventricular geometry and their effect on TR were expanded by collecting measurements of the annulus, leaflet tethering and the individual PMs. The technique of using 3D echo to measure PM positions may also prove helpful for clinicians to determine which PM is contributing to the TR and target their repair efforts. It is impossible to know the initial position of any given PM, as patients do not routinely undergo echo examination until the disease has already manifested. For this reason it may be important to determine the location of the PMs in the diseased state relative to a reference, in which the normal relative distance of the PMs to the reference is known. This normal distance may be possibly discovered from a large scale clinical study. Furthermore the clinician could determine if the PM displacement observed as a result of disease could be used to explain the presence or grade of TR. The most relevant

reference in this case may be the annulus, as displacement of the PMs away from the annulus may result in leaflet tethering and prevent proper coaptation.

With regards to displacement of the PMs, patients with isolated RV dilatation had significant displacement of all PMs. As would be expected, all PMs moved away from the annulus. Although previous studies have speculated displacement of the APM on the free wall, this is the first study demonstrating movement of the PMs on the septum: SPM and PPM moving towards the LV as a result of RV dilatation (Fig. 7.1).

The resulting RV geometry observed is most likely due to the restricted space within the pericardial sack. The combination of displacement of all PMs and annular dilatation may account for the patients with isolated RV dilatation having the largest percentage of severe TR. We can conclude that the APM, SPM and PPM are moving away from the center of the annulus. Even though the annulus is dilated, we expect that the center of the annulus, the reference, would remain in a similar location, as the septum is being displaced into the LV and the free wall is moving out. It is however possible that while the septal and posterior PMs may have moved from their original position in the patients with a dilated LV and both ventricles dilated, no difference was seen from control because the relative position to the annulus remained the same. In the patients with a dilated LV it may have been that while the annulus size remained the same, the original position of the annulus was displaced along with the septal and posterior PMs as the septum is pushed into the RV with LV dilatation. Additionally, with combined RV and LV dilatation both the annulus center may moves along with the all PMS, resulting in no relative difference in PM position (Fig. 7.1).

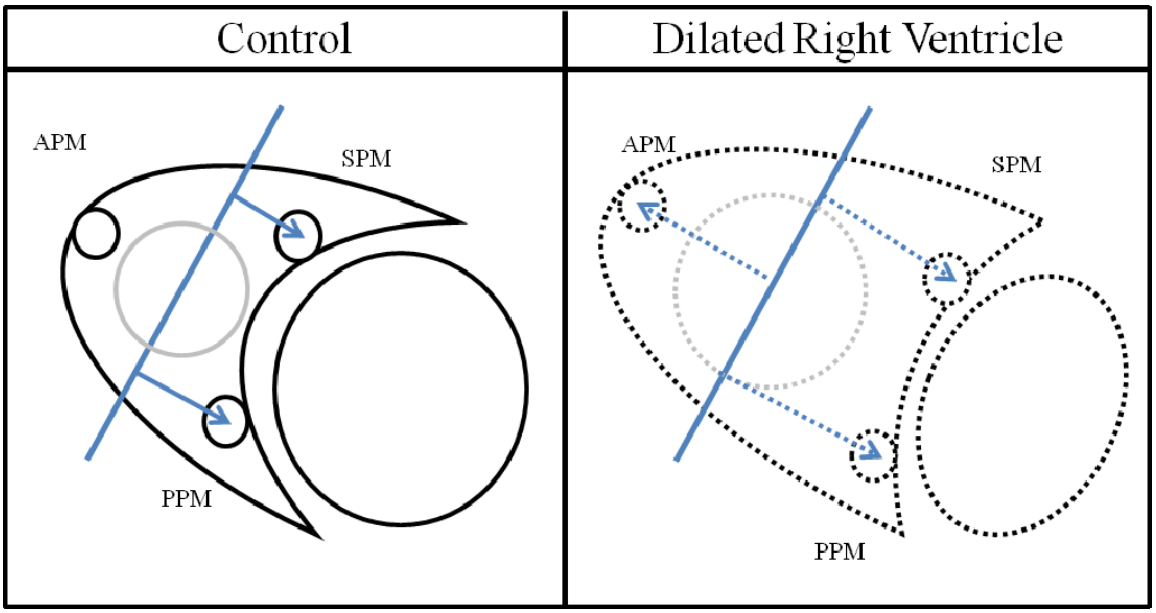

Fig. 7.1: Depiction of RV dilatation and resulting PM displacement away from the center of the RV as compared to control. Blue line depicts lateral reference, with grey showing annulus.

While displacement of the SPM towards the RV was observed in patients with a dilated LV using MRI, there were no changes observed in the lateral direction using echo. The explanation for this may be manifested in the difference in patients, or with the differences in references. While the MRI study used the centroid of the three PMs as a reference; the reference in the echo analysis was the center of the annulus. As a result of LV dilatation, the center of the annulus may be displaced when the septum moves towards the RV. Thus, no difference may be seen in the displacement of the SPM and PPM as they would move relative to the reference. This is depicted in the below figure (7.2). This may explain why the presence of clinically significant TR was much lower in these patients.

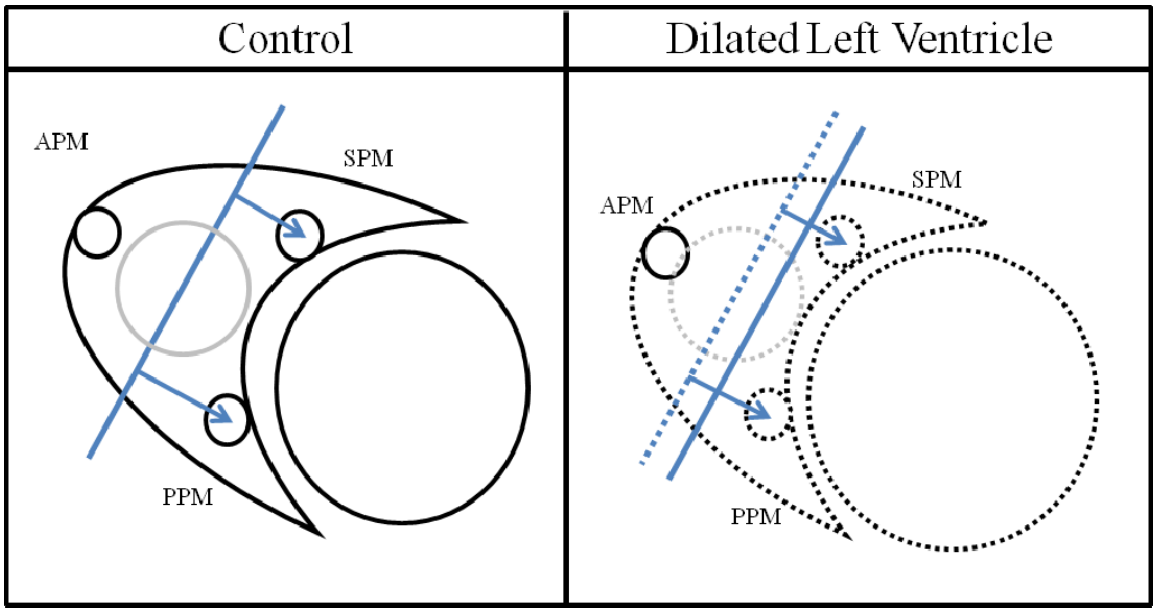

Fig. 7.2: Depiction of LV dilatation and resulting lateral PM displacement. Control is shown with a solid line and disease is shown with a dashed line. Blue line depicts lateral reference, with grey showing annulus.

The same cannot be said for patients with combined RV/LV dilatation, as their reference may be moved, as the LV pushes against the expanding RV. While it may have been that the reference (annulus) and septal wall were moving together, the resulting distance from the reference to the PMs remained the same in the control patients as in patients with a dilated RV (Fig 7.3).

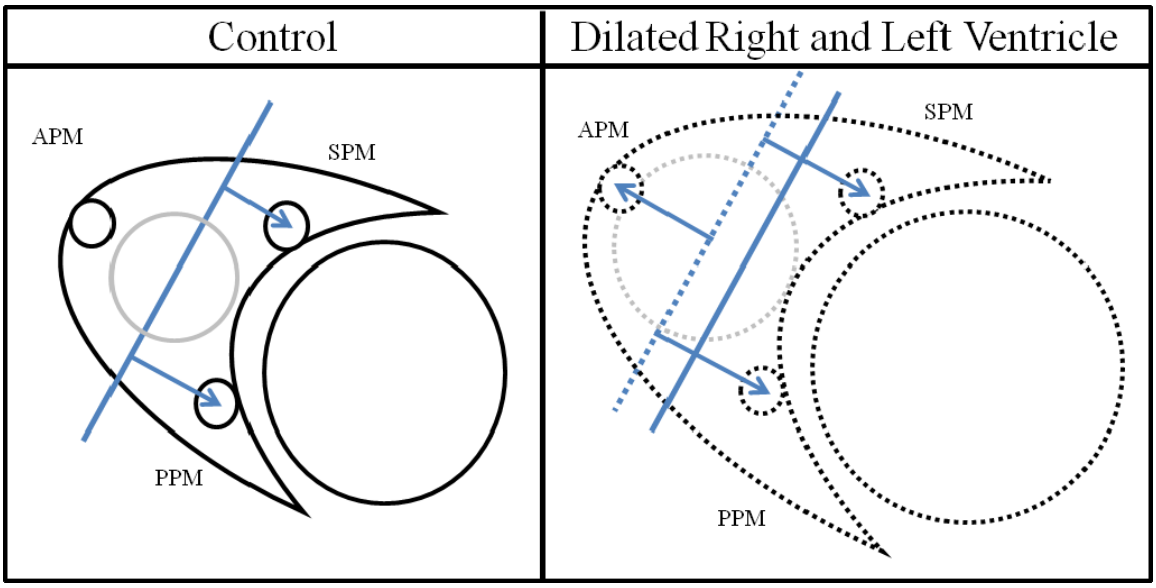

Fig. 7.3: Depiction of combined RV and LV dilatation and resulting lateral PM displacement. Control is shown with a solid line and disease is shown with a dashed line. Blue line depicts lateral reference, with grey showing annulus.

If this is true, it cannot be conclusively stated that the SPM and PPM have moved into the LV. It is however important to point out, that it is most likely the relative position between the PMs and the annulus which matters the most. For instance, if the annulus was moving in the same direction and magnitude as the PMs, it should not affect proper valve closure, as the relative distances would be the same. It is important to observe that while the lateral displacement of the PMs to the reference remained constant, the apical distance did not. As the PMs are pulled away from the center of the annulus, tethering may be induced in conjunction with the increased orifice size due to annular dilation and further exacerbate TR. Previous studies have quantified this both in the tricuspid[20-22, 33] and mitral valves [27].

Apical displacement of APM was seen in all patient groups with dilatation of the RV, LV or both. This indicates that either the PM is moving away from the annulus plane, which is the *z* reference, or the reference annulus plane is moving. Previous studies

by Ton-Nu et al.[12] and Fukuda et al.[33] demonstrated that the annulus plane becomes more planar in patients with annular dilatation, as opposed to saddle shape in normal subjects. Unfortunately both studies used a plane of best fit to the annulus as their reference; therefore it cannot be determined if the points on the saddle were moving towards the apex or atrium. If, in fact, the PMs are being displaced apically, the rationale behind their movement may be due to the remodeling and shape change of the ventricles, which are yet to be characterized. Thus it cannot be determined which is moving, the annulus plane or the PMs. However, as pointed out previously, it is the relative position that is most important, as apical displacement of the PMs, away from the annulus is likely to result in leaflet tethering.

When investigating annulus area it was seen that patients with RV dilatation whether isolated or in addition to LV dilatation had the largest annulus area. Additionally, it was shown that while the size of the annulus with patients with trace and mild TR was similar, patients with moderate to severe TR had much larger annulus areas. This further strengthens our belief that annulus area does in fact play a role in determining the severity of TR.

Next, the investigation of the role of PA pressure found it to be the highest amongst patients with a dilated RV. This patient group also demonstrated the highest levels of TR, thus it was not unexpected that PA pressure and TR were highly correlated in all statistical comparisons. Although it has long been accepted that pulmonary hypertension may result in TR, clinical correlations are difficult to find in the literature. Not only was this study able to correlate the two, it may also provide an explanation as to why this happens. PA pressure was found to be correlated with RV geometry (RVEDA, r

= 0.51). RV geometry was correlated with annular dilatation (r = 0.60), as well as PM displacements, which were also shown to be correlated to TR (Fig. 7.4).

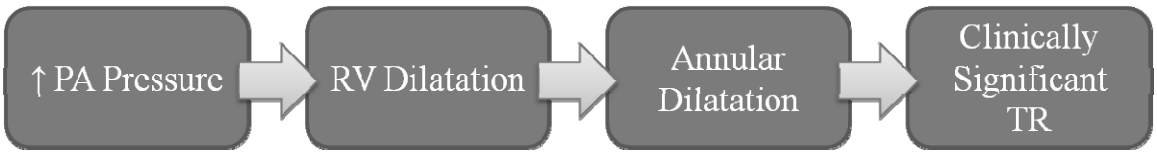

Fig. 7.4: Relation of increases in PA pressure to clinically significant TR through the dilatation of the RV resulting in annular dilatation.

This can be explained by understanding that increases in PA pressure result in RV dilatation, which dilates the annulus and displaces the PMs. Increases in PA pressure may explain this high interdependence and the cause of the geometric alterations. This study has shown that increased PA pressure alters the geometry of the ventricle; whether these geometric changes can be reversed when the PA pressures are decreased to normal levels is yet to be proven.

Additionally, a significant correlation between the size of the ventricles and the grade of TR was found. This can be explained by the changes in the valvular and subvalvular apparatus as a result of ventricular dilatation which may prevent the valve from forming a proper seal. Furthermore, the correlation of RV size to tricuspid annulus area shows that patients with a dilated RV are more likely to have a dilated annulus. This information has been shown before[13, 23], however, it is interesting to note that not all patients with a dilated RV had significant increases in annulus area. Although the number of patients was small, it is still important to note that the RV may become dilated without the annulus being affected. Annulus area was also correlated with TR (r = 0.51) which is consistent with many previous studies [22, 23, 38].

This study, as well as previously published studies[20-22], have shown leaflet tethering to be a contributor to the presence of TR. Displacements in the PMs would be

expected to contribute to leaflet tethering, which may explain why both were correlates to the grade of TR. Interestingly our study was able to show apical displacement of the APM to be a better predictor of TR, as tethering measurements dropped out of the multivariate regression. While tethering remains a clinically important metric in TR, attempts to identify and quantify the position of the APM may provide more insight.

The initial MRI investigation and 3D echo study was essential as they showed that changes in the PM positions may also play an important role in TR. If PM displacement impacts TV function and lead to TR, residual TR may result after the repair. This may result if the PM positions were altered and not addressed with the repair. Traditionally, the most common surgical intervention for non-rheumatic disease focuses on reducing the dilated annulus to its original size with the placement of an annuloplasty ring. Studies have found that restoring the annulus to a normal size may not eliminate TR completely and in many cases it returns [26, 33]. Hence, solely reducing the annulus may be insufficient to permanently correct TR [26, 55]. While papillary muscle displacement may be one contributor to this recurrence of TR, this study also demonstrates that it may be important to assess the impact of the LV size and septal motion on RV function, even before surgery is attempted. These outcomes suggest that the underlying pathophysiology associated with TR is perhaps not well understood. Previous studies have attempted to correlate RV PM displacement to TR and found tethering and restriction of leaflet mobility caused by PM displacement to be an independent predictor of TR after TV annuloplasty [26, 55]. Although the relation of LV dilatation to durability of TV repairs has yet to be proven, this study demonstrates the geometric relation between the two ventricles. Futures studies may aim to determine pre and post operative PM position and

determine the relation to patient outcome. For the first time, this study demonstrates the 3D echo as a useful tool in locating and measuring PM positions which can be implemented on both normal and disease patients.

7.2 *In vitro*

The *in vitro* part of the thesis sought to investigate the effects of disease on the tricuspid valve annular and subvalvular apparatus in a controlled environment. In this section, quantitative measurements were made to understand the changes in TR and attempt to explain these changes by analyzing residual leaflet length, leaflet mobility and finally chordal force distribution.

7.2.1 Model Development

A large portion of the initial thesis was devoted to development of the *in vitro* model for the TV *in vitro* studies. Based on previous experience with mitral valves, it was hypothesized that a modification of the left heart simulator for mitral valve studies with an additional PM muscle and annular geometry would suffice for TV studies. While the implementation of the third PM was simple, the simulation of physiologic and pathologic annular geometry was more complex. Dilatation of the TV is not symmetric and only occurs along the anterior and posterior sections[12, 13]. While the plate construction was similar to that of the MV annulus plate with a spring and internal wire, a rigid tube was added to the septal section to ensure it did not dilate. In conjunction with dilatation, the TV annulus also adjusts from a triangular to circular shape[29, 32]. Thus, initial design of the annulus plate required an additional wire between the anterior and posterior sections to control the amount of triangulation. With the second-generation annulus plate, this was no longer needed as the wire and spring alone were able to simulate accurate geometries when the wire exited the plate on the septal/posterior segment, as opposed to septal/anterior segment. In addition, the second generation plate replaced the rigid tube with a separate spring to allow for implementation of a physiological saddle shape.

Measurements of the annular plate at normal and dilated sizes were within acceptable ranges for *in vivo* human measurements.

The implementation of a saddle shape was added to the second-generation annulus plate to make the normal condition more physiologic. Addition of the saddle shape did not have a significant impact on TR even though it was used as a control for comparison to disease conditions. Further investigation of the saddle shape was conducted to investigate its effects on the stretch of the leaflets. The findings from the study can be found in the appendix J. This additional study was motivated by the introduction of the MC^3 (Edwards Lifesciences, Irvine, CA) tricuspid specific 3D ring. Interestingly, the saddle shape significantly increased the stretch of the anterior leaflet of the TV but not the posterior leaflet. This trend differed from that observed in the MV, where a saddle was shown to decrease the stretch on both leaflets[80]. This may be attributed to the inherent 3D geometrical differences between the tricuspid and mitral valves. In the MV, the apical motion of the commissures results in a saddle, and each leaflet is flanked by two annular high points[81, 82]. However in the TV, the posterior leaflet is flanked by two annular points with apical motion (low points) similar to the MV, while the anterior leaflet is flanked by one annular point with apical motion (low point) and one annular point with basal motion (high point)[12, 33]. The result of two adjacent annulus points moving in opposite directions resulted in more tethering and deformation of the anterior leaflet than the posterior leaflet. Thus the stretch configuration of the anterior leaflet is not comparable to the MV.

Since the tricuspid valve has three leaflets, the saddle applied at two points may affect each leaflet's curvature differently. Additionally, the TV is in a lower pressure

environment, which may cause the leaflets to possess different material properties than the MV. For the posterior leaflet, two high points exist on either side of the leaflet, similar to what is seen in the mitral valve. However, there was no significant impact on the stretch of the posterior leaflets with a saddle shape as compared to flat, where it has been observed with the mitral valve. When comparing the effect of the saddle on the TV to the MV, it is important to understand that the annular height to commissural width ratio (AHCWR) observed in the TV is approximately 10% whereas the MV is 20%. The saddle which is present in the TV has not been investigated as rigorously as compared to the MV[81, 82], as the importance, if any, of the saddle in the TV is still not well understood. Previous studies investigating the effect of saddle on MV leaflet strains, reported no differences with 10% AHCWR, and it was not until the AHCWR was increased to 20% that the strains were significantly decreased with a saddle shape as compared to flat[68, 80].

Once the flow simulator was adapted to account for geometric differences, between the TV and MV, alterations to the loop configuration from the MV set up were necessary to maintain a cardiac output of 5 liters/minute with a much lower driving force of only 40 mmHg from the right ventricle. It was necessary to minimize the length of all tubing and increase the diameter to 1.5 inch to reduce the resistance to all flow within the system. Another major change involved the atrial and pulmonary compliance. It was essential to make it as easy as possible for the ventricle to expel its volume within the allotted time. This was achieved by increasing the size of the pulmonary reservoir container, as detailed in the materials section. The pulmonary reservoir overflowed into the atrial reservoir, resulting in a consistent water column for both reservoirs.

7.2.2 Isolated Annular Dilatation

Investigation of annular dilatation, found that TR was highly dependent on annular dilatation with significant TR occurring at only a 40% increase in annular area. This was seen at 75% dilatation in *in vitro* mitral valve studies[59]. It may be the increased mechanical complexity of bringing three flexible surfaces together which causes the TV to leak earlier. A central zone of leaflet malcoaptation was consistently seen in all valves with annular dilatation, demonstrating the dependence on the three leaflets coapting simultaneously. Previous studies of TR repair have determined varying thresholds for deciding when to clinically repair the annulus. In a study by Dreyfus et al., they repaired any TV that was larger than 70 mm in diameter by direct measurement [9] and Carpentier et al. repaired the valve if the surgeon could insert 3 fingers width into the annulus [8]. In the present study, annular dilatation of 40% corresponded to an annulus area of 88 ± 2 mm^2 and septal lateral diameter of 23 ± 0. 5 mm, which is less dilatation then previously recommended for repair.

While annular dilatation has been shown to cause TR, it was important to understand the mechanism behind it in order to gain insight as to why some patients with annular dilation have TR and others do not. As the annulus dilates the anterior and posterior sections are displaced, causing the posterior and anterior leaflets to be pulled away from the central coaptation line. This results in the reduction of RLL at the point of coaptation. When the RLL is reduced to an insufficient length, the three leaflets cannot properly coapt, resulting in gaps, wrinkles, and leaflet mismatch (Fig. 7.5).

A significant increase in TR coincided with a visible gap and an RLL of 5 mm as such a minimum RLL of 5 mm or less of any leaflet may be a predictor of tricuspid

regurgitation. Even if the leaflets have RLL available for coaptation, the complexity of coaptation may require more than 5 mm of tissue from each leaflet to form a seal and prevent regurgitation. This study found anterior leaflet RLL to be most affected by annular dilatation. It may be because the anterior leaflet extends to compensate for the increase in the orifice area, created by dilatation of the annulus. It is interesting to note that multiple studies have reported the anterior leaflet to be the longest and largest in area as compared to the posterior and septal leaflets [32, 40]. This ratio may be the body's attempt to compensate for annular dilatation up to a certain level. In contrast to the anterior leaflet, the septal leaflet experienced little change in RLL as an effect of dilatation[83]. This may be explained by previous studies which have commented on the large number of chordae inserting into the septal leaflet from the septum[32] and thus the possibility for restricted motion. When these findings are compared to the mitral valve it is the posterior section of the annulus which dilates, with the anterior leaflet covering the increased orifice [84]. Thus whereas it is the leaflet on the annulus segment that is dilating (anterior) which is effected with TV dilatation it is the opposite with the MV (anterior). It is however interesting to point out that the leaflets of both the MV and TV which compensate for the dilatation are both the largest leaflets.

Next, the leaflet mobility and coaptation geometry were investigated with the use of 3D echo, in which measurements of tenting height and tenting area were taken at the three coaptation lines. Dilatation of the annulus did not significantly alter leaflet mobility or coaptation geometry. This may be because the leaflets are free to adjust and adapt as no PM displacement if present, to the changes although the annular diameter is increased.

It is only the residual leaflet length that displays a significant change, not the leaflet coaptation geometry.

Although the coaptation geometry did not change with dilatation, investigation of the chordal forces showed an increase in forces in all six measured chords: anterior marginal, anterior intermediate, anterior strut, posterior marginal, posterior intermediate, posterior strut. This may be due to many factors at play. As the annulus dilates, the surface area of the leaflet exposed to pressure increases, as force is proportional to pressure and area. Thus, the maximum chordal force required to prevent billowing of the leaflets increases. In addition, it is believed that the marginal and intermediate chordal forces increased with dilatation as they were no longer in the coaptation zone and were engaged. This is compared to a normal configuration where these chordae were within the coaptation region and may have been slack. This explains the findings that marginal and intermediate chords had the largest increases in force as compared to control. Finally, the relative position of the point of leaflet insertion to PM attachment of the chord is altered. The annulus is moved, however the PMs remain in their normal position. Similar trends were seen with dilatation above 40%, with the most extreme case at 100% dilatation. The below schematic depicts significant alterations from normal when the valve was dilated to 100%.

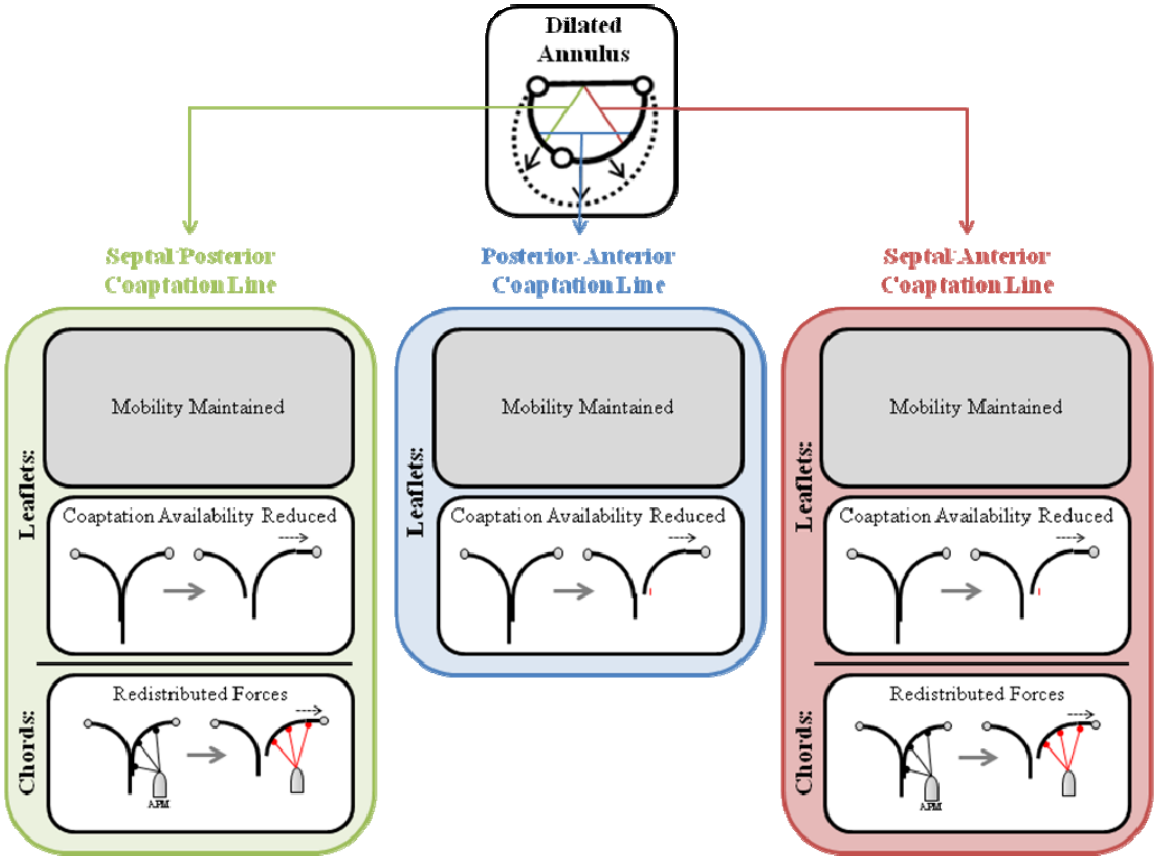

Figure 7.5: Schematic of significant alterations in the leaflets and chords as observed with dilatation. The schematic shows leaflet mobility, residual leaflet length and chordal forces along the three coaptation lines. Specific significant alterations are shown in bright red.

7.2.3 Isolated Papillary Muscle Displacement

While it is accepted that annular dilatation may result in TR, it is not the only mechanism which can cause TR. The effect of PM displacement on valve function has been investigated on the left side of the heart, both *in vivo* and *in vitro*, but has only recently been investigated on the right side. While this has been shown through *in* vivo studies in this thesis, previously published studies have yet to correlate PM displacement to TR. However, studies have correlated changes in RV geometry to increases in TR[21, 23,

[24]. It is believed that as the RV dilates, the PMs become displaced and this results in leaflet tethering[20, 22].

In the previously discussed *in vivo* MRI study, it was found that dilatation of the LV can affect RV PM positions. The septal PM displaced towards the center of the RV in patients with a dilated LV[25]. Although the previous study was unable to specifically correlate the presence of TR in these patients to the PM displacement, the results presented may give us an idea of how the lateral displacement reported in patients may cause TR. Additionally, the *in vivo* portion of this thesis provided a direct correlation of PM displacement to the grade of TR.

Through the *in vitro* investigation of PM displacement, it was demonstrated that PM displacement alone may lead to significant TR. As with the case of isolated PM displacement, significant levels of TR in the presence of the displacement of the APM, PPM/SPM and all PMs could be seen. While numerous PM displacements were investigated, severe displacement with the APM, S/PPM and all PMs displaced in multiple directions simultaneously was the only condition which resulted in significant TR. Although lateral displacement of the SPM/PPM resulted in significant TR in some of the cases, the high variability did not allow for a statistical comparison of the group to control. This variability may be a result of the high variability in chordae insertion into the septal leaflet. In addition, septal leaflet RLL was highly affected by all PM changes as it experienced a reduction for all PM displacements. It is believed that the septal leaflet is most impacted by changes in PM displacement since it has many chordal insertions, with those coming from the septal PM being the shortest[32]. While displacement of the PMs

without concurrent annular dilatation is rare, it is important to understand what may happen if the annulus is repaired and the PMs are left displaced.

In addition to the creation of TR, multidirectional PM displacement also affected proper coaptation of the leaflets. Changes in coaptation were most significant when all PMs were displaced in all directions corresponding to increased mobility of the septal leaflet and restriction of the other leaflets. With this increased mobility, the coaptation line of the three leaflets was more towards the center of the annulus, thus the septal leaflet covered more of the orifice, but was not long enough to do so, as it is the shortest leaflet [32, 40], which resulted in a central zone of malcoaptation.

With evidence that PM displacement in the presence of a normal sized annulus may result in TR, the impact of these alterations on leaflet mobility and coaptation was used to better understand valve mechanics. With PM displacement, the only changes in septal/anterior and posterior/septal coaptation geometry were seen with multidirectional displacement of all PMs. This may be due to the small length of the chords from the septal PM. Observationally, it was found that the septal PM is not always well defined and often fused, and thus the chords are often the shortest and thinnest. Because of this phenomenon, small changes in PM position may result in large changes in leaflet mobility, especially since all chordae are displaced by the same amount (10 mm) for all PMs. Additionally, combined displacement in the apical or lateral directions of the APM resulted in tethering at the AP coaptation zone, while isolated directional displacement of the APM did not. This suggests that tethering is a local phenomenon, in that changes at a given coaptation zone are a direct result of the PM at that location. For example, alterations in the AP coaptation line would be indicative of displacement of the APM.

This may be useful, in that while it is possible to clinically visualize the PMs, it may not always be feasible. Thus one could potentially use the coaptation geometry to assess which PM or multiple PMs are displaced.

Finally the investigation of PM displacement on chordal forces revealed increases only in the forces on the posterior strut chordae. While force tended to increase with apical APM displacement, significant increases were observed with severe PM displacement. Thus, significant alteration in the coaptation geometry of the valve is needed in order to redistribute forces in the case of isolated PM displacement. These findings are important, as they emphasize that in the case of PM displacement the mechanics of the valve and subvalvular apparatus are altered. Thus an annuloplasty procedure may not be sufficient to restore the valve mechanics to normal. The below schematics showcase the conditions in which isolated PM displacement resulted in significant differences in leaflet mobility, as assessed with echo, leaflet coaptation, as assessed with RLL, and chordal forces. This is depicted for apical (Fig. 7.6), combined lateral and apical (Fig. 7.7) displacements of the APM, and for all PMs displaced (Fig. 7.8). Only conditions which resulted in significant alterations from control are shown.

With isolated apical displacement of the APM the anterior leaflet length available for coaptation increased as the leaflet was restricted apically. No further changes were observed in any other conditions measured. Thus, these alterations were not drastic enough to result in a significant amount of TR.

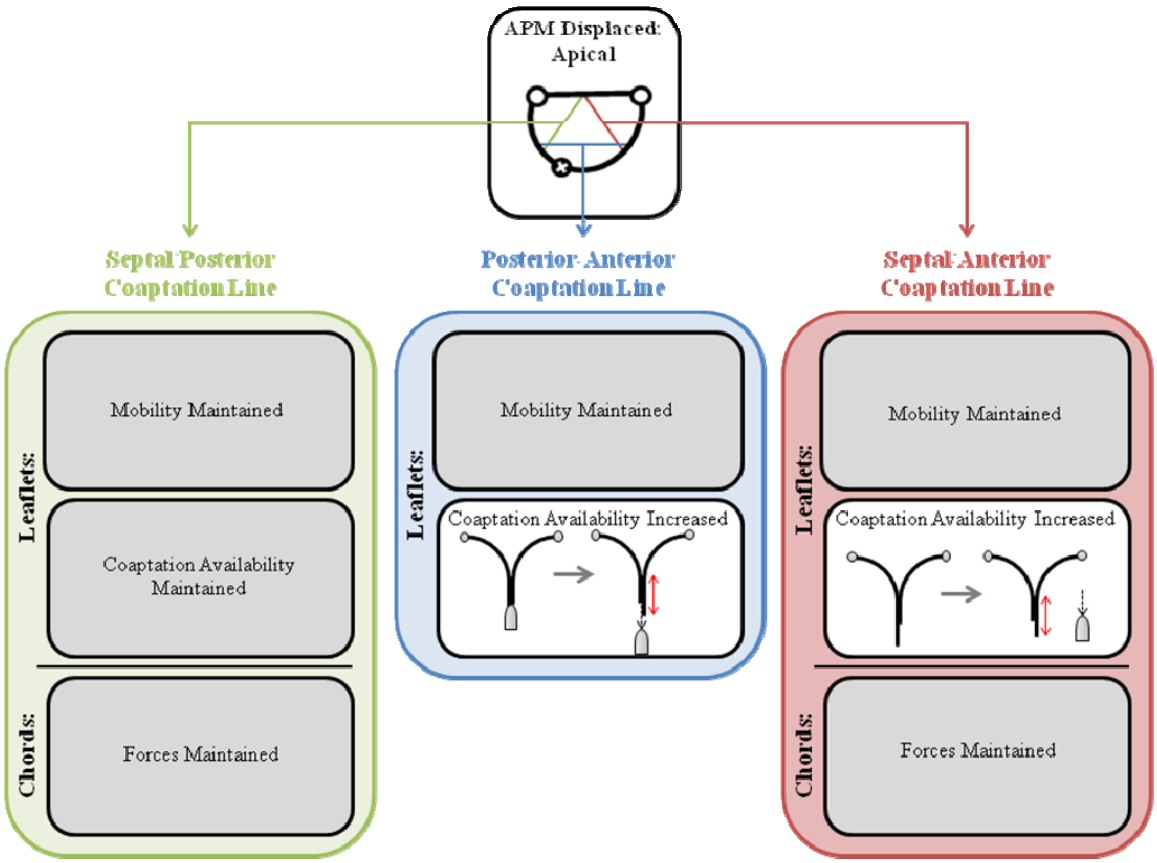

Figure 7.6: Schematic of significant alterations in the leaflets and chords as observed with apical displacement of the APM. The schematic shows leaflet mobility, residual leaflet length and chordal forces along the three coaptation lines. Specific significant alterations are shown in bright red.

With the addition of lateral displacement to apical displacement of the APM, the mobility of the anterior and posterior leaflets was decreased. Apical displacement restricts the mobility of the anterior leaflet initially. However, the combined lateral displacement moves the APM away from the center of the valve, further restricting mobility of the anterior leaflet resulting in tethering. Changes in leaflet tethering were only observed at the anterior/posterior coaptation line as this is where the chords from the APM insert into the leaflets.

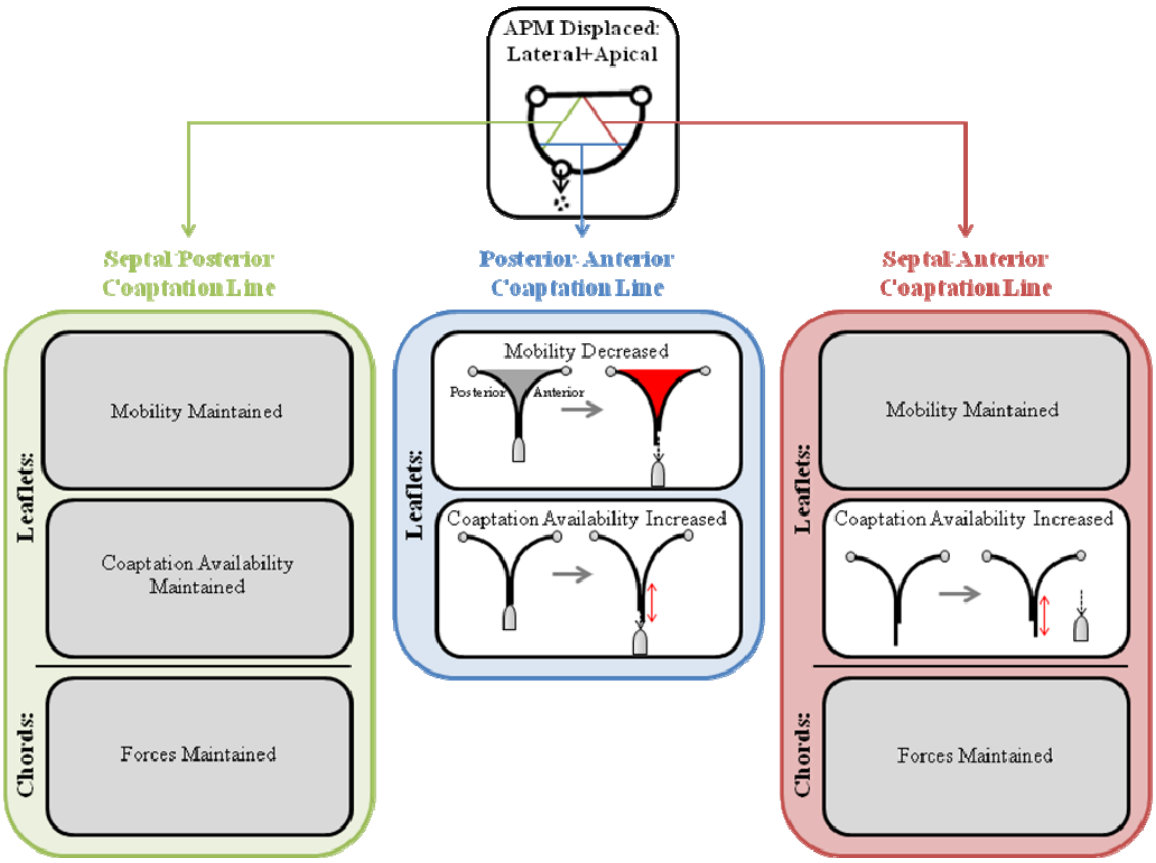

Figure 7.7: Schematic of significant alterations in the leaflets and chords as observed with combined lateral and apical displacement of the APM. The schematic shows leaflet mobility, residual leaflet length and chordal forces along the three coaptation lines. Specific significant alterations are shown in bright red.

Finally, with displacement of the anterior (lateral and apical), septal (anterior, lateral and apical) and posterior (posterior, lateral and apical) PMs the most drastic changes in valve mechanics with isolated PM displacement were observed. The leaflet tethering observed with lateral and apical displacement of the APM, was no longer seen. The coaptation line was moved more towards the anterior and posterior sections of the annulus due to displacement of the septal and posterior PMs. This resulted in a reduction in the leaflet mobility across both coaptation lines for the septal leaflet. As a result, the posterior leaflet contributed more to coaptation, as the length of the posterior leaflet which was available for coaptation increased since it was restricted. Furthermore,

displacement of all three PMs was the only condition of isolated PM displacement which resulted in a significant increase in chordal forces. Combined PM displacement resulted in severe changes in the coaptation geometry. Consequently, the posterior strut chord restricted the motion of the posterior leaflet as measured as an increasing force, resulting in an increased RLL and leaflet tethering. The numerous alterations in the valve mechanics may explain why this condition had the highest levels of TR with isolated PM displacement.

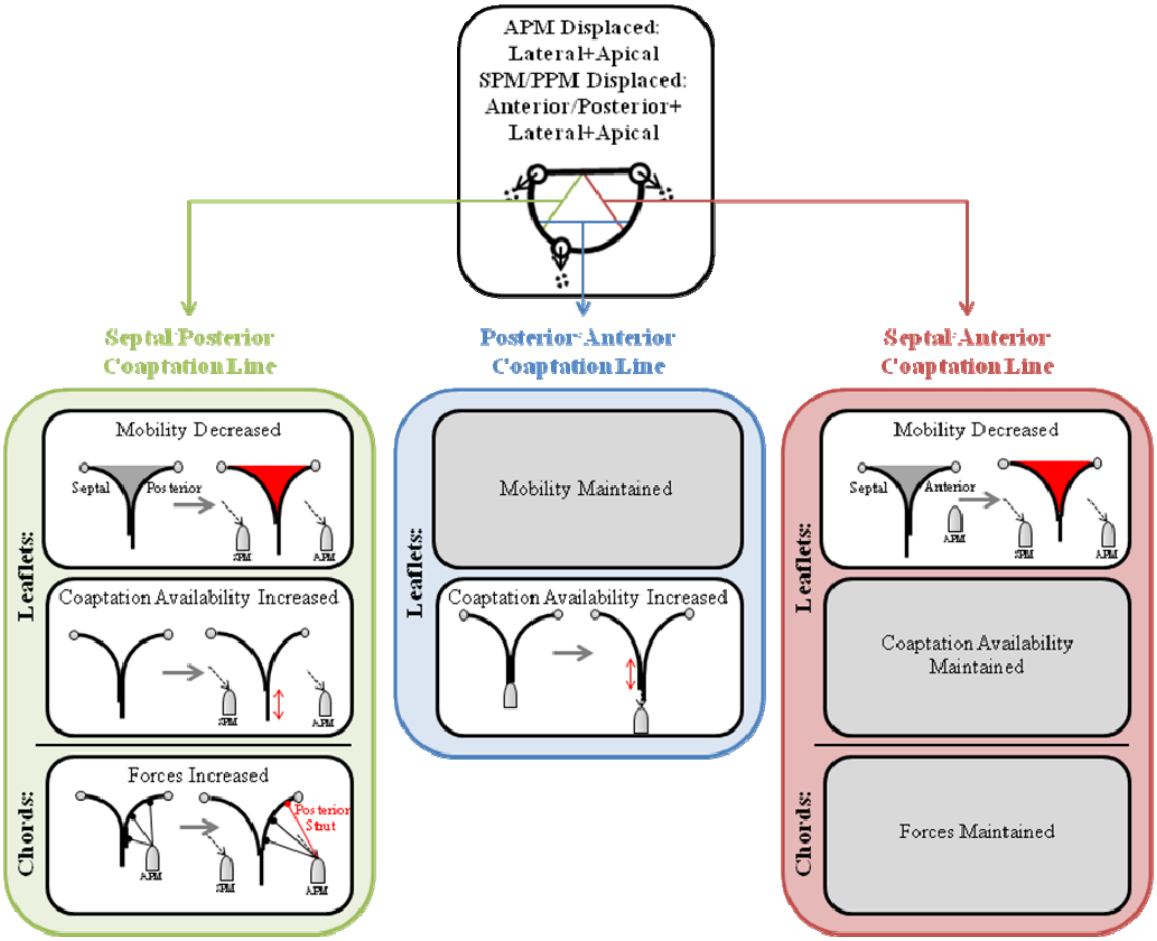

Figure 7.8: Schematic of significant alterations in the leaflets and chords as observed with combined displacement of the APM, SPM and PPM. The schematic shows leaflet mobility, residual leaflet length and chordal forces along the three coaptation lines. Specific significant alterations are shown in bright red.

7.2.4 Combined Annular Dilatation and Papillary Muscle Displacement

The next logical step was to combine these two disease manifestations, to investigate the combined effect of annular dilatation and PM displacement. It was shown that in the combined case of annular dilatation, greater than or equal to 40%, and all PMs displaced in all directions the highest levels of TR were achieved. It is a combination of multiple mechanisms that results in the increased levels of TR. The anterior and posterior leaflets are pulled away from the central line of coaptation due to annular dilatation, increased leaflet mobility of the septal leaflet with SPM and PPM displacement (as discussed previously), and restriction of the anterior leaflet mobility with displacement of the APM all contribute to the high levels of regurgitation.

When these two conditions, annular dilatation and PM displacement, were combined, more information as to the role of these disease states was obtained. Combined cases were observed to have more impact on the leaflet geometry. This is most likely true because with annular dilatation the orifice area is increased, and with PM displacement the leaflet mobility is restricted. Consequently, the leaflets are no longer free to coapt normally as was the case with annular dilatation. Multidirectional displacement of the PMs resulted in significant changes in leaflet coaptation which was evident by the alterations in leaflet geometry across all coaptation lines. In the case of apical displacement of the APM with dilatation, only the AP coaptation line was affected, resulting in local restriction of the anterior and posterior leaflet mobility. By adding further displacement of the APM in the lateral direction the SA coaptation line was affected. This may be due to the lateral restriction of the anterior leaflet. At the same time, the anterior leaflet still attempts to compensate for the dilatation and thus it was

pulled away from the SA coaptation line. When all three PMs were displaced in all directions, leaflet mobility was affected at all coaptation lines, which is evident by significant changes in the coaptation geometry. There was never a case in which changes were observed in tenting height and not in tenting area. This suggests that measurements of tenting area alone may provide enough information as to alterations in leaflet geometry, thus it may not be of additional value to measure tenting height.

With an understanding of the combined role of annular dilatation and PM displacement on leaflet coaptation and leaflet mobility, the final step was to investigate chordal forces. Alterations in chordal forces will be discussed by condition and explained in conjunction with the altered mechanics for each condition.

Overall combined conditions of annular dilatation and PM displacement resulted in the most severe alterations in valve mechanics. The following images depict the alterations in valve mechanics as seen with the combination of annular dilatation and each type of PM displacement (Fig.7.9-7.14).

While no change was observed in valve mechanics with isolated lateral displacement of the APM, when combined with annular dilatation significant changes were observed. With lateral displacement of the APM away from the center of the annulus the anterior leaflet became restricted as is evident with an increase in RLL. As the anterior leaflet attempts to assist in covering the enlarged orifice due to dilatation, it cannot as it is tethered. This results in an increase in force in all the chords inserting into the anterior leaflet from the APM.

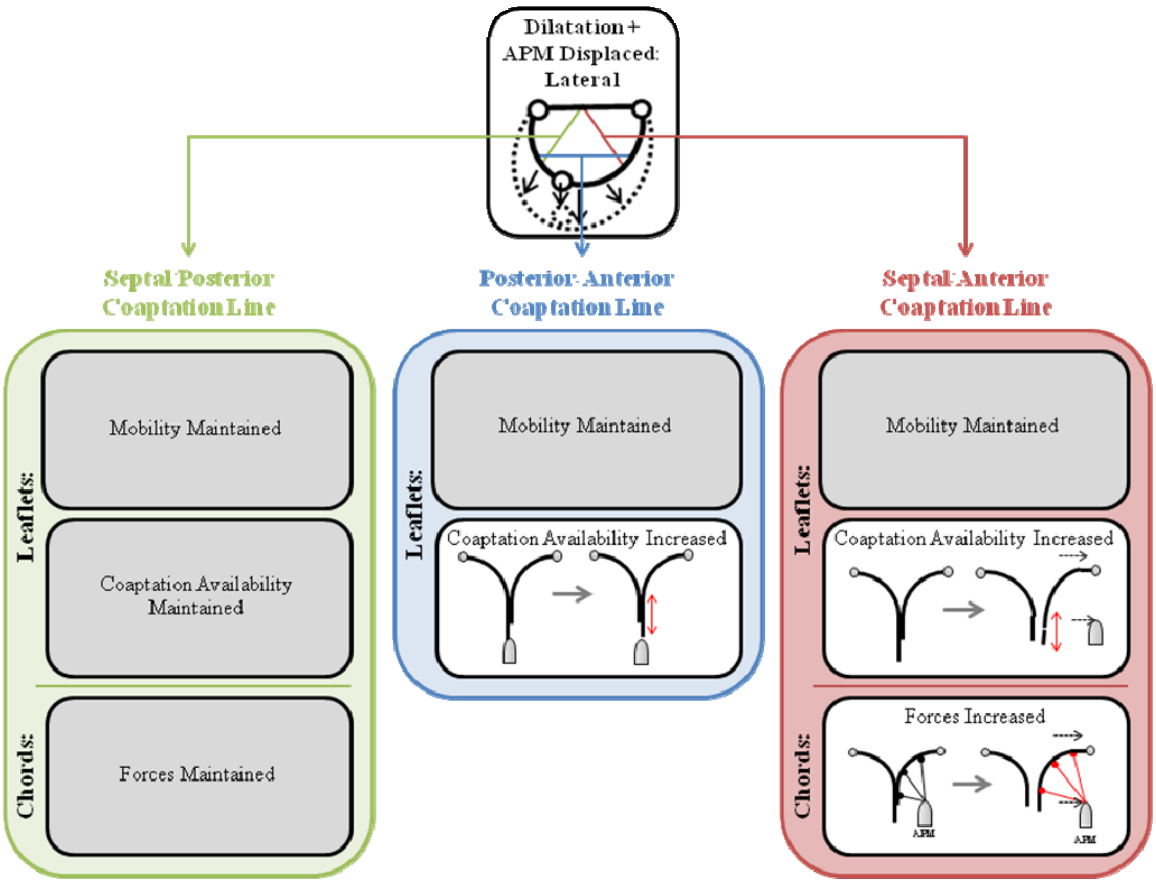

Figure 7.9: Schematic of significant alterations in the leaflets and chords as observed with combined annular dilatation and lateral APM displacement. The schematic shows leaflet mobility, residual leaflet length and chordal forces along the three coaptation lines. Specific significant alterations are shown in bright red.

Combined annular dilatation and apical displacement of the APM affected valve mechanics across all three coaptation lines. This resulting combination displaced the anterior/posterior coaptation zone apically, resulting in an increase in anterior RLL, as the anterior leaflet mobility was decreased as a result of tethering. Finally the chords from the APM inserting into both the anterior and posterior leaflets were affected. The strut and marginal chordal forces increased. The increase in strut chord forces may be due to the apical displacement. The increase in marginal chordal force may have been observed only on the anterior leaflet as this leaflet attempted to cover the enlarged orifice, due to annular dilatation, to prevent TR.

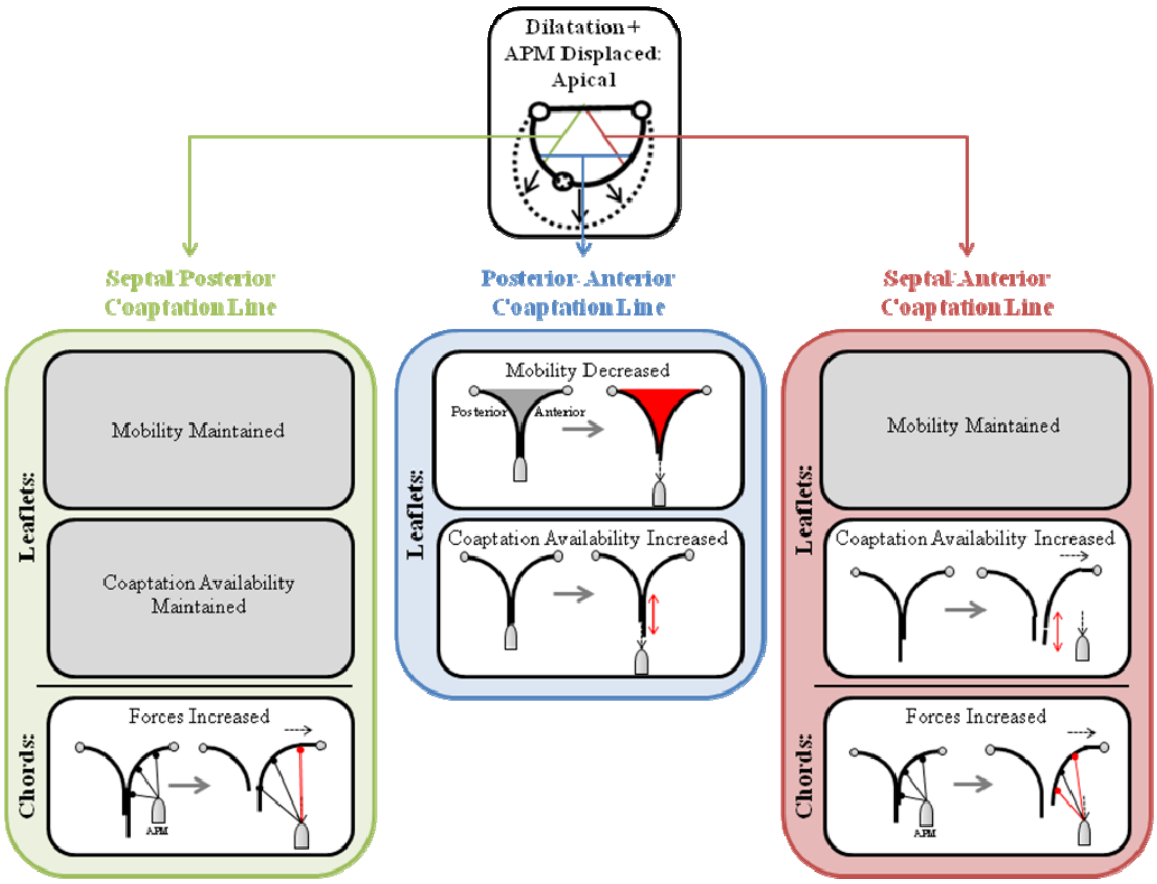

Figure 7.10: Schematic of significant alterations in the leaflets and chords as observed with combined annular dilatation and apical APM displacement. The schematic shows leaflet mobility, residual leaflet length and chordal forces along the three coaptation lines. Specific significant alterations are shown in bright red.

When the APM was displaced both laterally and apically and combined, with annular dilatation, a combination of the alterations seen in apical and lateral displacement was observed. Only the coaptation lines of the anterior and posterior leaflet were observed to be altered. Apical and lateral displacement restricted the mobility of the anterior leaflet with an increase in leaflet tethering at the anterior/posterior coaptation and an increase in RLL. As the leaflet was restricted, less of the leaflet covered the orifice, leaving more leaflet available for coaptation. As with lateral APM displacement and annular dilatation, forces on all chords from the APM inserting into the anterior leaflet were increased, further demonstrating the restriction of the anterior leaflet.

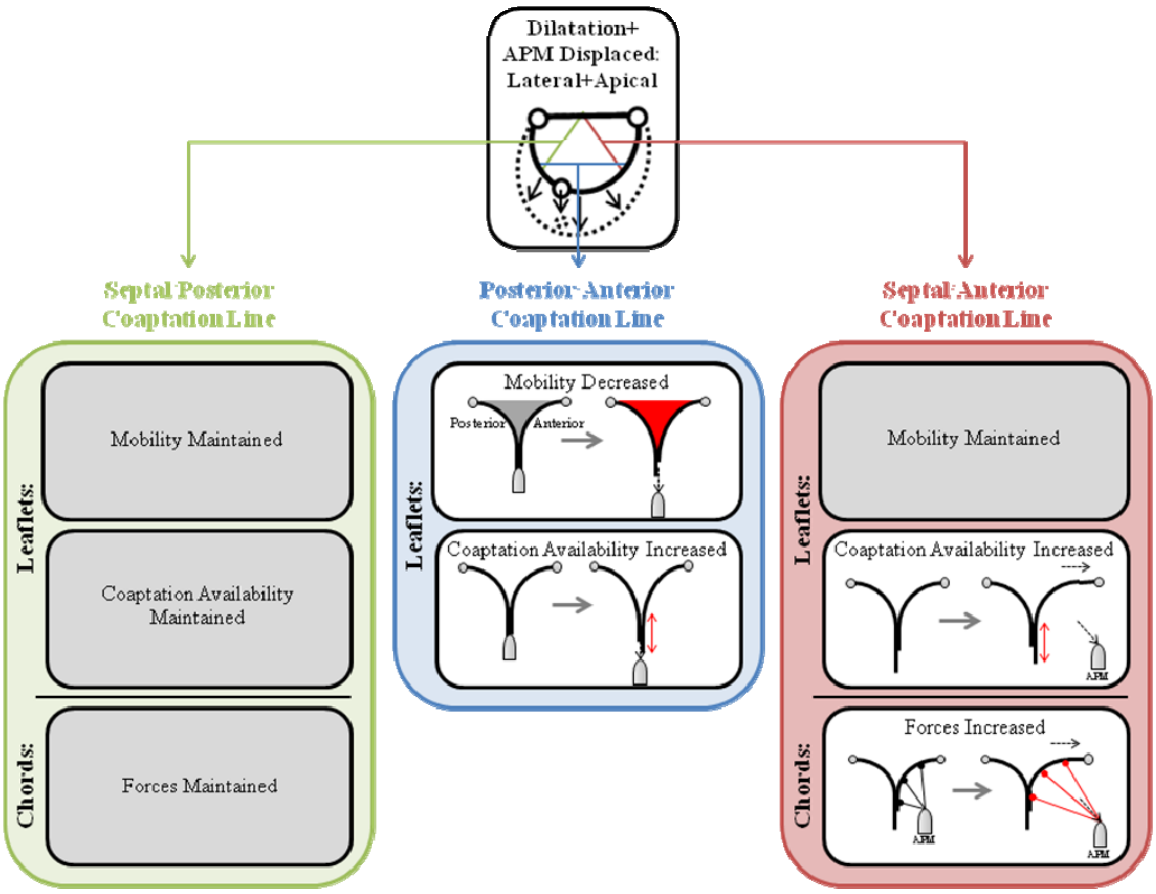

Figure 7.11: Schematic of significant alterations in the leaflets and chords as observed with combined annular dilatation and combined lateral and apical APM displacement. The schematic shows leaflet mobility, residual leaflet length and chordal forces along the three coaptation lines. Specific significant alterations are shown in bright red.

While apical displacement of the septal and posterior PMs had little effect on leaflet mechanics, it did result in a decrease in leaflet mobility at the septal/posterior coaptation line. The reason this was observed at the line of coaptation between the septal leaflet and anterior leaflet and not the posterior leaflet may be due to two reasons. First, with annular dilatation, the anterior leaflet is responsible for covering a majority of the orifice, thus restriction in the mobility of the leaflet may drastically alter coaptation. Secondly, it is important to note that the chords inserting into the septal PM are the shortest. Thus as the septal PMs is displaced by 10 mm, the septal/anterior zone may be

more affected since this is the location of the SPM and insertion of the chords into the anterior and septal leaflets.

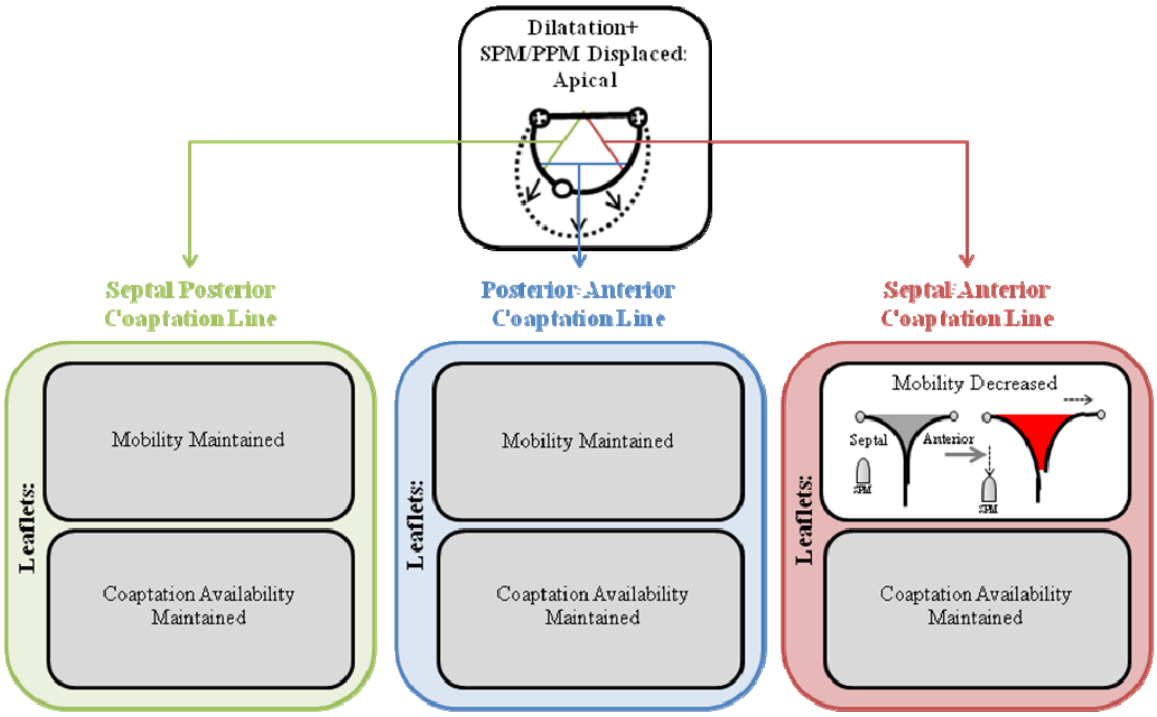

Figure 7.12: Schematic of significant alterations in the leaflets and chords as observed with combined annular dilatation and apical SPM and PPM displacement. The schematic shows leaflet mobility, residual leaflet length and chordal forces along the three coaptation lines. Specific significant alterations are shown in bright red.

Similar observations were made with displacement of the septal and posterior PMs in the anterior/posterior, lateral and apical directions as with isolated apical displacement. The decrease in mobility at the septal/anterior coaptation line may be explained with the same rationale as mentioned above.

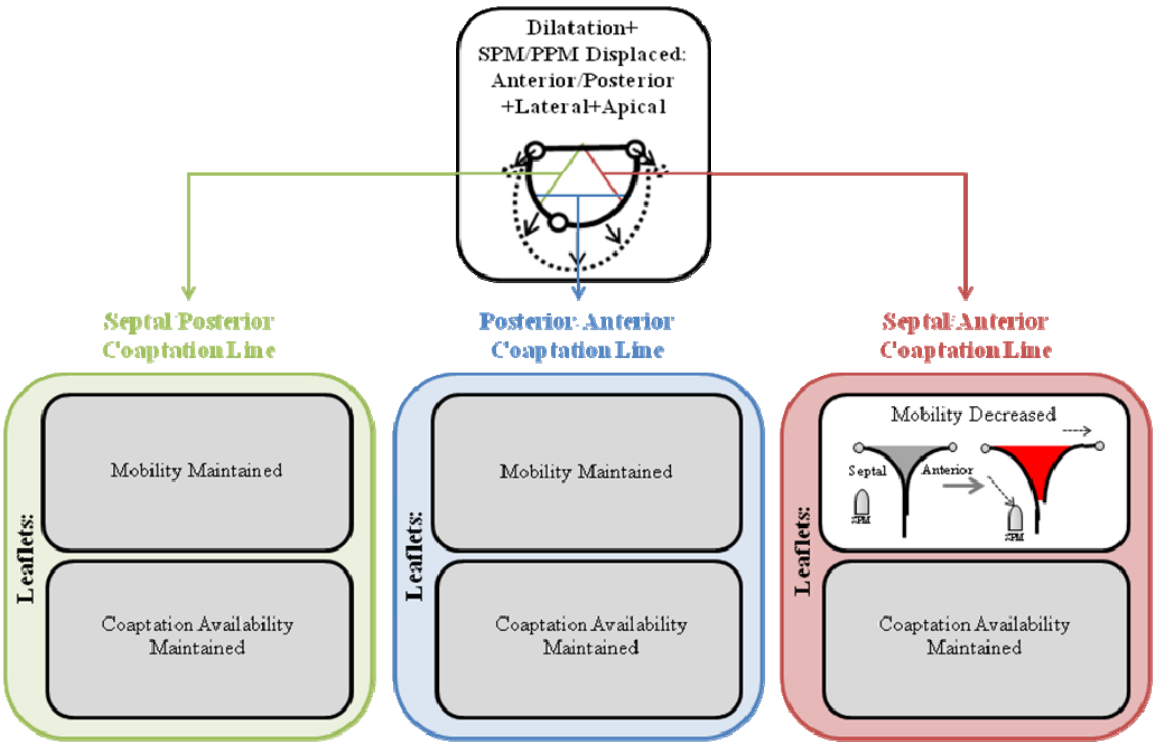

Figure 7.13: Schematic of significant alterations in the leaflets and chords as observed with combined annular dilatation and combined anterior, lateral and apical SPM and combined posterior, lateral and apical PPM displacement. The schematic shows leaflet mobility, residual leaflet length and chordal forces along the three coaptation lines. Specific significant alterations are shown in bright red.

As expected the most severe alterations in the annular and subvalvular apparatus resulted in the most severe changes in leaflet mechanics, as observed with changes along all three coaptation lines. Leaflet mobility was decreased along all three coaptation lines. As was reported with isolated displacement of all three PMs the line of coaptation was more towards the anterior/posterior annulus segment. The septal leaflet mobility was increased with lateral displacement of the septal and posterior PMs and the anterior leaflet mobility was decreased with lateral and apical displacement of the APM. Coaptation is further altered with the addition of annular dilatation as the anterior and posterior annular segments are displaced and the septal leaflet attempts to cover the increased orifice size since the anterior leaflet is restricted. The greatest levels of TR are

seen in this condition, both for annular dilatation of 40% and 100% because the septal leaflet is too short to cover the increasing orifice. Both anterior and posterior strut chordal forces increased, which can be attributed to the apical displacement of the APM and not the lateral displacement. The reason for this is that the lateral displacement when combined with annular dilatation reorients the APM with the annulus to a more normal state.

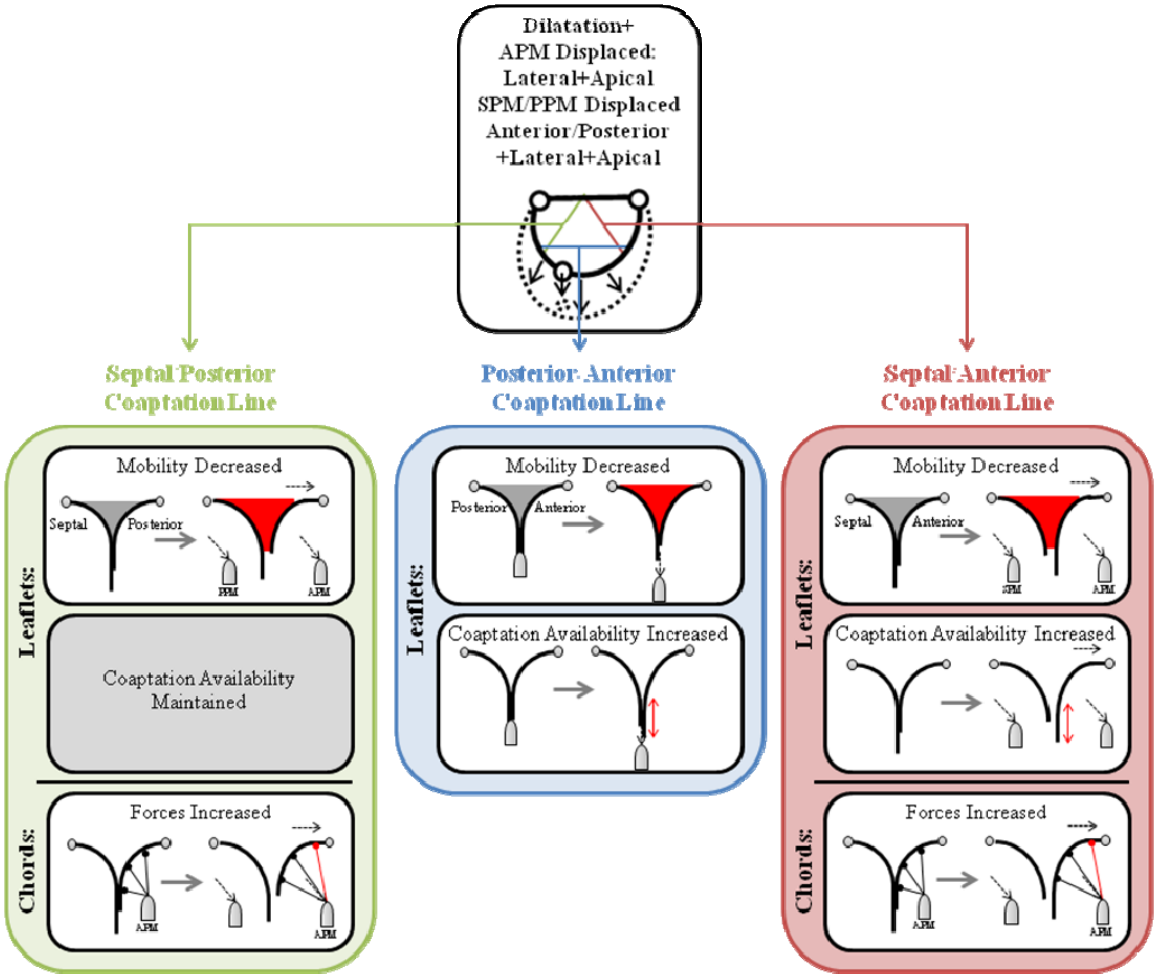

Figure 7.14: Schematic of significant alterations in the leaflets and chords as observed with combined annular dilatation and APM, SPM and PPM displacement. The schematic shows leaflet mobility, residual leaflet length and chordal forces along the three coaptation lines. Specific significant alterations are shown in bright red.

7.3 *In Vivo*/*In Vitro* Comparison

Since the *in* vivo (specific aim1) and *in* vitro (specific aims 2 and 3) sections were done simultaneously, it was not feasible to test PM positions which were found to be significant in aim 1 in both aims 2 and 3. For this reason, the relevance and comparison between the *in vivo* findings and *in vitro* simulations will be discussed here. Assumptions were made for *in vitro* simulations of PM displacement as no previous studies had been conducted to define actual PM displacement. *In vitro* experiments were done to systematically explore the effect of PM displacement, which cannot be done in patients. Displacement of the PMs was simulated by displacing the PMs on the septal wall simultaneously (PPM/SPM), simulating left ventricle (LV) dilatation[69], and the sole displacement of the APM to simulate right ventricle (RV) dilatation[23, 24]. Combined RV and LV dilatation was combined displacement of the anterior, septal and posterior PMs.

Completion of the *in vivo* study revealed different PM displacements than those simulated *in vitro*. Figure 7.15 demonstrates the overlap between the conditions simulated *in vivo* and *in vitro*.

	In Vitro	In Vivo		
	PM Displacement	RV Dilatation	LV Dilatation	RV/LV Dilatation
RV Dilatation	APM (Lateral)			
	APM (Apical)	x	x	x
	APM (Lateral+Apical)			
LV Dilatation	SPM/PPM (Anterior/Posterior)			
	SPM/PPM (Lateral)			
	SPM/PPM (Apical)	x		x (only SPM)
	SPM/PPM (Anterior/Posterior+Lateral+Apical)			
RV/LV Dilatation	APM (Lateral+Apical) SPM/PPM (Anterior/Posterior+Lateral+Apical)			

Figure 7.15: Overlapping *in vivo* and *in vitro* PM displacements.

While RV dilatation was simulated *in vitro* with only APM displacement, SPM and PPM displacement was measured *in vivo*. This was based on the assumption that RV dilatation would not result in displacement of the septal wall into the LV. It was believed that even with elevated RV pressures, the LV pressure remains higher than the RV pressure. *In vivo* echo measurements disproved this theory demonstrating displacement of the septal and posterior PMs towards the LV. As pointed out previously in the discussion, it may be an artifact of the *x*-reference, which is the center of the TV annulus, which may have moved laterally. This may account for the significant changes in SPM/PPM displacement, but not lateral APM displacement. As seen in the above figure apical displacement of the APM was observed for all *in vivo* cases, and was simulated *in vitro* but not in conjunction with apical displacement of other PMs as was observed *in vivo*. There was however a condition in which all PMs were displaced apically, but it was combined with displacement of the PMs in multiple other directions. While isolated LV

dilatation was simulated with SPM and PPM displacement, as it was assumed that the LV would dilate into the RV, only apical displacement was observed *in vivo*. Both the SPM and PPM were displaced apically *in vitro* but did not result in significant TR alone, which is consistent with *in vivo* findings of patients with dilated LVs having lower levels of TR. *In vitro* simulation of combined RV/LV dilatation was more severe than was seen *in vivo* as only the APM and SPM were displaced apically.

Comparison of the *in vivo* to *in vitro* results can help to provide a better understanding of the data. For example, *in vivo* results showed that patients with significant levels of TR were patients with a dilated RV or both ventricles. Interestingly these patients had a dilated annulus as well as PM displacement. When dilatation and PM displacement were combined *in vitro*, significant levels of TR were always observed irrespective of the type of PM displacement. Although displacement of the septal and posterior PM differed *in vivo* as compared to *in vitro*, *in vivo* studies demonstrated that TR was very sensitive to displacement of the septal and posterior PPM, as seen in both echo and MRI studies [72].

While differences did exist in the conditions found *in vivo* and those created *in vitro*, it is important to point out that all possible PM displacements may not have been observed in the patient population. Additionally, the *in* vivo results of PM displacements are show as an average of the population sampled and any deviations from the mean may have been lost with averaging. Thus, future *in vivo* studies may aim to target more specific patient populations with various types of dilatation and papillary muscle positions. Furthermore, the *in vitro* simulations demonstrate what conditions, both in isolation and combination, may result in TR but do not include all possibilities.

Comparing the annulus sizes measured *in vivo* and those simulated *in vitro* shows that the annulus size of patients with trace and mild TR, 8.7 cm^2 and 8.9 cm^2 is comparable to approximately 40% dilatation of the *in vitro* annulus, resulting in an annulus area of 8.4 cm^2. While this was the level of dilatation at which statistically significant TR was observed, it was not necessarily clinically significant, with levels of TR similar to those of mild TR *in vivo*. While the annulus size found in patients with moderate TR (11.4 cm^2) was similar to *in vitro* levels of TR measured with isolated dilatation of 100% (12 cm^2), the annulus size measured in patients with severe TR was much larger than what was simulated *in vitro*. With isolated annular dilatation of 100% as our max we were only able to create mild to moderate levels of TR *in vitro*. Based upon the *in vivo* findings, the creation of more dilatation would have resulted in higher levels of TR. Future studies should investigate annular dilatation greater than 100%.

7.4 Clinical Relevance

First and foremost it is important to understand a problem before it can be accurately corrected. For this reason the information presented in this thesis is of importance not only to the scientific community, to fill a gap in knowledge, but the clinical community as well. This thesis provides clinicians with a better understanding of how the tricuspid valve mechanics are altered with disease and an explanation of the resulting TR. If one were to look through the literature they would find some information on the tricuspid valve, but mostly about its anatomy, and little to nothing on the mechanics of the valve. As our lab has been instrumental in providing the clinical community with in depth information on the mitral valve for close to 20 years, this thesis serves as the first step in doing this for the tricuspid valve.

There is an increasing interest in the changes that occur in the anatomy of the tricuspid valve apparatus and the correlation of these changes with the severity of tricuspid regurgitation. In our study with the use of 3D Echocardiography the position of the RV PMs was identified for the first time and reported how their position was altered with ventricular dilatation. This study also showed the presence of leaflet tethering with PM displacement resulting in significant TR in patients. A detailed investigation of the parameters responsible for clinically significant TR, as presented here, can guide the clinician to target repairs to the direct cause of TR and thus may result in more durable repairs. In addition to highlighting the importance of geometry and pulmonary pressures in TR, this study also presented a reliable non-invasive technique which may serve to provide more patient-specific diagnosis and treatment. These findings help to change the future diagnosis and therapies of clinically relevant TR.

While this study consistently found that dilatation of the annulus area by 40% resulted in significant TR, the valves were of relatively similar size. Clinically, not all patients with annular dilation have regurgitation, and it is believed that this may be due to variations in leaflet and sub-valvular anatomy, with some patients' valves being larger to begin with and tolerate more dilatation. Additionally, some believe that the leaflets may possibly remodel *in vivo* to compensate for the altered environment, which cannot be simulate in vitro. This study showed that the anterior leaflet is responsible for compensating for an increase in orifice area as a result of annular dilatation in most cases. Thus, it may be important for the clinician to not only look at annulus size, but also at RLL to determine the potential for regurgitation. Although it may be difficult to measure RLL *in vivo* with current 2D and 3D echocardiograph techniques, leaflet length as

measured just before coaptation and coaptation length may be used to assess the valve. Future studies should be conducted to determine if in fact patients with annular dilatation but no TR have longer leaflets, specifically the anterior leaflet.

This has already begun to take place as knowledge and understanding of the tricuspid valve increase, changes are being made to clinical standards to incorporate this information. For example, AHA/ACC guidelines recommend repair for patients with tricuspid annular dilatation, specifically recommending annuloplasty to correct annular dilatation during left-side repair when mild TR is present[14]. Currently this decision only requires the consensus of clinicians and does not state the size at which the tricuspid valve annulus is considered dilated as with the mitral valve. Current repairs for functional TR focus mainly on reducing the size of the annulus to normal. This study shows that it may also be important to restore the available leaflet length for coaptation, providing as much overlap as possible, specifically in the central region. Repairing the annulus to its true size with a ring annuloplasty may not be enough in the presence of PM displacement, if the PMs are displaced enough to severely affect the mechanics of proper leaflet closure. With evidence that PM displacement alone can lead to TR, it may be important to investigate PM position and ventricular size, both RV and LV, in addition to annulus area when deciding to treat a patient. Potential adjunct procedures in the setting of leaflet tethering and PM displacement could include downsizing ring annuloplasty (a mainstay repair strategy in functional mitral regurgitation), or leaflet augmentation[57] to increase the amount of leaflet area available for coaptation. More specifically, evidence-based guidelines are ultimately needed to ensure patients are treated appropriately.

Furthermore, it is interesting to note that not all patients with RV dilatation had a dilated annulus. Annulus size within this patient group ranged from a very small sized annulus (4.3 cm^2) to an extremely dilated annulus (23.4 cm^2). While it cannot be elucidated from this data it is of interest to determine if in fact RV dilatation occurs first with remodeling of the ventricular, along with annular dilatation occurring secondary. The converse may also be true in that patients may first present with isolated annular dilatation, possibly due to enlargement of the right atrium, which may then result in remodeling of the RV. Thus, the combination of both annular dilatation and RV dilatation is most likely a more chronic condition.

Additionally, the alterations reported in tricuspid valve mechanics, through measurements of leaflet mobility, residual leaflet length and chordal force may help to provide clinicians with a road map to target repairs. This thesis used 3D echo for the first time, not only to identify and measure the PMs *in vivo*, but also to interrogate leaflet mobility across the three coaptation lines. By taking a closer look at the alterations in individual leaflet geometry and understanding displacement of which PMs are responsible, clinicians may be able to correct leaflet tethering with repairs to the PM responsible for tethering. Leaflet tethering continues to be a clinical relevant metric as studies correlate leaflet tethering to TR. Additionally, leaflet tethering is easily measured in the clinic and assessed by the clinician. The chordal force data are important to clinicians to better understand the role of individual chords to better guide repairs which reposition or even cut different chords. All cases of severe TR also experienced significant alterations in valve mechanics. For this reason to restore the valve to its

normal state, which is the ultimate goal, not only should regurgitation be addressed but an attempt made to restore valve mechanics to their original state.

7.5 Limitations

7.5.1 *In Vivo*

While the MRI study was limited to the effects of LV dilatation on the posterior and septal PMs, as they are located on the septal wall, the echo study was able to include both isolated and combined RV and LV dilatation. In addition, the 3D echo study allowed for direct correlations of alterations in the tricuspid valve annular and subvalvular apparatus to the grade of TR.

With the 3D echo study, the small number of patients within each group resulted in high variability within the group classifications. Future studies should aim to recruit additional patients and look at PM displacements in specific disease patterns, as those with different disease manifestations would be expected to have different remodeling characteristics. In addition, it would be interesting to determine if the severity of ventricular dilatation correlates to the magnitude of PM displacement. As noted in the discussion, although relative position of PMs to the annulus plane is important, it would be of interest to determine if the reference (annulus plane) or the PMs are moving in these patients, as it is difficult to identify a reference that does not move with disease. For example, the annulus plane was used as a reference in the study, but was found to be dilated and thus the center of the annulus in the diseased patients was not in the same relative position as in the normal patients.

It is important to point out the fact that in this study and in typical clinical practice, PA pressure is determined directly from the TR jet velocity. Although TR was

determined from the size of the TR jet, this is not completely independent of the velocity of the jet. The TR jet is dependent on both the orifice size and velocity; thus, the higher the PA pressure, the higher grade of TR. Previous studies which measured PA pressure both indirectly and directly, found PA pressure to be correlated with TR [16, 19]. Although not ideal, to truly investigate the correlation between TR and PA pressure, direct high fidelity catheter measurement of PA pressure should be conducted to confirm these findings.

It was not always feasible to identify all three PMs in a single patient as the septal and posterior PMs were often difficult to view. In addition it was often difficult to see the PM protruding from the wall, particularly in the case of the SPM and PPM. If the PM was not visible, the insertion point of the chordae into the wall was taken instead. Although the direct insertion of the chordae into the wall may not be evidence of the existence of a PM, it is the changes in the attachment location (chordae insertion) that are important, not necessarily the existence of a PM. Previous classifications of PM types have reported some PMs to be "fused", in which the chordae attached directly into the wall [42]. The same study reported there to be several PMs tips and chordae insertions for both the SPM and PPM, whereas the APM is usually one distinct PM [42, 43].

7.5.2 *In Vitro*

Although the rigidity of the right ventricle is not physiologic, it does not significantly impact the results of this study as this analysis is focused on the valve itself. Interactions between the right ventricle and valve apparatus are simulated by displacement of the PMs themselves. Many previous mitral studies[60, 61, 68, 85] have been published using a rigid ventricle box and have been instrumental in providing a better

mechanistic understanding of the valve under both physiological and pathologic conditions. With regards to the rigid annulus model used, it is believed that this is essential since these PM holders maintain a rigid position, thus the relative position between the two remains constant, which is supported by the literature [35]. Since measurements were made during systole, this system is maintained in a systolic state, for both the annulus and PMs. This is an accepted limitation of the study, and thus the impact of the results may be limited by the static nature of the ventricle and annulus.

Measurement of RLL reported here is an estimate of the leaflet available for coaptation as it does not take into account any curvature, stretching or compression which may occur when the leaflet surfaces join and thus may underestimate the actual length. The common technique which is currently practiced is to measure coaptation length, a surrogate of RLL, which provides a global measurement for the coapting leaflet length, but cannot distinguish individual leaflets. The method used here allowed us to determine each individual leaflets contribution to coaptation. The technique cannot be directly applied to clinical applications but only as a method to provide further information about leaflet mechanics.

Echo measurements for assessment of leaflet mobility were made across the three coaptation lines, whereas the location of malcoaptation was centrally located at the three leaflets. As it was of interest to understand how each individual leaflet was affected by disease it was impossible to take measurements as the center of the annulus as this is the point where the three leaflets come together, and therefore impossible to distinguish between the leaflets, specifically the anterior and posterior leaflets.

Finally, while a saddle shaped annulus similar to that reported in humans [12, 33] was used on the control conditions for the PM displacement and combined cases, isolated annular dilatation studies had a flat annulus. It is believed that the presence or absence of a saddle in this study did not affect the results as the closing volume between valves (n = 8) with and without a saddle in a control position (normal annulus size and PM location) was compared and found no significant difference ($p \leq 0.05$).

CHAPTER 8

CONCLUSIONS

Through both *in vivo* and *in vitro* investigations, the mechanics of the tricuspid regurgitation and the role of annular and subvalvular alterations were investigated. *In vivo* analysis was able to determine PM displacements of disease patients as compared to controls and correlate them and annulus area to TR. *In vitro* investigations extended this analysis and provided detailed mechanics responsible for TR.

The *in vivo* study showed that 3D echocardiography can be used to identify and measure the position of all three PMs of the tricuspid valve for normal and diseased patients. This study found that dilatation of both ventricles results in displacement of the RV PMs. Apical and lateral displacement of all PMs was significantly correlated to the grade of TR and leaflet tethering, with the exception of lateral displacement of the APM. PA pressure, classification based upon RV and LV size, annulus area, and apical displacement of the APM were all predictors of the severity of TR. Increases in PA pressure lead to geometric changes in the ventricles, which results in alterations to the TV apparatus including both the annulus and PMs. A complete investigation of the parameters responsible for clinically significant TR as presented here can help the clinician to target repairs to the direct cause of TR and thus may result in more durable repairs. In addition to highlighting the importance of geometry and pulmonary pressures in TR, this study also presented a reliable non-invasive technique which may serve to provide more patient-specific diagnosis and treatment.

The *in vitro* study demonstrates that while annular dilatation can alone lead to TR, isolated PM displacement can also cause TR, with the most severe TR achieved with a combination of these conditions. Alterations in either the annulus size or PM position result in the distortion of proper coaptation mechanics. With annular dilatation the anterior leaflet attempts to compensate for the dilatation since it is the section which is most commonly dilated. While no changes were observed in leaflet mobility, marginal chords were engaged as a result of dilatation as they were no longer in the coaptation zone and assisted in preventing leaflet prolapsed. With isolated PM displacement the septal leaflet has the largest reduction in RLL, which may be attributed to numerous chordae insertions into the leaflet. Overall, severe displacement of the PMs, with all PMs displaced simultaneously in multiple directions, was necessary to cause alterations in leaflet mobility. In addition the strut chordal forces increased with multidirectional displacement of the PMs. In combined cases of annular dilatation and PM displacement, the increased annulus diameter (annular dilatation) and leaflet tethering (PM displacement), drastically changed leaflet coaptation and altered chordal forces.

This study showed that with disease, as simulated with annular and subvalvular geometric alterations, leaflet coaptation is initially altered which results in redistribution of chordal forces. This study helps to identify situations in which the valve mechanics are significantly altered and may provide insight for targeting repairs of the tricuspid valve. In conclusion, addressing annular size and PM location may be important for effectiveness and durability of tricuspid valve repairs.

CHAPTER 9

RECOMMENDATIONS

With regards to the *in vivo* study, the small number of patients within each group resulted in high variability within the group classifications. Future studies should aim to recruit additional patients and look at PM displacements in specific disease patterns, as those with different disease manifestations would be expected to have different remodeling characteristics. In addition, it would be interesting to determine if the severity of ventricular dilatation correlates to the magnitude of PM displacement. As noted in the discussion, relative position of PMs to the annulus plane is important. Thus, it would be of interest to determine if the reference (annulus plane) or the PMs are moving in these patients, as it is difficult to identify a relevant reference that does not move with disease.

It is important to point out the fact that in this study, and in typical clinical practice, PA pressure is determined directly from the TR jet velocity. Although TR was determined in this study from the size of the TR jet, this measurement is not completely independent of the velocity of the jet. The TR jet is dependent on both the orifice size and velocity; thus, the higher the PA pressure, the higher grade of TR. Previous studies which measured PA pressure both indirectly and directly, found the values to be correlated with TR [16, 19]. Although not ideal, to truly investigate the correlation between TR and PA pressure, direct high fidelity catheter measurement of PA pressure should be collected to confirm these findings.

The logical next step for the *in vivo* and *in vitro* work is to investigate the effects of pulmonary hypertension of TR, as this is of particular interest to the clinical community. While PA pressure is accepted as a contributor to TR and was confirmed with the *in vivo* findings in this thesis, the mechanisms by which this occurs are still unknown. In vivo studies may aim to determine which PA hypertension patients present

with severe TR, and if there are any geometrical correlations. Furthermore, it would be of interest to see if current treatment for PA hypertension also results in a reduction of TR, and if so by what mechanism. Long term studies may be important to determine the outcome of patients in which the TR is reserved with PA hypertension treatment. If in fact patients in which the TR remains have poor outcomes repair for the tricuspid valve may be necessary. The in vitro flow loop provides an ideal system to isolate parameters to see if it is the increase in pressure, providing a greater force on the TV apparatus, or the secondary change in geometry, or a combination of the two which contributes to TR.

Additional conditions of PM displacement which were identified *in vivo* should be investigated *in vitro*. For example, in vitro studies assumed only the APM was displaced with RV dilatation, but *in vivo* findings showed that in addition to the APM, the SPM and PPM are also displaced. While no significant increase in TR was seen with APM displacement alone *in vitro*, significant TR was created when all PMs were displaced, although the SPM and PPM were displaced in the opposite direction, towards the RV, as reported *in vivo*. Combined displacement of the APM, SPM, and PPM away from the RV, would be expected to further exacerbate TR.

While the role of a saddle shaped annulus was not shown to have a significant effect on the TR as well as leaflet strain, future studies may look to investigate the effect of chordal forces. Saddle shape may result in a redistribution of chordal forces as it would alter the distance from the annulus to the PMs at certain locations of the annulus.

This thesis focused solely on functional tricuspid regurgitation and did not investigate any of the many congenital abnormalities with result in significant TR. For example, Ebstein's is a disease in which the leaflets of the tricuspid valve are often attached directly to the ventricle wall or septum, resulting in severe TR. While tricuspid valve alterations occur with many congenital defects the resulting geometries are widely variable. Any information into the mechanism behind the TR in these cases may further assist the clinicians with repairing the valve and eliminating TR.

APPENDIX A

COMPARISON OF HUMAN AND PORCINE TRICUSPID VALVES

A study was completed to investigate to compare the anatomy of human tricuspid valves to those of porcine valves. Porcine measurements were taken of the annulus, leaflets, chords and papillary muscles. These measurements were compared to similar measurements found in literature for human tricuspid valves.

AN APPROPRIATE MODEL FOR THE HUMAN TRICUSPID VALVE: THE PORCINE TRICUSPID VALVE

INTRODUCTION

Interest in the tricuspid valve and its role in tricuspid regurgitation (TR) are on the rise. TR was previously thought of as benign, but recent studies have found it to affect morbidity and mortality [1]. With an increased interest, research studies are being conducted to understand the valve *in vivo* for both human and animal subjects. Although *in vivo* studies have provided us with initial insight into the disease, to truly understand the mechanics of the valve, animal testing and *in vitro* studies are necessary. Such studies would allow the investigator to understand the valve in a controlled environment. Acquisition of disease free human hearts for research purposes is often challenging as normal hearts are typically allocated for transplant recipients, and those typically used for research purposes have heart disease. In addition, the source of the human hearts is most often limited and inconsistent. Since the acquisition of human valves is difficult, we must first determine an appropriate animal model for the human tricuspid valve to be studied *in vitro*.

Studies have looked at both ovine [35, 36] and porcine [42, 43] specimens to serve as a model for the human tricuspid valve. However, these studies did not focus in detail on the size and shape of the annulus or leaflets. Although many studies have looked at various components of the TV, no study exists that both looks at the valve in its entirety and compares an alternative species to a human valve. Although the porcine heart is typically accepted as a good model for the human heart [31, 43] it has not been investigated in detail

for the tricuspid valve and its valvular and subvalvular components, which has been done for the mitral valve [86, 87]. This study will compare the annulus, leaflets, chordae tendineae and papillary muscles of the human tricuspid valve to the porcine valve to demonstrate that the porcine valve is an appropriate model for the human tricuspid valve.

MATERIALS AND METHODS

Porcine specimens were obtained from a local abattoir (Holifield Farms, Covington GA) from female non pregnant pigs ages 6-12 months, 600 lbs.. Porcine hearts had an average weight of 941 $\pm$ 86 grams. Measurements were taken on fresh hearts within 4 hours of slaughter. Hearts were selected which had an approximate annulus area of 10 cm^2. Hearts were removed from the study if there was damage to the TV as a result of slaughter. The various measurement methods used for porcine hearts were comparable to those used to obtain the reference human data. Specific descriptions as to why each method was selected for comparison are detailed below.

Annulus: The right atria was removed from the flaccid porcine hearts (n = 10) to expose the tricuspid valve and the ventricle was statically pressurized to 40 mmHg to simulate normal systolic ventricular pressure. Pressurization was achieved by placing a tube in the RV through the pulmonary valve. A bucket was then attached to the end of the tube and elevated to a height to achieve a static pressure head of 40 mmHg when filled with water. A ruler was placed in the annulus plane for reference. Pictures were then taken of the pressurized valve. The annulus area and diameter were measured both in the septal/lateral (SL) and posterior/anterior (AP) directions. The annulus was traced in Matlab R2007a (Mathworks, Natick, MA) to determine the area. The centers of the anterior and posterior

annulus segments were selected and the distance was measured using Matlab to determine AP diameter. This same procedure was repeated for the SL diameter with the center of the septal and anteroposterior segments. Human measurements of diameter (SL [22, 33, 37] and AP [22, 33]) and annulus area [34, 37, 38] were taken from studies that used 2D and 3D *in vivo* measurements. Human measurements during diastole were used since they are most similar to the statically pressurized porcine hearts, as they are not contracted.

Porcine annulus segment length and circumference measurements were performed on intact flattened hearts (n = 10) in which an incision was made through the right ventricle at the free wall connection between the septal and posterior leaflets. Pictures were then taken of the valve with a reference ruler at the annulus. Segment lengths were traced in Matlab along the annulus between the posteroseptal (PS) and anteroseptal (AS) commisures, and along the septal leaflet for the septal segment and the anterior and posterior leaflets for the anteroposterior (AP) segment (Fig. 1a) to determine distance.

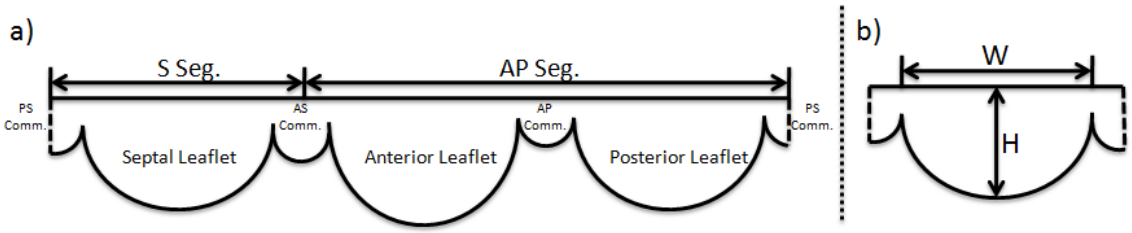

Figure A.1: Schematic of annulus and leaflet measurements. a) Segment length measurements: septal segment (S Seg.) measured from the posterior/septal (PS) commisure to the anterior/septal (AS) commisure across the septal leaflet, anteroposterior segment (AP Seg.) measured from the anterior/septal commisure (AS Comm.) to the posterior/septal commisure (PS Comm.) across the anterior and posterior leaflets. b) Location of width (W) and height (H) measurement of each leaflet.

Circumference was calculated as the addition of the two segments. This method mimicked that of Fernando et al. on fresh human hearts [88] which was used for human comparison.

Leaflets: Porcine leaflet measurements were made using the same methods as previously described to measure segment lengths with intact flattened hearts. Leaflet height and width were measured with a ruler (Fig. 1b). Leaflet area was calculated by analyzing images in Matlab by identifying the reference distance on the ruler to determine pixel spacing and tracing the leaflet perimeter to define the analysis area. Human leaflet height, width and area data from fixed hearts [31, 40] was used for comparison as there have been no accurate methods of in vivo quantification of leaflet length and width. In order to account for changes due to fixation, normalization was also investigated in which the values of the measurements were normalized by the circumference of the fixed hearts. Relative leaflet size was compared to 3D echocardiographic human findings of Shah [39] and Anwar [37].

Papillary Muscles: Porcine observations of the papillary muscles (PM) were made on intact flattened hearts (n = 10) ensuring that all PM structures were maintained. The PMs were defined using relative leaflet position, with the anterior PM located between the anterior and posterior leaflets, septal PM, also known as the medial or conus muscle, between the septal and anterior leaflets, and posterior PM located between the septal and posterior leaflets. The size of the PMs was also noted and whether the PM had multiple heads or was fused to the wall. In addition to the three main PMs, observations were made as to the presence and location of the moderator band, which extends from the free wall to the septal wall. Comparison to human PMs were made to observations of cadaver hearts by Crick et al. [43].

Chordae Tendineae: Valves were exposed as previously described for annulus measurement and then excised with annulus, leaflets, chords and PMs intact. Porcine

chordae tendineae were classified into similar groups as seen in humans based upon insertion location: 1 - Free Edge/Marginal (n = 26), 2 - Rough Zone/Supplemental (n = 27), 3 - Deep/Strut (n = 24) for each leaflet (Fig. 2).

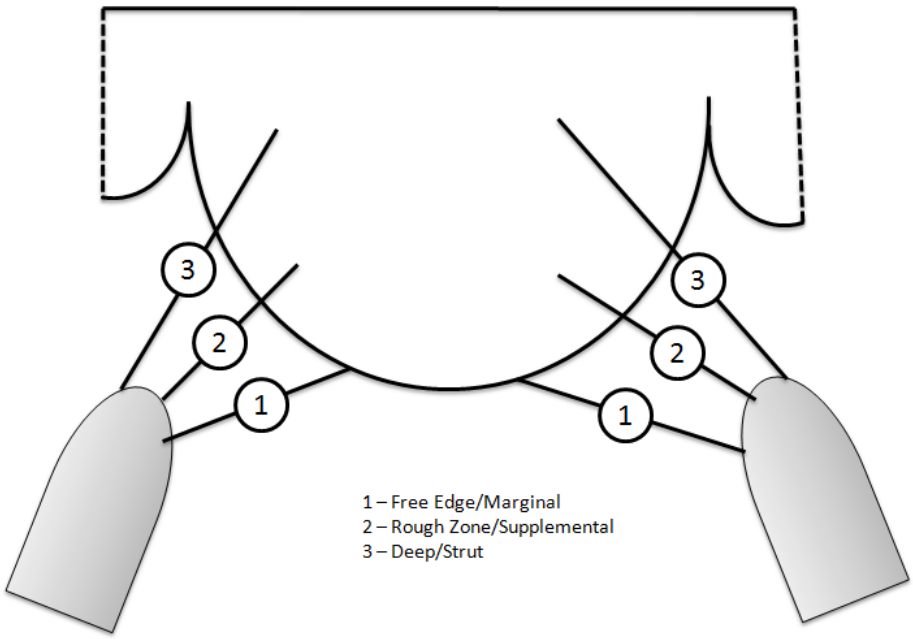

Figure A.2: Insertion location of chordae tendineae, with classification based upon insertion location into leaflet.1) marginal/primary - inserting into the free edge of the leaflet, 2) rough zone/supplemental - inserting between the marginal and intermediate chords, and deep/secondary - inserting into the belly of the leaflet.

Chordae were cut at the PM tip and leaflet insertion location. Laser micrometry was used to obtain chordae diameter along the entire length of the chord and an average diameter was then calculated. Human chordae measurements were taken from Silver et al. [31] and normalized by leaflet width to account for fixation.

Statistical Analysis: All statistical analyses were completed in Minitab 15 (Minitab Inc., State College, PA). A 2 sample t-test with summarized data was used for comparison. Summarized data, which included sample size, mean, and standard deviation, was used as raw values were not available from previously published data. Results are presented as mean $\pm$ standard deviation. A significant difference was determined at a 99% confidence

level, to minimize the differences due to chance since the comparisons are across studies, with the assumption that the sample population was normally distributed.

RESULTS

Minimal significant differences were seen between porcine and human anatomy when normalized. The comparison is divided into annulus, leaflet, PM and chordae tendineae measurements.

Annulus: Results for the comparison between human and porcine for annulus measurements can be found in Table A.1.

Table A.1: Annulus measurements for both human and porcine specimens. Both absolute and normalized values are shown.

	Absolute Value					Normalized by Annulus Area				
	Human		Porcine			Human		Porcine		
	Mean	± SD	Mean	± SD		Mean	± SD	Mean	± SD	
Diameter (cm)										
SA (SL)	3.28	0.64	3.19	0.25		0.32	0.06	0.32	0.03	
AP	3.58	0.49	4.70	0.41	*	0.35	0.05	0.47	0.04	*
Area (cm^2)	10.34	2.55	9.99	1.33						
Circumference (cm)	11.80	1.27	15.50	0.98	*	1.15	0.12	1.55	0.10	*
Segment Lengths (cm)						Normalized by Circumference				
AnteroPosterior	8.54	0.83	9.60	0.53	*	0.72	0.07	0.62	0.03	*
Septal	3.20	0.85	5.90	0.53	*	0.27	0.07	0.38	0.03	*

* = $p<.01$ as compared to human

There were no significant differences between human and porcine when comparing annulus area as this was used for inclusion criteria. Human circumference (11.8 $\pm$ 1.27 cm) was significantly ($p < 0.01$) smaller than porcine valves (15.5 $\pm$ 0.98 cm). Comparison of normalized human measurements of the SL (n = 52) [22, 33, 37] diameter to measured porcine valves found no significant difference, while comparison of the AP (n = 22) [22, 33] diameter to measured porcine valves found a significant difference ($p < 0.01$)

when normalized by annulus area for comparison. There was a significant difference ($p < 0.01$) between the anteroposterior and septal segment lengths for porcine when compared to human measurements on flattened hearts ($n = 30$) [88]. Human and porcine segment length measurements were normalized by the circumference for comparison.

Leaflets: Results for the comparison between human and porcine leaflet measurements can be found in Table A.2.

Table A.2: Leaflet measurements for both human and porcine specimens, including length/height, width and area for all leaflets. Both absolute and normalized values are shown.

	Absolute Value					Normalized by Circumference				
	Human		Porcine			Human		Porcine		
	Mean	± SD	Mean	± SD		Mean	± SD	Mean	± SD	
Length/Height (cm)										
Anterior	2.90	0.44	3.20	0.38	*	0.24	0.04	0.21	0.02	*
Septal	2.33	0.39	2.70	0.81	*	0.19	0.03	0.17	0.05	
Posterior	2.55	0.41	3.20	0.23	*	0.20	0.03	0.21	0.01	
Width (cm)										
Anterior	3.42	0.85	3.80	0.63	*	0.28	0.07	0.25	0.04	
Septal	3.37	0.85	4.20	0.57	*	0.28	0.07	0.27	0.04	
Posterior	2.59	0.91	2.80	0.23	*	0.21	0.07	0.18	0.01	*
Area (cm^2)										
Anterior	4.53	1.72	7.90	1.23	*	0.37	0.14	0.51	0.08	*
Septal	4.04	1.74	7.70	3.09	*	0.33	0.14	0.50	0.20	
Posterior	3.11	1.73	4.80	1.36	*	0.25	0.14	0.31	0.09	

* = $p<.01$ as compared to human

Minimal differences were seen in porcine leaflet geometry when compared to human leaflet height and width measurements on intact fixed hearts [31, 40] and *in vivo* 3D real-time echo measurement of height[22] and area [37, 40]. When normalized by circumference, significant differences ($p < 0.01$) were seen in posterior leaflet width, with human (0.21 ± 0.07) wider than porcine (0.18 ± 0.01) and anterior leaflet length, with human (0.24 ± 0.04) being larger than porcine (0.21 ± 0.02) and anterior leaflet area, with human ($0.37 \pm$

0.14) larger than porcine (0.51 $\pm$ 0.08). A further comparison between groups was completed to better understand the relative dimensions of the leaflets to each other (Fig. 3).

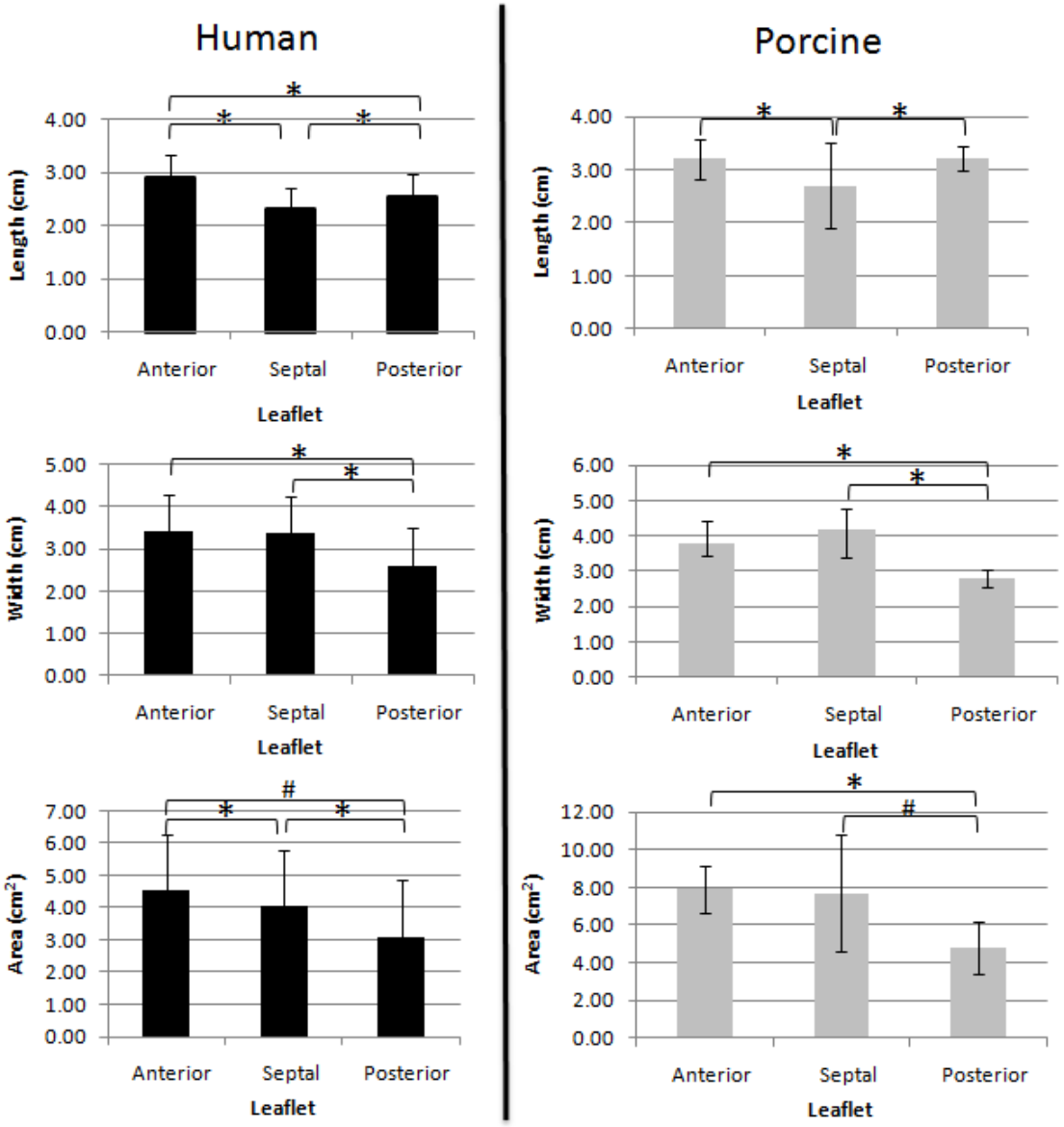

Figure A.3: Relative comparison within human and porcine specimens for leaflet length, width and height. * = $p \leq 0.05$, # = $p \leq 0.10$ using a two sample T-test.

The septal leaflet was the shortest for both human and porcine. The posterior leaflet was the smallest in width for both human and porcine. For both human and porcine the posterior leaflet had the smallest area.

Papillary Muscles: The comparison between human and porcine PMs on flattened hearts was qualitative. A representative image from a porcine heart and a normal human heart, obtained for this study, are shown in figure 4.

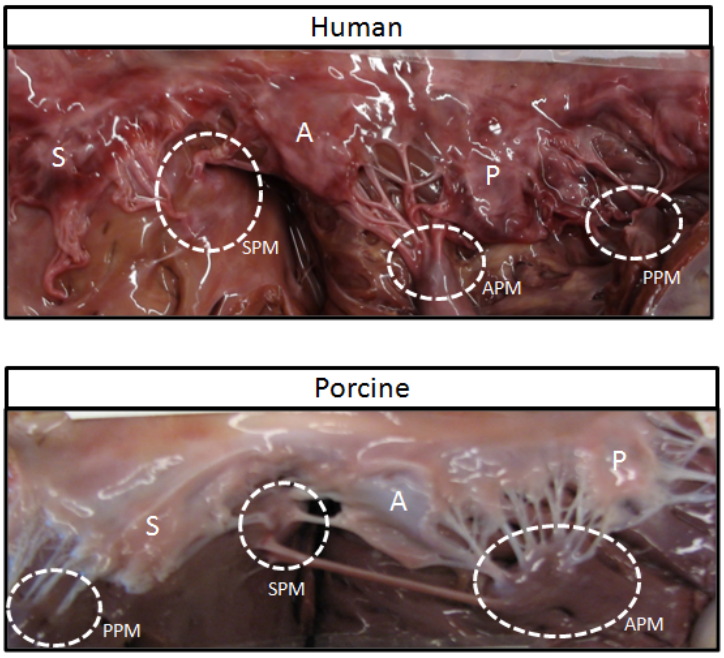

Figure A.4: Representative images of a flattened human tricuspid valve and porcine tricuspid valve comparing papillary muscle morphology and insertion location. Abbreviations: A-Anterior Leaflet, P-Posterior Leaflet, S-Septal Leaflet, APM-Anterior papillary muscle, PPM-Posterior papillary muscle, SPM-Septal papillary muscle.

Observations in the porcine PMs were similar to those previously reported by Joudinaud [42] on 50 porcine hearts. Both human and porcine hearts had similar PM insertion location into the ventricle, with the anterior PM on the free wall and the posterior and septal PMs on the septum. Porcine and human PMs are of similar type, with protruding, fused and multiple muscle heads and can be classified in the same manner, by location. The anterior

PM is the largest and most well defined [43], with the posterior PM having many attachments, and the septal PM the smallest and often fused to the wall [42], with chordae inserting directly into the free wall. Relative location was similar in both species.

The moderator band was present on all porcine hearts analyzed. Diameter of the moderator band was variable but consistent with attachment from the free wall to the septal wall was observed. A previous study comparing human to porcine anatomy reported the moderator band to be present in both porcine and human hearts [43]. They reported the structure to be more prominent in the porcine heart and located further from the apex as compared to humans.

Chordae Tendineae: Porcine chordae tendineae were observed for all groups which have previously been reported in the human TV [31], with the marginal/primary, inserting into the free edge of the leaflet, rough zone/supplemental inserting between the marginal and strut chords, and deep/strut inserting into the belly of the leaflet. A representative image of porcine and human chordal insertions can be seen in figure 5.

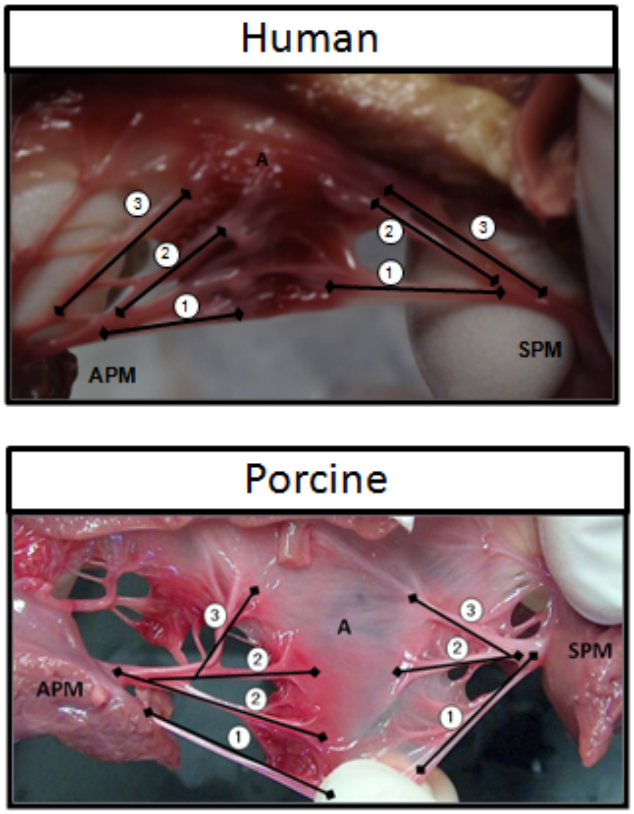

Figure A.5: Representative image of chordae tendineae classification for both human and porcine tricuspid valves. Free Edge/Marginal (1), Rough Zone/Supplemental (2), and Deep/Strut (3) chordae are shown.

Variation exists between chords from valve to valve, but the main chordae groups were present [32]. Human measurements taken from Silver et al. [31] were compared to porcine measurements of all chordae and found a significant difference ($p < 0.01$) between chordae diameter was only seen in rough zone/supplemental for the septal leaflet when normalized by anterior leaflet width (Table 3).

Table 3: Chordae tendineae measurements for both human and porcine specimens, including free edge/marginal, rough zone/supplemental and deep/intermediate for all leaflets. Both absolute and normalized values are shown.

	Absolute Value				Normalized by Ant. Leaflet Width				
	Human		Porcine		Human		Porcine		
	Mean	± SD	Mean	± SD	Mean	± SD	Mean	± SD	
Diameter (mm)									
Anterior Leaflet									
Free Edge/Marginal	0.80	0.20	1.12	0.36	0.23	0.06	0.30	0.09	
Rough Zone/Supplemental	1.10	0.40	1.09	0.18	0.32	0.12	0.29	0.05	
Deep/Strut	1.00	0.40	1.37	0.45	0.29	0.12	0.36	0.12	
Posterior Leaflet									
Free Edge/Marginal	0.80	0.20	1.03	0.25	0.23	0.07	0.27	0.07	
Rough Zone/Supplemental	0.90	0.20	0.96	0.34	0.26	0.07	0.25	0.09	
Deep/Strut	0.90	0.30	1.12	0.44	0.26	0.10	0.29	0.12	
Septal Leaflet									
Free Edge/Marginal	0.80	0.30	0.62	0.17	0.23	0.10	0.16	0.04	
Rough Zone/Supplemental	0.90	0.20	0.62	0.09	0.26	0.07	0.16	0.02	*
Deep/Strut	0.80	0.30	0.87	0.23	0.23	0.10	0.23	0.06	

* = $p<.01$ as compared to human

DISCUSSION

The main difference in the human and porcine heart is the position in the body as the human stands upright while porcine specimens are on all fours. While this may affect the naming of the leaflets, this study demonstrated that the structure of the tricuspid valve is similar between porcine and human species, irrespective of the orientation of the heart in the body. In this study, the leaflets were named as if the heart was sitting on its apex (septal, anterior and posterior) [89] and not as if anatomically oriented in the heart (septal, antero-superior, and inferior). Controversies over the proper naming of the leaflets continue to exist [90]. The leaflets in this study were named as such to be consistent with recent publications in the field [9, 39, 42, 88].

Comparisons of the annulus indicated a difference in the AP diameter. This may be due to the fact that human measurements were completed using echocardiography, and the difference seen may be due to the low echo resolution. Also, determining the AP diameter *in vivo* is subjective as it is very difficult to determine the exact center of the anterior and posterior annulus segments. The measurements performed on the porcine hearts may be more accurate than what is possible with echocardiography. It is important to note that although the annulus area measurements were similar the circumference was not. The study in which the circumference data was extracted did not report the annulus or heart size; it only stated that the hearts were from adult cadavers, thus they may have differed in size than the human hearts used to determine annulus area. The difference seen in the circumference between species is most likely due to the difference in size of the porcine hearts used in this study and the typical adult human heart. For this reason the circumference was used as a normalization factor throughout the study. Segment lengths also differed for human and porcine. Since segment lengths were determined between the commissures, there is variability in choosing the center of the commissure accounting for this difference.

The leaflet geometry was in overall agreement. Although there were differences seen between species in length, width and area, further investigation found no difference in the relative sizes when compared within the species. It is the relative sizes that are most important when the valve as a whole is used to study mechanics, since investigation is conducted to understand how the entire valve works together. Comparison of leaflets was restricted to the main leaflets and did not include the scallops due to the large variability in number and size of the scallop leaflets as reported in both humans and

porcine valves [42]. Measurements in this study were conducted on the three main leaflets, although studies have reported a variable number of leaflets, with 2 to 7 leaflets present [32, 91].

This study also provides a baseline for porcine valve selection for *in vitro* studies. In this study the difference in the specimens were minimized when normalized to account for the difference in size of the hearts. It may be possible to select for valves that are more similar in size to humans and to exclude those with large structural differences. Valves should be selected to minimize differences in annulus area, leaflet height and width, with similar PM structure and chordae insertion location.

Human vs. Porcine Measurement Method Comparison

The human hearts that were used in reported studies were normal, with no clinical implication of tricuspid valve disease. Human measurements, which were used for comparison, were taken from several literature sources.

Justifications for comparisons of reported human measurements to measured porcine valves can be made. Human measurements taken from Silver et al. [31] which were used to compare chordae tendineae diameter were normalized by leaflet width as this was the only appropriate normalization parameter provided in the human study. We expect similar effects in structure due to fixation on chordae as to leaflet width, due to similar collagen alignment. Diastolic measurements were used for all *in vivo* human data, as this is most similar to an excised heart which is in a relaxed state. Despite best efforts to mimic measurement techniques used on existing human data, some of the difference may be attributed to measurement discrepancy. Indexing was used for comparison, as there are not only variations across species but within the species themselves. It is not uncommon

for a normalization factor to be utilized when analyzing clinical data, thus we have chosen to do so in this study. Ideally it would be best to obtain human hearts and porcine hearts of similar size for a direct comparison. Even with this method, some differences are to be expected due to the fact that there is a large amount of variability within each species.

Accounts of human observations on the TV and its components are limited, especially with respect to PMs. It is necessary for future studies to do an exhaustive analysis of the human TVs which includes the location and structure of the PMs. Most studies of the human TV have been limited to the annulus [22, 29, 33-36, 38, 88], which may coincide with recent attempts to surgically repair the annulus. Studies of the annulus *in vivo* have not only looked at size, but shape as well [12, 33] and have commented on the 3D nature of the annulus. This amount of detail as to 3D shape was not completed in this study as the porcine hearts were excised and as such would not be expected to retain its natural 3D geometry.

In conclusion, this investigation provides a complete and thorough examination of the porcine tricuspid valve and its similarities to the human valve. We found the porcine tricuspid valve to be an appropriate model for the human valve due to minimal significant differences in valvular and subvalvular anatomy. The porcine tricuspid valve may thus be used as a model for *in vitro* testing as the relative structure of the valve is maintained within the two species. The specimens share similar geometric measurements of the annulus, leaflets, chordae tendineae and papillary muscles.

The identification of an appropriate model for *in vitro* investigation will greatly aid research as it is not always feasible to obtain human valves, due to cost and

availability of healthy valves. It is important to note that the purpose of this study was to identify an acceptable model for *in vitro* testing and the authors make no claims for a replacement to a native human valve *in vivo*.

REFERENCES

[1] Bruce CJ, Connolly HM. Right-sided valve disease deserves a little more respect. Circulation 2009;119:2726-2734.

[2] Jouan J, Pagel MR, Hiro ME, Lim KH, Lansac E, Duran CMG. Further information from a sonometric study of the normal tricuspid valve annulus in sheep: Geometric changes during the cardiac cycle. Journal of Heart Valve Disease 2007;16:511-518.

[3] Hiro ME, Jouan J, Pagel MR, Lansac E, Lim KH, Lim HS, Duran CMG. Sonometric study of the normal tricuspid valve annulus in sheep. Journal of Heart Valve Disease 2004;13:452-460.

[4] SIMON J. CRICK MNS, SIEW YEN HO, LIOR GEBSTEIN,, ANDERSON RH. Anatomy of the pig heart: comparisons with normal human cardiac structure. J Anat 1998;193:105-119.

[5] Joudinaud TM, Flecher EM, Duran CMG. Functional terminology for the tricuspid valve. Journal of Heart Valve Disease 2006;15:382-388.

[6] Silver MD, Lam JH, Ranganat.N, Wigle ED. CLASSIFICATION OF TRICUSPID VALVE CHORDAE TENDINEAE. American Journal of Pathology 1971;62:A105-&.

[7] Kunzelman KS, Cochran RP, Verrier ED, Eberhart RC. Anatomic basis for mitral valve modelling. J Heart Valve Dis 1994;3:491-496.

[8] Perloff JK, Roberts WC. The mitral apparatus. Functional anatomy of mitral regurgitation. Circulation 1972;46:227-239.

[9] Fukuda S, Saracino G, Matsumura Y, Daimon M, Tran H, Greenberg NL, Hozumi T, Yoshikawa J, Thomas JD, Shiota T. Three-dimensional geometry of the tricuspid annulus in healthy subjects and in patients with functional tricuspid regurgitation - A real-time, 3-dimensional echocardiographic study. Circulation 2006;114:I492-I498.

[10] Anwar AM, Geleijnse ML, Soliman OII, McGhie JS, Frowijn R, Nemes A, van den Bosch AE, Galema TW, ten Cate FJ. Assessment of normal tricuspid valve anatomy in adults by real-time three-dimensional echocardiography. International Journal of Cardiovascular Imaging 2007;23:717-724.

[11] Park YH, Song JM, Lee EY, Kim YJ, Kang DH, Song JK. Geometric and hemodynamic determinants of functional tricuspid regurgitation: A real-time three-dimensional echocardiography study. International Journal of Cardiology 2008;124:160-165.

[12] Kwan J, Kim GC, Jeon MJ, Kim DH, Shiota T, Thomas JD, Park KS, Lee WH. 3D geometry of a normal tricuspid annulus during systole: A comparison study with the mitral annulus using real-time 3D echocardiography. European Journal of Echocardiography 2007;8:375-383.

[13] Tei C, Pilgrim JP, Shah PM, Ormiston JA, Wong M. THE TRICUSPID-VALVE ANNULUS - STUDY OF SIZE AND MOTION IN NORMAL SUBJECTS AND IN PATIENTS WITH TRICUSPID REGURGITATION. Circulation 1982;66:665-671.

[14] Fernando ANTONIALI DMB, Glória Maria Braga POTÉRIO, Cledicyon Eloy da, COSTA MML, Gustavo Calado de Aguiar RIBEIRO, Luciano dos Santos TARELHO. Proportion among the segments of the normal tricuspid valve annulus: parameter for valve annuloplasty. Braz J Cardiovasc Surg 2006;21:262-271.

[15] M. Skwarek JH, M. Dudziak, M. Grzybiak. The morphology of the right atrioventricular
valve in the adult human heart. Folia Morphol 2006;65:200-208.

[16] Shah PM, Raney AA. Tricuspid valve disease. Current Problems in Cardiology 2008;33:47-84.

[17] Silver MD, Lam JHC, Ranganat.N, Wigle ED. MORPHOLOGY OF HUMAN TRICUSPID VALVE. Circulation 1971;43:333-&.

[18] Carpentier A, Adams D.H., Filsoufi, F. Reconstructive Valve Surgery. Maryland Heights: Saunder Elsevier, 2010.

[19] Cook AC, Anderson RH. Attitudinally correct nomenclature. Heart 2002;87:503-506.

[20] Dreyfus GD, Corbi PJ, Chan J, Bahrami T. Secondary tricuspid regurgitation or dilatation: Which should be the criteria for surgical repair? Annals of Thoracic Surgery 2005;79:127-132.

[21] Victor S, Nayak, V.M. The Tricuspid Valve Is Bicuspid. Journal of Heart Valve Disease 1994;3:27-36.

[22] Anwar AM, Soliman OII, Nemes A, van Geuns RJM, Geleijnse ML, ten Cate FJ. Value of assessment of tricuspid annulus: real-time three-dimensional echocardiography

and magnetic resonance imaging. International Journal of Cardiovascular Imaging 2007;23:701-705.

[23] Ton-Nu TT, Levine RA, Handschumacher MD, Dorer DJ, Yosefy C, Fan DL, Hua LQ, Jiang L, Hung J. Geometric determinants of functional tricuspid regurgitation - Insights from 3-dimensional echocardiography. Circulation 2006;114:143-149.

APPENDIX B

VALVE SELECTION

Form completed for every valve prior to experimentation. Valves which passed all selection criteria were used for experimentation.

Valves will be selected which best represent the human anatomy
Pass/Fail

☐ 1 Begin by selecting a valve which is small and has minimal gashing. Ensure that the TV is intact.

Estimation of annulus size can be achieved by comparing to TV ring sizer 32.

Do not select a heart if the RV is distended.

☐ 2 Examine the PMs to ensure that there are no abnormalities and three distinct groups are present

Septal	
Anterior	
Posterior	

☐ 3 Ensure chords insert into PM groups.

☐ 4 Examine the leaflets.

3 Main Cusps - Anterior, Posterior, Septal

Post Smallest Leaflet

☐ 5 Pressurize the heart. Ensure there is no/minimal leakage. If there is a distinct regurgitant jet the valve will not be chosen for experimentation.

☐ 6 Take a picture of the pressurized valve with a reference ruler placed on the plane of the annulus.

☐ 7 Measure the Annulus

Perimeter (10.5 ± 1.27 cm)	
Septal Segment (3.06 ± 0.37 cm)	
Anteroposterior Segment (7.4 ± 0.94 cm)	

☐ 8 Open the RV. Prior to excising the valve measure the leaflets.

Anterior:

Height (2.16 ± 0.44 cm)	
Width (3.42 ± 0.85 cm)	

Septal:

Height (1.74 ± 0.39 cm)	
Width (3.37 ± 0.85 cm)	

Posterior:

Height (1.90 ± 0.41 cm)	
Width (2.59 ± 0.91 cm)	

☐ 9 Excise valve and subvalvular apparatus. Ensure no damage to leaflets, annulus, PMs and Chords

APPENDIX C

VENTRICULAR CHAMBER DRAWINGS

The right ventricle consisted of multiple parts which were assembled to make the complete chamber. All necessary drawings needed to manufacture the chamber are provided along with necessary materials.

Bottom Plate

Note: All Units Shown in cm.
Material. Clear Cast 1.27cm Acrylic.

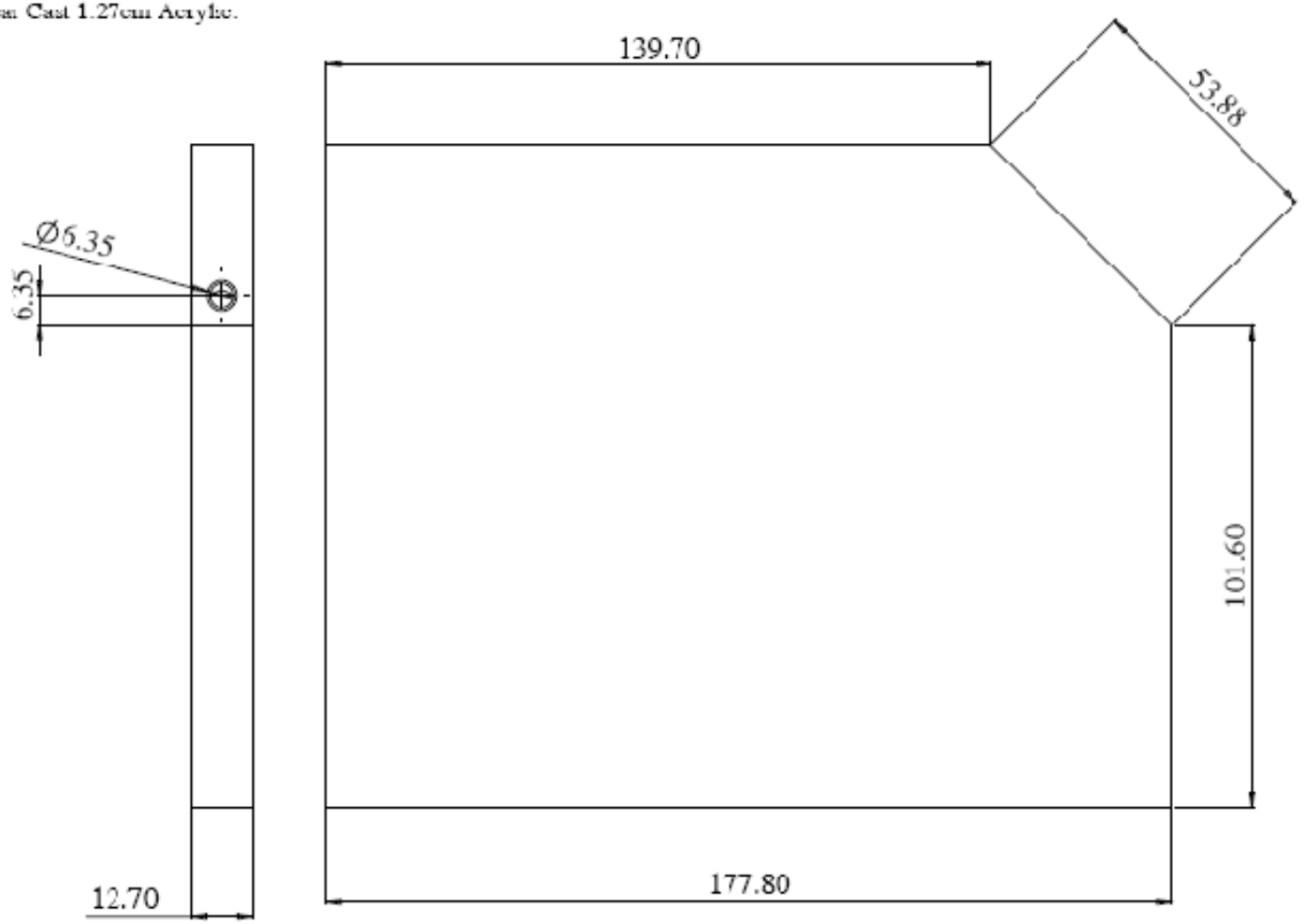

Pulmonary Valve Plate

Note: All Units Shown in cm.
Material: Clear Cast 1.27cm Acrylic.

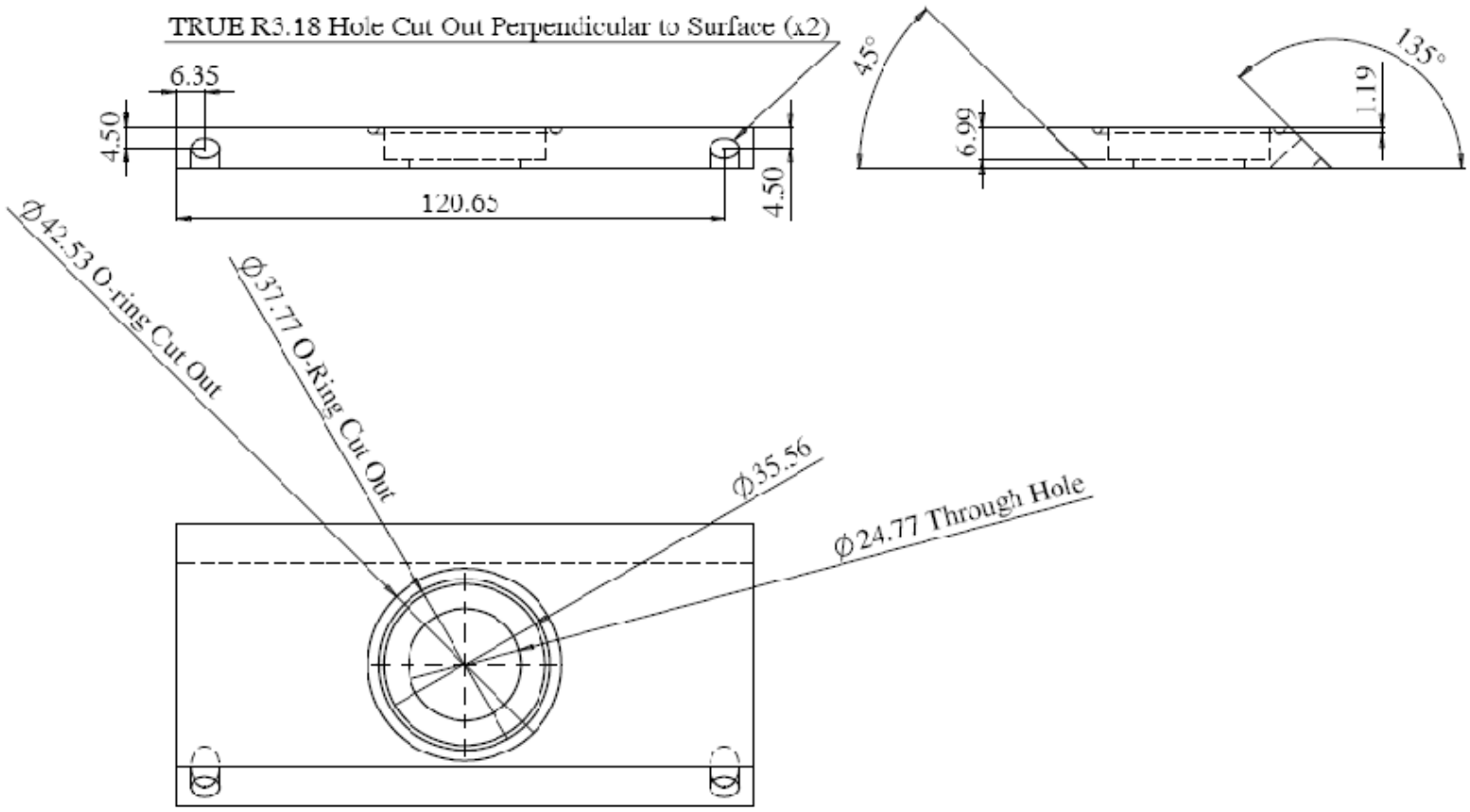

Pulmonary Valve Top Plate

Note: All Units Shown in cm.
1. Press Fit, 25.40 cm long, 38.10 OD, 37.15 ID, Clear Acrylic Tube
Material: Clear Cast 1.27cm Acrylic.

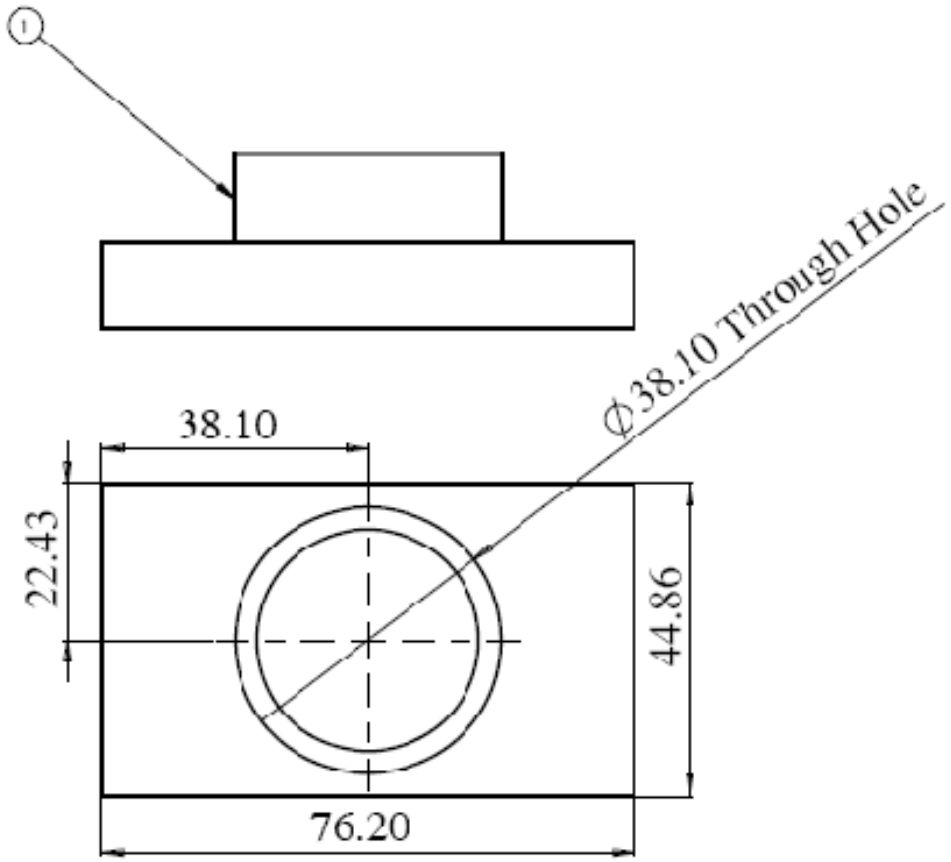

Back Plate

Note: All Units Shown in cm.
1. Press Fit, 25.40 cm long, 38.10 cm OD, 37.15 cm ID, Clear Cast Acrylic Tube.
Material: Clear Cast 1.27cm Acrylic.

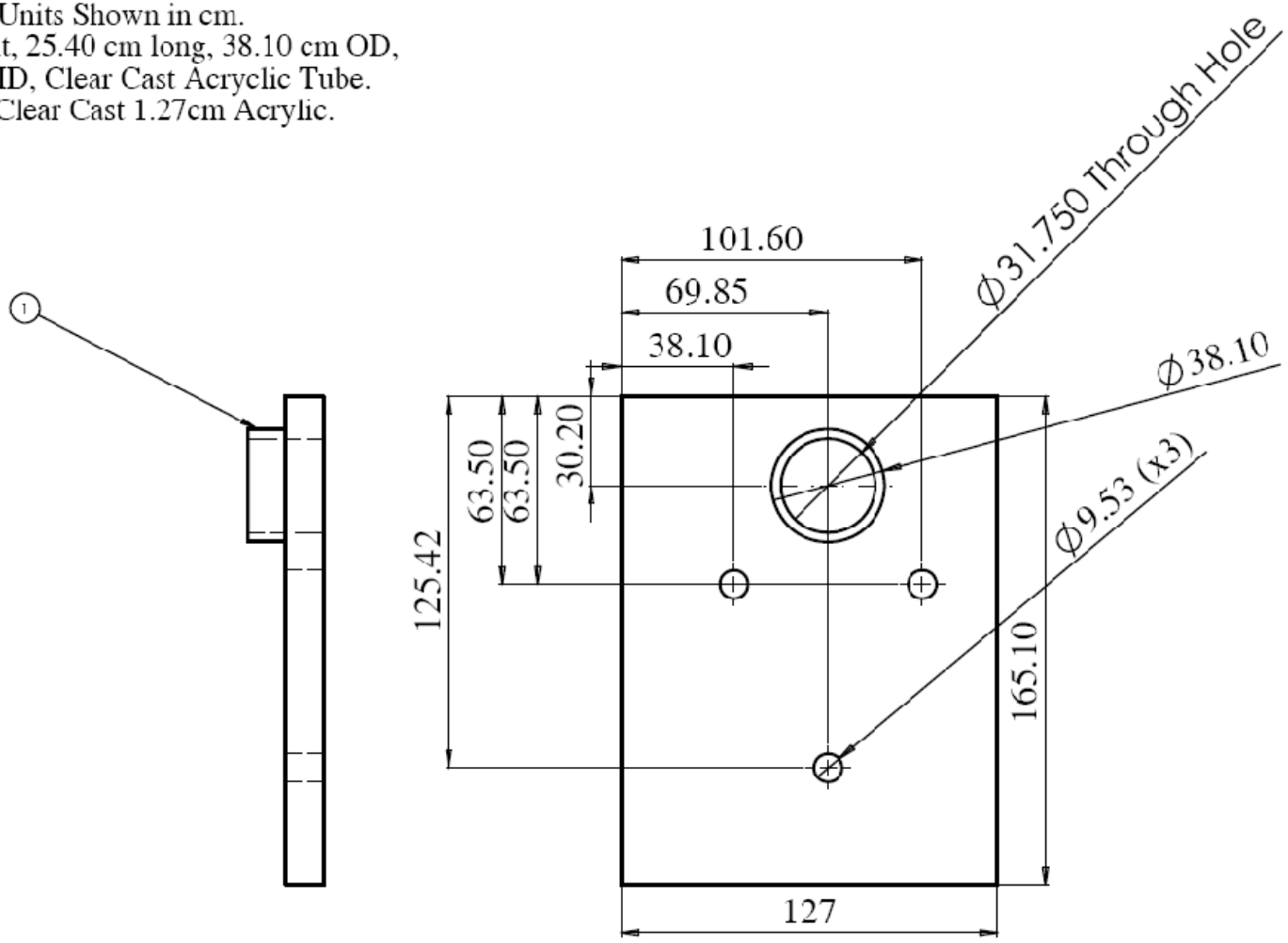

Side Plate_Right

Note: All Units Shown in cm.
Material: Clear Cast 1.27cm Acrylic.

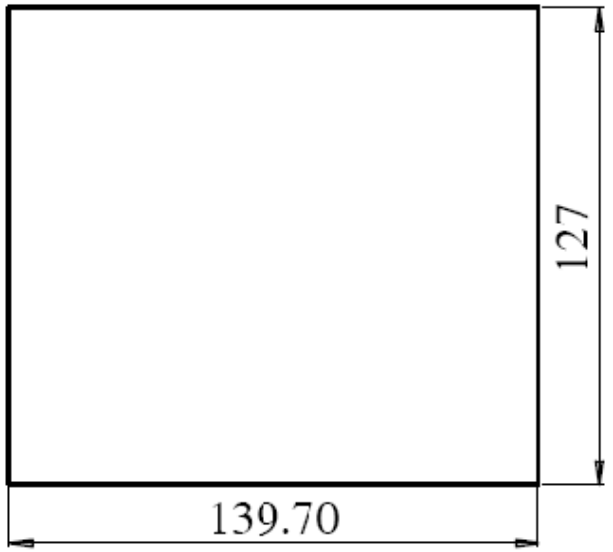

Side Plate_Left

Note: All Units Shown in cm.
Material: Clear Cast 1.27cm Acrylic.

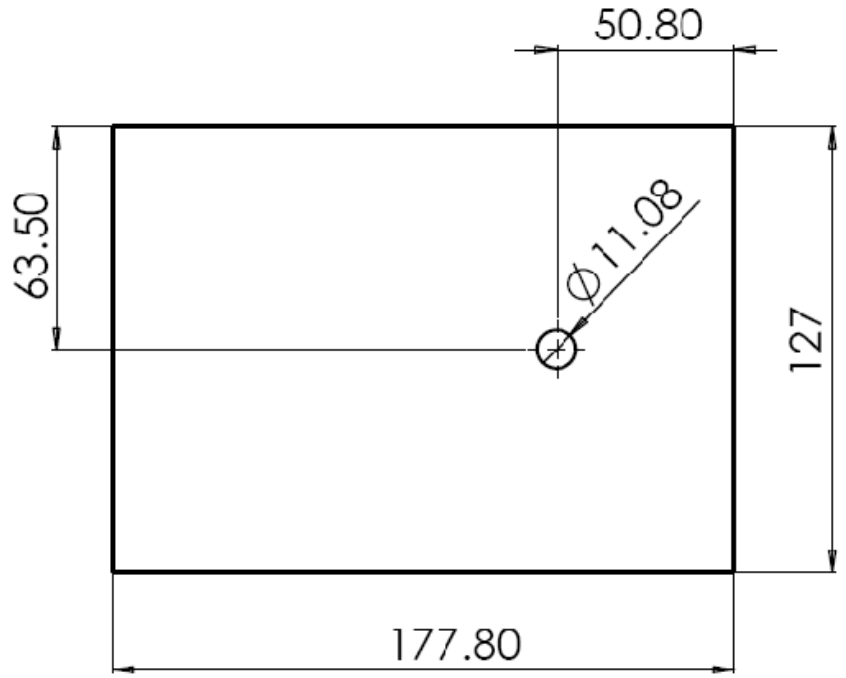

Wedge

Note: All Units Shown in cm.
Material: Clear Cast 1.27cm Acrylic.

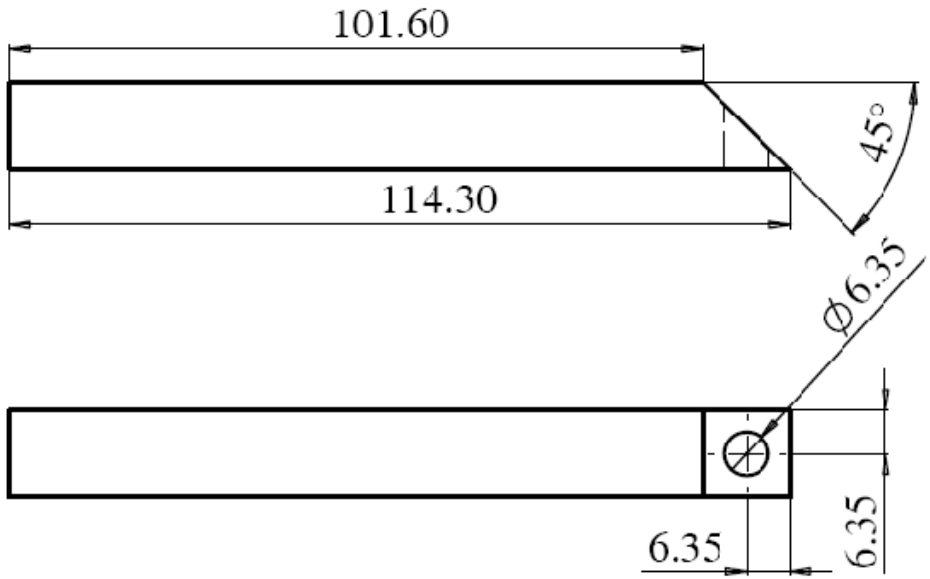

Top Plate

Note: All Units Shown in cm.
Material: Clear Cast 1.27cm Acrylic.

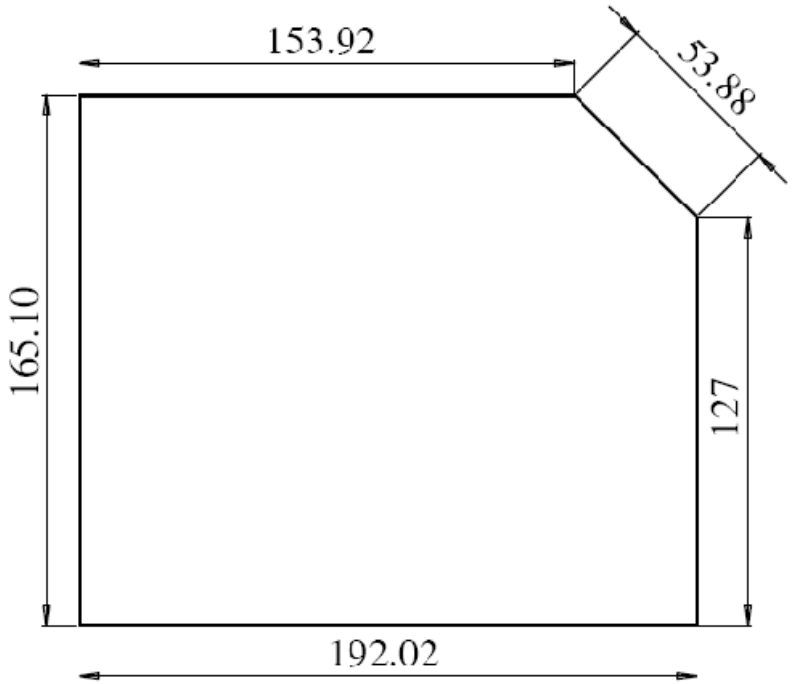

Top Plate Gasket

Note: All Units Shown in cm.
Material: 0.2 cm Neoprene Rubber

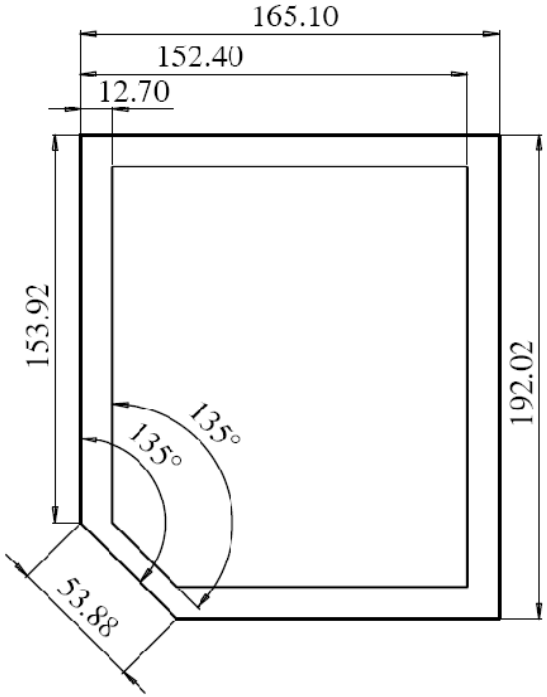

Back Plate Gasket

Note: All Units Shown in cm.
Material: 0.2 cm Neoprene Rubber

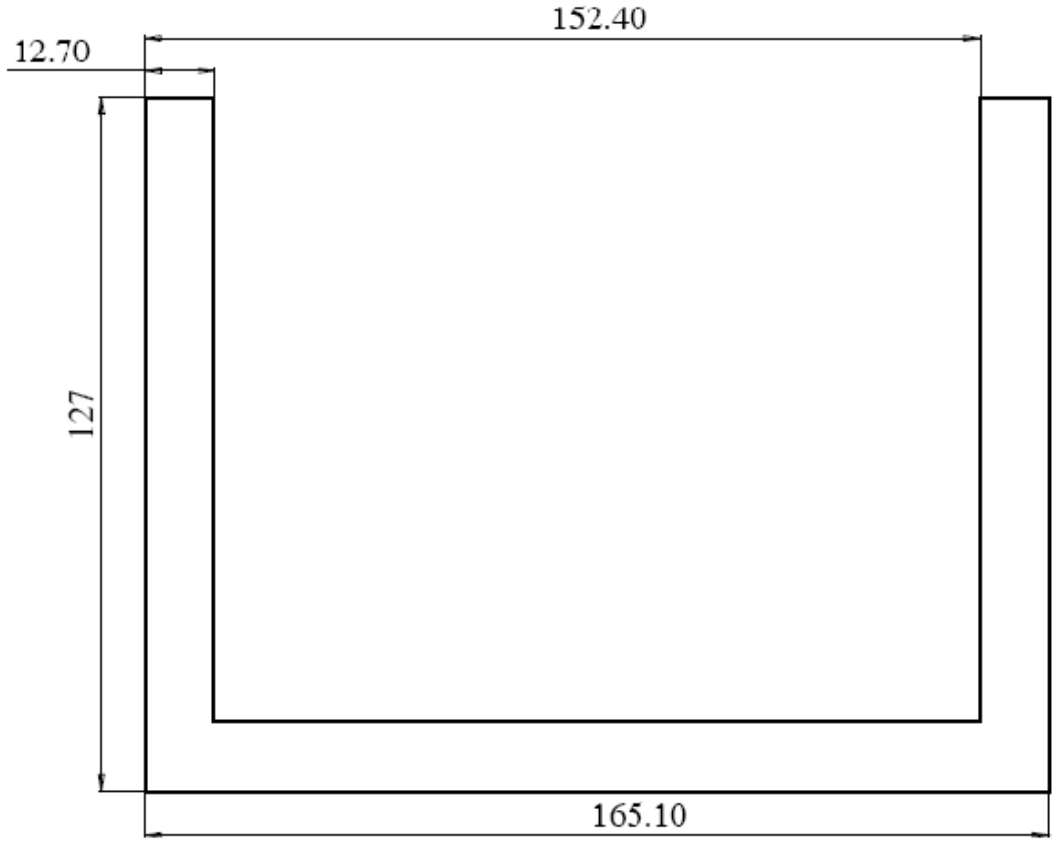

Front Plate Gasket

Note: All Units Shown in cm.
Material: 0.2 cm Neoprene Rubber

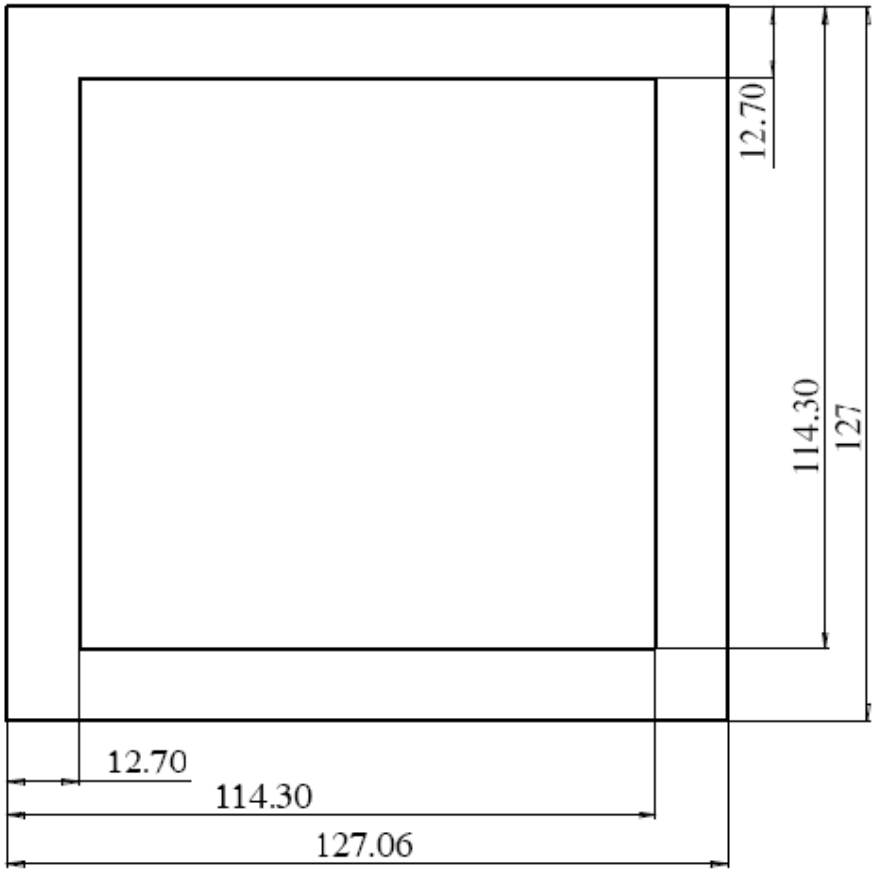

Bottom Plate

Note: All Units Shown in cm.
Material: Clear Cast 1.27cm Acrylic.

Top Plate and Gasket Pattern

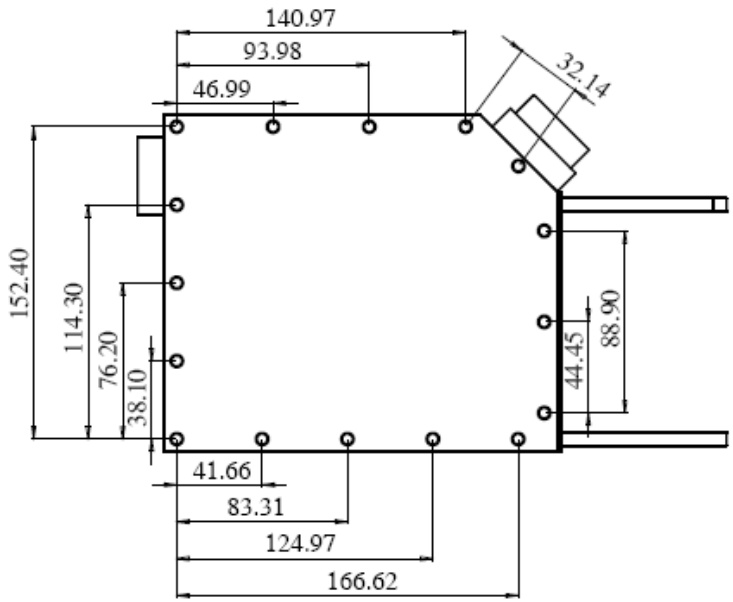

Back Plate and Gasket Pattern

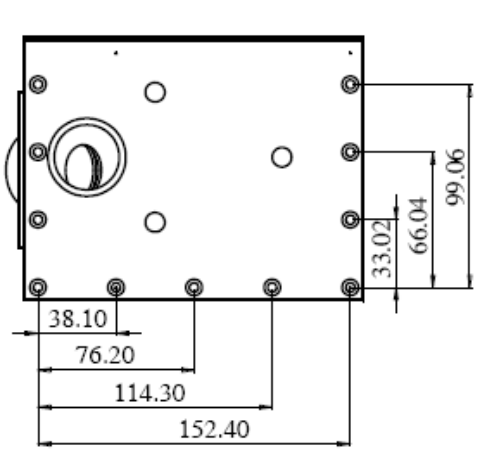

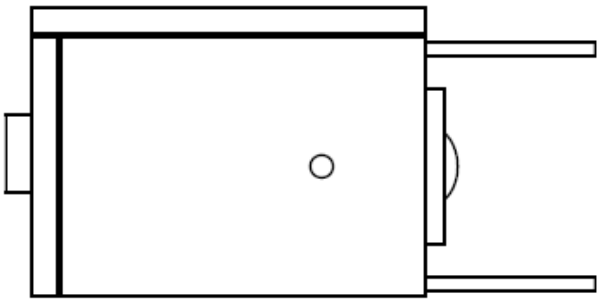

Top Plate Gasket Pattern

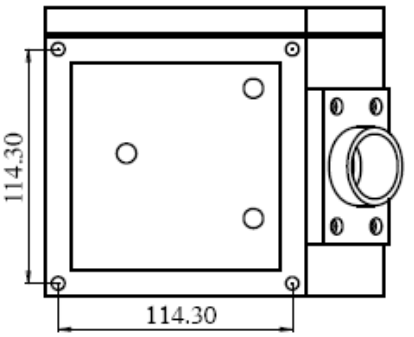

APPENDIX D

PAPILLARY MUSCLE DISPLACEMENT SHEET

An excel sheet was used to input the current position of the three papillary muscle rods and determine repositioning needed to simulate disease.

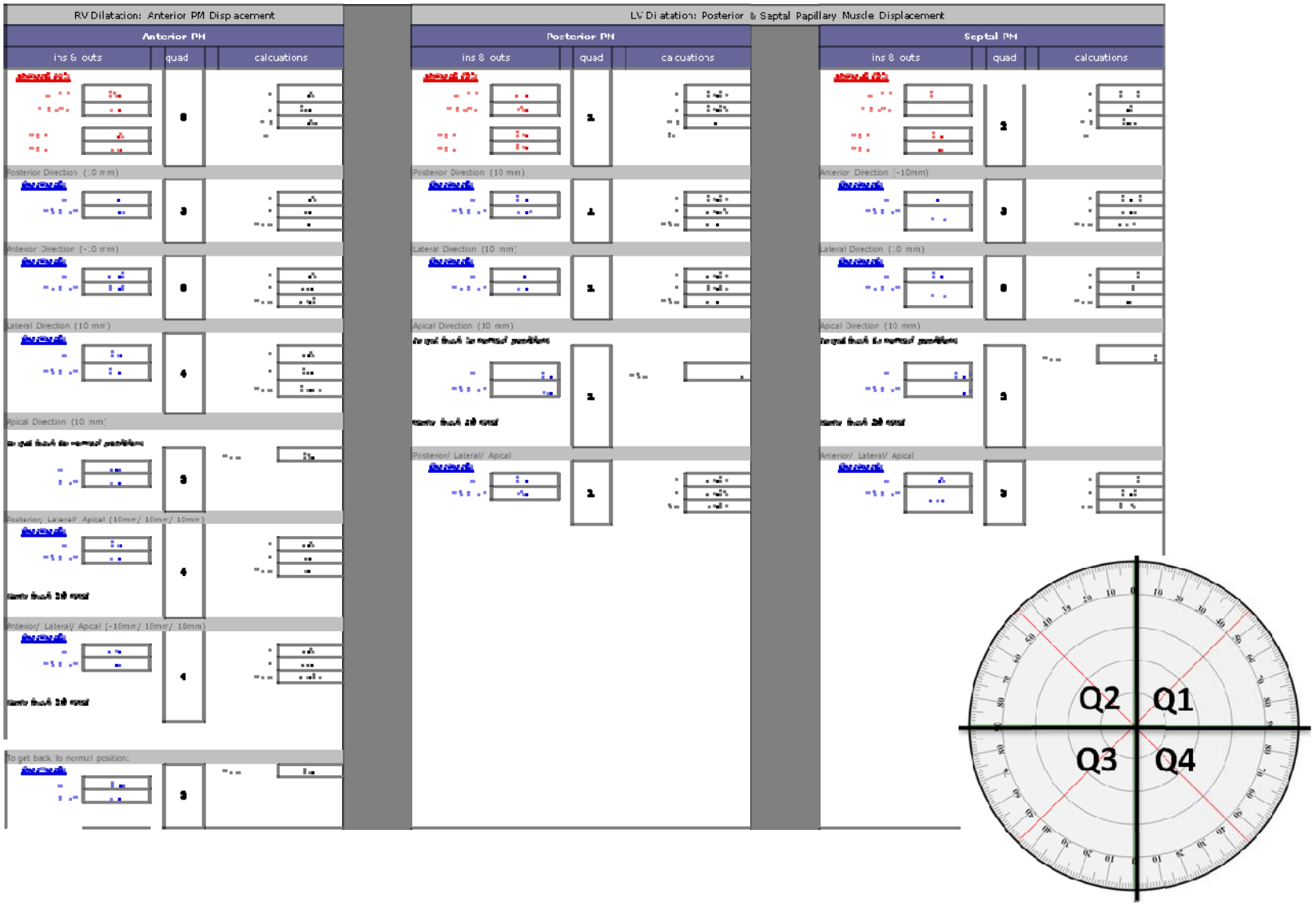
RV Dilatation: Anterior PM Displacement
Anterior PM
ins & outs
quad
calcuations
Posterior Direction (-10 mm)
Anterior Direction (-10 mm)
Lateral Direction (10 mm)
Apical Direction (10 mm)
Posterior/ Lateral/ Apical (10mm/ 10mm/ 10mm)
Anterior/ Lateral/ Apical (-10mm/ 10mm/ 10mm)
To get back to normal position:
LV Dilatation: Posterior & Saptal Papillary Muscle Displacement
Posterior PM
ins & outs
quad
calcuations
Posterior Direction (10 mm)
Lateral Direction (10 mm)
Apical Direction (10 mm)
Posterior/ Lateral/ Apical
Septal PM
ins & outs
quad
calcuations
Anterior Direction (-10mm)
Lateral Direction (10 mm)
Apical Direction (10 mm)
Anterior/ Lateral/ Apical
Q2
Q1
Q3
Q4

APPENDIX E

IN VIVO IRB PROTOCOL

Protocol as submitted to the Emory IRB for review and acceptance of *in vivo* patient study.

IRB Study: IRB00013027

Protocol – Version Date: 10/2009

Title of Study: Echocardiographic study of Right Ventricular Papillary Muscle position in normal, dilated RV, dilated LV and dilated LV/RV patients

Short Title: Echocardiographic Right Ventricular Papillary Muscle Displacement Study

Principle Investigator: Stamatios Lerakis, M. D.

Emory Department: Cardiology

Phone Number: 404-778-5414

Co-Investigators: Erin Spinner, B.S.

Abstract:

Although recent advancements have been made for the specific repair of tricuspid regurgitation (TR), many patients are still left with residual TR or later develop recurrent TR. Current repairs seek to fix the valvular apparatus but do not attempt to restore subvalvular function, such as papillary muscle (PM) position. It is believed PM displacement is a common result of ventricular dilatation, in addition to the annular dilatation. This displacement may cause leaflet tethering and improper leaflet coaptation, thus contributing to the latent TR.

This study will seek to identify and quantify the amount of papillary muscle displacement that occurs in patients with TR. We will use echocardiographic images to examine quantitative changes in patient anatomy with left ventricular (LV) and right ventricular (RV) dilatation. Anatomical measurements can be made once the images are acquired using commercially available software

Patients will be assigned to one of four categories: 1) those with normal sized and functioning right and left ventricles (RVEDV < 110 ml and LVEDV < 130 ml); 2) those with RV dilation or (RVEDV > 110 ml); 3) those with LV dilation (LVEDV > 130ml); and 4) those with combined RV and LV dilation. The normal patient group may have

trace TR while the dilated group will have mild to severe grade TR. We will use echocardiographic data to take specific measurements of the placement of the three papillary muscles in the RV with respect to the annulus plane. Eight patient data sets from each group (normal, LV dilatation, RV dilatation, and RV/LV dilatation) will be analyzed for a total of 32 patients. The distance for all three PMs will be recorded and compared between the groups to determine if dilatation has a significant impact on RV PM location.

This information will provide insight into the mechanism of how PM displacement may cause tricuspid regurgitation. We can then begin to understand if there are additional changes that affect proper closing of the leaflets.

1. Introduction – Background

Currently, 16.8 million people in the US (5.6% of the population) have tricuspid valve regurgitation (TR) [7], which results in back flow of blood from the right ventricle to the right atrium. Out of this population, 8,000 per year go on to receive some type of treatment [8], either complete valve replacement or repair such as an annuloplastry, which reduces the size of the valve opening to its original size. Current repairs offer limited success, with 10% of surgeries unsuccessful, and a majority of reoperations due to returning levels of TR [47]. This number of unsuccessful repairs may be due to the incomplete understanding of the cause of the TR.

In most cases, TR is caused by annular dilatation, in which the fibrous ring that attaches the valve to the heart wall becomes enlarged so that the leaflets cannot completely cover the orifice in order to prevent regurgitation. In conjunction with a dilated annulus, the ventricle also dilates. Fixing the annulus size does not eliminate TR completely and in many cases it returns [26, 33]. Studies that found recurring TR after annuloplasty have concluded that reducing the annulus may not be enough to correct TR [26, 55]. Thus, additional mechanisms have been investigated, specifically the effects of PM

displacement. It has been shown that TV tethering, restriction of leaflet mobility, caused by PM displacement is an independent predictor of TR after tricuspid valve annuloplasty [26, 55], but the amount of displacement has yet to be quantified. The proposed mechanism for this relationship is that as the free wall dilates the anterior papillary muscle, which is located on the free wall of the ventricle and attaches through chordae tendineae to the valve leaflets, moves outward, thus tethering the leaflets [92]. In addition to the proposed motion of the anterior PM in RV dilation, it is of interest to determine if the PMs on the septal wall, the posterior and septal PMs, move in conjunction with RV or LV dilation. Although it is possible for the septal and posterior PMs to be affected by LV dilation since the two ventricles are connected, it has not yet been identified. If in fact there is an effect on the PMs in the RV due to LV dilatation, this may further support the belief that the dynamics on the left side of the heart affect the right side of the heart.

2. Objectives

The purpose of this study is to utilize echocardiography to examine anatomical changes in patients with dilated right and left ventricles in association with tricuspid regurgitation.

The specific aims of this project are as follows:

1. Determine RV papillary muscles displacement due to isolated RV and LV dilatation and combined RV/LV dilatation, from patient Echocardiographic images
2. Compare RV papillary muscles location in normal, RV dilated, LV dilated and RV/LV dilated patients and determine effect of papillary muscles displacement on TR

3. Study Design and Methods

Echocardiographic images of the heart will be acquired following the standard clinical procedures, including 4 chamber and RV views. Procedures that differ from standard practice are limited to the subsequent additional data analysis. The echocardiographer will maintain a spreadsheet in which they will identify eligible patients for the study and assign a reference number to protect patient privacy. All echocardiographic patient images will be stored according to current hospital practice on secure servers. Images will then be analyzed using commercially available software to measure the distance of all three RV PM tips to the annulus plane. Results from data analysis will also be stored, but no patient data will be contained on these files, only the assigned reference number.

Since this study is purely data analysis and requires no additional involvement as far as the patients is concerned, there are no risks to the patient. At the same time the patient will receive no immediate benefits from participating in the study.

4. Participant Selection

Patients who come in for an echocardiography which fit into one of the four categories listed below will be asked for verbal consent to participate. The echocardiographer will ask the patients when they are in the echo suite prior to beginning the exam if they are interested in participating in a research study. The technician will then inform them of the study and read the verbal consent script. If the patient says yes, their information will be noted in the list stating they have consented, and the exam will proceed according to standard operating procedure. If the patient says no, their name will not be placed on the eligible patient list and the will proceed with their exam.

<u>Eligibility Criteria</u>

a. Physician Ordered Echocardiogram
b. Age >18 years of Age
c. Normal Patients:

a. N = 25 patients
b. Normal LV : LVEDV< 130 ml
c. Normal RV: RVEDV < 110 ml
d. Maximum TR Grade: Trace

d. RV Dilatation Patients:
    a. N = 25 patients
    b. Normal LV: LVEDV< 130 ml
    c. Dilated RV: RVEDV > 110 ml
    d. TR Grade: Mild - Severe

e. LV Dilatation Patients:
    a. N = 25 patients
    b. Dilated LV: LVEDV> 130 ml
    c. Normal RV: RVEDV < 110 ml
    d. TR Grade: Mild- Severe

f. RV/LV Dilatation patients:
    a. N = 25 patients
    b. Dilated LV: LVEDV> 130 ml
    c. Dilated RV: RVEDV > 110 ml
    d. TR Grade: Mild - Severe

Ineligibility Criteria:

During data analysis if we are unable to accurately identify and measure all three RV PMs the patient data will be removed from the study.

5. Statistical Analysis

Measurements will need to be normalized by body surface area (BSA) to minimize error due to various sized anatomies. All data will first be accessed for

normality, and then based upon normality the data will be assessed for statistical difference from the normal patients measurements and additionally between the groups.

6. Adverse Event Reporting

Although, the likelihood of an adverse event is negligible, any events that may occur will be reported in writing to the IRB board, as per standard procedure.

7. Data and Safety Monitoring Plan (DSMP)

A list will be maintained by the echocardiographer as to which patients are eligible for the study and what group they are in. This spreadsheet will also be used to assign a reference number to the patient in order to protect patient privacy. The spreadsheet will be stored in a locked cabinet. The safety of the patients involved will not be addressed in this IRB since the echo is part of the standard of care for these patients and no additional protocols will be needed.

8. References

1. *Framingham Heart Study*. [cited; Available from: http://www.nhlbi.nih.gov/about/framingham/.
2. *STS Adult CV Surgery National Database - Fall 2008 Executive Summary*.
3. Bajzer, C.T., et al., *Tricuspid valve surgery and intraoperative echocardiography - Factors affecting survival, clinical outcome, and echocardiographic success.* Journal of the American College of Cardiology, 1998. **32**(4): p. 1023-1031.
4. Fukuda, S., et al., *Mechanism of recurrent or residual functional tricuspid regurgitation mid-term after tricuspid annuloplasty.* Circulation, 2005. **112**(17): p. U556-U556.
5. Fukuda, S., et al., *Determinants of recurrent or residual functional tricuspid regurgitation after tricuspid annuloplasty.* Circulation, 2006. **114**: p. I582-I587.

6. Fukuda, S., et al., *The effect of tricuspid valve surgery on right ventricular function in patients with functional tricuspid regurgitation.* Journal of the American College of Cardiology, 2005. **45**(3): p. 365A-365A.

7. Fukuda, S., et al., *Tricuspid valve tethering predicts residual regurgitation after tricuspid annuloplasty.* Journal of the American College of Cardiology, 2005. **45**(3): p. 362A-362A.

APPENDIX F

IN VIVO CONSENT FORM

All patients were consented prior to admittance into the research study. A script was provided to the technician to read to the patients.

IRB Study: IRB00013027
Verbal Consent Script – Version Date: 11/13/2008
Title of Study: Echocardiographic study of Papillary Muscle position in normal, dilated RV, dilated LV and dilated LV/RV patients
Short Title: Echocardiographic Papillary Muscle Displacement Study

Principle Investigator: Stamatios Lerakis, M.D.
Emory Department: Cardiology
Phone Number: 404-778-5414

You are being asked to participate in a study which will seek to identify and quantify the amount of right ventricle papillary muscle displacement which occurs in patients with TR. In this study, we will use echocardiographic images to examine the changes in patients with left ventricular (LV) and right ventricular (RV) dilatation. There is no difference in the time or procedure of acquisition of your echocardiogram. This study will simply use your echo images, which are taken as standard procedure as have already been ordered by your doctor, to take measurements afterward.

Your participation and data is strictly confidential. Your data will be assigned a reference number in order to protect patient privacy. Since this study is purely data analysis and requires no additional involvement as far as you, the patients is concerned, there are no additional risks involved. At the same time you will receive no immediate benefits from participating in the study.

Your participation in this study is voluntary. It is entirely your choice. If you decide to take part, you can change your mind later on and withdraw from the research study. The decision to join or not join the research study will not cause you to lose any medical benefits. If you decide not to take part in this study, your doctor will continue to treat you.
Do you give verbal consent to participate in this study?
If, yes state yes and your data will be included as part of this study.
If no, state no, and your data will not be used as part of this study.

APPENDIX G

RLL MATLAB CODE

A Matlab code was written to transpose the marker data into a matrix and then plot the diseased leaflet on the static leaflet. The following protocol and three codes were used.

PROTOCOL

1. Increase contrast in all 42 pictures (includes static images). Save.
2. Crop all 42 pictures. Save as file_cropped.jpg in a new folder.
3. Places cropped pictures in ppt template. Save as date.
4. EITHER:
    - Place cropped pictures (3 on each page) in word doc. Print and connect-the-dots for each leaflet with a pen/pencil.
    - Open each of the 42 pictures in Photoshop, or similar program. Connect-the-dots for each leaflet with a thin paintbrush.
    - TIP: darken the dots first to make it easier to connect-the-dots.
5. Start with one leaflet. Count the dots on each row for each of the 14 conditions (includes static). Write the numbers down next to the picture to make it easier for step 6.
6. Enter this info in the leaflet's corresponding makeMatrix.m file.
    - DO NOT CHANGE anything in this file. Just run it, and fill in the blanks in the command window.
    - TIP: Must do all 40 entries for the one leaflet in one sitting. So, be sure you've done step 5 in its entirety (and clearly), so you can do this quickly without any mistakes.
7. Open the areaPlotInitial.m file for that leaflet and run it. That's it.
    - DO NOT CHANGE anything in this file.
8. Open the plotAll.m file for that leaflet and run it.
    - DO NOT CHANGE anything in this file.
    - Save all the newly formed jpgs in a new folder.
9. Places these newly formed jpgs in the ppt.
10. Make a line showing the residual leaflet length on the jpg in ppt, and enter the data in the table. Do this for each of the 39 experimental conditions.
11. Repeat 5 – 9 for the other two leaflets.

Matlab CodeL: makeMatrix.m

```
% User Status Information
fprintf('When there are no more rows, just press enter.\n')
fprintf('Enter row info as a vector.\n');
fprintf('Example: [0 14 0] would be one empty spot, 14 markers, and
then one empty spot\n\n');

% Get the bottom row and create the empty matrix
counter = 30;
fprintf('Input ant_1_0\n');
row = input('Enter bottom row info: ');
mat = zeros(counter,row);
mat(end, :) = 1;

% Ask for each row
while length(row) > 0
   row = input('Enter row info: ');
```

```
   firstOne = find(mat(counter,:),1); % finds the first occurance of a
marker in the previous row

   zerosBefore = find(row,1) - 1;
   markers = row(zerosBefore+1);
   zerosAfter = find(row(end:-1:1),1) - 1;

   lastOne = length(mat(counter,:)) - find(mat(counter,end:-1:1),1) +
1;
   totalOnes = lastOne - firstOne + 1;

   if isempty(zerosBefore)
       zerosBefore = 0;
   end
   if isempty(markers)
       markers = 0;
   end
   if isempty(zerosAfter)
       zerosAfter = 0;
   end


  if      totalOnes ~= (zerosBefore + markers + zerosAfter) &&
length(row) > 0
          row = input('WRONG INPUT.  TRY AGAIN. Enter row info: ');
          firstOne = find(mat(counter,:),1); % finds the first
occurance of a marker in the previous row
          zerosBefore = find(row,1) - 1;
          markers = row(zerosBefore+1);
          zerosAfter = find(row(end:-1:1),1) - 1;
   end

   counter = counter-1;
   mat(counter,firstOne+zerosBefore:firstOne+zerosBefore+markers-1)=1;
end

status = 'Now adding reference point...'
xcor = input('What is the X coordinate of the reference point: ');
ycor = input('What is the Y coordinate of the reference point: ');
mat(end-ycor+1,xcor) = 2;

while length(find(mat(1,:),1)) == 0
    mat(1,:) = [];
end

status = 'Finished.'

ant1_0 = mat
```

Matlab Code: areaPlotInital.m

```
function [x, y, refx, refy] = areaPlotInitial(sample, color1)
% septal, initial, 10/07/08, 100708_full.jpg
```

```
  sample = [ 0     0     0     0     0     1     1     1     0     0
0     0     0     0     0
     0     0     0     0     0     1     1     1     1     1     1
1     1     0     0
     0     0     0     0     1     1     1     1     1     1     1
1     1     0     0
     0     0     0     0     1     1     1     1     1     1     1
1     1     0     0
     0     0     0     0     1     1     1     1     1     1     1
1     1     0     0
     0     0     0     0     1     1     1     2     1     1     1
1     1     0     0
     0     1     1     1     1     1     1     1     1     1     1
1     1     0     0
     0     1     1     1     1     1     1     1     1     1     1
1     1     0     0
     0     1     1     1     1     1     1     1     1     1     1
1     1     0     0
     0     1     1     1     1     1     1     1     1     1     1
1     1     0     0
     1     1     1     1     1     1     1     1     1     1     1
1     1     1     0
     1     1     1     1     1     1     1     1     1     1     1
1     1     1     1
     1     1     1     1     1     1     1     1     1     1     1
1     1     1     1];
tempTitle = 'Anterior Leaflet';
%% sample leaflet adjustments
% separate leaflet into positive and negative slopes
max = find( sample(1,:), 1);
% size the original leaflet
[rows cols] = size(sample);
% add a border of zeros around it
sample = [zeros(1,cols+2)
          zeros(rows,1) sample zeros(rows,1)
          zeros(1,cols+2)];
% flip it vertically for proper graphing
sample = sample(end:-1:1,:);

%% sample leaflet locations
% find bottom left corner of leaflet
x = [find(sample(2,:),1,'first')];
y = [find(sample(:,2),1,'first')];
% find bottom right corner of leaflet
xend = [find(sample(2,:),1,'last')];
yend = [find(sample(:,2),1,'first')];
% find reference X point of leaflet
[refy refx] = find(sample==2,1);

%% plotting
% plot the base of leaflet
plot([x xend], [y yend],color1);
% setup axis and plot holding
axis([1,cols+2,1,rows+2]);
hold on
```

```
% iterate through left side (positive sloping)
for c=1:max+1
    for r=1:rows+1
        if sample(r,c) == 1
            if sample(r+1,c) == 0 || (sample(r,c-1)==0 && sample(r-1,c-
1)==1)
                x = [x c];
                y = [y r];
            end
            plot(c,r,'r.');
        end
    end
end

% iterate through right side (negative sloping)
for c=max+1:cols+1
   for r=rows+1:-1:1
       if sample(r,c) == 1
           if sample(r+1,c) == 0 || (sample(r,c+1)==0 && sample(r-
1,c+1)==1)
               x = [x c];
               y = [y r];
           end
           plot(c,r,'r.');
       end
   end
end

% add the bottom right corner
x = [x xend];
y = [y yend];

% plot reference point
plot(refx,refy,'kx');

% plot black border of leaflet
plot(x,y,color1)

xlabel('Distance (mm/2)'); ylabel('Distance (mm/2)');
title(tempTitle);
```

Matlab Code: plotAll.m
Code shown for Anterior Leaflet (plotAllAnterior.m) code is modified for each leaflet by altering the leaflet name.

```
%%Plot Static Leaflet
leafletName = 'Anterior Leaflet';

date = '031909';

color1 = 'k';
color2 = 'b';
color3 = 'g';
color4 = 'c';
```

```
color5 = 'm';
color6 = 'r';
color7 = 'y';

colorName1 = 'Black';
colorName2 = 'Blue';
colorName3 = 'Green';
colorName4 = 'Cyan';
colorName5 = 'Pink';
colorName6 = 'red';
colorName7 = 'yellow';

leftTextCoor = -1;
rightTextCoor = 16;

%%%%%%%%%%%%%%%%%%%%%%%%

colorAll = 56;
colorNameAll = {colorName1 colorName2 colorName3 colorName4 colorName5
colorName6 colorName7};

[rows cols] = size(ant_S);
[x1, y1, refx1, refy1] = areaPlotInitial(ant_S,colorAll{1});
%% Plot Ant_1_0
[x2, y2, refx2, refy2] = areaPlot(ant_1_0);
%plot(refx2+(refx1-refx2),refy2+(refy1-refy2),'go'); % plot the ref
point
plot(x2+(refx1-refx2),y2+(refy1-refy2),colorAll{2}); % plot the border
plot([x2(1) x2(end)]+(refx1-refx2),[y2(1) y2(end)]+(refy1-
refy2),colorAll{2}); % plot the base
%% Plot Ant_1_40
[x3, y3, refx3, refy3] = areaPlot(ant_1_40);
plot(x3+(refx1-refx3),y3+(refy1-refy3),colorAll{3}); % plot the border
plot([x3(1) x3(end)]+(refx1-refx3),[y3(1) y3(end)]+(refy1-
refy3),colorAll{3}); % plot the base
%% Plot Ant_1_100
[x4, y4, refx4, refy4] = areaPlot(ant_1_100);
plot(x4+(refx1-refx4),y4+(refy1-refy4),colorAll{4}); % plot the border
plot([x4(1) x4(end)]+(refx1-refx4),[y4(1) y4(end)]+(refy1-
refy4),colorAll{4}); % plot the base
%% Plot Ant_2_0
[x5, y5, refx5, refy5] = areaPlot(ant_2_0);
plot(x5+(refx1-refx5),y5+(refy1-refy5),colorAll{5}); % plot the border
plot([x5(1) x5(end)]+(refx1-refx5),[y5(1) y5(end)]+(refy1-
refy5),colorAll{5}); % plot the base

%% Plot Ant_2_40
[x6, y6, refx6, refy6] = areaPlot(ant_2_40);
plot(x6+(refx1-refx6),y6+(refy1-refy6),colorAll{6}); % plot the border
plot([x6(1) x6(end)]+(refx1-refx6),[y6(1) y6(end)]+(refy1-
refy6),colorAll{6}); % plot the base

%% Plot Ant_2_100
[x7, y7, refx7, refy7] = areaPlot(ant_2_100);
plot(x7+(refx1-refx7),y7+(refy1-refy7),colorAll{7}); % plot the border
```

```
plot([x7(1) x7(end)]+(refx1-refx7),[y7(1) y7(end)]+(refy1-
refy7),colorAll{7}); % plot the base
%% Plot Ant_3_0
[x8, y85, refx8, refy8] = areaPlot(ant_3_0);
plot(x8+(refx1-refx8),y8+(refy1-refy8),colorAll{8}); % plot the border
plot([x8(1) x8(end)]+(refx1-refx58),[y8(1) y8(end)]+(refy1-
refy8),colorAll{8}); % plot the base

%% Plot Ant_3_40
[x9, y9, refx9, refy9] = areaPlot(ant_3_40);
plot(x9+(refx1-refx9),y9+(refy1-refy9),colorAll{9}); % plot the border
plot([x9(1) x9(end)]+(refx1-refx9),[y9(1) y9(end)]+(refy1-
refy9),colorAll{9}); % plot the base

%% Plot Ant_3_100
[x10, y10, refx10, refy10] = areaPlot(ant_3_100);
plot(x10+(refx1-refx10),y7+(refy1-refy10),colorAll{10}); % plot the
border
plot([x10(1) x10(end)]+(refx1-refx10),[y10(1) y10(end)]+(refy1-
refy10),colorAll{7}); % plot the base


strTop = [colorNameAll{1} ' = Static ... ' colorNameAll{2} ' = Normal
... ' colorNameAll{3} ' = Dilated 20% ... ' colorNameAll{4} ' = Dilated
40%'];
strBottom = [colorNameAll{5} ' = Dialated 60% ... ' colorNameAll{6} ' =
Dialated 80% ... ' colorNameAll{7} ' = Dialated 100%'];
title(strTop);
xlabel(strBottom);
text(leftTextCoor,0,leafletName);
text(rightTextCoor,0,date);
axis image
YL = YLIM; XL = XLIM;
YLIM([YL(1)-1 YL(2)+1]);
XLIM([XL(1)-1 XL(2)+1]);
```

APPENDIX H

MRI ASSESSMENT OF RIGHT VENTRICLE PAPILLARY MUSCLE POSITION

MRI was used to investigate the right ventricle (RV) PM position in normals and patients with a dilated left ventricle (LV). A significant difference was seen in the septal PM position, towards the center of the RV, in patients with a dilated LV as compared to normal subjects. Dilatation of the LV was shown to impact the geometry of the RV through the septum.

Spinner EM, Sundareswaran K, Dasi LP, Thourani VH, Oshinski J, Yoganathan AP. Altered right ventricular papillary muscle position and orientation in patients with a dilated left ventricle. *The Journal of thoracic and cardiovascular surgery.* 2011;141(3):744-749.

Altered Right Ventricular Papillary Muscle Position and Orientation in Patients with a Dilated Left Ventricle

Erin M. Spinner BS[1], Kartik Sundareswaran PhD[1], Lakshmi Prasad Dasi PhD[1], Vinod H. Thourani MD[2], John Oshinski PhD[2], Ajit P. Yoganathan PhD[1]

1. Wallace H. Coulter Department of Biomedical Engineering, Georgia Institute of Technology and Emory University, Atlanta, Georgia USA
2. Department of Surgery, Division of Cardiothoracic Surgery, Emory University School of Medicine, Atlanta, Georgia USA

ABSTRACT

Objective: To investigate the impact of left ventricular (LV) dilatation on right ventricular (RV) papillary muscle (PM) displacement.

Methods: Thirteen patients underwent high resolution cardiac magnetic resonance imaging (CMR) at Emory University Hospital: **7** patients with congestive heart failure and a dilated LV composed the Dilated LV Group and 6 normal subjects were used as a control. 120 CMR slices were acquired in a short axis view at end-diastole for each subject. CMR slices were used to identify the papillary muscle tip position in 3 dimensional coordinates for the septal, posterior and anterior PMs. The centroid of the PM coordinates was used as the reference point for comparison between subjects. The relative orientation between the right ventricular papillary muscles was evaluated and compared between the Dilated LV Group and normal subjects.

Results: Dilatation of the LV resulted in a significant ($p=0.05$) displacement of the septal RV PM towards the centroid, Normal group: 0.0285 ± 0.036 mm/mm vs. Dilated LV Group: 0.1437 ± 0.026 mm/mm. More specifically the septal PM significantly ($p=0.03$) moved away from the septal wall (Normal Group: 0.61 ± 0.09 mm/mm, Dilated LV

Group: 0.379±0.037 mm/mm). Specific locations of all three RV PMs were reported for normal subjects and patients with a dilated LV.

Conclusions: Patients with a dilated LV have significantly increased displacement of the septal RV PM away from the septum when compared to normal controls. This demonstrates pathophysiologic contribution of the LV to specific papillary muscle alterations within the RV.

Left sided heart disease is traditionally thought to impact the right side of the heart through pulmonary hypertension [16, 93] and increased after load on the right ventricle (RV). LV dilatation and dysfunction, even in the absence of pulmonary hypertension, can have a detrimental impact on the RV and may be a potential mechanism for high occurrence of TR in patients with MR. In this study, it is hypothesized that in addition to pulmonary hypertension geometric changes on the left side may also directly affect the right side as the RV and LV are connected through the interventricular septum [69]. The volume in which the LV and RV can fill is restricted by the pericardial sack, thus, a dilated LV may not only enlarge into the pericardial space but also into the RV as it is a lower pressure chamber. Changes in RV geometry induced from LV geometric changes may contribute to secondary tricuspid regurgitation through papillary muscle displacement, improper muscle contraction or other complications.

Changes in RV geometry may lead to alterations in the positions of the PMs of the tricuspid valve as they are directly connected to the ventricle. Studies by Jouan et al. and Hiro et al. investigated the RV PM position in sheep over the cardiac cycle, but did not report how these positions may change in a diseased state [35, 36]. Studies have

implicated RV dilatation as a cause of anterior PM displacement [23, 24]. The speculated mechanism for pathological PM displacement is that as the free wall of the right ventricle dilates, the anterior PM, located on the free wall of the ventricle and attaching through chordae tendineae to the valve leaflets, moves outwardly, thus tethering the tricuspid valve leaflets [92]. In addition to the proposed motion of the anterior PM due to RV dilation, it is of interest to determine if the PMs on the septal wall, the posterior and septal PMs, are displaced due to LV dilation. Although it is probable that the septal and posterior PMs are affected by LV dilation through the interventricular septal motion, it has yet to be demonstrated in human subjects. The specifics of which PMs are displaced with specific etiologies, the direction of displacement, and how much they are displaced remain unknown.

If in fact there is an effect on the PMs in the RV due to LV dilatation, this may further support the belief that the dynamics on the left side of the heart affect the right side of the heart. We hypothesize that geometric changes in the left ventricle (LV), as a result of LV dilatation, may also alter RV geometry and displace the PMs located on the septal wall.

In this study, we identify and compare the position of RV PMs in normal subjects and patients with LV dilation to quantitatively establish the RV PM positions and the influence of LV dilation on RV PM displacement. Magnetic Resonance Imaging (MRI) was the imaging modality chosen for this study because it has the potential to image cardiac structures in high resolution with no radiation dosage.

METHODS

Patient Selection

A total of 13 subjects were scanned as part of a high resolution geometric protocol at Emory University Hospital Midtown, Atlanta GA. Of these, 7 were congestive heart failure patients (Dilated LV Group) with the following implications: mild (n=2) to severe (n=5) mitral valve regurgitation, a dilated left ventricle (LVEDV 234.7 $\pm$ 70.8 ml), mean age of 65 ± 14, NYHA class 2(n=2), 3(n=4), 4(n=1), pulmonary regurgitation (n=3), pulmonary hypertension mild(n=3) to moderate(n=3), normal systolic function(n=6), and mild tricuspid regurgitation(n=5). The remaining 6 were normal subjects, with no known heart conditions and used as controls for the study (Normal Group), mean age(n=5) 25 ± 2.5. The study was approved by the Emory University Institutional Review Board for human subjects, and patient privacy was protected according to HIPPA regulations and all patient identifiers were removed from data used in this study. Informed consent was obtained from all participants in the study.

Image Acquisition

All scans were acquired on a Philips Intera CV 1.5 T system using a cardiac coil. High resolution, ECG and navigator echo gated 'whole heart' gradient echo sequence was used in the short axis orientation spanning both the right and left ventricles during end-diastole [94]. Pixel size ranged from 0.53 – 0.70 mm, slice thickness from 1.5 – 2.0 mm, and echo time from 1.3 – 2.1 ms. Approximately 120 slices were acquired at end-diastole, as confirmed with cine images, to cover the entire LV and RV.

Data Processing

XnView 1.92 was used for visualization and post processing. References in the x, y, and z direction were identified to compare the PMs in 3D space. An annulus reference slice was identified in order to calculate the z distance relative to the annulus reference plane (ARP). The annulus plane was selected as a reference plane so the relative proximity and change could be related to the annulus plane. The ARP was identified as the slice in which the right coronary artery and aortic leaflets were visible. The diameter of the ascending aorta was measured and recorded in the ARP. Papillary muscle tip position was manually identified in the various images by identifying the regions of low intensity (the PM) among regions ofhigh intensity (blood), in the right ventricle (RV) (Fig H.1).

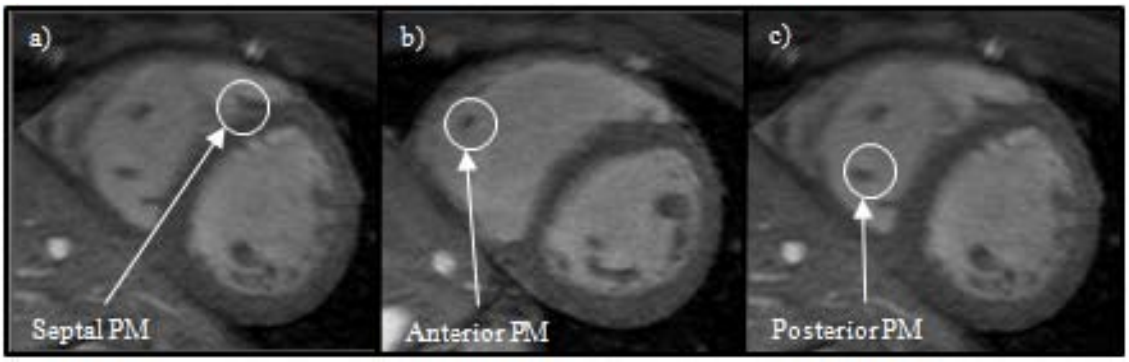

Figure H.1: MRI visualization of papillary muscles. a) Septal PM, b) Anterior PM, c) Posterior PM

The first slice in which the PM was visible was recorded to obtain the z distance with respect to the ARP. The x and y coordinates of the center of the PM tip was recorded to give the full 3D position.

3D coordinates were recorded for all three papillary muscles: septal, posterior and anterior in all subjects. All images were registered to the MRI coordinate system for purposes of position and orientation [95].

The centroid of the three PM coordinates was calculated for the three PMs for each patient and used as a reference point. All distances were normalized by ascending aortic diameter to minimize patient variability. X, y and z distances from the centroid (Fig H.2a) were calculated for each PM as well as the distance from each PM to the centroid (Fig H.2c). In addition, the triangle formed by the 3 PMs was used to investigate the relative position of the PMs. The distance of each triangle side length (Fig H.2b) and area of the triangle formed by the three PMs (Fig 2d) was reported.

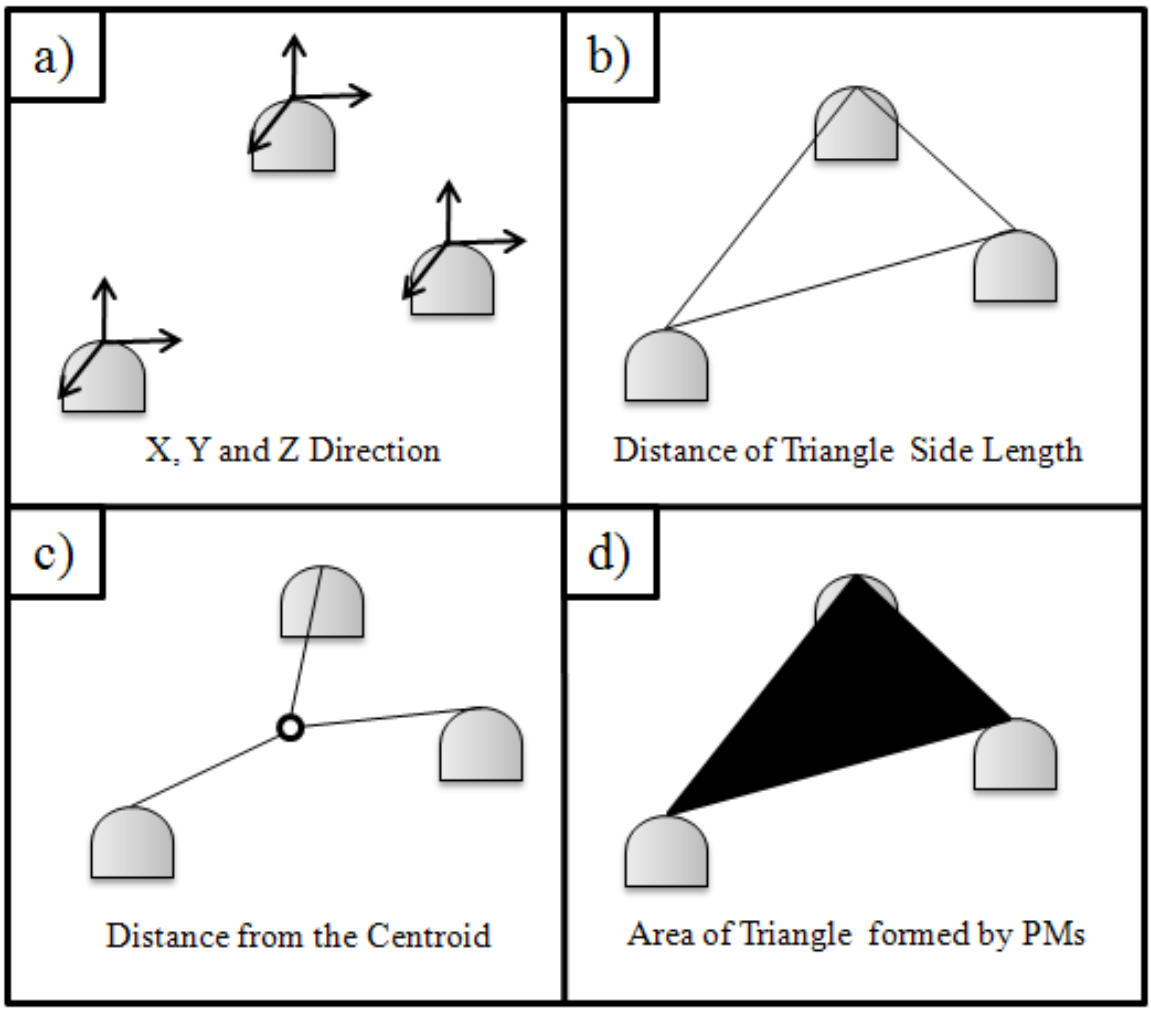

Figure H.2: Schematic of measurements of PMs. X-direction = (+) septal/(-) lateral, Y- direction = (+) anterior/(-) posterior, Z-direction: distance from annulus reference plane.

Papillary muscles were classified into groups based upon their location; (i) anterior: located on the free wall (ii) septal: located on the anterior portion of the septum; and (iii) posterior: located on the posterior portion of the septum.

Statistical Methods

An Anderson Darling test was used to test for normality. A two-sample student's t-test was performed to determine statistically significant differences between normal and diseased patients at a significance level of $p < .05$. Values are expressed as mean $\pm$

standard error. A post hoc power analysis was conducted on groups in which a significant difference was noted to confirm appropriate power (≥ 0.7).

RESULTS

Normal Group

All measurements for normal PM position can be found in Table H.1.

Table H.1: Numerical Measurements of PMs for Normal and Dilated LV groups. List of abbreviations: LV (Left Ventricle), Avg. (Average), SE (Standard Error), Dist. (Distance), Ant. (Anterior), Post. (Posterior), Sept. (Septal).

	Normal Group			Dilated LV Group			
	Avg.		SE	Avg.		SE	p-value
X Dist. – Ant. PM	0.61	±	0.09	0.38	±	0.04	0.06
Y Dist. – Ant. PM	0.20	±	0.04	0.30	±	0.04	0.11
Z Dist. – Ant. PM	0.20	±	0.05	0.15	±	0.03	0.44
X Dist. – Post. PM	0.00	±	0.07	0.03	±	0.06	0.76
Y Dist. – Post. PM	-0.35	±	0.04	-0.33	±	0.06	0.83
Z Dist. – Post. PM	0.65	±	0.03	0.62	±	0.03	0.48
X Dist. – Sept. PM	-0.61	±	0.08	-0.41	±	0.07	0.09
Y Dist. – Sept. PM	0.14	±	0.03	0.03	±	0.04	0.03*
Z Dist. – Sept. PM	0.85	±	0.07	0.74	±	0.05	0.24
Dist. Ant. PM	0.69	±	0.08	0.49	±	0.06	0.07
Dist. Post. PM	0.76	±	0.04	0.65	±	0.10	0.32
Dist. Sept. PM	1.07	±	0.08	0.76	±	0.11	0.05*
Triangle Area	0.13	±	0.02	0.09	±	0.02	0.23
Dist. Sept.-Ant. PM	1.40	±	0.15	1.04	±	0.08	1.08
Dist. Sept.-Post. PM	0.84	±	0.10	0.63	±	0.11	0.19
Dist. Post.-Ant. PM	0.99	±	0.07	0.90	±	0.07	0.35

*=$p \leq 0.05$ as compared to normal

It is notable that the sides of the triangle formed by the PMs were of similar length. The Septal PM was the furthest from the centroid with a normalized distance of 1.07$\pm$ 0.08 mm/mm. The anterior PM was the most apical and furthest from the ARP of the three PMs (0.20 $\pm$ 0.04 mm/mm) with the septal PM the closest to the ARP (0.85 $\pm$ 0.07 mm/mm). A 3D depiction of normal PMs and their position in the heart can be seen in Figure H.3.

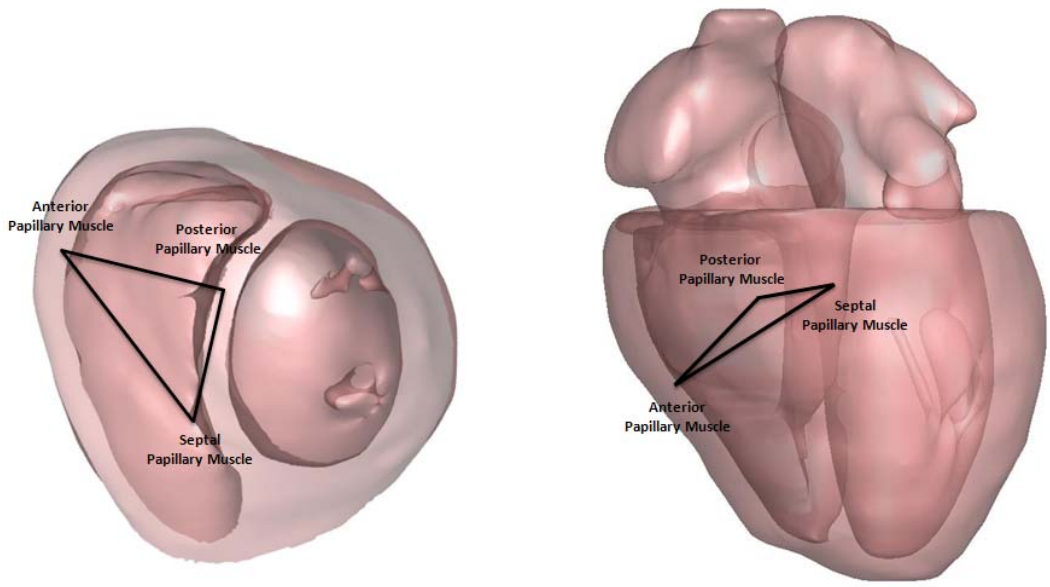

Figure H.3: Anatomical representation of PM position in the right ventricle.

Dilated LV Group

All measurements for diseased PM position can be found in Table H.1. The same relative position and orientation of all three PMs was noted in the diseased patients as in normal patients. The septal PM was furthest from the centroid (0.76 $\pm$ 0.11 mm/mm). The anterior PM was furthest away from the ARP (0.15 $\pm$ 0.03 mm/mm) while the septal PM was the closest (0.74 $\pm$ 0.05 mm/mm).

Differences

Significant differences between normal and diseased patients were only detectable with the septal PM. The differences were observed in the y distance ($p = 0.03$) of the septal PM (Diseased 0.38 $\pm$ 0.04 mm/mm, Normal 0.61 $\pm$ 0.09 mm/mm) and thus displaced in a posterior direction. In addition the septal PM was also displaced towards the centroid ($p = 0.05$) in diseased patients (Dilated 0.029 $\pm$ 0.04 mm/mm, Normal 0.144 $\pm$ 0.03 mm/mm), and therefore away from the septum. Significant differences of PM displacement are visually depicted in Figure H.4.

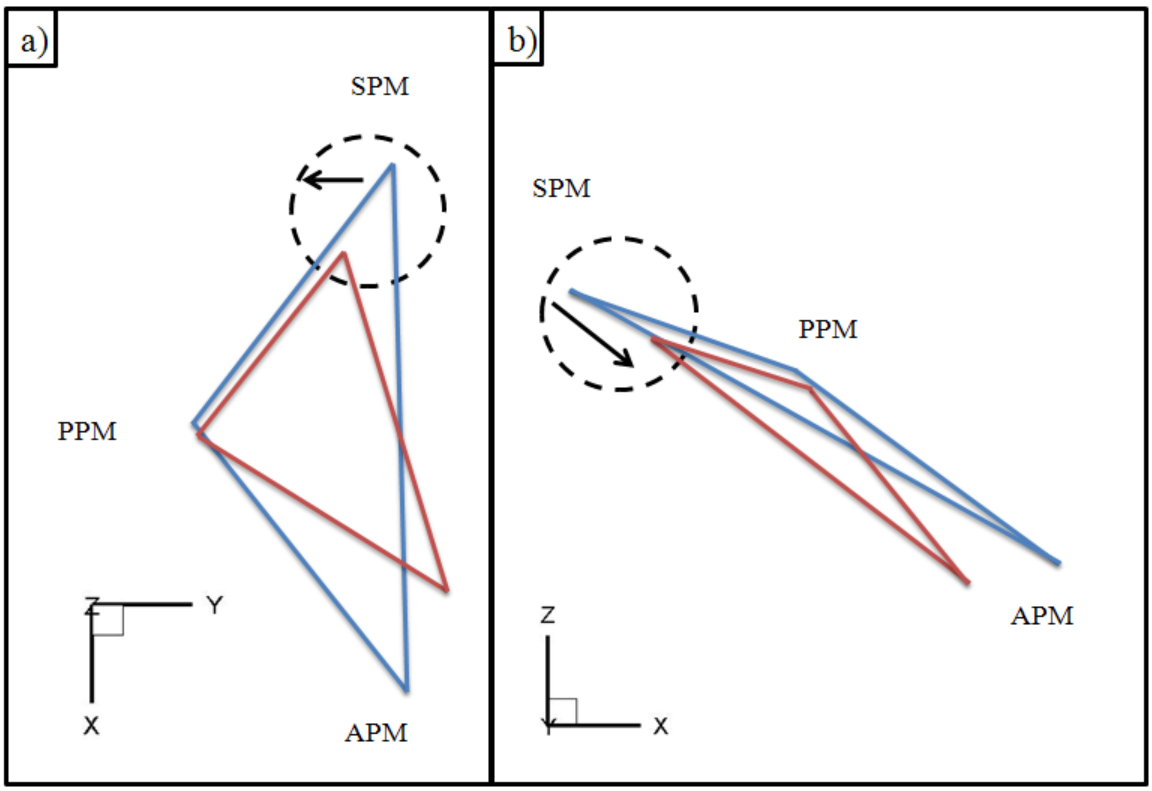

Figure H.4: Visualization of triangle formed by normal (blue) and diseased (red) patients. a) Y displacement of the Septal PM in diseased patients b) Displacement of the Septal PM towards then centroid in diseased patients.

DISCUSSION

To our knowledge this is the first report describing the specific locations of all three RV PMs in normal and patients with a dilated LV using cardiac MRI. Comparison between RV PM position in normal patients and patients with a dilated left ventricle revealed a significant difference in the relative position of the septal PM. In this study, we found that left ventricular dilatation resulted in the inward displacement of the septal PM towards the centroid of the three PMs, which may be due to the displacement of the septal wall into the RV with the increased left ventricular volume. LV dysfunction has typically been related to RV dysfunction through pulmonary hypertension [16, 18, 77], but changes in the LV geometry may be transferred to the RV though the interventricular

septum [2]. Anyanwu et al. proposed LV dysfunction or dilatation as a mechanism of TR with normal pulmonary hypertension [24]. Weber and Janicki discuss in detail interventricular septum effects and the displacement of the septum into the RV with acute LV distention [69]. Our results clearly show the interplay of ventricle volume and the effect of the septum displacement into the RV on the PMs. In addition, we believe that motion of the septal wall into the RV, may translate to the septal leaflet as it is attached to the septum through chordae tendineae and the septal an posterior PMs. Specific identification of the effects of the septal PM displacement on the leaflets was outside the scope of this study and therefore we cannot conclude if this displacement leads to tricuspid valve tethering or prolapse of the leaflets. However, there is evidence that prolapse and tethering of the leaflets result in TR [20, 22, 65]. As the PMs are displaced, the tension in the chordae may be decreased, but this study only investigated the PM motion. We speculate that the PM displacement observed in the diseased group may have contributed to the TR present in five of the 7 patients. Our analysis is a first step in demonstrating that left sided disease has a direct impact on right sided anatomic structures, resulting in a configuration that may lead to tricuspid valve leaflet prolapse and tethering. Further studies are needed to investigate the direct impact of PM displacement on valve function. Such studies are currently underway to confirm these phenomena.

In addition to the role of annular dilatation in TR, which is widely accepted, we believe changes in the PM positions may also play an important role in TR. If PM displacement does in fact impact TV function and lead to TR, this may lead to residual TR after repair, if the PM positions were altered and not addressed with the repair. Traditionally, the most common surgical intervention for non-rheumatic TV focuses on

reducing the dilated annulus to its original size with the placement of an annuloplasty ring. Studies have found that restoring the annulus to a normal size may not eliminate TR completely and in many cases it returns [26, 33]. Hence, solely reducing the annulus may be insufficient to permanently correct TR [26, 55]. While papillary muscle displacement may be one contributor to this recurrence of TR, this study also demonstrates that it may be important to assess the impact of the LV size and septal motion on RV function, even before surgery is attempted. These outcomes suggest that the underlying pathophysiology associated with TR is perhaps not well understood. Previous studies have attempted to correlate RV PM displacement to TR and found tricuspid valve (TV) tethering and restriction of leaflet mobility caused by PM displacement ~~is~~ to be an independent predictor of TR after TV annuloplasty [26, 55]. Although the relation of LV dilatation to durability of TV repairs has yet to be proven, this study demonstrates the geometric relation between the two ventricles. Futures studies may aim to determine pre and post operative PM position and determine the relation to patient outcome. This study demonstrates a useful tool which can be implemented to measure PM position in both normal and disease patients.

LIMITATIONS

This study was limited to the effects of LV dilatation on the posterior and septal PMs, as they are located on the septal wall. Due to the retrospective nature of this study, only PM positions at end-diastole were acquired, while future studies of the dynamic position of the PMs through the cardiac cycle are required. Although the images used for this study were at end-diastole, after careful observation of the ventricle throughout the

cardiac cycle we found the position of the PMs did not move from the time at which analyzed until beginning systole when the ventricle began to contract. It is of importance to note that while TR is a systolic phenomenon, the displacement of the PMs elucidated in this study are expected have an effect on the TV apparatus during systole and may even be further exacerbated. This can be determined by future studies which investigate the PMs not only at peak systole but throughout the entire cardiac cycle.

CONCLUSION

Dilatation of the left ventricle resulted in a significant displacement of the septal papillary muscle position. This change in PM position is due to change in geometry of the LV with dilatation and movement of the septal wall into the RV. Implications the displacement of septal and posterior PMs in the role of tricuspid valve function are yet to be determined.

ACKNOWLEDGEMENTS

Boston Scientific for providing funding for the MRI scans.

American Heart Association Predoctoral Fellowship for EM Spinner (#09PRE2380090)

REFERENCES

1. Singh, J.P., et al., *Prevalence and clinical determinants of mitral, tricuspid, and aortic regurgitation (The Framingham Heart Study) (vol 83, pg 897, 1999).* American Journal of Cardiology, 1999. **84**(9): p. 1143-1143.
2. *STS Adult CV Surgery National Database*. Fall 2008 Executive Summary.
3. Calafiore, A.M., et al., *Mitral Valve Surgery for Functional Mitral Regurgitation: Should Moderate-or-More Tricuspid Regurgitation Be Treated? A Propensity Score Analysis.* Annals of Thoracic Surgery, 2009. **87**(3): p. 698-703.
4. Bruce, C.J. and H.M. Connolly, *Right-sided valve disease deserves a little more respect.* Circulation, 2009. **119**(20): p. 2726-34.
5. Chang, B.C., et al., *Long-term clinical results of tricuspid valve replacement.* Annals of Thoracic Surgery, 2006. **81**(4): p. 1317-1324.
6. Bernal, J.M., et al., *Reoperations after tricuspid valve repair.* Journal of Thoracic and Cardiovascular Surgery, 2005. **130**(2): p. 498-503.
7. Fukuda, S., et al., *Mechanism of recurrent or residual functional tricuspid regurgitation mid-term after tricuspid annuloplasty.* Circulation, 2005. **112**(17): p. U556-U556.
8. Fukuda, S., et al., *Determinants of recurrent or residual functional tricuspid regurgitation after tricuspid annuloplasty.* Circulation, 2006. **114**: p. I582-I587.
9. Fukuda, S., et al., *The effect of tricuspid valve surgery on right ventricular function in patients with functional tricuspid regurgitation.* Journal of the American College of Cardiology, 2005. **45**(3): p. 365A-365A.

10. Sadeghi, H.M., et al., *Does lowering pulmonary arterial pressure eliminate severe functional tricuspid regurgitation?* Journal of the American College of Cardiology, 2004. **44**(1): p. 126-132.

11. Bonow, R.O., et al., *ACC/AHA guidelines for the management of patients with valvular heart disease - A report of the American College of Cardiology American Heart Association Task Force on practice guidelines (Committee on Management of Patients with Valvular Heart Disease).* Journal of the American College of Cardiology, 1998. **32**(5): p. 1486-1582.

12. Weber, K.T., et al., *CONTRACTILE MECHANICS AND INTERACTION OF THE RIGHT AND LEFT-VENTRICLES.* American Journal of Cardiology, 1981. **47**(3): p. 686-695.

13. Jouan, J., et al., *Further information from a sonometric study of the normal tricuspid valve annulus in sheep: Geometric changes during the cardiac cycle.* Journal of Heart Valve Disease, 2007. **16**(5): p. 511-518.

14. Hiro, M.E., et al., *Sonometric study of the normal tricuspid valve annulus in sheep.* Journal of Heart Valve Disease, 2004. **13**(3): p. 452-460.

15. Kim, H.K., et al., *Determinants of the severity of functional tricuspid regurgitation.* American Journal of Cardiology, 2006. **98**(2): p. 236-242.

16. Anyanwu, A.C., J. Chikwe, and D.H. Adams, *Tricuspid valve repair for treatment and prevention of secondary tricuspid regurgitation in patients undergoing mitral valve surgery.* Curr Cardiol Rep, 2008. **10**(2): p. 110-7.

17. Fukuda, S., et al., *Tricuspid valve tethering predicts residual regurgitation after tricuspid annuloplasty.* Journal of the American College of Cardiology, 2005. **45**(3): p. 362A-362A.

18. Weber, O.M., A.J. Martin, and C.B. Higgins, *Whole-heart steady-state free precession coronary artery magnetic resonance angiography.* Magn Reson Med, 2003. **50**(6): p. 1223-8.

19. Association, N.E.M., *Digital Imaging and Communications in Medicine (DICOM)*, in *Information Object Definitions*. 2004: Rosslyn. p. 876.

20. Hinderliter, A.L., et al., *Frequency and severity of tricuspid regurgitation determined by Doppler echocardiography in primary pulmonary hypertension.* American Journal of Cardiology, 2003. **91**(8): p. 1033-1037.

21. Sukmawan, R., et al., *Geometric changes of tricuspid valve tenting in tricuspid regurgitation secondary to pulmonary hypertension quantified by novel system with transthoracic real-time 3-dimensional echocardiography.* Journal of the American Society of Echocardiography, 2007. **20**(5): p. 470-476.

22. Rogers, J.H. and S.F. Bolling, *The tricuspid valve: current perspective and evolving management of tricuspid regurgitation.* Circulation, 2009. **119**(20): p. 2718-25.

23. Fukuda, S., et al., *Echocardiographic insights into atrial and ventricular mechanisms of functional tricuspid regurgitation.* American Heart Journal, 2006. **152**(6): p. 1208-1214.

24. Carpentier, A., *CARDIAC-VALVE SURGERY - THE FRENCH CORRECTION.* Journal of Thoracic and Cardiovascular Surgery, 1983. **86**(3): p. 323-337.

25. Miyatake, K., et al., *EVALUATION OF TRICUSPID REGURGITATION BY PULSED DOPPLER AND TWO-DIMENSIONAL ECHOCARDIOGRAPHY.* Circulation, 1982. **66**(4): p. 777-784.

26. Park, Y.H., et al., *Geometric and hemodynamic determinants of functional tricuspid regurgitation: A real-time three-dimensional echocardiography study.* International Journal of Cardiology, 2008. **124**(2): p. 160-165.

APPENDIX I

UTILITY OF 3D ECHOCARDIOGRAPHY FOR VISUALIZATION OF THE TRICUSPID VALVE

As the interest in repairing the tricuspid valve (TV), to correct tricuspid regurgitation (TR) is increasing, so are attempts to better visualize the TV. Recent advances in 3D echocardiography provide for optimal visualization of both normal and diseased TVs, including the valvular and subvalvular apparatus. Previous 2D methods were restricted to only the planes acquired, whereas 3D provides the entire geometry for analysis. By acquiring a 3D transthoracic image focusing on the right ventricle one can visualize TV leaflet motion and identify the papillary muscles (PM). While the leaflet motion can be visualized in the 3D image, it is necessary to interrogate the 3D images along the long axis to identify the PMs. All images were acquired at Emory University Hospital using a GE Vivid 7, under an IRB approved protocol. 2D slices along the apical 4-chamber and para-sternal short axis were extracted from the 3D image using GE EchoPAC.

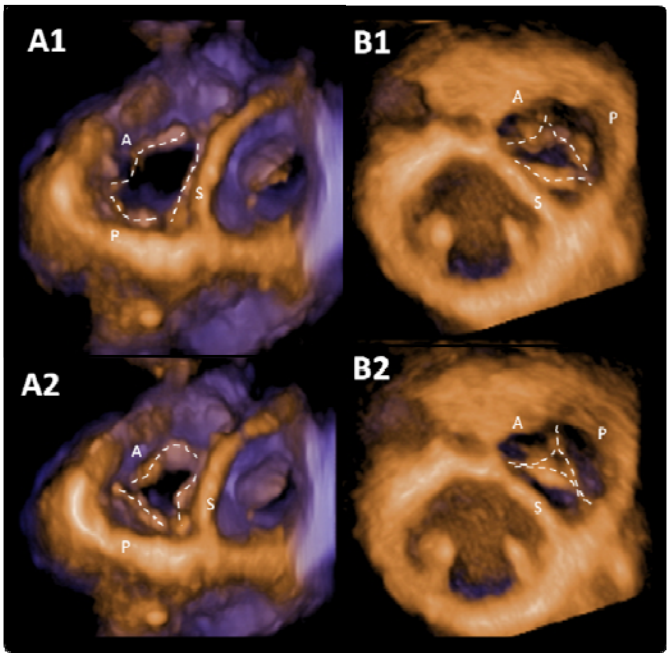

Figure I.1: Visualization of the tricuspid valve leaflets from the ventricle during diastole (A1) and systole (A2), and the atrium during diastole (B1) and systole (B2). Three distinct leaflets can be identified and are labeled: anterior (A), posterior (P) and septal (S) (click images A and B for videos)

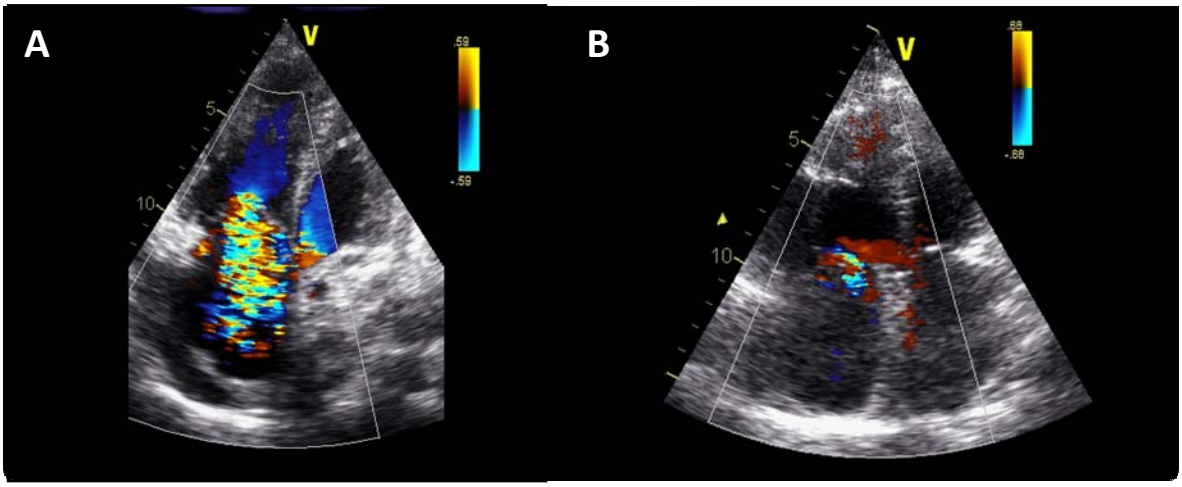

Figure I.2: 3D echocardiography can be utilized to interrogate the TV apparatus of diseased patients. Regurgitation jets can be visualized in the four chamber view and are seen above in patients with severe pulmonary hypertension, with severe (A) and moderate (B) TR jets (click image A for video).

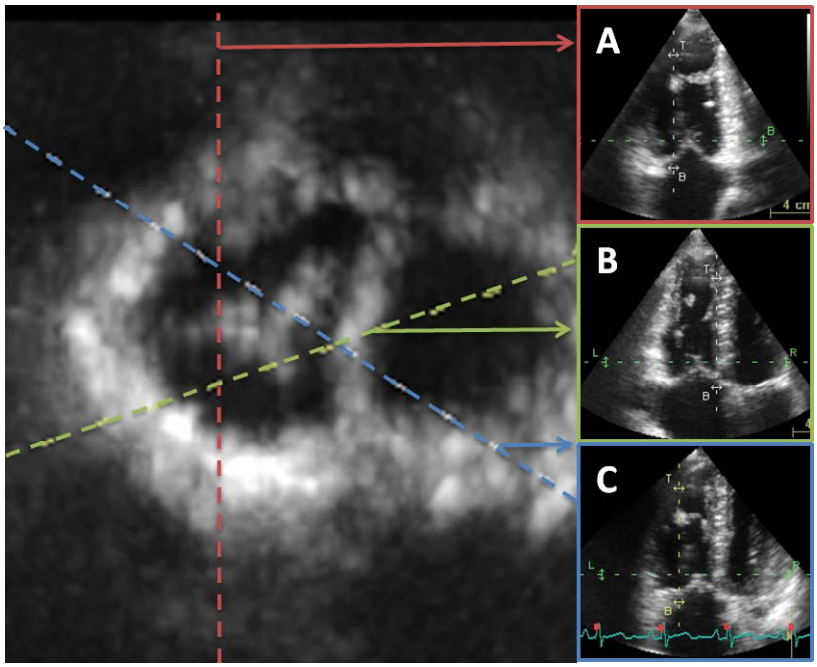

Figure I.3: With acquisition of the complete 3D geometry, a more detailed description of the valve as compared to traditional 2D methods can be obtained. Post processing can be conducted to visualize the three leaflets by taking a cross section of the valve, whereby the 2D coaptation lines of the three leaflets can then be interrogated. Coaptation images of the A) septal and anterior; B) anterior and posterior; and C) posterior and septal leaflets are shown. Quantitative measurements such as tenting height and area can then be quantified for each coaptation line.

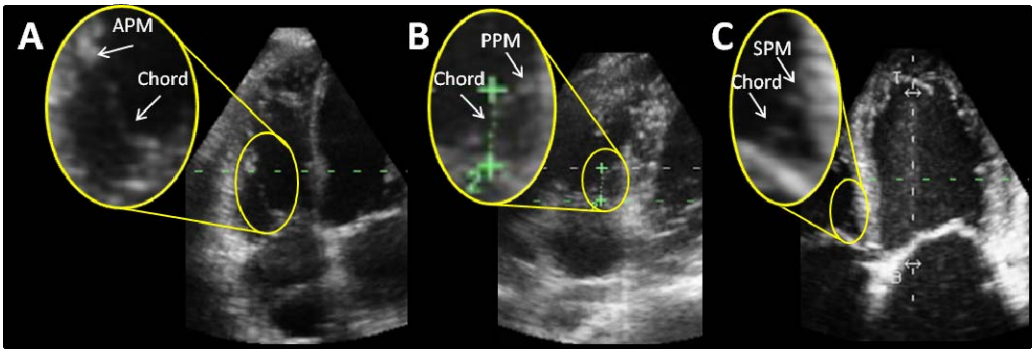

Figure I.4: Through interrogation of the 3D image, with 2D planes in the long axis view of the RV, the PMs can be identified. Visualization of the chordae, which can be traced back to their PM insertions, is used to locate the PM tip. Images of the A) anterior PM (APM), B) posterior PM (PPM), and C) septal PM (SPM) are shown.

APPENDIX J

MEASUREMENT OF STRAIN ON THE TV LEAFLETS

The following manuscript investigates the effect of both disease and a saddle shape annulus of the strain on the anterior and posterior leaflets.

The Effects a Three-Dimensional, Saddle-Shaped Annulus on Anterior and Posterior Leaflet Stretch and Regurgitation of the Tricuspid Valve

Erin Spinner BS, Dana Buice BS, Choon Hwai Yap MS, Ajit P. Yoganathan PhD

Wallace H. Coulter Department of Biomedical Engineering Georgia Institute of Technology and Emory University, & Parker H. Petit Institute for Bioengineering & Bioscience, Georgia Tech, Atlanta, GA USA

16/20 Pages (references, no figures or tables), 7/~8 Figures, 2 Tables

Correspondence to:

Ajit P. Yoganathan, PhD

Wallace H. Coulter Department of Biomedical Engineering

Georgia Institute of Technology

313 Ferst Drive, Suite 2119

Atlanta, GA 30332-0535

404-894-2849

404-894-4243 (Fax)

ajit.yoganathan@bme.gatech.edu

ABSTRACT

Tricuspid regurgitation (TR) is present in trace amounts or more in 85% of the population and is greater than mild in 14% of the population. In severe cases, it can contribute to right heart failure and adversely affects mitral valve repair durability. One major cause of TR is the dilation of the tricuspid annulus, which alters the geometry of the annulus from a saddle-shape to a more planar profile. Another cause of TR is the displacement of the papillary muscles, which results from right ventricular dilation. The objective of this study was to identify the effect of a saddle annulus on native tricuspid leaflets stretch mechanics and TR. In addition, the effects of geometric alterations, including annular dilatation and PM displacement, on leaflet stretch was investigated.

Fresh porcine tricuspid valves (n=8) were excised and sutured to an adjustable three-dimensional annulus plate (allowing for dilatation and saddle-shape) and three PM attachment rods. The valve was then placed in the *in vitro* Georgia Tech right heart simulator. Dual-camera photogrammetry, was used to quantify the stretch ratio experienced by the valve leaflets at peak systole for the following conditions: physiologically normal, 100% annular dilatation, displaced papillary muscles, and a combination of annular dilatation and papillary muscle displacement. In addition, a saddle and flat annulus was implemented for each of the four conditions. Papillary muscle displacement was simulated by displacing all papillary muscles by 10 mm in all directions (laterally, apically, posteriorly/anteriorly). The physiologically normal condition - normal annulus area, saddle-shaped annulus with PMs in a normal position, was used as a control.

The results showed that the posterior leaflet exhibited significantly ($p \leq 0.05$)

higher stretch ratios than the anterior leaflet at peak systole for all conditions tested in both the major and areal directions. While no significant ($p \leq 0.05$) difference was seen in stretch when a flat annulus was compared to saddle in any disease simulated, there was a significant ($p \leq 0.05$) difference in the normal condition. The posterior leaflet stretch was increased with saddle as compared to a flat annulus for both major (1.22 ± 0.12) and areal directions (1.19 ± 0.09). Investigation of the impact of disease found a significant increase in stretch in the posterior leaflet with a combination of annular dilatation and PM displacement (2.01 ± 0.68) as compared to the normal condition with a saddle annulus (1.43 ± 0.20). In addition to the impact of a saddle shaped annulus on the stretch of the leaflets, a significant ($p \leq 0.05$) reduction in TR was also observed in the presence of PM displacement, although the actual volume reduced was minimal (1.2 mL).

Stretch values were measured for the anterior and posterior leaflet under both physiologic and pathologic conditions for the first time. Further, these results provide an understanding of the effects of geometric parameters on valve mechanics and function, which may lead to improved tricuspid valve repairs.

INTRODUCTION

The tricuspid valve (TV) is one of two atrioventricular valves, and of the two, it is the least understood. It has, however, been shown that in severe cases, tricuspid regurgitation (TR), can negatively impact mitral valve (MV) repairs[1,2] and contribute to right heart failure[3]. Severe TR is also associated with an increased mortality rate[4]. TR is surprisingly common, and is detectable in 82 – 86% of the US population, with 14 – 18% of this population having clinically severe TR[5].

The tricuspid valve consists of an annulus, three leaflets, numerous chordae and three main papillary muscle (PM) groupings. These components work together to provide proper coaptation and maintain unidirectional blood flow. Alterations in this balance may result in improper closure of the leaflets, altering valve mechanics and leading to TR. Specifically, stretch on the leaflets may be impacted when this balance is disturbed.

Previous studies on the MV concluded that stretch in the central region of the anterior and posterior leaflet was reduced with increasing annular saddle curvature[6,7] Thus, saddle was thought to be an important component of mitral valve annular restoration. Additionally, studies have shown that as with the MV, alterations in the three-dimensional geometry of the tricuspid valve are present in patients with TR[8,9]. Recent clinical studies using 3-dimensional echocardiography have shown the TV annulus in healthy patients has a saddle-shape[9,10]. More specifically, the posteroseptal and anterolateral segments of the annulus were shown to be more apical, (low points), and the anteroseptal and posterolateral segments were more basal (high points). These studies also showed that with functional TR, the annulus became more planar. This information may not be similarly applied to the TV as the saddle shape differs as well as

the presence of an additional leaflet. It is however, it is unclear whether saddle aides in reducing TR or in minimizing leaflet stretch.

Changes in the 3D geometry of the TV annulus occur in conjunction with annular dilatation, the major cause of TR[11]. In the case of dilatation, the leaflets are unable to compensate for the enlarged orifice. TR resulting from isolated annular dilatation is rare[12], while combined annular dilatation and papillary muscle (PM) displacement is more common. This is due to the fact that dilatation is typically a secondary condition, and is associated with a dilated right ventricle[2]. Additionally, PM displacement also contributes to TR. The role of annular dilatation and PM displacement have been demonstrated to have a significant impact on TR, through both *in vivo*[13,14] and *in vitro* investigations[15]. The anterior PM is displaced with right ventricular dilatation, as it is located on the free wall; while the septal and posterior PM is displaced with left ventricular dilatation, since they are located on the septal wall.

Fully understanding the effects of disease on tricuspid valve leaflet stretch is necessary as alterations in the mechanical loading environment may have long term detrimental affects to the leaflet tissue properties through adverse remodeling. The current study will help us understand the effects of annulus shape, annular size and PM position on the stretch experienced by the anterior and posterior leaflets of the TV. The role of a saddle shaped annulus on TR will also be investigated.

MATERIALS AND METHODS

Valve Selection

Fresh porcine hearts (n=8) were obtained from a local abattoir (Holifield Farms,

Covington, GA). Tricuspid valves with 6 cm^2 annulus area, and leaflet heights and widths similar to physiological human measurements[16-18] were selected. Each leaflet height and width was measured. The relative size of the leaflets was confirmed, ensuring the anterior was the largest and the septal was the smallest. The valves were excised, preserving the valvular and sub-valvular components: annulus, leaflets, chordae tendineae, and papillary muscles as detailed in previously published TV in vitro studies[15,19,20].

Experimental Set-Up

The valve was sutured to an annulus plate with an adjustable silicone ring, allowing for physiological annular dilatation and saddle-shape adjustments. The normal annulus had an area of 6 cm^2 with an area of 12 cm^2 when dilated by 100%. Annular dimensions were determined from previous published *in vivo* studies[9,21]. Saddle-shape was implemented based on the clinical data reported by Fukuda et. al. The posteroseptal and anterolateral segments of the annulus were pulled into the ventricular chamber 6 mm each, resulting in a saddle height of 3mm on either side of the annulus plane, apical and basal[9] (Figure J.1).

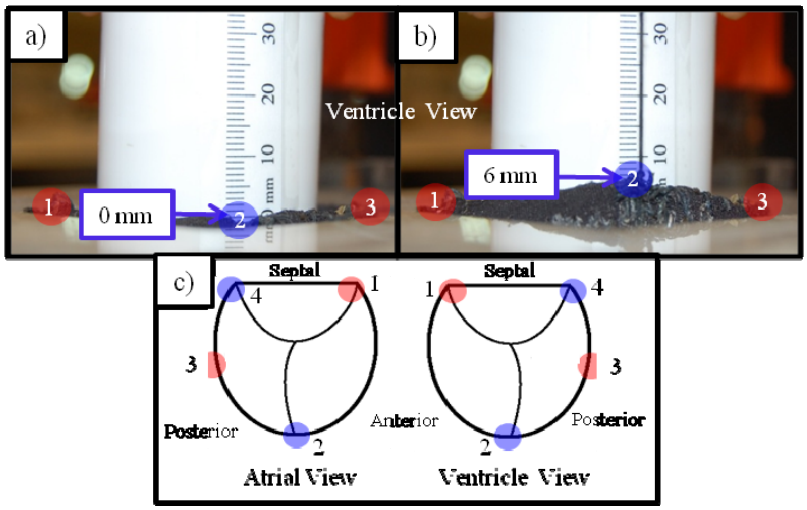

FIGURE J.1: Implementation of a saddle shape on the annulus plate A) flat configuration, B) saddle configuration with peak to peak saddle height of 6mm. C) Schematic of high (red) and low (blue) saddle points, with posteroseptal and anterolateral segments of the annulus low and the anteroseptal and posterolateral segments high.

Dacron cloth and a button was sutured to the papillary muscles to allow for attachment to the 3D adjustable PM rods. The valve was then placed in the *in vitro* Georgia Tech right heart simulator (Figure J.2) to simulate physiologic hemodynamic conditions[15].

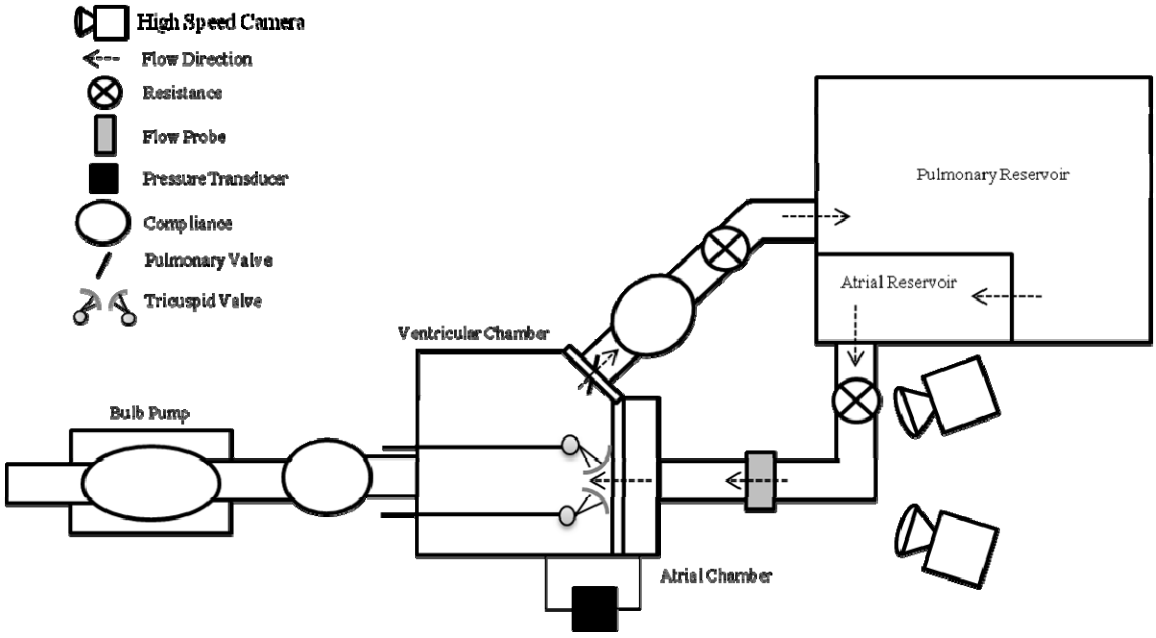

FIGURE J.2: Georgia Tech Right Heart Simulator used to hold tricuspid valve and simulate both physiologic and pathologic conditions. High speed cameras are places in front of the right atrial chamber to visualize the leaflet markers though out the cardiac cycle.

The rods were used to achieve a normal PM configuration and subsequently displaced to mimic PM positions which result from ventricular dilatation. For this study, PM displacement was simulated by displacing the anterior PM (APM) laterally and apically, and both the posterior (PPM) and septal (SPM) PMs together, laterally, anterior/posteriorly and apically. All PMs were displaced 10 mm in each direction. The pressure was generated by a compressor system and triggered by an electronic pulse programmer box. The flow loop was tuned by adjusting compliances and resistances to maintain the following hemodynamic conditions: heart rate of 70 beats per minute; mean systolic transvalvular pressure of 40mmHg; and cardiac output of 5 liters per minute. A flow probe (600 Series, Carolina Medical Electronics, North Bend, SC) in line with the flow, upstream of the atrial chamber, with a differential pressure transducer (DP9-30, Validyne Engineering Corp., Northridge, CA) attached to the atrial and ventricle

chambers. Flow and pressure were monitored and recorded using an in-house LabVIEW data acquisition program.

The following conditions were simulated in this study.: 1) control, with a normal annulus size and PMs in normal positions, 2) a dilated annulus with normal PM positions, 3) a normal annulus size with PMs and 4) a dilated annulus with displaced PMs (Figure J.3).

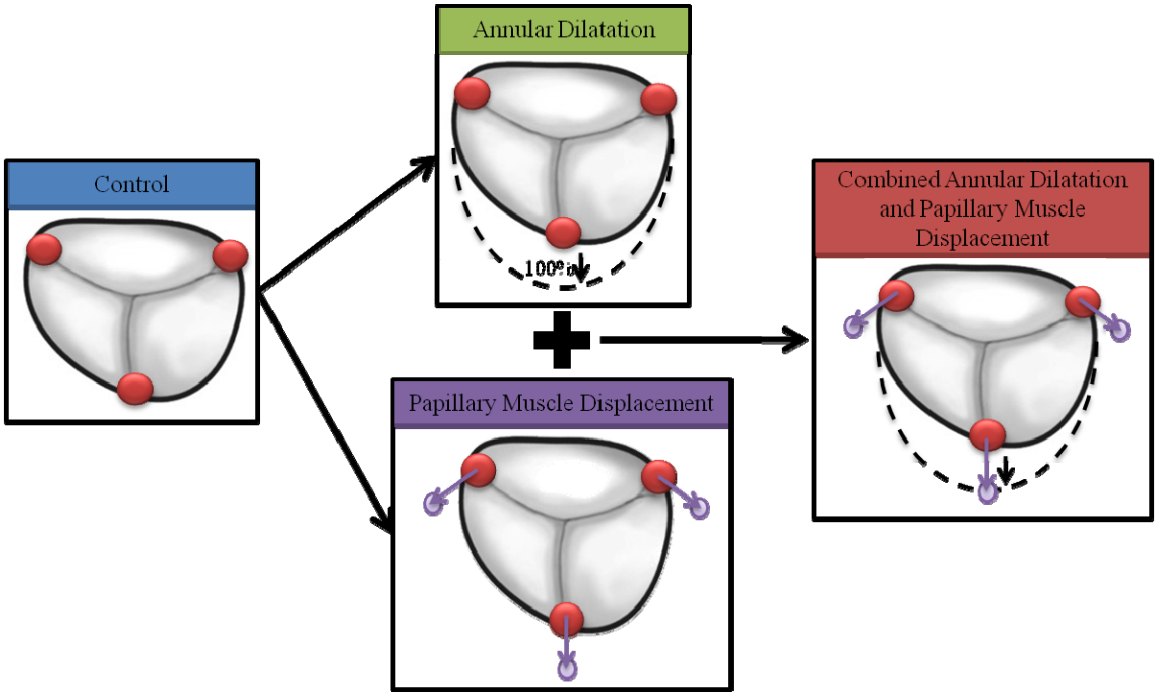

FIGURE J.3: Marker grid on the surface of the TV leaflets. Location of the markers selected for analysis are highlighted.

The four conditions were performed with and without a saddle shape, yielding a total of eight conditions. It was verified that the valve coapted properly without regurgitation before beginning experimentation. This was achieved with the PMs located at the commissures ensuring chords were slightly taught and perpendicular to annulus plane.

Hemodynamic Data Processing

Tricuspid regurgitation (TR) was determined for each condition by integrating the

negative portion of the flow curve and subtracting the closing volume. Closing volume was determined as the negative flow in the normal condition. This was averaged over 15 cardiac cycles for each condition.

Dual Camera Photogrammetry

Dual camera photograpmmetry was used to acquire images for measuring stretch ratios experienced by the tricuspid leaflets, as previously applied to the mitral and aortic valve leaflets [22,23]. Markers were placed in a 2mm x 2mm grid (Figure J.4) on the anterior and posterior leaflets with tissue dye (Black Tissue Marking Dye, Thermoelectron, Pittsburgh, PA) before inserting the annulus plate into the simulator.

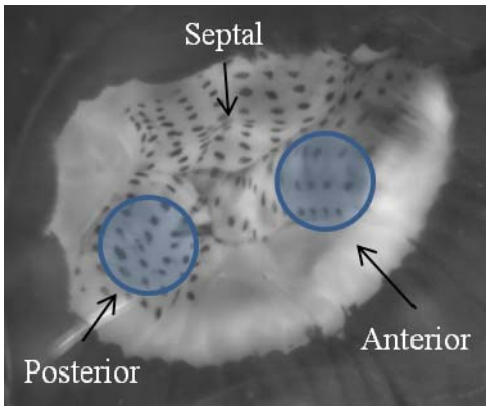

FIGURE J.4: Experimental conditions: A) Normal, B) Isolated annular dilatation, C) Isolated PM displacement and C) combined annular dilatation and PM displacement. PM displacement: lateral and apical displacement of all papillary muscles, posterior and anterior displacement for the posterior and septal PMs, respectively, 10 mms in all directions.

Two high-speed cameras (Basler camera A504K, Basler) with a resolution of 1280 x 1023 pixels were placed approximately 30 degrees apart on the same plane directed through the atrial chamber pointing at the annulus plane. Images were acquired at 500 frames per second, using an image grabbing system (EPIX CL3SD, Buffalo Grove, IL).

At the end of each experiment, images were taken of the valve leaflets in the

stress free state. This stress-free state was achieved by allowing pressures in the atrial and ventricular chambers to equilibrate. These images were used as the zero-stretch, stress-free reference configurations for the stretch ratio calculations. Lastly images of a 10 mm cube in the plane of the annulus at the center of the valve were taken for the direct linear transformation (DLT) calibration.

Leaflet Strain Data Processing

The following method was used to determine principal stretch ratios at peak systole for all experimental conditions. Images from both cameras were imported into MatLab (R2010a, Mathworks, Natick MA) and marker grids were manually selected and tracked. For the anterior leaflet, the coordinates were found for 16 markers in a 4x4 grid (n=8). For the posterior leaflet, since a smaller leaflet area was visible, 9 markers were selected in a 3x3 grid (n=6). The same grid for each valve was tracked across all experimental conditions for peak systole and the reference "stress-free" state. Peak systole was defined as the time point where the leaflets did not move in subsequent frames and stretch was maximal.

The seven visible vertices of the calibration cube were used to resolve the angle between the two cameras in order to obtain 3D coordinates of the leaflet markers, using the DLT algorithm[23]. The 3D marker coordinates were then analyzed for leaflet deformation. Shell-based 2D isoparametric finite element shape functions were used to fit the surface geometry and cover the different groups of markers on the leaflets for interpolation. The C-0 continuous quadratic 9 node Lagrangian shape functions were used for interpolation, and were fitted to coordinates of arrays of 9 markers (3x3) where possible. This was only completed once for the posterior leaflet and repeated four times

for the anterior leaflet to include all 16 markers. The following equation was used where summation notation applies[24]:

$$R_p = N_i^{jk}(\xi_p, \eta_p) R_i^{jk} \quad ; \qquad \text{i} = 1,9 \; ; \; \text{j,k} = 0 \qquad (1)$$

where N_i was the shape function for each node, R_i was the known coordinates at the nodes, and Rp was the interpolated coordinates at the specific location defined by ξ and η. j and k are differential indices with respect to ξ and η.

The shape functions were subsequently used to compute stretch ratios and strains at peak systole. Principal Almansi strains (e) and principal stretch ratios (λ) were calculated as follows:

$$e_{\alpha\beta} = \frac{1}{2}(g'_{\alpha\beta} - g_{\alpha\beta}) \qquad (2)$$

$$\lambda_{\alpha\beta} = \sqrt{2e_{\alpha\beta} + I} \qquad (3)$$

Where $g'_{\alpha\beta}$ and $g_{\alpha\beta}$ are components of the metric tensor in the deformed configuration and in the stress-free reference configuration, respectively. The methodology for the computation of stretch ratio and strains has been described previously by Smith et al. [24].

Statistical Analysis

Leaflet stretch ratio was compared between anterior and posterior leaflets for the same PM and annulus geometry, and for each leaflet among different PM and annulus geometry. An Anderson Darling test was first used to assess the normality of the data. A paired, two-tailed t-test was used, as natural pairing existed within different conditions being simulated on the same valve. A one-way ANOVA was used for comparison of the absolute stretch of the anterior leaflet to the posterior leaflet, as the data could not be

paired for all experiments. Furthermore, a GLM was used to assess the effect of disease on leaflet strain with the valve as a random factor to allow for pairing and comparison of multiple disease conditions. If data was not normal a Wilcoxon rank test was used in place of a paired t-test, Kruskal-Wallis for a One Way ANOVA and a Friedman's test instead of the GLM. All values are expressed as mean ± standard deviation. Minitab® (Minitab 16, State College, PA) was used for all statistical analysis.

RESULTS

Hemodynamics

Hemodynamic data are shown in Figure J.5.

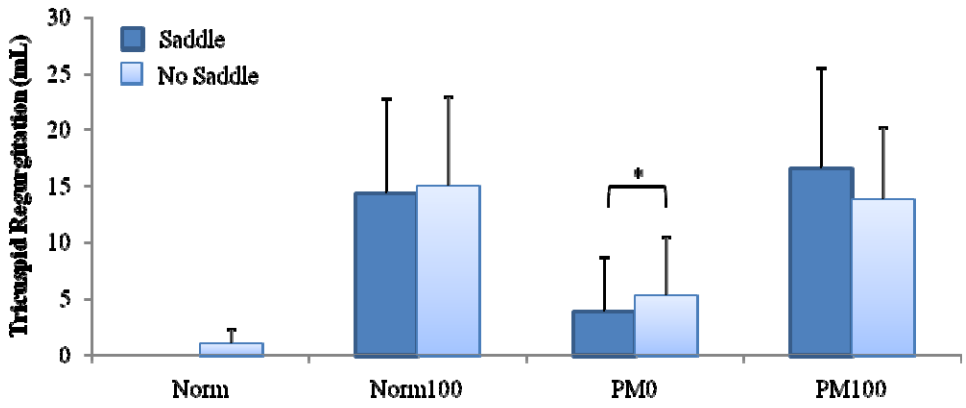

FIGURE J.5: Tricuspid regurgitation as an effect of a saddled annulus on tricuspid regurgitation on both normal and diseased conditions. Significance $p \leq 0.05$ (*), saddle vs. no saddle, average and standard error shown.

TR was examined to determine the effect of the presence of the saddle-shape in physiologically normal and diseased conditions on regurgitation. Statistical significance was only observed with isolated PM displacement ($p = 0.009$), where a decrease in TR was seen with the saddle shape. As has been reported previously[15] TR increased with both isolated annular dilatation and PM displacement, with the most severe TR observed

with a combinations of these anatomical parameters.

Leaflet Stretch Ratios

Major, minor and areal stretch ratios for the anterior leaflet are listed in Table 1 and Figure 6a, while values for the posterior leaflet are listed in Table 2 and in Figure 6b.

From one valve to the next, significant variability in stretch ratios under the same transvauvlar pressure were found, with standard deviations of stretch under normal conditions ranging from 0.07 to 0.12, which are consistent with results observed for the mitral valve and aortic valve leaflets[6,7,23].

For the anterior leaflet, the saddle-shape displayed major and minor axis stretch ratios of 1.22 ± 0.12 and 0.98 ± 0.06. Without a saddle-shaped annulus, the stretch values were found to be 1.17 ± 0.07 and 0.98 ± 0.07, respectively (Table J.1).

Table J.1: Anterior Leaflet: Major, minor, and areal stretch ratios for normal and diseased conditions, with and without saddle.

	Major Axis Stretch Ratio		Minor Axis Stretch Ratio		Areal Stretch Ratio	
	No Saddle	Saddle	No Saddle	Saddle	No Saddle	Saddle
Normal	1.17±0.07#	1.22±0.12***,#**	0.98±0.07	0.98±0.05	1.14±0.08#	1.19±0.09***,#**
100% Dilatation	1.22±0.12#	1.21±0.07#	1.02±0.10	1.01±0.05	1.25±0.23#	1.22±0.09#
PM Displacement	1.17±0.13#	1.17±0.14#	0.91±0.19	0.93±0.19	1.07±0.26	1.10±0.29#
Dilatation and PM Displacement	1.24±0.14#	1.22±0.13#	0.99±0.13	0.98±0.12	1.25±0.30#	1.19±0.23#

*****=p ≤ 0.05 as compared to same condition, same leaflet, saddle vs. no saddle, paired t-test
#=p ≤ 0.05 as compared to same condition, anterior vs. posterior leaflet, One Way ANOVA
#=p ≤ 0.05 as compared to same condition, anterior vs. posterior leaflet, Kruskal-Wallis

For the posterior leaflet control position with saddle-shape, major and minor axis stretch ratios were found to be 1.53 ± 0.32 and 0.96 ± 0.32. While the stretch ratios

without a saddle-shaped annulus were 1.54 ± 0.33 and 0.96 ± 0.15, respectively (Table J.2).

Table J.2: Posterior Leaflet: Major, minor, and areal stretch ratios for normal and diseased conditions, with and without saddle.

	Major Axis Stretch Ratio		Minor Axis Stretch Ratio		Areal Stretch Ratio	
	No Saddle	Saddle	No Saddle	Saddle	No Saddle	Saddle
Normal	1.54±0.32	1.53±0.32	0.96±0.15	0.96±0.16	1.45±0.24	1.43±0.20
100% Dilatation	1.57±0.24	1.65±0.34	1.04±0.24	1.01±0.19	1.62±0.47	1.63±0.25
PM Displacement	1.56±0.48	1.56±0.29	1.06±0.28	1.05±0.25	1.71±0.97	1.64±0.55
Dilatation and PM Displacement	1.84±0.49	1.62±0.28	1.10±0.23	1.08±0.19	2.01±0.68*	1.74±0.45

*=p ≤ 0.05 as compared to control (normal annulus size, saddle), normal vs. disease

Normal (Anterior and Posterior)

Between the posterior and anterior leaflets, significant differences in stretch ratios (major and areal stretch ratios) were observed for all conditions at p≤0.05. Major axis stretch ratios on the posterior leaflet were greater. Minor axis stretch ratios, however, did not exhibit any significant difference between the two leaflets.

Saddle vs. Flat Annulus (Anterior and Posterior)

For the anterior leaflet in the normal condition, the saddle-shaped annulus resulted in significantly greater major and areal stretch values (p= 0.07; 0.07) compared to the flat annulus. When the annulus was dilated and/or PMs were displaced, there was no significant difference in stretch ratios between the saddle-shaped and flat annulus. Additionally, no significant difference was found between saddle and flat for normal or

disease conditions for the posterior leaflet.

Normal vs. Disease (Anterior and Posterior)

No difference in stretch ratio was observed for disease as compared to normal for the anterior leaflet. However, a significant increase in stretch as a result of combined dilation and PM displacement was observed in the posterior leaflet in the major (p=0.024) and areal (p=0.024) stretches as seen in Figure J.6.

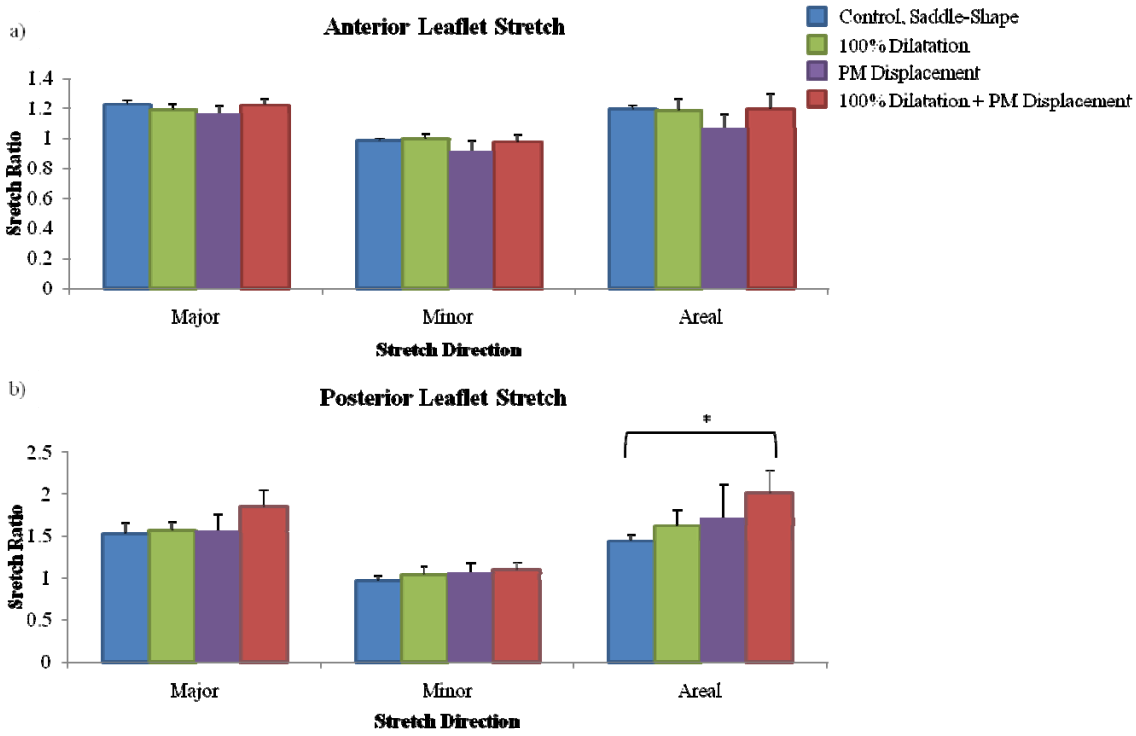

FIGURE J.6: A) Major, minor and areal anterior leaflet stretch ratio for control (saddle), 100% annular dilatation (flat), PM Displacement (flat) and combined annular dilatation and PM displacement (flat). B) Major, minor and areal posterior leaflet stretch ratio for control (saddle), 100% annular dilatation (flat), PM Displacement (flat) and combined annular dilatation and PM displacement (flat). Significance $p \leq 0.05$ (*), average and standard error shown.

DISCUSSION

Hemodynamics

A statistical difference was seen in TR between an annulus with and without a saddle in the presence of PM displacement, although the difference was minimal at only

2%. The reduction was only about 1 ml on the average, and most likely has very limited clinical impact. This difference would not be clinically alarming, as this value is within current accepted error associated with measurement techniques of TR, which can vary by technique or viewing window. Saddle-shape did not significantly affect TR in the normal or dilated conditions. Thus, this small difference may not warrant the implantation of a saddle ring as opposed to a flat ring, to further reduce TR.

Normal Leaflet Mechanics (Anterior and Posterior)

For the first time, physiological stretch ratios were recorded for the anterior and posterior leaflets of the tricuspid valve. The major principal stretch ratios during peak systole observed on the anterior leaflet, with (1.22 ± 0.12) and without saddle (1.17 $\pm$ 0.07) were comparable to peak leaflet stretch of the mitral valve leaflets measured in our laboratory. Previous mitral valve studies have reported stretch ratios on the anterior 1.30 ± 0.18 and posterior 1.23 ± 0.14 leaflets[22,25]. This similarity is not unexpected, as while the valves are under different loading conditions, the leaflet structures may be similar. The rationale for this is that during peak systole the valve is at its maximum stretch. Further investigating into the behavior of the collagen fibers shows that while the response curve is gradual at first, it then becomes steep[6,26]. We believe that both the mitral and tricuspid valves are within this steep range of the stress-strain curve, in which large changes in force have little effect on the stretch as the collagen fibers have already locked. While, we believe it is possible that the valve leaflets experience similar stretch, it is important to note that the references used in the MV studies were not the same as those used here for the TV. The study presented here uses a stress free state as a reference, whereas previous MV studies used a low stretch reference. The use a stress

free reference ensures proper measurement, and eliminates the possibility of under estimating the stretch with a pre-stretched reference which may be the case for previously referenced MV studies.

Interestingly, when comparing the TV anterior and posterior leaflets, the posterior leaflet exhibited significantly greater stretch than the anterior leaflet. To better understand why the posterior leaflet had higher stretch than the anterior leaflet, leaflet thickness and collagen structure were investigated. Back lit images of six valves were taken, focusing on the ventricular side of the anterior and posterior leaflets. A representative image (Figure J.7) highlights the anterior and posterior leaflet regions analyzed for this paper.

FIGURE J.7: Representative image of ventricular side of TV with anterior PM and anterior and posterior leaflets. Location of strain measurement is highlighted. Deep insertion of strut chordae is clearly present on the anterior leaflet, but not the posterior leaflet.

A difference in the leaflet structure was observed between the two leaflets in the region in which stretch was measured. More specifically, the strut chordae insert deep into the belly of the anterior leaflet, which was not as pronounced on the posterior leaflet. This increased localization of collagen structures does not allow the leaflet to stretch as much at or near the location of chordal insertion. This phenomenon has been presented previously in which a reduced stretch was observed at the location on the leaflet closest to strut chordae insertion[27,28]. For the posterior leaflet, the insertion of the chordae did not extend as deep into the leaflet belly, thus this phenomenon was not present in the region

in which we measured stretch, This may also explain why the differences in the leaflets were only seen in the major and areal directions, as the anterior leaflet may have been restricted by the increased collagen content.

The results thus suggest that different TV leaflets can have very different stretch responses to transvalvular pressure. Detailed information on the mechanics of the valve leaflets will aid in FEA modeling studies by providing realistic physiologic inputs . While a previous finite element simulation was published which predicted the stretch on the leaflets, its results were contradictory to those presented here. Stevanella et al performed finite element analysis of the tricuspid valve[29] and reported the posterior leaflet to have the less stretch as compared to the anterior leaflet, whereas this study found no difference between the leaflet stretch. This may be due to the fact that their model assumed the same material properties for the leaflets. Both our stretch findings as well as physical observations of the leaflets lead us to believe that the structure and material properties of the leaflets are different. Thus further detailed studies of the fiber architecture and stretch response mechanics of the TV leaflets are warranted.

Saddle vs. Flat Annulus (Anterior and Posterior)

Interestingly, the saddle shaped annulus led to a significantly increased stretch on the anterior leaflet of the TV, but not the posterior leaflet. This finding differed from that observed in the MV, where a saddle was shown to decrease the stretch on both leaflets[6]. This may be attributed to the inherent 3D geometrical differences between the tricuspid and mitral valves. In the MV, the apical motion of the commissures results in a saddle, with each leaflet flanked by a dip in the saddle at the commissures[30,31]. In the case of the TV, the posterior leaflet is flanked by two annular points with apical motion (low points)

similar to the MV, while the anterior leaflet is flanked by one annular point with apical motion (low point) and one annular point with basal motion (high point)[8,9]. The result of two adjacent annulus points moving in opposite directions may explain the larger stretch observed in the anterior leaflet as compared to the posterior leaflet, as it experiences in more tethering and deformation as a result of the saddle. Thus the stretch configuration of the anterior leaflet of the TV is not comparable to the MV.

Since the tricuspid valve has three leaflets, the saddle applied at two points may affect each leaflet's curvature differently. Additionally, the TV is in a lower pressure environment, and the leaflets may possess different material properties than the MV. For the posterior leaflet, two high points exist on either side of the leaflet, similar to what is seen in the mitral valve. However, no significant decrease in stretch, as seen with the MV, was observed when comparing the saddle to the flat annulus for this leaflet. When comparing the effect of saddle on the TV to the MV, it is important to understand that the annular height to commissural width ratio (AHCWR) observed in the TV is approximately 10%, whereas for the MV it is 20%[30,31]. Previous studies investigating the effect of the saddle on MV leaflet strains, saw no differences with 10% AHCWR. It was not until the AHCWR was increased to 20% that the strains were significantly decreased with a saddle shape as compared to flat[6,7].

Normal vs. Disease (Anterior and Posterior)

Only combined annular dilation and PM displacement resulted in significantly increased stretch for the posterior leaflet; while the anterior leaflet showed no changes. These finding are consistent with MV studies which were unable to show a difference in stretch as an effect of PM displacement[22]. Since neither isolated annular dilatation nor

PM displacement resulted in increased stretch, significant changes in valve geometry appeared to be necessary for any significant alterations to stretch patterns. The mechanism of this alteration has been demonstrated previously[19] was as such: the PM displacement restricts leaflet mobility, tethering the leaflets away from the annulus, while annular dilatation forced the leaflets to stretch further and compensate for the increased orifice area.

While restoring the tricuspid valve to its anatomic state is appealing, through implantation of a 3-dimensional annuloplasty ring, its benefits have yet to be demonstrated. Thus additional studies are needed to support the benefit of a 3D ring as compared to a traditional flat ring.

LIMITATIONS

The major limitation of this study was variability of the location of the stretch ratio measurements on the leaflets. Although a similar area was chosen, the grid was not always in the exact same location for every valve.

The intrinsic limitations of using an in vitro system exist, such as the rigid ventricle which is not physiologic. We do not believe this significantly impacts the results of this study as this study is focused on analyzing the stretch on the leaflets at peak systole. As such a dynamic ventricle is not necessary as annulus and PM positions are simulated at peak systole. In vitro experiments such as these have been successful in providing mechanistic understanding of the mitral and aortic valves under both physiological and pathologic conditions[6,7,23,27].

CONCLUSIONS

In conclusion, physiological stretch ratios of the TV leaflets were investigated for the first time in vitro. In addition, the affects of annular geometry and disease were examined and shown to increase strain in the case of combined annular dilatation and PM displacement. This study provides a better understanding of how the valve mechanics are altered with disease, which could allow for improved valve repair procedures in the future. The data/results from this study may also be of used to validate future numerical FEA models.

ACKNOWLEDGEMENTS

The authors thank Jean-Peirre Rabbah for his intellectual discussion and critical review of the manuscript and Holifield Farms for donation of the porcine hearts.

FUNDING

American Heart Association Predoctoral Fellowship 09PRE2380090, Wallace H. Coulter Distinguished Faculty Chair Endowment and Georgia Institute of Technology, Tom and Shirley Gurley and the Georgia Tech Presidential Undergraduate Research Award.

REFERENCES

1. Antunes MJ, Barlow JB. Management of tricuspid valve regurgitation. *Heart.* Feb 2007;93(2):271-276.

2. Anyanwu AC, Chikwe J, Adams DH. Tricuspid valve repair for treatment and prevention of secondary tricuspid regurgitation in patients undergoing mitral valve surgery. *Curr Cardiol Rep.* Mar 2008;10(2):110-117.

3. Shah PM, Raney AA. Tricuspid valve disease. *Curr Probl Cardiol.* Feb 2008;33(2):47-84.

4. Nath J, Foster E, Heidenreich PA. Impact of tricuspid regurgitation on long-term survival. *J Am Coll Cardiol.* Feb 4 2004;43(3):405-409.

5. Singh JP, Evans JC, Levy D, et al. Prevalence and clinical determinants of mitral, tricuspid, and aortic regurgitation (the Framingham Heart Study). *Am J Cardiol.* Mar 15 1999;83(6):897-902.

6. Jimenez JH, Liou SW, Padala M, et al. A saddle-shaped annulus reduces systolic strain on the central region of the mitral valve anterior leaflet. *J Thorac Cardiovasc Surg.* Dec 2007;134(6):1562-1568.

7. Padala M, Hutchison RA, Croft LR, et al. Saddle Shape of the Mitral Annulus Reduces Systolic Strains on the P2 Segment of the Posterior Mitral Leaflet. *Annals of Thoracic Surgery.* Nov 2009;88(5):1499-1505.

8. Ton-Nu TT, Levine RA, Handschumacher MD, et al. Geometric determinants of functional tricuspid regurgitation - Insights from 3-dimensional echocardiography. *Circulation.* Jul 2006;114(2):143-149.

9. Fukuda S, Saracino G, Matsumura Y, et al. Three-dimensional geometry of the tricuspid annulus in healthy subjects and in patients with functional tricuspid

regurgitation - A real-time, 3-dimensional echocardiographic study. *Circulation.* Jul 2006;114:I492-I498.

10. Ton-Nu TT, Levine RA, Handschumacher MD, et al. Geometric determinants of functional tricuspid regurgitation: insights from 3-dimensional echocardiography. *Circulation.* Jul 11 2006;114(2):143-149.

11. Dreyfus GD, Corbi PJ, Chan J, Bahrami T. Secondary tricuspid regurgitation or dilatation: Which should be the criteria for surgical repair? *Annals of Thoracic Surgery.* Jan 2005;79(1):127-132.

12. Marui A, Mochizuki T, Mitsui N, Koyama T, Horibe M. Isolated tricuspid regurgitation caused by a dilated tricuspid annulus. *Ann Thorac Surg.* Aug 1998;66(2):560-562.

13. Park YH, Song JM, Lee EY, Kim YJ, Kang DH, Song JK. Geometric and hemodynamic determinants of functional tricuspid regurgitation: A real-time three-dimensional echocardiography study. *International Journal of Cardiology.* Feb 2008;124(2):160-165.

14. Seo HS, Ha JW, Moon JY, et al. Right ventricular remodeling and dysfunction with subsequent annular dilatation and tethering as a mechanism of isolated tricuspid regurgitation. *Circulation Journal.* Oct 2008;72(10):1645-1649.

15. Spinner EM, Shannon P, Buice D, et al. In Vitro Characterization of the Mechanisms Responsible for Functional Tricuspid Regurgitation. *Circulation.* Accepted for Publication 2011.

16. Park YH, Song JM, Lee EY, Kim YJ, Kang DH, Song JK. Geometric and hemodynamic determinants of functional tricuspid regurgitation: a real-time

three-dimensional echocardiography study. *Int J Cardiol.* Feb 29 2008;124(2):160-165.

17. Silver MD, Lam JH, Ranganathan N, Wigle ED. Morphology of the human tricuspid valve. *Circulation.* Mar 1971;43(3):333-348.

18. Skwarek M, Hreczecha J, Dudziak M, Grzybiak M. The morphology of the right atrioventricular valve in the adult human heart. *Folia Morphol (Warsz).* Aug 2006;65(3):200-208.

19. Spinner EM, Troxler LG, Yoganathan AP. An In Vitro Investigation of the Effects of Disease on Tricuspid Valve Mechanics: Leaflet Mobility and Chordal Forces. *Journal of the American College of Cardiology.* In Review, 2011.

20. Toxler LG, Spinner EM, Yoganathan AP. Measurement of Strut Chordal Forces of the Tricuspid Valve using Miniature C Rings. *Journal of Biomechanics.* In Review, 2011.

21. Tei C, Pilgrim JP, Shah PM, Ormiston JA, Wong M. The tricuspid valve annulus: study of size and motion in normal subjects and in patients with tricuspid regurgitation. *Circulation.* Sep 1982;66(3):665-671.

22. He Z, Ritchie J, Grashow JS, Sacks MS, Yoganathan AP. In vitro dynamic strain behavior of the mitral valve posterior leaflet. *J Biomech Eng.* Jun 2005;127(3):504-511.

23. Yap CH, Kim HS, Balachandran K, Weiler M, Haj-Ali R, Yoganathan AP. Dynamic deformation characteristics of porcine aortic valve leaflet under normal and hypertensive conditions. *Am J Physiol Heart Circ Physiol.* Feb 2010;298(2):H395-405.

24. Smith DB, Sacks MS, Vorp DA, Thornton M. Surface geometric analysis of anatomic structures using biquintic finite element interpolation. *Ann Biomed Eng.* Jun 2000;28(6):598-611.

25. He ZM, Sacks MS, Baijens L, Wanant S, Shah P, Yoganathan AP. Effects of papillary muscle position on in-vitro dynamic strain on the porcine mitral valve. *Journal of Heart Valve Disease.* Jul 2003;12(4):488-494.

26. Grashow JS, Yoganathan AP, Sacks MS. Biaixal stress-stretch behavior of the mitral valve anterior leaflet at physiologic strain rates. *Annals of biomedical engineering.* Feb 2006;34(2):315-325.

27. Padala M, Sacks MS, Liou SW, Balachandran K, He ZM, Yoganathan AP. Mechanics of the Mitral Valve Strut Chordae Insertion Region. *J Biomech Eng-T Asme.* Aug 2010;132(8):-.

28. Chen L, Yin FCP, May-Newman K. The structure and mechanical properties of the mitral valve leaflet-strut chordae transition zone. *J Biomech Eng-T Asme.* Apr 2004;126(2):244-251.

29. Stevanella M, Votta E, Lemma M, Antona C, Redaelli A. Finite element modelling of the tricuspid valve: A preliminary study. *Med Eng Phys.* Dec 2010;32(10):1213-1223.

30. Kaplan SR, Bashein G, Sheehan FH, et al. Three-dimensional echocardiographic assessment of annular shape changes in the normal and regurgitant mitral valve. *American Heart Journal.* Mar 2000;139(3):378-387.

31. Levine RA, Triulzi MO, Harrigan P, Weyman AE. The Relationship of Mitral Annular Shape to the Diagnosis of Mitral-Valve Prolapse. *Circulation.* Apr 1987;75(4):756-767.

APPENDIX K

IN VIVO RAW DATA

The raw data for all *in vivo*, for both MRI and echocardiograph studies is included in this section. The echocardiograph data is divided into patient characteristic and measurements.

MRI Data

Table K.1: MRI measurements for normal subjects to determine PM position. Abbreviations: Papillary Muscle (PM).

Aorta Diameter (mm)		Image #	Coordinate		Distance (mm)			
			x	y	x	y	z	3D
BSCI_1 (Normal)								
33.1 (slice 33)	Annulus Reference Plane	28					0	
	Anterior PM	17	166	182	182	12	9	183
	Posterior PM	8	204	242	10	-20	9	24
	Septal PM	13	300	188	-40	8	1	41
	PM Centroid	13	223	204	0	0	0	
BSCI_2 (Normal)								
30.1 (slice 47)	Annulus Reference Plane	49					0	
	Anterior PM	35	198	260	11	-13	6	18
	Posterior PM	29	239	258	-18	-12	6	22
	Septal PM	32	203	205	7	25	0	26
	PM Centroid	32	213	241	0	0	0	
BSCI_3 (Normal)								
29.5 (slice 45)	Annulus Reference Plane	44					0	
	Anterior PM	29	88	43	13	8	1	16
	Posterior PM	24	81	78	18	-16	9	26
	Septal PM	33	152	44	-32	8	9	34
	PM Centroid	29	107	55	0	0	0	
BSCI_4 (Normal)								
31.5 (slice 37)	Annulus Reference Plane	37					0	
	Anterior PM	19	179	254	19	-3	5	20
	Posterior PM	23	200	283	5	-23	3	24
	Septal PM	22	241	214	-24	26	1	35
	PM Centroid	21	207	250	0	0	0	
BSCI_5 (Normal)								
29 (slice 37)	Annulus Reference Plane	41					0	
	Anterior PM	56	211	321	6	-23	23	33
	Posterior PM	68	253	300	-16	-12	41	45
	Septal PM	57	205	211	9	35	24	43
	PM Centroid	60	223	277	0	0	0	
BSCI_6 (Normal)								
37.8 (slice 41)	Annulus Reference Plane	45					0	
	Anterior PM	66	205	230	15	-13	32	37
	Posterior PM	68	252	235	-18	-16	35	42
	Septal PM	67	222	169	3	29	33	44
	PM Centroid	67	226	211	0	0	0	

Table K.2: MRI measurements for diseased subjects to determine PM position. Abbreviations: Papillary Muscle (PM).

Aorta Diameter (mm)		Image #	Coordinate		Distance (mm)			
			x	y	x	y	z	3D
BSCI_7 (Abnormal)								
29.4 (slice 40)	Annulus Reference Plane	42					0	
	Anterior PM	58	92	174	10	-13	28	33
	Posterior PM	62	127	173	-14	-12	35	40
	Septal PM	54	102	118	3	25	21	33
	PM Centroid	58	107	155	0	0	0	
BSCI_8 (Abnormal)								
36.6 (slice 46)	Annulus Reference Plane	44					0	
	Anterior PM	62	81	205	17	-9	27	33
	Posterior PM	62	133	227	-19	-24	27	40
	Septal PM	70	103	145	2	32	39	51
	PM Centroid	65	106	192	0	0	0	
BSCI_9 (Abnormal)								
28.9 (slice 46)	Annulus Reference Plane	48					0	
	Anterior PM	64	276	350	10	-8	24	8
	Posterior PM	61	300	367	-5	-18	20	12
	Septal PM (fused)	63	302	296	-6	26	23	17
	PM Centroid	63	293	338	0	0	0	
BSCI_10 (Abnormal)								
30.3 (slice 50)	Annulus Reference Plane	50					0	
	Anterior PM	31	209	304	13	-5	29	32
	Posterior PM	32	253	313	-17	-12	27	34
	Septal PM	34	221	271	5	17	24	30
	PM Centroid	32	228	296	0	0	0	
BSCI_11 (Abnormal)								
41.6 (slice 57)	Annulus Reference Plane	57					0	
	Anterior PM	36	206	284	13	-13	32	36
	Posterior PM (fused)	35	249	285	-17	-14	33	40
	Septal PM	37	218	224	4	28	30	41
	PM Centroid	36	224	264	0	0	0	
BSCI_12 (Abnormal)								
32 (slice 52)	Annulus Reference Plane	56					0	
	Anterior PM	71	195	259	18	-15	23	32
	Posterior PM	74	251	263	-21	-18	27	39
	Septal PM	71	216	187	3	34	23	41
	PM Centroid	72	221	236	0	0	0	
BSCI_13 (Abnormal)								
38 (slice 48)	Annulus Reference Plane	52					0	
	Anterior PM	63	172	260	15	-9	17	24
	Posterior PM	68	215	286	-15	-27	24	39
	Septal PM	70	194	195	0	36	27	45
	PM Centroid	67	194	247	0	0	0	

Echo Patient Data

Table K.3: Echocardiograph data for all patients. Abbreviations: Body Surface Area (BSA), Pulmonary Arterial Pressure (PA Press.), Mitral Regurgitation (MR), Tricuspid Regurgitation (TR), Right Ventricle (RV), Left Ventricle (LV).

Patient	Gender	Age	BSA (m^2)	PA Press. (mmHg)	MR Grade	TR Grade	Group	RV area (cm^2)	LV area (cm^2)
1	M	42	1.80	24.4	1	1	1	10	26
3	M	83	1.58	61.0	3	3	4	29	32
4	F	46	1.74	24.4	1	2	1	9	19
6	M	56	1.6	56.2	1	4	2	43	5
8	M	43	2.17	21.0	2	1	1	28	40
9	F	53	1.86	75.2	2	3	2	38	17
10	F	52	2.02	97.4	1	4	2	46	10
15	M	57	2.02	61.2	4	3	4	41	47
16	M		1.92	26.2	1	1	1	5	8
17	M		2.15			1	1	4	25
18	M	58	2.15	33.4	2	1	1	23	24
19	M	91	1.64	47.5	3	1	1	12	42
20	M	34	2.06	26.2	1	1	1	18	22
21	F	85	1.77	86.4	2	3	1	15	9
22	F	90	1.56	66.9	3	2	3	11	43
23	F	60	1.86	30.0	4	2	3	16	33
24	M		2.06	23.0	1	1	1	6.5	15
25	M	50	2.02	53.6	3	4	4	39	48
26	M	27	1.84	28.0	1	1	1	32	38
27	M		2.12	22.0	1	1	1	13	15
28	M	42	2.24	19.4	1	1	1	31	34
29	M		1.75		1	1	1	22	31
30	M		1.87	32.1	1	1	1		
31	M		1.91	32.9	1	2	1	2	7
32	M	28	2.04	41.0	1	3	2	47	29
33	M	49	2.08	22.6	2	1	3	8	44
34	F	63	1.47	76.0	2	3	2	26	11
35	F	57	1.71	85.6	3	4	4	37	51
36	F	60	1.87	41.4	3	4	4	36	41
37	M	35	2.11	49.6	1	1	2	34	27
38	F	36	1.61	43.6	4	4	3	24	45
39	F	66	1.67	59.0	3	4	3	14	36
40	M	21	2.36	32.0	2	3	2	45	50
41	F	25	1.15	32.0	1	1	1	25	15
42	F	33	1.55	112.2	1	4	2	51	12
43	F	45	1.69	108.4	1	3	2	21	37

Patient	Gender	Age	BSA (m^2)	PA Press. (mmHg)	MR Grade	TR Grade	Group	RV area (cm^2)	LV area (cm^2)
44	M	41	2.10	59.0	1	4	2	48	23
45	M	60	1.83	80.6	1	4	2	40	30
46	F	20	1.68	37.0	2	3	4	35	35
47	M	69	1.87	74.8	1	4	2	49	3.5
48	F	47	1.96	23.0	1	1	2	44	18
49	M	37	1.96	37.0	3	1	3	20	49
50	F	32	1.67	33.0	1	3	1	6.5	28
51	F	20	1.85	46.4	1	2	1	17	39
52	F	47	1.52	44.2	2	2	3	19	46
53	F	45	1.99	94.0	1	4	1	27	21
54	M	26	2.23	46.0	2	3	4	22	54.3
55	F	51	1.80	108.4	1	3	2	28.2	32.7
56	F	57	1.90	84.0	2	3	2	35.6	33.9
57	M	78	2.19	50.0	2	3	4	38.2	36.6
58	M	46	2.05	35.0	1	1	2	26	30.8
59	M	52	1.72	46.0	1	4	4	17.8	52.7
60	F	58	1.87	59.8	2	3	2	23.1	33.1
61	M	60	2.04	58.6	3	2	3	20.2	51.4
62	M	84	1.74	61.6	2	3	4	15.6	33
63	F	34	2.08	36.4	3	2	3	14	57.7
64	M	63	1.87	21.0		2	3	14	35.1
65	M	45	1.99	25.2	2	1	4	22.3	42.4
66	F	50	2.06	71.8	3	4	3	16.5	58.5
67	M	43	1.92	58.6	4	3	3	17.3	44.6
68	M	76	1.69	61.8	3	2	4	24.1	43.3
69	F	77	1.63	49.9	1	2	1	18.2	29.5
70	M	63	1.84	31.2	2	2	3	13.3	55.9
71	F	33	2.05	47.0	2	2	4	19	49

Echo Measurements

Table K.4: Echocardiograph measurements for all patients. Abbreviations: Annulus (Ann.) (BSA), Anterior Papillary Muscle (APM), Septal Papillary Muscle (SPM), Posterior Papillary Muscle (PPM), 4-Chamber View (4ch), Tenting Area (TA), Tenting Height (TH), Septal/Anterior Coaptation (S/A), Septal/Posterior Coaptation (S/P), Anterior/Posterior Coaptation (A/P).

Patient	Ann.	APM			SPM			PPM			4ch		S/A		S/P		A/P	
		x	y	z	x	y	z	x	y	z	TA	TH	TA	TH	TA	TH	TA	TH
1	3.2	-0.3	-1.1	0.9	0.7	0.0	0.7	0.0	-0.4	0.6	1.9							
3	5.9	-0.2	-1.3	2.0	0.9	0.3	1.1	0.5	-0.9	1.3								
4	4.1	0.1	-0.7	0.9	0.2	0.3	0.6	0.1	-0.7	0.9	0.5	0.4	0.6	0.4	0.5	0.3	0.8	0.4
6	10.1	-1.8	-1.0	2.3	1.3	0.4	0.9	1.1	-1.6	0.9	3.3	1.2	3.4	1.2	3.6	1.5	2.9	1.2
8	7.8	-0.4	-0.5	1.7	0.6	0.6	0.7	0.1	-0.3	1.0	2.3	0.7	2.3	0.7	2	0.5	2.2	0.9
9	3.8	-0.5	-0.4	1.8	1.0	0.4	1.5	0.5	0.0	1.0	1.4	0.7	1.5	0.8	1.1	0.6	0.6	2.0
10	6.3	-0.6	-0.2	1.6	0.0	0.7	1.6	0.6	-0.7	1.3	2.4	1.3	1.6	0.8	2.0	1.0	1.6	1.0
15	5.3	-1.1	-0.9	1.7	0.7	0.3	0.9	0.7	-1.2	0.6	2.2	1.3	2.3	1.3	1.6	0.9	2.2	1.3
16	3.3	-0.2	-0.4	1.2	0.4	0.3	0.7	0.3	-1.1	1.0	0.7	0.5	0.5	0.3	0.5	0.4	0.7	0.5
17	3.2	-0.1	-0.3	1.4	0.3	0.7	0.7	0.4	-0.8	0.5	0.6	0.6	0.9	0.6	0.4	0.5	0.9	0.3
18	5.1	-0.1	-0.5	1.6	0.7	0.3	1.1	0.6	-0.9	0.5								
19	5.0	0.0	0.0	1.8	0.4	0.2	0.7	0.7	-0.5	0.9								
20	3.9	-0.4	0.0	1.8	0.6	0.0	0.9	0.6	-0.3	1.0	1.5	0.9	1.2	0.7	0.8	0.6		
21	5.1	-0.5	-0.4	1.4	0.8	0.0	0.4	0.6	-0.8	0.7	1.0	0.4	0.8	0.3	1.0	0.6	0.8	0.4
22	5.4	-0.3	-0.5	2.2	0.6	0.6	1.0	0.6	-0.3	0.8	1.1	0.5	0.7	0.4	1.0	0.3	0.8	0.5
23	4.8	-0.3	-0.5	1.5	0.8	0.3	0.4	0.9	-0.6	0.5								
24	3.4	-0.4	-0.6	1.5	0.5	0.0	0.4	0.7	-0.2	0.3	1.2	0.5	1.0	0.7	0.6	0.4	1.0	0.6
25	5.7	-0.4	0.0	1.7	0.9	0.2	0.7	0.9	-0.9	0.9	5	1.2	4.8	1.2	4.6	1.1	3.1	1.2
26	4.3	-0.2	-0.4	1.6	0.9	0.0	1.0	0.5	-0.9	0.8	0.9	0.5	0.6	0.3	1.1	0.5	0.8	0.6
27	3.3	0.0	-0.5	1.4	0.6	0.2	0.7	0.6	-0.6	0.6	1.3	0.6	0.8	0.5	1.2	0.7	0.9	0.6
28	3.7	-0.3	-0.5	1.5				0.4	-0.8	0.7	1.2	0.5	0.8	0.4	0.6	0.5	0.9	0.5
29	3.7	0.0	-0.6	1.4	0.6	0.0	0.5				1.2	0.5	1.3	0.5			0.5	0.6
30	4.8	-0.4	-0.7	2.0	0.2	1.1	0.9	0.8	-0.5	0.8								
31	3.9	-0.7	-0.2	1.4	0.7	0.0	0.5	0.4	-0.7	0.6	1.3	0.7	1.0	0.5	0.6	0.4		
32	4.0	-0.8	-0.7	1.7	0.7	0.2	0.9	0.6	-0.7	1.2	2.9	1.1	2.6	1.1	1.1	0.9	1.5	1.2
33	4.0	-0.6	-1.1	1.2	0.4	-0.3	0.7	0.3	-1.3	1.1	1.0	0.6	0.7	0.5	1.1	0.6	1.1	0.5
34	5.9	-0.5	0.0	2.2	0.9	0.2	0.7	0.6	-0.5	1.6	2.6	1.0	2.7	1.1	1.6	0.7	2.2	1.0
35	6.5	-0.3	-0.6	2.7	0.8	0.0	0.9	0.6	-0.9	1.7	2.7	1.1	1.9	0.9	1.9	1.0	2.2	1.0
36	7.0	-0.8	0.0	2.5	0.6	0.2	1.2				2.4	1.0	2.5	1.0	2.3	1.0	2.4	1.2
37	3.9	-0.3	-0.3	2.0	0.9	0.2	0.9				2.4	1.1	2.1	0.9	2.0	0.7	1.4	0.8
38	7.0	-0.5	0.0	2.7	0.4	0.1	1.1	0.6	-1.3	1.0	3.1	1.2	2.6	1.2	3.1	1.2	2.6	1.0
39	5.7	0.0	-0.5	1.3	0.5	0.0	0.9	0.6	-0.7	0.8	1.2	0.6						
40	5.4	-1.0	-0.6	1.1	0.6	0.2	0.6	0.6	-0.5	1.1	2.1	1.1	2.0	0.6	1.5	1.0	0.6	0.6

Patient	Ann.	APM			SPM			PPM			4ch		S/A		S/P		A/P	
		x	y	z	x	y	z	x	y	z	TA	TH	TA	TH	TA	TH	TA	TH
41	5.5	-1.2	-0.5	1.8				0.7	-0.3	1.4	0.9	0.5	1.0	0.5	0.6	0.5	0.9	0.5
42	15.1	0.3	-1.0	4.2	2.3	-0.1	1.0	2.6	-0.8	2.3	4.5	1.1	3.3	1.0	2.7	1.2	2.9	1.3
43	6.4	-0.9	-0.5	1.7	0.8	0.0	1.1	0.8	0.2	1.4	2.4	1.4	2.8	1.4	1.8	0.8	1.4	0.8
44	6.8	-1.0	-0.3	1.0	1.5	0.5	1.7	1.0	0.0	1.3	3.6	1.3	3.3	1.4	4.3	1.5	2.0	1.0
45	6.2	-0.7	-0.4	1.2				0.6	-0.2	1.2	2.0	0.9	2.2	1.0	1.1	0.6	2.2	0.9
46	6.3	-1.3	-0.5	1.6				0.2	-0.2	1.0	1.5	0.9	1.7	0.8	1.5	0.9	2.2	0.8
47	6.9	-0.7	0.0	2.9	1.2	0.5	1.2	1.1	-0.2	1.9	2.7	0.9	2.8	0.9	2.8	1.1	2.2	1.1
48	4.4	-0.5	-0.3	2.4	0.7	-0.2	1.2	0.9	-0.3	1.0	2.9	1.3	2.6	1.1	2.0	0.9	1.4	1.0
49	7.3	0.3	0.2	2.2	0.2	0.7	0.7	0.6	-0.4	0.7	2.7	1.0	2.3	0.8	1.5	0.9	1.2	0.8
50	6.0	-0.3	0.0	1.7	0.8	0.4	0.8	0.7	0.0	0.7	0.9	0.7	0.8	0.6	1.8	0.6	1.3	0.7
51	5.4	-0.6	-0.2	1.8				0.4	-0.5	0.9	0.8	0.5	0.8	0.5	1.1	0.6	0.9	0.5
52	8.6	-1.9	0.8	2.7	0.9	0.9	1.2				3.5	1.3	2.6	1.0	1.9	1.0	3.5	1.3
53	6.6	0.8	-0.4	1.1	0.7	0.2	0.9	0.6	-0.5	1.4								
54	4.3	-0.4	0.0	2.2	0.6	0.1	0.9	0.7	0.0	0.4	1.9	0.9	2.0	0.9	1.7	0.8	1.7	0.6
55	7.0	-0.8	0.8	1.8	1.0	0.1	1.3	0.8	-0.8	1.2	3.0	1.6	2.5	1.1	2.0	1.4	2.9	1.0
56	4.8	0.0	0.0	2.1	0.8	0.4	1.1	1.3	-0.3	1.2	2.8	0.4	2.8	1.3	3.6	1.2	1.9	0.8
57	7.1	-0.3	-0.5	1.9	0.8	0.2	1.1	0.8	-0.1	0.9	4.1	1.0	2.6	1.0	4.3	1.5	2.9	1.4
58	4.1	0.0	-0.5	1.7	0.8	0.2	0.8	0.6	0.0	0.7	1.8	1.1	1.4	0.7	1.6	1.0	0.9	0.5
59	7.6				0.6	-0.2	1.6	0.9	-0.4	1.3	4.0	1.7	3.9	1.5	4.5	1.8	1.9	0.9
60	2.6	0.6	0.4	1.2	0.9	0.4	0.9	0.4	-0.4	1.0	1.3	0.8	1.0	0.6	0.9	0.7	0.6	0.7
61	2.7	0.0	0.0	2.0	0.4	0.0	0.8	0.3	-0.3	0.8	1.3	0.6	1.2	0.6	0.8	0.6	1.1	0.9
62	7.1	0.0	0.0	1.7	0.9	0.5	0.9				1.8	0.6	2.1	0.8	1.6	0.6	2.2	0.8
63	4.1	0.0	0.0	2.4	0.3	0.1	0.5	0.5	0.7	0.7	1.8	0.7	1.8	0.7	0.8	0.7	0.7	0.4
64	4.1	0.5	-0.4	1.1	0.4	0.3	0.9	0.6	-0.5	0.9	1.9	0.6	0.7	0.5	1.3	0.6	1.3	0.5
65	6.1	-0.6	0.0	1.7				0.5	-0.8	0.8	2.5	1.0	1.8	0.8	1.8	0.9	1.5	0.8
66	5.3	0.5	-0.5	2.0	0.4	0.3	0.6	0.6	-0.2	0.7	2.6	1.2						
67	9.6	0.3	0.3	2.2	1.0	0.6	0.7	0.9	-0.2	1.1	3.2	1.1	3.1	1.1	2.4	1.3	3.1	1.0
68	6.5	-0.6	0.8	2.0	0.6	0.0	0.9	0.8	-0.7	1.3	1.3	0.7	1.2	0.6	1.5	0.8	0.5	0.4
69	4.6	1.2	0.1	1.0	0.6	0.0	1.2	0.8	-0.2	1.0	1.2	0.6	1.4	0.6	0.9	0.5		
70	5.6	0.3	-0.5	2.7	0.9	0.6	1.1	0.7	-0.4	1.1	1.2	0.8	1.5	0.7	1.4	0.4	1.4	0.7
71	5.1	0.4	-0.1	2.2	0.4	0.3	0.7	0.6	-1.4	0.5	2.9	1.1	1.8	0.9	3.2	1.4		

APPENDIX L

IN VITRO RAW DATA

The raw data for all *in vitro* studies is included in this section including: hemodynamics, residual leaflet length, echocardiograph and force measurements. Within each section the data is divided into isolated annular dilatation, isolated PM displacement and combined annular dilatation and PM displacement.

Hemodynamics: Isolated Annular Dilatation

Table L.1: Hemodynamics results for all experiments for isolated annular dilatation for 0%, 20%, 40%, 60%, 80%, 100%. Abbreviations: Stroke Volume (SV), Tricuspid Regurgitation (TR).

Date	Percent Dilatation											
	0		20		40		60		80		100	
	SV	TR	SV	TR	SV	TR	SV	TR	SV	TR	SV	TR
31909	73.7	9.9	72.8	12.7	73.2	15.1	73.7	19.1	70.4	20.3	71.3	25.4
32109	71.3	7.4	71.7	11.4	71.0	20.0	72.2	23.0	74.6	31.0	71.1	34.0
32509	72.5	17.2	74.1	18.6	73.3	24.7	71.6	26.8	72.5	31.4	73.5	34.7
33009	69.3	19.4	69.3	25.3	75.4	31.7	73.4	33.5	72.5	39.7	68.5	43.2
40109	75.3	19.0	72.1	22.1	67.3	28.1	73.7	32.1	72.8	40.7	69.6	45.1
40209	74.9	17.9	72.1	20.7	70.8	25.4	73.4	30.1	71.7	34.6	75.1	42.3
40609	69.2	12.0	72.6	15.5	75.4	18.8	76.1	20.6	75.2	24.3	71.5	30.1
40909	72.1	14.9	73.4	15.9	66.0	17.2	70.3	18.9	74.4	22.5	74.2	23.6

Hemodynamics: Isolated PM Displacement

Table L.2: Hemodynamics results for all experiments for isolated anterior papillary muscle (APM) displacement. Abbreviations: Stroke Volume (SV), Control Volume (CV), Negative Volume (NV), Tricuspid Regurgitation (TR).

Date	Control			APM (Lateral)			APM (Apical)			APM (Apical+Lateral)		
	SV	CV	TR	SV	NV	TR	SV	NV	TR	SV	NV	TR
92309	71.2	7.1	0.0	68.4	7.7	0.6	74.1	15.7	8.6	69.6	12.3	5.2
93009	74.4	5.2	0.0	71.1	5.2	0.0	72.9	6.5	1.3	70.2	5.5	0.3
100709	67.1	9.5	0.0	69.7	10.6	1.1	71.2	11.9	2.4	72.2	11.0	1.5
102109	70.4	13.5	0.0	71.3	15.8	2.3	70.3	15.9	2.4	69.1	19.5	6.0
110409	67.1	17.9	0.0	70.8	23.9	6.0	71.9	31.0	13.1	68.9	30.4	12.5
111009	70.5	16.8	0.0	69.9	17.4	0.6	71.6	17.7	0.9	70.3	18.8	2.0
111109	71.7	15.4	0.0	70.6	18.6	3.2	75.9	20.6	5.2	70.0	23.6	8.2
111309	69.5	18.6	0.0	71.2	18.9	0.3	70.6	17.7	-0.9	71.2	20	1.4

Table L.3: Hemodynamics results for all experiments for isolated septal and posterior papillary muscle (SPM/PPM) displacement. Abbreviations: Stroke Volume (SV), Control Volume (CV), Negative Volume (NV), Tricuspid Regurgitation (TR).

Date	Control			SPM (Anterior) PPM (Posterior)			SPM/PPM (Lateral)			SPM/PPM (Apical)			SPM (Anterior+Lateral+Apical) PPM (Posterior+Lateral+Apical)		
	SV	CV	TR	SV	NV	TR	SV	NV	TR	SV	NV	TR	SV	NV	TR
92309	71.2	7.1	0.0	73.1	13.9	6.8	67.2	20.7	13.6	71.4	14.8	7.7	69.9	14.4	7.3
93009	74.4	5.2	0.0	71.6	8.0	2.8	72.1	7.3	2.1	73.6	8.5	3.3	68.6	8.7	3.5
100709	67.1	9.5	0.0	71.3	11.8	2.3	70.9	12.0	2.5	69.9	13.4	3.9	72.3	13.4	3.9
102109	70.4	13.5	0.0	68.9	17.5	4.0	69.9	16.1	2.6	68.7	18.8	5.3	71.2	20.6	7.1
110409	67.1	17.9	0.0	73.2	23.2	5.3	76.2	36.6	18.7	71.2	18.5	0.6	70.5	17.2	-0.7
111009	70.5	16.8	0.0	69.5	18.7	1.9	69.8	19.0	2.2	68.5	21.2	4.4	69.6	21.3	4.5
111109	71.7	15.4	0.0	70.5	18.6	3.2	69.9	17.3	1.9	71.8	18.4	3.0	70.6	18.8	3.4
111309	69.5	18.6	0.0	67.6	23.9	5.3	70.5	26.6	8.0	70.7	21.0	2.4	74.6	25.3	6.7

Table L.4: Hemodynamics results for all experiments for isolated displacement of the anterior (APM), septal (SPM) and posterior (PPM) papillary muscles. Abbreviations: Stroke Volume (SV), Control Volume (CV), Negative Volume (NV), Tricuspid Regurgitation (TR).

Date	Control			APM(Lateral+Apical) SPM (Anterior+Lateral+Apical) PPM (Posterior+Lateral+Apical)		
	SV	CV	TR	SV	NV	TR
92309	71.2	7.1	0.0	70.5	15.8	8.7
93009	74.4	5.2	0.0	72.7	9.1	3.9
100709	67.1	9.5	0.0	73.2	13.7	4.2
102109	70.4	13.5	0.0	71.7	22.4	8.9
110409	67.1	17.9	0.0	69.8	31.3	13.4
111009	70.5	16.8	0.0	70.8	21.3	4.5
111109	71.7	15.4	0.0	67.3	22.1	6.7
111309	69.5	18.6	0.0	74.4	26.7	8.1

Hemodynamics: Combined 40% Dilation and PM displacement

Table L.5: Hemodynamics results for all experiments for combined annular dilatation (40%) and anterior papillary muscle (APM) displacement. Abbreviations: Stroke Volume (SV), Control Volume (CV), Negative Volume (NV), Tricuspid Regurgitation (TR).

Date	Control			APM (Lateral)			APM (Apical)			APM (Apical+Lateral)		
	SV	CV	TR	SV	NV	TR	SV	NV	TR	SV	NV	TR
92309	70.3	12.2	0.0	68.5	12.9	0.7	70.5	22.3	10.1	72.5	22.0	9.8
93009	69.3	8.6	0.0	72.0	9.3	0.7	72.3	10.4	1.8	75.0	11.0	2.4
100709	71.0	14.8	0.0	67.6	14.6	-0.2	70.4	16.2	1.4	68.9	15.6	0.8
102109	71.9	17.2	0.0	68.3	21.8	4.6	70.7	21.4	4.2	70.3	24.2	7.0
110409	69.5	26.6	0.0	61.5	28.8	2.2	69.6	36.5	9.9	70.4	35.2	8.6
111009	67.9	24.4	0.0	73.5	22.4	-2.0	70.2	22.9	-1.5	68.0	23.5	-0.9
111109	67.8	22.9	0.0	67.4	26.1	3.2	72.4	28.5	5.6	67.9	32.2	9.3
111309	70.8	26.1	0.0	77.6	22.3	-3.8	71.8	25.9	-0.2	67.4	28.0	1.9

Table L.6: Hemodynamics results for all experiments for combined annular dilatation (40%) and septal and posterior papillary muscle (SPM/PPM) displacement. Abbreviations: Stroke Volume (SV), Control Volume (CV), Negative Volume (NV), Tricuspid Regurgitation (TR).

Date	Control			SPM (Anterior) PPM (Posterior)			SPM/PPM (Lateral)			SPM/PPM (Apical)			SPM (Anterior+Lateral+Apical) PPM (Posterior+Lateral+Apical)		
	SV	CV	TR	SV	NV	TR	SV	NV	TR	SV	NV	TR	SV	NV	TR
92309	70.3	12.2	0.0	72.5	18.8	6.6	68.8	29.8	17.6	67.1	20.3	8.1	73.2	19.3	7.1
93009	69.3	8.6	0.0	73.4	12.1	3.5	71.9	13.0	4.4	73.0	13.7	5.1	74.9	13.0	4.4
100709	71.0	14.8	0.0	69.0	17.6	2.8	68.5	17.9	3.1	69.0	18.9	4.1	70.9	19.4	4.6
102109	71.9	17.2	0.0	71.1	21.5	4.3	70.4	20.1	2.9	72.9	22.1	4.9	69.5	24.1	6.9
110409	69.5	26.6	0.0	73.2	30.8	4.2	71.6	45.7	19.1	70.6	26.0	-0.6	73.1	27.5	0.9
111009	67.9	24.4	0.0	67.1	26.0	1.6	72.3	25.3	0.9	71.6	30.1	5.7	72.1	30.3	5.9
111109	67.8	22.9	0.0	67.4	24.0	1.1	69.3	23.7	0.8	68.5	27.8	4.9	73.3	28.0	5.1
111309	70.8	26.1	0.0	68.4	35.8	9.7	68.2	35.3	9.2	68.2	28.4	2.3	73.2	34.1	8

Table L.7: Hemodynamics results for all experiments for combined annular dilatation (40%) and displacement of the anterior (APM), septal (SPM) and posterior (PPM) papillary muscles. Abbreviations: Stroke Volume (SV), Control Volume (CV), Negative Volume (NV), Tricuspid Regurgitation (TR).

Date	Control			APM(Lateral+Apical) SPM (Anterior+Lateral+Apical) PPM (Posterior+Lateral+Apical		
	SV	CV	TR	SV	NV	TR
92309	70.3	12.2	0.0	72.6	22.4	10.2
93009	69.3	8.6	0.0	69.8	14.9	6.3
100709	71.0	14.8	0.0	70.6	18.9	4.1
102109	71.9	17.2	0.0	68.2	25.6	8.4
110409	69.5	26.6	0.0	71.4	37.3	10.7
111009	67.9	24.4	0.0	67.5	26.5	2.1
111109	67.8	22.9	0.0	73.5	32.8	9.9
111309	70.8	26.1	0.0	69.5	41.8	15.7

Hemodynamics: Combined 100% dilation and PM displacement

Table L.8: Hemodynamics results for all experiments for combined annular dilatation (100%) and anterior papillary muscle (APM) displacement. Abbreviations: Stroke Volume (SV), Control Volume (CV), Negative Volume (NV), Tricuspid Regurgitation (TR).

Date	Control			APM (Lateral)			APM (Apical)			APM (Apical+Lateral)		
	SV	CV	TR	SV	NV	TR	SV	NV	TR	SV	NV	TR
92309	68.5	17.3	0.0	67.9	17.8	0.5	75.1	22.9	5.6	70.2	25.9	8.6
93009	75.5	13.0	0.0	74.9	13.5	0.5	72.1	15.6	2.6	71.3	15.0	2.0
100709	75.7	19.2	0.0	74.2	19.6	0.4	75.1	19.7	0.5	75.3	19.9	0.7
102109	72.8	21.0	0.0	68.8	25.5	4.5	70.5	24.9	3.9	69.6	29.8	8.8
110409	69.4	30.5	0.0	71.0	32.5	2.0	67.6	38.3	7.8	69.9	38.2	7.7
111009	68.8	30.6	0.0	71.9	28.8	-1.8	69.4	28.5	-2.1	69.3	28.7	-1.9
111109	69.3	29.2	0.0	67.5	31.3	2.1	71.1	34.2	5.0	69.3	39.0	9.8
111309	69.5	32.8	0.0	71.2	18.9	-13.9	77.6	22.3	-10.5	73.3	37.6	4.8

Table L.9: Hemodynamics results for all experiments for combined annular dilatation (100%) and septal and posterior papillary muscle (SPM/PPM) displacement. Abbreviations: Stroke Volume (SV), Control Volume (CV), Negative Volume (NV), Tricuspid Regurgitation (TR).

Date	Control			SPM (Anterior) PPM (Posterior)			SPM/PPM (Lateral)			SPM/PPM (Apical)			SPM (Anterior+Lateral+Apical) PPM (Posterior+Lateral+Apical)		
	SV	CV	TR	SV	NV	TR	SV	NV	TR	SV	NV	TR	SV	NV	TR
92309	68.5	17.3	0.0	72.7	23.3	6.0	68	37.5	20.2	73.3	24.6	7.3	72.3	22.5	5.2
93009	75.5	13.0	0.0	72.6	17.5	4.5	73.0	17.0	4.0	71.1	17.9	4.9	69.9	17.0	4.0
100709	75.7	19.2	0.0	72.2	22.0	2.8	70.2	21.5	2.3	69.4	24.4	5.2	69.7	25.3	6.1
102109	72.8	21.0	0.0	70.4	25.1	4.1	70.1	20.6	-0.4	71.7	25.4	4.4	68.1	28.9	7.9
110409	69.4	30.5	0.0	72.2	22.5	-8.0	68.5	49.4	18.9	71.4	28.9	-1.6	69.3	31.8	1.3
111009	68.8	30.6	0.0	70.8	31.2	0.6	70.0	30.1	-0.5	68.1	36.2	5.6	66.4	38.8	8.2
111109	69.3	29.2	0.0	70.6	31.0	1.8	70.5	30.7	1.5	68.3	34.2	5.0	72.4	32.5	3.3
111309	69.5	32.8	0.0	67.6	43.1	10.3	68.6	36.6	3.8	68.4	32.1	-0.7	68.6	47.3	14.5

Table L.10: Hemodynamics results for all experiments for combined annular dilatation (100%) and displacement of the anterior (APM), septal (SPM) and posterior (PPM) papillary muscles. Abbreviations: Stroke Volume (SV), Control Volume (CV), Negative Volume (NV), Tricuspid Regurgitation (TR).

Date	Control			APM(Lateral+Apical) SPM (Anterior+Lateral+Apical) PPM (Posterior+Lateral+Apical		
	SV	CV	TR	SV	NV	TR
92309	68.5	17.3	0.0	71.6	28.7	11.4
93009	75.5	13.0	0.0	72.8	20.2	7.2
100709	75.7	19.2	0.0	73.6	22.3	3.1
102109	72.8	21.0	0.0	66.5	32.5	11.5
110409	69.4	30.5	0.0	70.3	41.6	11.1
111009	68.8	30.6	0.0	63.2	28.6	-2.0
111109	69.3	29.2	0.0	71.3	38.3	9.1
111309	69.5	32.8	0.0	68.3	48.2	15.4

Residual Leaflet Length: Isolated Annular Dilatation

Table L.11: Residual leaflet length measurements for all experiments for isolated annular dilatation for 0%, 20%, 40%, 60%, 80%, 100%. Abbreviations: Posterior Leaflet (P), Septal Leaflet (S), Anterior Leaflet (A).

Date	Percent Dilatation																	
	0			20			40			60			80			100		
	P	S	A	P	S	A	P	S	A	P	S	A	P	S	A	P	S	A
31909	1.2	0.2	1.8	1.0	0.0	1.0	0.8	0.2	0.8	0.8	0.2	0.6	0.8	0.2	0.4	0.6	0.0	0.4
32109	1.8	1.4	0.6	1.6	1.2	0.4	1.6	0.4	0.4	1.4	0.4	0.4	1.2	0.4	0.0	0.8	0.2	0.0
32509	2.0	0.8	1.6	1.6	0.6	1.4	1.4	0.6	0.8	1.4	0.4	0.0	1.4	0.2	0.0	1.4	0.2	0.0
33009	2.0	0.2	1.2	1.8	0.2	1.2	1.6	0.2	0.6	1.6	0.0	0.2	1.6	0.0	0.2	1.4	0.0	0.0
40109	1.2	0.6	0.8	1.2	0.6	0.2	0.8	0.8	0.2	0.8	0.6	0.2	1.0	0.8	0.2	1.2	0.4	0.0
40209	1.4	0.8	0.8	1.2	0.6	0.8	1.0	0.6	0.6	1.0	0.4	0.6	1.0	0.6	0.6	0.8	0.6	0.6
40609	1.0	0.8	1.0	1.0	0.8	0.8	0.8	0.8	0.6	0.8	0.6	0.4	0.6	0.6	0.4	0.6	0.6	0.4
40909	1.6	1.8	1.0	1.6	1.6	0.8	1.4	1.4	0.2	1.2	1.6	0.2	1.0	1.6	0.2	0.8	1.6	0.0

Residual Leaflet Length: Isolated PM Displacement

Table L.12: Residual leaflet length measurements for all experiments for isolated anterior papillary muscle (APM) displacement. Abbreviations: Posterior Leaflet (P), Septal Leaflet (S), Anterior Leaflet (A).

Date	Control			APM								
				Lateral			Apical			Apical+Lateral		
	P	S	A	P	S	A	P	S	A	P	S	A
92309	1.0	0.6	1.6	1.2	0.6	1.4	0.8	0.6	2.0	1.0	0.2	1.6
93009	1.4	1.2	1.0	1.4	0.8	1.4	1.6	0.6	1.8	1.6	0.6	1.8
102109	0.4	2.0	1.0	0.4	1.4	1.2	0.6	1.2	1.0	0.4	1.4	1.0
110409	0.2	0.6	0.8	0.4	0.6	1.0	0.6	0.8	1.0	0.4	0.8	1.2
111009	0.6	0.8	0.6	0.4	0.8	0.8	0.4	0.8	1.0	0.8	0.6	1.0
111309	1.0	1.4	0.8	1.2	1.0	0.8	1.2	1.2	1.0	1.4	0.8	1.0
120309	1.6	0.8	2.4	1.6	0.6	2.2	1.6	0.8	2.6	1.6	0.8	2.6

Table L.13: Residual leaflet length measurements for all experiments for isolated septal (SPM) and posterior (PPM) papillary muscle displacement. Abbreviations: Posterior Leaflet (P), Septal Leaflet (S), Anterior Leaflet (A).

Date	Control			SPM/PPM											
				Anterior/Posterior			Lateral			Apical			Anterior/Posterior +Lateral+Apical		
	P	S	A	P	S	A	P	S	A	P	S	A	P	S	A
92309	1.0	0.6	1.6	1.4	0.4	2.4	1.0	0.0	2.4	1.0	0.2	1.6	1.6	0.4	2.2
93009	1.4	1.2	1.0	1.8	0.6	1.6	1.8	0.4	1.6	0.2	0.8	1.8	1.6	0.6	2.0
102109	0.4	2.0	1.0	0.6	2.2	1.0	0.6	1.6	1.2	0.6	2.0	0.6	0.8	1.6	0.4
110409	0.2	0.6	0.8	0.2	0.6	0.6	0.6	0.4	1.4	0.2	0.6	0.8	0.4	0.6	0.0
111009	0.6	0.8	0.6	0.6	0.8	0.6	0.6	0.8	0.6	1.0	0.6	0.4	0.6	0.8	0.4
111309	1.0	1.4	0.8	1.6	0.8	1.2	0.4	1.6	1.0	1.0	1.4	1.2	1.6	0.8	0.8
120309	1.6	0.8	2.4	1.6	1.0	2.4	1.6	0.8	2.0	1.6	1.2	2.4	1.4	1.6	2.4

Table L.14: Residual leaflet length measurements for all experiments for isolated anterior (APM), septal (SPM) and posterior (PPM) papillary muscle displacement. Abbreviations: Posterior Leaflet (P), Septal Leaflet (S), Anterior Leaflet (A).

Date	Control			APM (Lateral+Apical) SPM (Anterior +Lateral+Apical) PPM (Posterior+Lateral+Apical)		
	P	S	A	P	S	A
92309	1.0	0.6	1.6	1.6	0.2	2.4
93009	1.4	1.2	1.0	1.6	0.6	2.2
102109	0.4	2.0	1.0	1.2	1.2	0.8
110409	0.2	0.6	0.8	0.4	0.6	1.4
111009	0.6	0.8	0.6	0.6	0.8	0.6
111309	1.0	1.4	0.8	2.0	0.6	0.8
120309	1.6	0.8	2.4	1.6	1.0	2.4

Residual Leaflet Length: Combined 40% Annular Dilatation and PM Displacement

Table L.15: Residual leaflet length measurements for all experiments for combined 40% dilatation and anterior (APM) papillary muscle displacement. Abbreviations: Posterior Leaflet (P), Septal Leaflet (S), Anterior Leaflet (A).

Date	Control			APM								
				Lateral			Apical			Apical+Lateral		
	P	S	A	P	S	A	P	S	A	P	S	A
92309	0.6	0.6	1.0	0.8	0.4	1.0	0.8	0.2	1.2	0.6	0.2	1.2
93009	1.0	1.0	0.2	1.2	0.6	0.4	1.4	0.6	0.4	1.0	0.6	0.6
102109	0.6	1.8	0.6	0.4	1.2	1.0	0.4	1.2	1.0	0.4	1.4	1.0
110409	0.0	0.6	0.0	0.2	0.6	0.0	0.4	0.6	0.2	0.4	0.6	0.0
111009	0.2	0.8	0.4	0.2	0.8	0.6	0.4	0.6	0.6	0.8	0.4	0.6
111309	1.0	1.0	0.0	1.2	1.0	0.2	1.2	1.0	0.4	1.4	0.8	0.2
120309	1.4	0.8	1.8	1.6	0.6	1.8	1.6	0.6	2.2	1.6	0.4	2.2

Table L.16: Residual leaflet length measurements for all experiments for combined 40% dilatation and septal (SPM) and posterior (PPM) papillary muscle displacement. Abbreviations: Posterior Leaflet (P), Septal Leaflet (S), Anterior Leaflet (A).

Date	Control			SPM/PPM											
				Anterior/Posterior			Lateral			Apical			Anterior/Posterior +Lateral+Apical		
	P	S	A	P	S	A	P	S	A	P	S	A	P	S	A
92309	0.6	0.6	1.0	1.2	0.4	1.6	0.6	0.0	1.2	0.6	0.2	1.4	1.2	0.4	1.8
93009	1.0	1.0	0.2	0.2	0.2	1.0	0.4	0.2	1.0	0.0	0.8	0.8	1.0	0.4	1.6
102109	0.6	1.8	0.6	0.4	1.8	0.8	0.6	1.4	0.8	0.4	1.8	0.6	0.6	1.4	0.2
110409	0.0	0.6	0.0	0.0	0.6	0.0	0.2	0.2	0.6	0.0	0.6	0.0	0.2	0.6	0.0
111009	0.2	0.8	0.4	0.6	0.6	0.4	0.6	0.6	0.4	0.6	0.8	0.4	0.4	1.0	0.4
111309	1.0	1.0	0.0	1.4	0.8	0.4	0.4	1.2	0.2	1.0	1.2	0.8	1.4	0.8	0.2
120309	1.4	0.8	1.8	1.4	0.8	2.2	1.4	0.6	2.0	1.4	1.2	2.0	1.4	1.0	2.0

Table L.17: Residual leaflet length measurements for all experiments for combined 40% dilatation and anterior (APM), septal (SPM) and posterior (PPM) papillary muscle displacement. Abbreviations: Posterior Leaflet (P), Septal Leaflet (S), Anterior Leaflet (A).

Date	Control			APM (Lateral+Apical) SPM (Anterior +Lateral+Apical) PPM (Posterior+Lateral+Apical)		
	P	S	A	P	S	A
92309	0.6	0.6	1.0	1.2	0.2	2.2
93009	1.0	1.0	0.2	1.0	0.4	1.8
102109	0.6	1.8	0.6	0.8	1.0	0.6
110409	0.0	0.6	0.0	0.4	0.4	0.4
111009	0.2	0.8	0.4	0.6	0.6	0.6
111309	1.0	1.0	0.0	1.8	0.6	0.2
120309	1.4	0.8	1.8	1.4	1.0	2.0

Residual Leaflet Length: Combined 100% Annular Dilatation and PM

Displacement

Table L.18: Residual leaflet length measurements for all experiments for combined 100% dilatation and anterior (APM) papillary muscle displacement. Abbreviations: Posterior Leaflet (P), Septal Leaflet (S), Anterior Leaflet (A).

Date	Control			APM								
				Lateral			Apical			Apical+Lateral		
	P	S	A	P	S	A	P	S	A	P	S	A
92309	0.6	0.2	0.8	0.6	0.4	0.8	0.8	0.0	1.0	0.6	0.2	1.0
93009	0.8	0.8	0.0	0.4	0.4	0.0	0.8	0.4	0.2	0.8	0.6	0.2
102109	0.6	1.8	0.6	0.4	1.2	1.0	0.2	1.0	0.8	0.4	1.4	1.0
110409	0.0	0.6	0.0	0.0	0.6	0.0	0.4	0.6	0.2	0.2	0.4	0.0
111009	0.2	0.6	0.2	0.0	0.6	0.6	0.4	0.6	0.6	0.4	0.4	0.6
111309	0.8	1.0	0.0	1.0	0.8	0.2	1.0	0.8	0.2	1.2	0.8	0.2
120309	1.0	0.6	1.2	1.4	0.4	1.8	1.4	0.4	2.0	1.2	0.4	2.0

Table L.19: Residual leaflet length measurements for all experiments for combined 100% dilatation and septal (SPM) and posterior (PPM) papillary muscle displacement. Abbreviations: Posterior Leaflet (P), Septal Leaflet (S), Anterior Leaflet (A).

Date	Control			SPM/PPM											
				Anterior/Posterior			Lateral			Apical			Anterior/Posterior +Lateral+Apical		
	P	S	A	P	S	A	P	S	A	P	S	A	P	S	A
92309	0.6	0.2	0.8	1.0	0.0	1.0	0.6	0.0	1.2	0.6	0.4	1.0	1.2	0.2	1.2
93009	0.8	0.8	0.0	0.0	0.2	0.4	0.2	0.2	1.0	0.0	0.4	0.6	0.8	0.4	1.4
102109	0.6	1.8	0.6	0.2	1.4	0.6	0.6	1.4	0.6	0.4	1.4	0.6	0.6	1.0	0.2
110409	0.0	0.6	0.0	0.0	0.6	0.0	0.0	0.2	0.0	0.0	0.6	0.0	0.0	0.6	0.0
111009	0.2	0.6	0.2	0.2	0.8	0.2	0.6	0.6	0.2	0.2	0.8	0.2	0.2	0.6	0.2
111309	0.8	1.0	0.0	1.2	0.8	0.2	0.2	1.0	0.2	0.6	1.2	0.2	1.4	0.8	0.0
120309	1.0	0.6	1.2	1.2	0.6	1.8	1.4	0.4	1.4	1.2	1.2	1.8	1.4	1.0	1.8

Table L.20: Residual leaflet length measurements for all experiments for combined 1000% dilatation and anterior (APM), septal (SPM) and posterior (PPM) papillary muscle displacement. Abbreviations: Posterior Leaflet (P), Septal Leaflet (S), Anterior Leaflet (A).

Date	Control			APM (Lateral+Apical) SPM (Anterior +Lateral+Apical) PPM (Posterior+Lateral+Apical)		
	P	S	A	P	S	A
92309	0.6	0.2	0.8	1.2	0.0	1.8
93009	0.8	0.8	0.0	1.0	0.4	1.8
102109	0.6	1.8	0.6	0.8	1.0	0.6
110409	0.0	0.6	0.0	0.4	0.4	0.2
111009	0.2	0.6	0.2	0.4	0.6	0.4
111309	0.8	1.0	0.0	1.6	0.6	0.2
120309	1.0	0.6	1.2	1.4	0.8	1.8

Leaflet Mobility: Isolated Annular Dilatation

Table L.21: Echocardiograph leaflet mobility measurements for all experiments for isolated annular dilatation for 0%, 40%, 100%. Abbreviations: Tenting Height (TH), Tenting Area (TA), Septal and Anterior Coaptation (SA), Septal and Posterior Coaptation (SP), Anterior and Posterior Coaptation (AP).

Date	Percent Dilatation																	
	0						40						100					
	TH			TA			TH			TA			TH			TA		
	SA	SP	AP	SA	SP	AP	SA	SP	AP	SA	SP	AP	SA	SP	AP	SA	SP	AP
92309	0.7	0.3	0.6	0.6	0.2	0.5	0.3	0.4	0.5	0.2	0.2	0.5	0.2	0.6	0.8	0.2	0.6	0.7
93009	0.5	0.7	0.8	0.3	0.8	0.6	0.7	0.8	1.0	0.4	0.9	1.0	0.8	0.8	0.8	0.8	1.0	1.1
100709	0.4	0.3	0.4	0.3	0.1	0.2	0.5	0.3	0.3	0.4	0.3	0.2	0.5	0.3	0.3	0.6	0.3	0.4
102109	0.7	1.1	0.5	0.3	0.9	0.3	0.8	1.2	0.6	0.7	0.8	0.5	0.8	1.1	0.6	1.0	0.8	0.5
110409	0.5	0.9	0.4	0.5	0.7	0.2	0.7	0.9	0.6	0.6	0.5	0.5	0.6	0.8	0.6	0.7	0.7	0.4
111009	0.7	0.8	0.3	0.5	0.6	0.3	0.7	0.7	0.4	0.7	0.6	0.2	0.5	0.8	0.5	0.3	0.4	0.3
111109	0.5	0.7	0.8	0.5	0.6	1.0	0.5	0.5	1.0	0.3	0.7	1.1	0.7	0.7	0.8	0.7	0.8	1.0
111309	0.6	1.0	0.6	0.3	0.9	0.5	0.9	1.1	0.6	0.3	1.0	0.3	1.0	1.2	0.7	0.6	1.2	0.5

Leaflet Mobility: Isolated Papillary Muscle Displacement

Table L.22: Echocardiograph leaflet mobility measurements for all experiments for isolated anterior papillary muscle (APM) displacement. Abbreviations: Tenting Height (TH), Tenting Area (TA), Septal and Anterior Coaptation (SA), Septal and Posterior Coaptation (SP), Anterior and Posterior Coaptation (AP).

Date	APM																	
	Lateral						Apical						Lateral+Apical					
	TH			TA			TH			TA			TH			TA		
	SA	SP	AP	SA	SP	AP	SA	SP	AP	SA	SP	AP	SA	SP	AP	SA	SP	AP
92309	0.3	0.4	0.3	0.3	0.3	0.3	0.4	0.4	0.8	0.3	0.3	0.5	0.3	0.3	0.6	0.5	0.4	0.7
93009	0.9	0.8	0.7	0.9	1.0	0.7	0.9	0.7	0.8	0.8	0.6	0.8	0.7	0.5	0.8	0.6	0.5	0.8
100709	0.5	0.3	0.3	0.5	0.2	0.1	0.4	0.3	0.6	0.3	0.3	0.5	0.3	0.3	0.5	0.3	0.3	0.5
102109	1.2	0.9	0.6	0.9	0.7	0.4	1.0	1.1	1.0	1.1	1.0	0.6	1.2	1.2	1.1	1.4	1.0	1.2
110409	0.5	1.0	0.4	0.4	0.8	0.2	0.5	0.6	0.5	0.4	0.5	0.2	0.7	0.5	0.6	0.6	0.6	0.5
111009	0.7	0.8	0.6	0.4	0.6	0.6	0.6	0.8	0.7	0.4	0.7	0.5	0.7	0.7	0.7	0.8	0.8	0.6
111109	0.5	0.6	0.6	0.5	0.5	0.9	0.8	0.4	0.9	0.6	0.3	0.6	1.1	0.4	0.7	0.9	0.3	0.7
111309	0.6	0.9	0.7	0.3	0.7	0.4	0.7	1.0	0.4	0.3	0.7	0.3	0.8	0.9	0.9	0.4	0.7	0.9

Table L.23: Echocardiograph leaflet mobility measurements for all experiments for isolated septal (SPM) and posterior (PPM) papillary muscle displacement. Abbreviations: Tenting Height (TH), Tenting Area (TA), Septal and Anterior Coaptation (SA), Septal and Posterior Coaptation (SP), Anterior and Posterior Coaptation (AP).

Date	SPM/PPM																							
	Anterior/Posterior						Lateral						Apical						Anterior/Posterior +Lateral+Apical					
	TH			TA			TH			TA			TH			TA			TH			TA		
	SA	SP	AP	SA	SP	AP	SA	SP	AP	SA	SP	AP	SA	SP	AP	SA	SP	AP	SA	SP	AP	SA	SP	AP
92309	0.5	0.4	0.5	0.3	0.5	0.5	0.6	0.5	0.9	0.8	0.7	1.0	0.6	0.6	0.3	0.5	0.8	0.3	0.6	0.4	0.3	0.5	0.6	0.4
93009	0.9	0.9	0.7	1.1	1.3	0.7	0.9	0.7	0.6	1.0	0.8	1.0	1.1	0.9	0.3	1.3	0.8	0.4	1.1	0.8	0.2	1	0.6	0.2
100709	0.6	0.4	0.6	0.4	0.3	0.5	0.8	0.6	0.3	0.8	0.6	0.4	0.6	0.8	0.5	0.4	0.8	0.5	1.2	0.8	1.0	0.9	0.9	0.9
102109	0.9	1.0	0.3	0.4	0.7	0.2	0.7	1.1	0.5	0.7	0.7	0.3	0.7	1.7	0.8	0.3	1.6	0.9	1.0	1.3	0.3	0.7	1.1	0.3
110409	0.6	0.6	0.5	0.4	0.5	0.3	0.2	0.6	0.6	0.1	0.4	0.3	0.9	0.9	0.5	0.6	0.7	0.3	0.8	0.9	0.5	0.7	1.1	0.5
111009	0.5	0.8	0.5	0.5	0.5	0.5	0.4	0.6	0.5	0.2	0.5	0.4	0.6	0.6	0.4	0.6	0.5	0.3	0.5	1.2	0.5	0.4	1.0	0.4
111109	0.8	0.5	0.5	0.6	0.3	0.4	0.8	0.7	0.8	0.5	0.4	0.8	0.5	0.8	0.5	0.7	0.4	0.4	0.7	1.0	1.0	0.5	1.2	1.1
111309	1.2	1.3	0.6	0.6	1.2	0.5	0.7	0.9	0.7	0.3	0.7	0.4	0.9	0.8	0.5	0.5	0.5	0.2	0.9	1.1	0.5	0.6	0.7	0.2

Table L.24: Echocardiograph leaflet mobility measurements for all experiments for isolated anterior (APM), septal (SPM) and posterior (PPM) papillary muscle displacement. Abbreviations: Tenting Height (TH), Tenting Area (TA), Septal and Anterior Coaptation (SA), Septal and Posterior Coaptation (SP), Anterior and Posterior Coaptation (AP).

Date	APM (Lateral+Apical) SPM (Anterior +Lateral+Apical) PPM (Posterior+Lateral+Apical)					
	TH			TA		
	S/A	S/P	A/P	S/A	S/P	A/P
92309	0.4	0.5	0.6	0.4	0.5	0.7
93009	1.2	0.7	0.6	1.4	0.9	0.8
100709	0.7	0.7	0.8	1.1	0.7	1.0
102109	1.2	1.1	0.4	0.8	1.0	0.3
110409	1.0	1.0	0.8	1.0	0.9	0.6
111009	1.1	1.1	0.9	1.4	1.4	0.9
111109	1.0	0.9	0.9	0.6	0.9	0.9
111309	0.8	1.1	0.9	0.8	1.1	0.3

Leaflet Mobility: Combined 40% Annular Dilatation and PM Displacement

Table L.25: Echocardiograph leaflet mobility measurements for all experiments for combined 40% dilatation and anterior papillary muscle (APM) displacement. Abbreviations: Tenting Height (TH), Tenting Area (TA), Septal and Anterior Coaptation (SA), Septal and Posterior Coaptation (SP), Anterior and Posterior Coaptation (AP).

Date	APM																	
	Lateral						Apical						Lateral+Apical					
	TH			TA			TH			TA			TH			TA		
	SA	SP	AP	SA	SP	AP	SA	SP	AP	SA	SP	AP	SA	SP	AP	SA	SP	AP
92309	0.3	0.3	0.5	0.3	0.2	0.6	0.5	0.6	1.0	0.6	0.7	1.2	0.4	0.5	0.8	0.4	0.5	0.8
93009	0.7	0.5	0.7	0.7	0.4	0.9	1.1	0.4	1.1	1.3	0.4	1.4	0.9	0.3	1.2	0.9	0.4	1.1
100709	0.4	0.3	0.3	0.4	0.2	0.2	0.5	0.4	0.6	0.5	0.5	0.6	0.4	0.4	0.4	0.3	0.4	0.5
102109	1.2	1.0	0.7	1.2	0.8	0.7	1.2	0.9	1.0	1.6	0.8	0.8	1.4	0.9	0.9	1.2	1.0	1.1
110409	0.4	0.8	0.4	0.4	0.5	0.2	0.3	0.5	0.6	0.3	0.4	0.7	0.2	0.4	0.6	0.1	0.3	0.5
111009	0.7	0.8	0.4	0.5	0.7	0.5	0.6	0.9	0.7	0.4	0.8	0.9	0.6	0.7	0.8	0.7	0.7	0.7
111109	0.7	0.6	0.9	0.7	0.6	1.3	0.8	0.4	0.9	0.5	0.3	0.7	0.5	0.6	0.7	0.3	0.3	0.6
111309	1.1	1.1	0.8	0.7	0.9	0.5	0.8	1.0	0.6	0.3	0.8	0.5	1.0	1.1	0.6	0.8	1.0	0.7

Table L.26: Echocardiograph leaflet mobility measurements for all experiments for combined 40% dilatation and septal (SPM) and posterior (PPM) papillary muscle displacement. Abbreviations: Tenting Height (TH), Tenting Area (TA), Septal and Anterior Coaptation (SA), Septal and Posterior Coaptation (SP), Anterior and Posterior Coaptation (AP).

Date	SPM/PPM																							
	Anterior/Posterior						Lateral						Apical						Anterior/Posterior +Lateral+Apical					
	TH			TA			TH			TA			TH			TA			TH			TA		
	SA	SP	AP	SA	SP	AP	SA	SP	AP	SA	SP	AP	SA	SP	AP	SA	SP	AP	SA	SP	AP	SA	SP	AP
92309	0.5	0.3	0.6	0.5	0.4	0.5	0.5	0.3	0.4	0.6	0.3	0.6	0.6	0.5	0.7	0.6	0.7	0.7	0.8	0.4	0.7	1.2	0.5	0.6
93009	0.9	0.7	0.7	0.6	0.9	0.8	0.7	0.3	0.3	0.6	0.3	0.4	0.6	0.9	0.7	0.4	0.7	0.8	1.1	1.1	0.1	0.8	1.0	0.1
100709	0.7	0.7	0.5	0.6	0.7	0.7	0.6	0.7	0.4	0.7	0.5	0.5	0.7	1.1	0.6	0.7	1.0	0.9	0.9	1.0	0.5	0.9	0.9	0.7
102109	1.3	0.9	0.3	1.1	0.7	0.2	0.6	0.8	0.6	0.6	0.7	0.4	0.9	1.6	0.6	0.7	1.2	0.7	1.2	1.4	0.5	0.8	1.0	0.7
110409	0.9	0.9	0.5	0.8	0.6	0.5	0.2	0.6	0.6	0.2	0.4	0.5	0.9	1.0	0.5	1.0	0.8	0.3	1.0	0.9	0.6	0.8	1.2	0.5
111009	0.6	0.8	0.4	0.3	0.6	0.2	0.5	0.7	0.4	0.4	0.7	0.6	0.9	0.9	0.4	0.7	1.0	0.2	0.9	1.1	0.5	0.7	1.0	0.3
111109	0.5	0.7	0.6	0.4	0.7	0.6	0.7	0.5	0.8	0.5	0.4	0.6	0.7	0.6	0.6	0.5	0.3	0.5	0.9	1.0	1.1	0.7	1.2	1.4
111309	0.7	1.4	0.8	0.5	1.2	0.7	0.8	1.0	0.8	0.4	0.6	0.5	0.8	1.0	0.7	0.4	0.8	0.3	1.0	1.3	0.9	0.6	0.7	0.5

Table L.27: Echocardiograph leaflet mobility measurements for all experiments for combined 40% dilatation and anterior (APM), septal (SPM) and posterior (PPM) papillary muscle displacement. Abbreviations: Tenting Height (TH), Tenting Area (TA), Septal and Anterior Coaptation (SA), Septal and Posterior Coaptation (SP), Anterior and Posterior Coaptation (AP).

Date	APM (Lateral+Apical) SPM (Anterior +Lateral+Apical) PPM (Posterior+Lateral+Apical)					
	TH			TA		
	SA	SP	AP	SA	SP	AP
92309	0.8	0.5	0.6	1.1	0.4	0.6
93009	1.0	0.7	1.1	0.7	0.7	1.1
100709	0.9	0.8	0.6	0.8	1.0	0.7
102109	1.5	1.2	0.9	1.6	1.1	0.9
110409	0.7	0.8	0.8	0.8	1.2	0.9
111009	1.1	0.9	0.9	1.3	0.8	1.1
111109	0.8	0.8	0.9	0.6	0.9	1.0
111309	1.1	1.1	0.8	0.8	0.8	0.5

Leaflet Mobility: Combined 100% Annular Dilatation and PM Displacement

Table L.28: Echocardiograph leaflet mobility measurements for all experiments for combined 100% dilatation and anterior papillary muscle (APM) displacement. Abbreviations: Tenting Height (TH), Tenting Area (TA), Septal and Anterior Coaptation (SA), Septal and Posterior Coaptation (SP), Anterior and Posterior Coaptation (AP).

Date	APM																	
	Lateral						Apical						Lateral+Apical					
	TH			TA			TH			TA			TH			TA		
	SA	SP	AP	SA	SP	AP	SA	SP	AP	SA	SP	AP	SA	SP	AP	SA	SP	AP
92309	0.5	0.3	0.7	0.7	0.5	1.2	0.5	0.4	1.1	0.4	0.5	1.3	0.5	0.5	1.1	0.4	0.4	1.5
93009	0.7	0.9	0.4	0.5	0.8	0.3	1.2	0.4	1.0	1.5	0.2	1.2	0.9	0.5	1.1	1.0	0.4	1.6
100709	0.4	0.3	0.2	0.3	0.1	0.2	0.5	0.4	0.7	0.5	0.4	0.9	0.4	0.6	0.5	0.5	0.8	0.8
102109	0.8	1.1	0.9	0.8	0.9	0.8							1.2	1.2	1.2	2.1	1.1	1.4
110409	0.4	0.7	0.4	0.4	0.6	0.4	0.2	0.6	0.7	0.3	0.4	0.6	0.3	0.6	0.8	0.3	0.5	0.8
111009	0.5	0.8	0.4	0.3	0.8	0.3	0.2	0.7	0.7	0.1	0.7	0.8	0.6	0.6	0.7	0.6	0.6	0.8
111109	0.6	0.7	0.9	0.4	0.5	1.4	0.5	0.9	1.1	0.5	0.4	1.1	1.0	0.7	1.0	1.2	0.9	1.3
111309	1.1	1.3	0.5	0.8	1.0	0.3	1.0	1.1	0.8	0.8	1.0	1.0	0.9	1.1	0.5	0.6	1.2	0.3

Table L.29: Echocardiograph leaflet mobility measurements for all experiments for combined 100% dilatation and septal (SPM) and posterior (PPM) papillary muscle displacement. Abbreviations: Tenting Height (TH), Tenting Area (TA), Septal and Anterior Coaptation (SA), Septal and Posterior Coaptation (SP), Anterior and Posterior Coaptation (AP).

Date	SPM/PPM																							
	Anterior/Posterior						Lateral						Apical						Anterior/Posterior+Lateral+Apical					
	TH			TA			TH			TA			TH			TA			TH			TA		
	SA	SP	AP	SA	SP	AP	SA	SP	AP	SA	SP	AP	SA	SP	AP	SA	SP	AP	SA	SP	AP	SA	SP	AP
92309	0.6	0.5	0.9	0.8	0.7	1.0	0.9	0.2	0.6	0.9	0.1	0.8	0.6	0.5	0.7	0.8	0.5	0.7	0.6	0.4	0.8	0.5	0.6	0.7
93009	0.9	0.7	0.6	1.0	0.8	1.0	0.9	0.4	0.4	0.6	0.4	0.4	1.1	0.9	0.2	1.3	1.0	0.4	1.1	1.2	0.2	0.8	1.4	0.1
100709	0.8	0.6	0.3	0.8	0.6	0.4	0.9	0.6	0.5	0.7	0.5	0.5	0.7	0.8	0.2	0.6	0.8	0.2	0.7	0.6	0.4	0.7	0.5	0.3
102109	1.1	1.2	0.4	1.0	0.8	0.4	0.6	0.9	0.7	0.4	0.4	0.6	1.1	1.4	0.7	1.1	1.3	1.0	1.1	1.2	0.5	0.8	1.1	0.6
110409	0.8	1.0	0.5	0.6	0.9	0.5	0.2	0.6	0.7	0.2	0.5	0.7	0.8	0.8	0.4	1.1	0.7	0.3	1.1	0.7	0.5	1.2	1.1	0.5
111009	0.7	0.9	0.4	0.3	0.6	0.3	0.5	0.6	0.6	0.2	0.5	0.7	1.1	1.2	0.2	0.8	1.1	0.1	1.0	1.1	0.5	0.8	0.8	0.3
111109	0.6	0.9	0.6	0.5	0.8	0.4	0.7	0.8	0.7	0.7	0.7	0.5	0.7	0.6	0.6	0.7	0.3	0.5	0.9	1.1	1.0	0.8	1.4	1.4
111309	0.9	1.4	0.6	0.4	1.3	0.5	0.8	1.1	0.8	0.6	0.8	0.4	0.8	0.6	0.7	0.7	0.4	0.4	1.0	1.0	0.8	0.8	0.6	0.5

Table L.30: Echocardiograph leaflet mobility measurements for all experiments for combined 100% dilatation and anterior (APM), septal (SPM) and posterior (PPM) papillary muscle displacement. Abbreviations: Tenting Height (TH), Tenting Area (TA), Septal and Anterior Coaptation (SA), Septal and Posterior Coaptation (SP), Anterior and Posterior Coaptation (AP).

Date	APM (Lateral+Apical) SPM (Anterior +Lateral+Apical) PPM (Posterior+Lateral+Apical)					
	TH			TA		
	SA	SP	AP	SA	SP	AP
92309	0.8	0.7	0.9	1.0	0.7	1.4
93009	1.0	0.8	1.2	0.9	1.0	1.2
100709	0.7	0.7	0.5	0.7	0.8	0.9
102109	1.2	1.4	0.9	1.3	1.4	0.9
110409	1.0	0.9	1.1	1.6	1.1	1.3
111009	1.1	1.3	0.8	1.0	1.7	1.3
111109	0.9	0.9	1.1	1.1	0.8	1.0
111309	1.4	0.9	0.8	1.0	0.9	0.8

Chordal Forces: Isolated Annular Dilatation

Table L.31: Chordal force measurements for all experiments for isolated annular dilatation for 0% and 100%.

Date	% Dilatation	Anterior			Posterior		
		Marginal	Intermediate	Strut	Marginal	Intermediate	Strut
41510	0			0.118	0.065	0.061	0.334
	100			0.221	0.129	0.083	0.345
42210	0			0.429	0.017		0.749
	100			0.961	0.046		0.961
52510	0	0.007		0.651	0.027	0.068	0
	100	0.037		0.808	0.085	0.172	0
52710	0	0.027	0.087	0	0.025		
	100	0.245	0.373	0	0.539		
60110	0		0.105	0.946		0.036	0.565
	100		0.369	1.315		0.114	0.598
60210	0	0.002	0.009			0.017	1.057
	100	0.018	0.017			0.034	1.071
60310	0		0.011	0.971		0.369	0.389
	100		0.029	1.259		0.618	0.465
60810	0						0.715
	100						0.989
61010	0	0.019	0.037	0.406	0.236	0.008	
	100	0.427	0.148	0.47	0.596	0.032	
61510	0	0.098	0.078		0.049	0.197	0.267
	100	0.344	0.254		0.189	0.33	0.433
61610	0		0.174	0.143		0.023	0.407
	100		0.374	0.276		0.112	0.788
61710	0			0.907	0.016		
	100			1.501	0.024		
62210	0	0.103	0.019		0.008		
	100	0.296	0.021		0.038		
62310	0	0.012					
	100	0.331					
62410	0		0.22		0.146		
	100		0.334		0.24		
70710	0	0.021					
	100	0.527					

Chordal Force: Isolated PM Displacement

Table L.32: Marginal chordal force measurements for all experiments for isolated displacement of the anterior (APM) papillary muscle and all papillary muscles (Anterior, APM, Septal, SPM, Posterior, PPM). Abbreviations: Anterior Leaflet (A), Posterior Leaflet (P).

Date	Control		APM						APM (Apical+Lateral) SPM (Anterior+Apical+Lateral) PPM (Posterior+Apical+Lateral)	
			Apical		Lateral		Apical+Lateral			
	A	P	A	P	A	P	A	P	A	P
41510		0.065		0.071		0.201		0.145		0.126
42210		0.017		0.026		0.039		0.034		0.035
52510	0.007	0.027	0.013	0.03	0.01	0.022	0.024	0.047	0.027	0.05
52710	0.027	0.025	0.018	0.315	0.027	0.496	0.048	0.428	0.049	0.199
60210	0.002		0		0.002		1E-03		0.002	
61010	0.019	0.236	0.004	0.223	0.005	0.15	0.069	0.266	0.008	0.173
61510	0.098	0.049	0.093	0.07	0.099	0.078	0.108	0.059	0.141	0.063
61710		0.016		0.011		0.016		0.035		0.023
622/10	0.103	0.008	0.115	0.009	0.1	0.005	0.041	0.018	0.025	0.008
62310	0.012		0.331		0.115		0.213		0.106	
62410		0.146		0.102		0.072		0.07		0.064
70710	0.021		0.089		0.09		0.034		0.142	

Table L.33: Intermediate chordal force measurements for all experiments for isolated displacement of the anterior (APM) papillary muscle and all papillary muscles (Anterior, APM, Septal, SPM, Posterior, PPM). Abbreviations: Anterior Leaflet (A), Posterior Leaflet (P).

Date	Control		APM						APM (Apical+Lateral) SPM (Anterior+Apical+Lateral) PPM (Posterior+Apical+Lateral)	
			Apical		Lateral		Apical+Lateral			
	A	P	A	P	A	P	A	P	A	P
41510		0.061		0.041		0.104		0.08		0.046
52510		0.068		0.139		0.092		0.148		0.195
52710	0.087		0.134		0.088		0.15		0.191	
60110	0.105	0.036	0.018	0.097	0.022	0.154	0.004	0.116	0.034	0.1
60210	0.009	0.017	0.004	0.014	0.002	0.01	0.002	0.015	0.011	0.049
60310	0.011	0.369	0.006	0.228	0.015	0.107	0.007	0.073	0.005	0.07
61010	0.037	0.008	0.005	0.004	0.029	0.008	0.164	0.01	0.274	0.013
61510	0.078	0.197	0.036	0.324	0.038	0.349	0.08	0.227	0.044	0.194
61610	0.174	0.023	0.187	0.005	0.169	0.006	0.223	0.052	0.448	0.03
622/10	0.103		0.011		0.025		0.005		0.025	
62310	0.193		0.161		0.242		0.058		0.09	
62410	0.22		0.238		0.225		0.24		0.151	

Table L.34: Strut chordal force measurements for all experiments for isolated displacement of the anterior (APM) papillary muscle and all papillary muscles (Anterior, APM, Septal, SPM, Posterior, PPM). Abbreviations: Anterior Leaflet (A), Posterior Leaflet (P).

Date	Control		APM						APM (Apical+Lateral) SPM (Anterior+Apical+Lateral) PPM (Posterior+Apical+Lateral)	
			Apical		Lateral		Apical+Lateral			
	A	P	A	P	A	P	A	P	A	P
41510	0.118	0.334	0.116	0.367	0.025	0.4	0.066	0.37	0.038	0.575
42210	0.429	0.749	0.416	0.874	0.461	0.617	0.509	0.882	0.39	1.12
52510	0.651		0.609		0.625		0.694		0.552	
60110	0.946	0.565	0.772	0.479	0.784	0.193	0.528	0.442	1.044	0.708
60210		1.057		1.127		0.834		1.056		0.889
60310	0.971	0.389	1.206	0.47	0.567	0.363	1.195	0.477	1.432	0.459
60810		0.715		0.827		0.727		0.499		1.224
61010	0.406		0.362		0.44		0.443		0.463	
61510		0.267		0.352		0.379		0.246		0.544
61610	0.143	0.407	0.261	0.929	0.285	0.527	0.185	0.232	0.468	0.72
61710	0.907		0.946		0.897		0.845		2.02	

Chordal Force: Combined 100% Annular Dilatation and PM Displacement

Table L.35: Marginal chordal force measurements for all experiments for combined 100% annular dilatation and displacement of the anterior (APM) papillary muscle and all papillary muscles (Anterior, APM, Septal, SPM, Posterior, PPM). Abbreviations: Anterior Leaflet (A), Posterior Leaflet (P).

Date	Control		APM						APM (Apical+Lateral) SPM (Anterior+Apical+Lateral) PPM (Posterior+Apical+Lateral)	
			Apical		Lateral		Apical+Lateral			
	A	P	A	P	A	P	A	P	A	P
41510		0.129		0.125		0.144		0.191		0.187
42210		0.046		0.042		0.033		0.054		0.04
52510	0.037	0.085	0.019	0.039	0.022	0.045	0.025	0.058	0.025	0.069
52710	0.245	0.539	0.146	0.468	0.243	0.77	0.103	0.603	0.069	0.713
60210	0.018		0.002		0.001		0.002		0.052	
61010	0.427	0.596	0.244	0.526	0.34	0.374	0.562	0.534	0.449	0.59
61510	0.344	0.189	0.327	0.192	0.348	0.204	0.475	0.264	0.329	0.212
61710		0.024		0.021		0.024		0.05		0.035
62210	0.296	0.038	0.211	0.014	0.285	0.014	0.041	0.018	0.06	0.017
62410		0.24		0.225		0.111		0.19		0.107
70710	0.527		0.255		0.262		0.251		0.331	

Table L.36: Intermediate chordal force measurements for all experiments for combined 100% annular dilatation and displacement of the anterior (APM) papillary muscle and all papillary muscles (Anterior, APM, Septal, SPM, Posterior, PPM). Abbreviations: Anterior Leaflet (A), Posterior Leaflet (P).

Date	Control		APM						APM (Apical+Lateral) SPM (Anterior+Apical+Lateral) PPM (Posterior+Apical+Lateral)	
			Apical		Lateral		Apical+Lateral			
	A	P	A	P	A	P	A	P	A	P
41510		0.083		0.065		0.067		0.099		0.087
42210										
52510		0.172		0.194		0.154		0.207		0.33
52710	0.373		0.289		0.395		0.27		0.202	
60110	0.369	0.114	0.159	0.138	0.209	0.184	0.055	0.221	0.118	0.161
60210	0.017	0.034	0.003	0.016	0.01	0.024	0.002	0.02	0.006	0.057
60310	0.029	0.618	0.021	0.379	0.027	0.173	0.021	0.219	0.009	0.152
60810										
61010	0.148	0.032	0.049	0.007	0.069	0.004	0.297	0.014	0.344	0.058
61510	0.254	0.33	0.218	0.458	0.193	0.464	0.392	0.375	0.197	0.4
61610	0.374	0.112	0.359	0.063	0.42	0.057	0.427	0.094	0.691	0.094
61710										
62210	0.021		0.022		0.011		0.005		0.013	
62410	0.334		0.327		0.346		0.359		0.193	

Table L.37: Strut chordal force measurements for all experiments for combined 100% annular dilatation and displacement of the anterior (APM) papillary muscle and all papillary muscles (Anterior, APM, Septal, SPM, Posterior, PPM). Abbreviations: Anterior Leaflet (A), Posterior Leaflet (P).

Date	Control		APM						APM (Apical+Lateral) SPM (Anterior+Apical+Lateral) PPM (Posterior+Apical+Lateral)	
			Apical		Lateral		Apical+Lateral			
	A	P	A	P	A	P	A	P	A	P
41510	0.221	0.345	0.227	0.375	0.014	0.314	0.055	0.394	0.116	0.533
42210	0.961	0.961	0.634	1.146	0.716	0.973	0.829	1.359	0.523	1.394
52510	0.808	0	1.067	0	0.92	0	1.238	0	1.088	0
52710	0		0		0		0		0	
60110	1.315	0.598	1.469	0.7	1.098	0.302	1.183	0.438	1.105	0.665
60210		1.071		1.365		0.857		1.235		0.966
60310	1.259	0.465	1.15	0.466	0.902	0.418	1.187	0.486	1.554	0.549
60810		0.989		1.11		0.826		0.816		1.369
61010	0.47		0.537		0.606		0.44		0.402	
61510		0.433		0.538		0.549		0.373		0.674
61610	0.276	0.788	0.52	1.309	0.489	0.988	0.199	0.314	0.587	1.086
61710	1.501		1.47		1.656		1.463		2.044	

APPENDIX M

LIST OF VIDEOS

Included in this section is the list of videos for the *in vitro* analysis of both residual leaflet length and echo measurements. All video files are available on the dvds.

Video Files

(In Vitro DVD 1) Folder: Residual Leaflet Length:

Folder: Isolated Annular Dilatation:

Folder: 031909 (All conditions are contained within single video)

Folder: 032109 (All conditions are contained within single video)

Folder: 032509 (All conditions are contained within single video)

Folder: 033009 (All conditions are contained within single video)

Folder: 040109 (All conditions are contained within single video)

Folder: 040209 (All conditions are contained within single video)

Folder: 040609 (All conditions are contained within single video)

Folder: 040909 (All conditions are contained within single video)

Folder: PM Displacement (Isolated and Combined)

Folder: 092309 (All conditions are contained within this folder)

Folder: 093009 (All conditions are contained within this folder)

Folder: 102109 (All conditions are contained within this folder)

Folder: 110409 (All conditions are contained within this folder)

Folder: 111009 (All conditions are contained within this folder)

Folder: 111309 (All conditions are contained within this folder)

Folder: 120309 (All conditions are contained within this folder)

Echocardiograph:

Isolated Annular Dilatation, Isolated PM Displacement and Combined Annular Dilatation and PM Displacement:

(In Vitro DVD 2) Folder: 092309 (All conditions contained within this folder)

(In Vitro DVD 3) Folder: 093009 (All conditions contained within this folder)

(In Vitro DVD 4) Folder: 100709 (All conditions contained within this folder)

(In Vitro DVD 5) Folder: 101409 (All conditions contained within this folder)

(In Vitro DVD 6) Folder: 110409 (All conditions contained within this folder)

(In Vitro DVD 7) Folder: 111009 (All conditions contained within this folder)

(In Vitro DVD 8) Folder: 111109 (All conditions contained within this folder)

(In Vitro DVD 9) Folder: 111309 (All conditions contained within this folder)

REFERENCES

1. Bruce CJ, Connolly HM. Right-sided valve disease deserves a little more respect. *Circulation.* 2009;119(20):2726-2734.

2. Rogers JH, Bolling SF. The tricuspid valve: current perspective and evolving management of tricuspid regurgitation. *Circulation.* 2009;119(20):2718-2725.

3. Antunes MJ, Barlow JB. Management of tricuspid valve regurgitation. *Heart.* 2007;93(2):271-276.

4. Bernal JM, Gutierrez-Morlote J, Llorca J, San Jose JM, Morales D, Revuelta JM. Tricuspid valve repair: An old disease, a modern experience. *Annals of Thoracic Surgery.* 2004;78(6):2069-2075.

5. Izumi C, Iga K, Konishi T. Progression of isolated tricuspid regurgitation late after mitral valve surgery for rheumatic mitral valve disease. *Journal of Heart Valve Disease.* 2002;11(3):353-356.

6. Ruel M, Rubens FD, Masters RG, Pipe AL, Bedard P, Hendry PJ, Lam BK, Burwash IG, Goldstein WG, Brais MP, Keon WJ, Mesana TG. Late incidence and predictors of persistent or recurrent heart failure in patients with aortic prosthetic valves. *Journal of Thoracic and Cardiovascular Surgery.* 2004;127(1):149-159.

7. Braunwald NS, Ross J, Jr., Morrow AG. Conservative management of tricuspid regurgitation in patients undergoing mitral valve replacement. *Circulation.* 1967;35(4 Suppl):I63-69.

8. Carpentier A, Deloche A, Hanania G, Forman J, Sellier P, Piwnica A, Dubost C, McGoon DC. Surgical management of acquired tricuspid valve disease. *J Thorac Cardiovasc Surg.* 1974;67(1):53-65.

9. Dreyfus GD, Corbi PJ, Chan J, Bahrami T. Secondary tricuspid regurgitation or dilatation: Which should be the criteria for surgical repair? *Annals of Thoracic Surgery.* 2005;79(1):127-132.

10. Chikwe J, Anyanwu AC. Surgical strategies for functional tricuspid regurgitation. *Semin Thorac Cardiovasc Surg.* 2010;22(1):90-96.

11. McCarthy PM, Bhudia SK, Rajeswaran J, Hoercher KJ, Lytle BW, Cosgrove DM, Blackstone EH. Tricuspid valve repair: Durability and risk factors for failure. *Journal of Thoracic and Cardiovascular Surgery.* 2004;127(3):674-685.

12. Ton-Nu TT, Levine RA, Handschumacher MD, Dorer DJ, Yosefy C, Fan DL, Hua LQ, Jiang L, Hung J. Geometric determinants of functional tricuspid regurgitation - Insights from 3-dimensional echocardiography. *Circulation.* 2006;114(2):143-149.

13. Kim MJ, Song JM, Park YH, Lee EY, Kim YJ, Kang DH, Song JK. Septal-lateral right ventricular dilatation determines the severity of functional tricuspid regurgitation with sinus rhythm: A Real-TimeThree-Dimensional echocardiography study. *Journal of the American College of Cardiology.* 2007;49(9):306A-306A.

14. Bonow RO, Carabello BA, Chatterjee K, de Leon AC, Faxon DP, Freed MD, Gaasch WH, Lytle BW, Nishimura RA, O'Gara PT, O'Rourke RA, Otto CM, Shah PM, Shanewise JS, Nishimura RA, Carabello BA, Faxon DP, Freed MD, Lytle BW, O'Gara PT, Sidney C, Jacobs AK, Buller CE, Creager MA, Ettinger SM, Krumholz HM, Kushner FG, Nishimura RA, Page RL, Tarkington LG, Yancy CW. 2008 focused update incorporated into the ACC/AHA 2006 guidelines for the management of patients with valvular heart disease - A report of the American College of Cardiology American Heart Association task force on practice guidelines (writing committee to revise the 1998 guidelines for the management of patients with valvular heart disease) - Endorsed by the Society of Cardiovascular Anesthesiologists, Society for Cardiovascular Angiography and Interventions, and Society of Thoracic Surgeons. *Journal of the American College of Cardiology.* 2008;52(13):E1-E142.

15. Vahanian A, Baumgartner H, Bax J, Butchart E, Dion R, Filippatos G, Flachskampf F, Hall R, Iung B, Kasprzak J, Nataf P, Tornos P, Torracca L, Wenink A, Valvular TFM. Guidelines on the management of valvular heart disease - The Task Force on the Management of Valvular Heart Disease of the European Society of Cardiology. *European Heart Journal.* 2007;28(2):230-268.

16. Sadeghi HM, Kimura BJ, Raisinghani A, Blanchard DG, Mahmud E, Fedullo PF, Jamieson SW, DeMaria AN. Does lowering pulmonary arterial pressure eliminate severe functional tricuspid regurgitation? *Journal of the American College of Cardiology.* 2004;44(1):126-132.

17. Ubago JL, Figueroa A, Ochoteco A, Colman T, Duran RM, Duran CG. ANALYSIS OF THE AMOUNT OF TRICUSPID-VALVE ANULAR DILATATION REQUIRED TO PRODUCE FUNCTIONAL TRICUSPID REGURGITATION. *American Journal of Cardiology.* 1983;52(1):155-158.

18. Hinderliter AL, Willis PW, Long WA, Clarke WR, Ralph D, Caldwell EJ, Williams W, Ettinger NA, Hill NS, Summer WR, de Boisblanc B, Koch G, Li S, Clayton LM, Jobsis MM, Crow JW. Frequency and severity of tricuspid regurgitation determined by Doppler echocardiography in primary pulmonary hypertension. *American Journal of Cardiology.* 2003;91(8):1033-1037.

19. Behm CZ, Nath J, Foster E. Clinical correlates and mortality of hemodynamically significant tricupsid regurgitation. *Journal of Heart Valve Disease.* 2004;13(5):784-789.

20. Fukuda S, Song JM, Gillinov AM, Daimon M, Kongsaerepong V, Greenberg N, Thomas JD, Shiota T. Tricuspid valve tethering predicts residual regurgitation after tricuspid annuloplasty. *Journal of the American College of Cardiology.* 2005;111:975-979.

21. Seo HS, Ha JW, Moon JY, Choi EY, Rim SJ, Jang Y, Chung N, Shim WH, Cho SY, Kim SS. Right ventricular remodeling and dysfunction with subsequent annular dilatation and tethering as a mechanism of isolated tricuspid regurgitation. *Circulation Journal.* 2008;72(10):1645-1649.

22. Park YH, Song JM, Lee EY, Kim YJ, Kang DH, Song JK. Geometric and hemodynamic determinants of functional tricuspid regurgitation: A real-time three-dimensional echocardiography study. *International Journal of Cardiology.* 2008;124(2):160-165.

23. Kim HK, Kim YJ, Park JS, Kim KH, Kim KB, Ahn H, Sohn DW, Oh BH, Park YB, Choi YS. Determinants of the severity of functional tricuspid regurgitation. *American Journal of Cardiology.* 2006;98(2):236-242.

24. Anyanwu AC, Chikwe J, Adams DH. Tricuspid valve repair for treatment and prevention of secondary tricuspid regurgitation in patients undergoing mitral valve surgery. *Curr Cardiol Rep.* 2008;10(2):110-117.

25. Spinner EM, Sundareswaran K, Dasi LP, Thourani VH, Oshinski J, Yoganathan AP. Altered right ventricular papillary muscle position and orientation in patients with a dilated left ventricle. *J Thorac Cardiovasc Surg.* 2010.

26. Fukuda S, Gillinov AM, McCarthy PM, Song JM, Kihara T, Daimon M, Tran H, Thomas JD, Shiota T. Mechanism of recurrent or residual functional tricuspid regurgitation mid-term after tricuspid annuloplasty. *Circulation.* 2005;112(17):U556-U556.

27. He SQ, Fontaine AA, Schwammenthal E, Yoganathan AP, Levine RA. Integrated mechanism for functional mitral regurgitation - Leaflet restriction versus coapting force: In vitro studies. *Circulation.* 1997;96(6):1826-1834.

28. Come PC, Riley MF. TRICUSPID ANULAR DILATATION AND FAILURE OF TRICUSPID LEAFLET COAPTATION IN TRICUSPID REGURGITATION. *American Journal of Cardiology.* 1985;55(5):599-601.

29. Anwar AM, Soliman OII, Nemes A, van Geuns RJM, Geleijnse ML, ten Cate FJ. Value of assessment of tricuspid annulus: real-time three-dimensional echocardiography and magnetic resonance imaging. *International Journal of Cardiovascular Imaging.* 2007;23(6):701-705.

30. Silver MD, Lam JH, Ranganat.N, Wigle ED. A CLASSIFICATION OF TRICUSPID VALVE CHORDAE TENDINEAE. *Circulation.* 1970;42(4):I199-&.

31. Silver MD, Lam JH, Ranganat.N, Wigle ED. CLASSIFICATION OF TRICUSPID VALVE CHORDAE TENDINEAE. *American Journal of Pathology.* 1971;62(2):A105-&.

32. Silver MD, Lam JHC, Ranganat.N, Wigle ED. MORPHOLOGY OF HUMAN TRICUSPID VALVE. *Circulation.* 1971;43(3):333-&.

33. Fukuda S, Saracino G, Matsumura Y, Daimon M, Tran H, Greenberg NL, Hozumi T, Yoshikawa J, Thomas JD, Shiota T. Three-dimensional geometry of the tricuspid annulus in healthy subjects and in patients with functional tricuspid regurgitation - A real-time, 3-dimensional echocardiographic study. *Circulation.* 2006;114:I492-I498.

34. Kwan J, Kim GC, Jeon MJ, Kim DH, Shiota T, Thomas JD, Park KS, Lee WH. 3D geometry of a normal tricuspid annulus during systole: A comparison study with the mitral annulus using real-time 3D echocardiography. *European Journal of Echocardiography.* 2007;8(5):375-383.

35. Hiro ME, Jouan J, Pagel MR, Lansac E, Lim KH, Lim HS, Duran CMG. Sonometric study of the normal tricuspid valve annulus in sheep. *Journal of Heart Valve Disease.* 2004;13(3):452-460.

36. Jouan J, Pagel MR, Hiro ME, Lim KH, Lansac E, Duran CMG. Further information from a sonometric study of the normal tricuspid valve annulus in sheep: Geometric changes during the cardiac cycle. *Journal of Heart Valve Disease.* 2007;16(5):511-518.

37. Anwar AM, Geleijnse ML, Soliman OII, McGhie JS, Frowijn R, Nemes A, van den Bosch AE, Galema TW, ten Cate FJ. Assessment of normal tricuspid valve anatomy in adults by real-time three-dimensional echocardiography. *International Journal of Cardiovascular Imaging.* 2007;23(6):717-724.

38. Tei C, Pilgrim JP, Shah PM, Ormiston JA, Wong M. THE TRICUSPID-VALVE ANNULUS - STUDY OF SIZE AND MOTION IN NORMAL SUBJECTS AND IN PATIENTS WITH TRICUSPID REGURGITATION. *Circulation.* 1982;66(3):665-671.

39. Shah PM, Raney AA. Tricuspid valve disease. *Current Problems in Cardiology.* 2008;33(2):47-84.

40. Skwarek M HJ, Dudziak M, Grzybiak M. The morphology of the right atrioventricular valve in the adult human heart. *Folia Morphol.* 2006;65(3):200-208.

41. Victor S, Nayak VM. Tricuspid valve is bicuspid. *Annals of Thoracic Surgery.* 2000;69(6):1989-1990.

42. Joudinaud TM, Flecher EM, Duran CMG. Functional terminology for the tricuspid valve. *Journal of Heart Valve Disease.* 2006;15(3):382-388.

43. Crick SJ SM, Ho SY, Gebstein L, Anderson RH. Anatomy of the pig heart: comparisons with normal human cardiac structure. *J. Anat.* 1998;193:105-119.

44. Nath J, Foster E, Heidenreich PA. Impact of tricuspid regurgitation on long-term survival. *Journal of the American College of Cardiology.* 2004;43(3):405-409.

45. Kim MJ, Suh IW, Jeong YH, Park CB, Lee SW, Song JM, Kang DH, Song H, Lee JW, Song MG, Song JK. Factors associated with development of significant tricuspid regurgitation late after successful left-sided valve surgery. *Journal of the American College of Cardiology.* 2006;47(4):277A-277A.

46. Topilsky Y, Khanna AD, Oh JK, Nishimura RA, Enriquez-Sarano M, Jeon YB, Sundt TM, Schaff HV, Park SJ. Preoperative Factors Associated With Adverse Outcome After Tricuspid Valve Replacement. *Circulation.* 2011;123(18):1929-1939.

47. Bajzer CT, Stewart WJ, Cosgrove DM, Azzam SJ, Arheart KL, Klein AL. Tricuspid valve surgery and intraoperative echocardiography - Factors affecting survival, clinical outcome, and echocardiographic success. *Journal of the American College of Cardiology.* 1998;32(4):1023-1031.

48. Singh JP, Evans JC, Levy D, Larson MG, Freed LA, Fuller DL, Lehman B, Benjamin EJ. Prevalence and clinical determinants of mitral, tricuspid, and aortic regurgitation (The Framingham Heart Study) (vol 83, pg 897, 1999). *American Journal of Cardiology.* 1999;84(9):1143-1143.

49. King RM, Schaff HV, Danielson GK, Gersh BJ, Orszulak TA, Piehler JM, Puga FJ, Pluth JR. SURGERY FOR TRICUSPID REGURGITATION LATE AFTER MITRAL-VALVE REPLACEMENT. *Circulation.* 1984;70(3):193-197.

50. Matsuyama K, Matsumoto M, Sugita T, Nishizawa J, Tokuda Y, Matsuo T. Predictors of residual tricuspid regurgitation after mitral valve surgery. *Annals of Thoracic Surgery.* 2003;75(6):1826-1828.

51. Abe T, Tukamoto M, Yanagiya M, Morikawa M, Watanabe N, Komatsu S. De Vega's annuloplasty for acquired tricuspid disease: Early and late results in 110 patients. *Annals of Thoracic Surgery.* 1996;62(6):1876-1877.

52. Kim JB, Spevack DM, Tunick PA, Bullinga JR, Kronzon I, Chinitz LA, Reynolds HR. The effect of transvenous pacemaker and implantable cardioverter defibrillator lead placement on tricuspid valve function: An observational study. *Journal of the American Society of Echocardiography.* 2008;21(3):284-287.

53. Gibson TC, Foale RA, Guyer DE, Weyman AE. CLINICAL-SIGNIFICANCE OF INCOMPLETE TRICUSPID-VALVE CLOSURE SEEN ON TWO-DIMENSIONAL ECHOCARDIOGRAPHY. *Journal of the American College of Cardiology.* 1984;4(5):1052-1057.

54. Sagie A, Schwammenthal E, Padial LR, Vazquez JA, Weyman AE, Levine RA. DETERMINANTS OF FUNCTIONAL TRICUSPID REGURGITATION IN INCOMPLETE TRICUSPID-VALVE CLOSURE - DOPPLER COLOR-FLOW STUDY OF 109 PATIENTS. *Journal of the American College of Cardiology.* 1994;24(2):446-453.

55. Fukuda S, Gillinov AM, Song JM, Daimon M, Kongsaerepong V, Kihara T, Greenberg N, Thomas JD, Shiota T. The effect of tricuspid valve surgery on right ventricular function in patients with functional tricuspid regurgitation. *Journal of the American College of Cardiology.* 2005;45(3):365A-365A.

56. Min SY, Song JM, Kim JH, Jang MK, Kim YJ, Song H, Kim DH, Lee JW, Kang DH, Song JK. Geometric changes after tricuspid annuloplasty and predictors of residual tricuspid regurgitation: a real-time three-dimensional echocardiography study. *European Heart Journal.* 2010;31(23):2871-2880.

57. Dreyfus GD, Raja SG, Chan KMJ. Tricuspid leaflet augmentation to address severe tethering in functional tricuspid regurgitation. *European Journal of Cardio-Thoracic Surgery.* 2008;34(4):908-910.

58. STS Adult CV Surgery National Database. Fall 2008 Executive Summary.

59. He S, Jimenez J, He Z, Yoganathan AP. Mitral leaflet geometry perturbations with papillary muscle displacement and annular dilatation: an in-vitro study of ischemic mitral regurgitation. *J Heart Valve Dis.* 2003;12(3):300-307.

60. Jimenez JH, Forbess J, Croft LR, Small L, He Z, Yoganathan AP. Effects of annular size, transmitral pressure, and mitral flow rate on the edge-to-edge repair: an in vitro study. *Ann Thorac Surg.* 2006;82(4):1362-1368.

61. Jimenez JH, Soerensen DD, He ZM, Ritchie J, Yoganathan AP. Effects of papillary muscle position on chordal force distribution: An in-vitro study. *Journal of Heart Valve Disease.* 2005;14(3):295-302.

62. Fukuda S, Gillinov AM, Song JM, Daimon M, Kongsaerepong V, Thomas JD, Shiota T. Echocardiographic insights into atrial and ventricular mechanisms of functional tricuspid regurgitation. *American Heart Journal.* 2006;152(6):1208-1214.

63. Nielsen SL, Soerensen DD, Libergren P, Yoganathan AP, Nygaard H. Miniature C-shaped transducers for chordae tendineae force measurements. *Annals of Biomedical Engineering.* 2004;32(8):1050-1057.

64. Weyman AE, MD. *Principles and Practice of Echocardiography*. Second ed. Malvern: Lea & Febiger; 1994.

65. Miyatake K, Okamoto M, Kinoshita N, Ohta M, Kozuka T, Sakakibara H, Nimura Y. EVALUATION OF TRICUSPID REGURGITATION BY PULSED DOPPLER AND TWO-DIMENSIONAL ECHOCARDIOGRAPHY. *Circulation.* 1982;66(4):777-784.

66. Kerut EK, McIlwain EF, Plotnick GD. *Handbook of echo-doppler interpretation*. 2nd ed. Elmsford, N.Y.: Blackwell Publishing; 2004.

67. He SQ, Lemmon JD, Weston MW, Jensen MOJ, Levine RA, Yoganathan AP. Mitral valve compensation for annular dilatation: In vitro study into the mechanisms of functional mitral regurgitation with an adjustable annulus model. *Journal of Heart Valve Disease.* 1999;8(3):294-302.

68. Padala M, Hutchison RA, Croft LR, Jimenez JH, Gorman RC, Gorman JH, Sacks MS, Yoganathan AP. Saddle Shape of the Mitral Annulus Reduces Systolic Strains on the P2 Segment of the Posterior Mitral Leaflet. *Annals of Thoracic Surgery.* 2009;88(5):1499-1505.

69. Weber KT, Janicki JS, Shroff S, Fishman AP. CONTRACTILE MECHANICS AND INTERACTION OF THE RIGHT AND LEFT-VENTRICLES. *American Journal of Cardiology.* 1981;47(3):686-695.

70. Ludbrook J. Statistics in biomedical laboratory and clinical science: Applications, issues and pitfalls. *Med Prin Pract.* 2008;17(1):1-13.

71. Weyman AE. *Principles and practice of echocardiography*. 2nd ed. Philadelphia: Lea & Febiger; 1994.

72. Spinner EM, Sundareswaran K, Dasi LP, Thourani VH, Oshinski J, Yoganathan AP. Altered right ventricular papillary muscle position and orientation in patients with a dilated left ventricle. *The Journal of thoracic and cardiovascular surgery.* 2011;141(3):744-749.

73. Lin G, Nishimura RA, Connolly HM, Dearani JA, Sundt TM, 3rd, Hayes DL. Severe symptomatic tricuspid valve regurgitation due to permanent pacemaker or implantable cardioverter-defibrillator leads. *Journal of the American College of Cardiology.* 2005;45(10):1672-1675.

74. Brock RC. The surgical and pathological anatomy of the mitral valve. *British heart journal.* 1952;14(4):489-513.

75. Burch GE, DePasquale NP, Phillips JH. The syndrome of papillary muscle dysfunction. *American Heart Journal.* 1968;75(3):399-415.

76. Nu TTT, Levine RA, Perez-Sanz TM, Scherrer-Crosbie M. Transition from mitral valve prolapse to incomplete mitral leaflet closure: Central role of papillary muscle position. *Circulation.* 2005;112(17):U396-U396.

77. Sukmawan R, Watanabe N, Ogasawara Y, Yamaura Y, Yamamoto K, Wada N, Kume T, Okura H, Yoshida K. Geometric changes of tricuspid valve tenting in tricuspid regurgitation secondary to pulmonary hypertension quantified by novel system with transthoracic real-time 3-dimensional echocardiography. *Journal of the American Society of Echocardiography.* 2007;20(5):470-476.

78. Levine RA, Vlahakes GJ, Lefebvre X, Guerrero JL, Cape EG, Yoganathan AP, Weyman AE. Papillary-Muscle Displacement Causes Systolic Anterior Motion of the Mitral-Valve - Experimental Validation and Insights into the Mechanism of Subaortic Obstruction. *Circulation.* 1995;91(4):1189-1195.

79. Sanfilippo AJ, Harrigan P, Popovic AD, Weyman AE, Levine RA. Papillary-Muscle Traction in Mitral-Valve Prolapse - Quantitation by 2-Dimensional Echocardiography. *Journal of the American College of Cardiology.* 1992;19(3):564-571.

80. Jimenez JH, Liou SW, Padala M, He Z, Sacks M, Gorman RC, Gorman JH, 3rd, Yoganathan AP. A saddle-shaped annulus reduces systolic strain on the central region of the mitral valve anterior leaflet. *J Thorac Cardiovasc Surg.* 2007;134(6):1562-1568.

81. Kaplan SR, Bashein G, Sheehan FH, Legget ME, Munt B, Li XN, Sivarajan M, Bolson EL, Zeppa M, Martin RW. Three-dimensional echocardiographic assessment of annular shape changes in the normal and regurgitant mitral valve. *American Heart Journal.* 2000;139(3):378-387.

82. Levine RA, Triulzi MO, Harrigan P, Weyman AE. The Relationship of Mitral Annular Shape to the Diagnosis of Mitral-Valve Prolapse. *Circulation.* 1987;75(4):756-767.

83. Spinner EM, Shannon P, Buice D, Jimenez J, Veledar E, Del Nido P, Adams DH, Yoganathan AP. In Vitro Characterization of the Mechanisms Responsible for Functional Tricuspid Regurgitation. *Circulation.* Accepted for Publication 2011.

84. Shudo Y, Matsue H, Toda K, Hata H, Fujita S, Taniguchi K, Sawa Y. A Simplified Echocardiographic Measurements of Direct Effects of Restrictive Annuloplasty on Mitral Valve Geometry. *Echocardiography-a Journal of Cardiovascular Ultrasound and Allied Techniques.* 2010;27(8):931-936.

85. He SQ, Jimenez J, He ZM, Yoganathan AP. Mitral leaflet geometry perturbations with papillary muscle displacement and annular dilatation: An in-vitro study of ischemic mitral regurgitation. *Journal of Heart Valve Disease.* 2003;12(3):300-307.

86. Kunzelman KS, Cochran RP, Verrier ED, Eberhart RC. Anatomic basis for mitral valve modelling. *J Heart Valve Dis.* 1994;3(5):491-496.

87. Perloff JK, Roberts WC. The mitral apparatus. Functional anatomy of mitral regurgitation. *Circulation.* 1972;46(2):227-239.

88. Fernando ANTONIALI DMB, Glória Maria Braga POTÉRIO, Cledicyon Eloy da, COSTA MML, Gustavo Calado de Aguiar RIBEIRO, Luciano dos Santos TARELHO. Proportion among the segments of the normal tricuspid valve annulus: parameter for valve annuloplasty. *Braz J Cardiovasc Surg.* 2006;21(3):262-271.

89. Carpentier A, Adams D.H., Filsoufi, F. *Reconstructive Valve Surgery*. Maryland Heights: Saunder Elsevier; 2010.

90. Cook AC, Anderson RH. Attitudinally correct nomenclature. *Heart.* 2002;87(6):503-506.

91. Victor S, Nayak, V.M. The Tricuspid Valve Is Bicuspid. *Journal of Heart Valve Disease.* 1994;3(1):27-36.

92. Fukuda S, Song JM, Gillinov AM, Daimon M, Kongsaerepong V, Greenberg N, Thomas JD, Shiota T. Tricuspid valve tethering predicts residual regurgitation after tricuspid annuloplasty. *Journal of the American College of Cardiology.* 2005;45(3):362A-362A.

93. Bonow RO, Carabello B, De Leon AC, Edmunds LH, Fedderly BJ, Freed MD, Gaasch WH, Mckay CR, Nishimura RA, O'Gara PT, O'Rourke RA, Rahimtoola SH. ACC/AHA guidelines for the management of patients with valvular heart disease - A report of the American College of Cardiology American Heart Association Task Force on practice guidelines (Committee on Management of Patients with Valvular Heart Disease). *Journal of the American College of Cardiology.* 1998;32(5):1486-1582.

94. Weber OM, Martin AJ, Higgins CB. Whole-heart steady-state free precession coronary artery magnetic resonance angiography. *Magn Reson Med.* 2003;50(6):1223-1228.

95. Association NEM. Digital Imaging and Communications in Medicine (DICOM). In: Association NEM, ed. *Information Object Definitions*. Rosslyn, Virginia; 2004:876.